GENES PRESERVING STEM CELL STATE IN MEDULLOBLASTOMA CONTRIBUTE TO THERAPY EVASION AND RELAPSE

GENES PRESERVING STEM CELL STATE IN MEDULLOBLASTOMA CONTRIBUTE TO THERAPY EVASION AND RECURRENCE

By DAVID BAKHSHINYAN, (H)B.Sc.

A Thesis Submitted to the School of Graduate Studies in Partial Fulfillment of the Requirements for the Degree Doctor of Philosophy

Descriptive note:

DOCTOR OF PHILOSOPHY (2019) - Biochemistry & Biomedical Sciences
McMaster University,
Hamilton, Ontario, Canada

TITLE: Genes Preserving Stem Cell State in Medulloblastoma, contribute to Therapy Evasion and Relapse

AUTHOR: David Bakhshinyan, Hon. B.Sc. (York University)

SUPERVISOR: Dr. Sheila K. Singh

NUMBER OF PAGES: 229

Lay abstract:

Medulloblastoma is the most common type of brain cancer that affects children. Out of the four main subgroups of medulloblastoma, tumors in Groups 3 and 4 are the most aggressive and are associated with a low overall survival in children diagnosed with this type of brain cancer. These two subtypes of medulloblastoma also account for the largest number of patients in which gold standard therapies fail and no additional therapies are available. Several studies have shown the existence of few cells within the tumor that alone can drive tumor growth. The aggressive behavior of these cells has in part been attributed to dysregulation of genes involved in cell replication and division. Further studies that will focus on understanding the significance of genes that regulate cell growth and replication can help discover a population of cells that is capable of evading therapy and contribute to tumor relapse. The identification and characterization of such population can lead to development of novel treatments for the children affected with aggressive medulloblastoma. In my thesis, I have developed a mouse model that replicates the aggressive therapy given to the medulloblastoma patients in order to study cells capable of escaping the harsh treatment and drive tumor comeback. Next, by profiling the gene expression and functional attributes of those cells, we identified genes that contribute to regulation of cell division and growth. The effects of both increasing and decreasing the activity of those genes were then tested in cells grown in the dish. Subsequently, the most promising results were verified in the established mouse models. The main objective of my thesis was to discover new opportunities in treatments the most aggressive type of brain

cancer affecting children, and thus not only improve the quality of treatment but also the overall survival of patients with medulloblastoma.

Abstract:

Medulloblastoma (MB) is the most common malignant pediatric brain tumor. Out of the four molecular subgroups (WNT, SHH, Group 3 and Group 4), Group 3 patients face the highest incidence of leptomeningeal spread and overall patient survival of less than 50%. Current clinical trials for recurrent MB patients based on genomic profiles of primary, treatment-naïve tumors, provide limited clinical benefit since recurrent metastatic MBs are highly genetically divergent from their primary tumors. The paucity of patient matched primary and recurrent MB samples has contributed to the lack of molecular targets specific to medulloblastoma recurrence, limiting relapsing MB patients to palliation. Our previous *in silico* analyses revealed enriched expression of many stem cell self-renewal regulatory genes in Group 3 MB.

In this work, *I have set out to investigate whether by identifying genes contributing to self-renewal of Group 3 MB cells, we can characterize a population of cells responsible for therapy evasion and subsequent tumor relapse.* Initially, we have adapted the existing COG (Children's Oncology Group) protocol for children with newly diagnosed high-risk MB for treatment of immuno-deficient mice intracranially xenografted with human MB cells. Cell populations recovered separately from brains and spines mice during the course of tumor development and therapy were comprehensively profiled for gene expression analysis, stem cell and molecular features to generate a global, comparative profile of MB cells through therapy. Additionally, we have investigated therapeutic potential of small molecules targeting BMI1, a known self-renewal regulating gene. In the setting of recurrent

Group 3 MB, pharmacological inhibition of BMI1, led to a remarkable decrease in cell proliferation and self-renewal *in vitro* as well as reduction of local and spinal metastatic disease *in vivo*. Finally, by combining the established therapy-adapted patient-derived xenograft mouse model and BMI1 inhibitor, PTC-596, we have demonstrated an additive effect of two modalities and provided the pre-clinical data for the upcoming Phase I trial.

Biological investigations into the drivers of MB recurrence will lead to development of new therapeutic options for children who are frequently limited to palliation. Clinically relevant mouse models of MB recurrence can serve as platforms for pre-clinical testing and validation of new treatments aimed to provide therapeutic intervention rather than palliation.

Acknowledgements:

Throughout my journey as a graduate student I have had the privilege to meet and work alongside many brilliant people, and to them I will always be thankful.

First and foremost, I would like to thank Dr. Sheila Singh for her truly exceptional mentorship, for granting me opportunities that most graduate students dream of, and for shaping my scientific thinking. You have provided guidance and continuous encouragement throughout my graduate journey and never stopped believing in me, or my work. Much like you, I hope to continue my career and become a neurosurgeon-scientist.

To my committee members, Dr. Kristin Hope and Dr. Thomas Farrell, thank you for helping elevate my scientific work and all the invaluable advice you have provided me with during our meetings.

The past five and a half years would have felt much longer, if not for Dr. Chitra Venugopal. Thank you for addressing a never-ending stream of questions with unwavering patience, and always taking the time to ensure that we, as students, always have the tools to succeed.

I cannot forget my fellow graduate students in the Singh lab and SCC-RI for being a big part of my time at McMaster University; not only in helping to complete experiments, but also being there throughout both the successes and frustrations. The SCC-RI softball team will forever be Division D champions, even if the standings did not reflect that. Another big thank you is due to Nicole McFarlane for all the advice she has given me that went far beyond the work in the lab.

Finally, I would like to thank my parents for being the foundation on which I had a chance to grow and build myself. As a token of appreciation, I am dedicating this thesis to them.

Table of Contents

List of Figures and Tables:

Chapter 2

Chapter 5:

List of key abbreviations

ASCR – autologous hematopoetic stem cell rescue

BMI1 – B lymphoma MO-MLV insertion region 1

BPIFB4 – bactericidal/permeability-increasing fold-containing-family-B-member-4

BTICs – brain tumor initiating cells

CNS – central nervous system

COG – Children's Oncology Group

CSC – cancer stem cell

DPI – diphenyleneidodonium chloride

eNOS – endothelial nitric oxide synthase

G3 MB – group 3 medulloblastoma

GNCPs – granule neuron precursor cells

IC50 – inhibitory concentration of 50%

ID - inhibitors of differentiation

ITH – intratumoral heterogeneity

H3K4me3 – histone 3 lysine 4 trimethylation

H3K27me3 – histone 3 lysine 27 trimethylation

HDCT – high dose chemotherapy

hNSC – human neural stem cells

L-NIO – N^5(1-Iminoethyl)-L-ornithine

MB – medulloblastoma

nNOS – neuronal nitric oxide synthase

OS – overall survival

PDX – patient derived xenograft

PRC1 – polycomb repressive complex 1

PRC2 – polycomb repressive complex 2

SoC - standard-of-care

TIC – tumor initiating cell

Declaration of academic achievement:

In my PhD, I have contributed to 16 research papers, 6 book chapters and had an opportunity to present my research at 12 scientific conferences.

The presented thesis is prepared in the "sandwich" format as outlined in the "Guide for the Preparation of Master's and Doctoral Theses" (2016). Chapter 1 provides the general introduction into medulloblastoma, highlighting clinical epidemiology, molecular mechanisms driving medulloblastoma progression, and cancer stem cell hypothesis. Additionally, Chapter 1 summarizes the hypothesis and overall aims of the described work. The chapter contains excerpts from the following first-authored published peer-reviewed book chapters:

- Bakhshinyan, D., A.A. Adile, M.A. Qazi, M. Singh, M.M. Kameda-Smith, N. Yelle, C. Chokshi, C. Venugopal, S.K. Singh, (2016) Chapter 1: Introduction to Cancer Stem Cells: Past, Present and Future. *Methods in Molecular Biology*

- Bakhshinyan D.*, Qazi M.*, N. Garg, C. Venugopal, N. McFarlane, S.K. Singh (2015) Chapter 8: Isolation and identification of neural cancer stem/progenitor cells. *Principles of Stem Cell Biology*

Chapter 2 represents the recently submitted manuscript titled *Stem cell longevity factor BPIFB4 is a driver of medulloblastoma recurrence* containing results of the established therapy-adapted patient derived xenograft model of recurrent medulloblastoma. Chapter 3 is a review paper titled *BMI1: a path to targeting cancer stem cells* highlighting importance

of epigenetic regulators such as BMI1 in driving tumor progression and therapy evasion. Chapter 4 is an original manuscript "*BMI1 is a therapeutic target in recurrent medulloblastoma"* describing the pre-clinical data validating the efficacy of small molecules targeting BMI1for treatment of recurrent medulloblastoma. Chapter 5 includes the unpublished work attempting to decipher the clonal dynamics and the molecular mechanisms by which medulloblastoma cells evade both conventional and targeted therapy. Chapter 6 provides the overall summary of the work along with the broader implications of this thesis.

Chapter 1: Introduction

1.1 Epidemiology

Following leukemia, central nervous system (CNS) tumors are the second most common pediatric malignancy, and remain the leading cause of cancer-related mortality in pediatric oncology(Taylor et al., 2012). Originating in the cerebellar region of the brain, medulloblastoma (MB) represents the most common malignant pediatric brain tumor. Although the overall incidence of MB has declined to 4.82 cases per 1,000,000 people(Johnston et al., 2014), it still represents 60% of childhood intracranial embryonal tumors. A small number of population-based studies have highlighted the fairly uniform levels of MB incidence across geographical regions and ethnicities(Ezzat et al., 2016).The median age of diagnosis of pediatric medulloblastoma is at ~6 years of age, with an overall male-to-female ratio of 1.8:1(Khanna et al., 2017).

1.2 Diagnosis, histology and risk stratification

The diagnosis of MB is based on clinical symptoms, brain and spine imaging, cerebrospinal fluid cytology, molecular and histopathological analysis. The multimodal standard-of-care (SoC) therapy for MB consists of surgical resection, chemotherapy and radiation for non-infant patients (over the age of 3 years). To distinguish MB from other radiographically similar brain tumors, the biological specimen obtained during surgical resection is used for histopathological and molecular analysis. Current histopathological stratification of MB includes five subtypes: (i) Classic MB, (ii) desmoplastic/nodular MB (D/N), (iii) MB with extensive nodularity (MBEN), (iv) large cells MB (LC), and (v) anaplastic (A) MB(Ellison,

2010). Although the differences in histological and cytogenetic characteristics between subtypes have addressed the issue of cellular and morphological heterogeneity of the bulk tumor, they provide very limited prognostic value that can be translated into clinical settings. The survival rates of MB reach 70-85% in standard-risk patients(Gajjar et al., 2006; Oyharcabal-Bourden et al., 2005; Packer et al., 2006), who are typically older than 3 years of age, have a gross total tumor resection, and do not present any metastatic lesions at diagnosis. On the other hand, patients who are younger than 3, have a subtotal resection and present with metastatic lesions at diagnosis are stratified into the high-risk category with a five-year OS of less than 70%(Gajjar et al., 2006; Gandola et al., 2009; Jakacki et al., 2012). Patients with radiological evidence of brain dissemination or spinal metastasis have been shown to have worse overall prognosis that those who have no evidence of dissemination(Taylor et al., 2005; Zeltzer et al., 1999)

1.3 Molecular classification of medulloblastoma

Given the limitations of current clinico-pathological parameters to accurately predict treatment response(Crawford et al., 2007; Gilbertson, 2004; Korshunov et al., 2010), multiple integrated genomic platforms have been used to characterize the aberrant expression of signaling pathways in MB. This has re-conceptualized the heterogeneity that exists within pathological subtypes, and has given context to the role of key stem cell signaling pathways in MB pathogenesis(Cho et al., 2011b; Kool et al., 2008; Northcott et al., 2011; Thompson et al., 2006). The unsupervised hierarchical clustering methods of segregating these data have produced four subgroups, of MB, WNT, SHH, Group 3 and

Group 4. While WNT and SHH MBs are characterized by upregulation of genes in the Wnt and Sonic hedgehog (Shh) pathways, respectively(Fattet et al., 2009; Kool et al., 2008; Northcott et al., 2011; Taylor et al., 2012; Thompson et al., 2006), little is known about the underlying pathways driving Group 3 and 4 MB pathogenesis. In contrast to WNT and SHH MBs, Group 3 and 4 MBs are associated with metastatic disease and poor patient outcome(Cavalli et al., 2017; Schwalbe et al., 2017). These aggressive MBs, which have been collectively labeled as "non-Shh/Wnt" subgroups(Ellison, 2010), remain refractory to current treatment modalities. Furthermore, recent genomic meta-analyses have revealed evidence for the existence of subtypes within Group 3 and 4 MBs, now labeled as 3α, 3β, 4α and 4β, each with distinct gene mutations and transcriptome profiles(Cavalli et al., 2017). Furthermore, genetic alterations unique to each MB subtype that can influence histone modification, DNA methylation and subsequent chromatin remodeling were shown to impact the underlying gene expression profile(Northcott et al., 2012a). In non-Wnt/Shh MB, the undifferentiated phenotype is preserved by the increase in histone 3 lysine 27 trimethylation (H3K27me3) and decrease in histone 3 lysine 4 trimethylation (H3K4me3)(Alimova et al., 2012; Dubuc et al., 2013; Robinson et al., 2012). Molecular subgroups of MBs further differ in the prevalence of metastatic disease. While metastatic dissemination is observed in 10% of WNT and 20% of SHH tumors, it is more common in Group 3 (45%) and Group 4 (30%) MBs(Cho et al., 2011b; Kool et al., 2008; Northcott et al., 2011; Pomeroy et al., 2002; Shih et al., 2014). Genetic studies on metastatic samples have shown the preservation of subgroup affiliations(Wang et al., 2015), and provided evidence of increased genetic divergence between primary and metastatic compartments

through the course of disease progression(Morrissy et al., 2016; Wu et al., 2012). Clinically, metastatic dissemination presents a significant challenge as over 50% of Group 4 patients are presented with metastasis at the time of relapse, while Group 3 patients are frequently presented with unresectable tumor nodules on the leptomeninges at presentation(Ramaswamy et al., 2013). The paucity of both human samples and mouse models able to recapitulate metastatic disease has contributed to the lack of molecular targets, and remain to be an area of active investigation.

1.4 Recurrent MB

Relapse still remains the single most adverse event in MB progression. Despite the advances of multimodal therapies, current treatment schemes fail to cure 25-40% of SHH, Group 3 and Group 4 patients(Shih et al., 2014). The studies on recurrent MB have been hindered by the low incidence of the disease and the lack of standardized treatment regimens across institutions(Dunkel et al., 1998; Fouladi et al., 2006; Gajjar et al., 2006; Pizer et al., 2011). For the last three decades, relapsing patients have been treated with either salvage therapy or high dose chemotherapy (HDCT) followed by autologous hematopoetic stem cell rescue (ASCR). Although combination of HDCT-ASCR led to disease free survival of over 3 years in almost 10% of relapsing patients, the responding patients were almost uniformly radiotherapy-naïve(Gururangan et al., 2008; Shih et al., 2008). The long term benefit of HDCT-ASCR is still unclear in patients over the age of 3 and who have been treated with radiation(Gajjar et al., 2006; Gururangan et al., 2008; Pizer et al., 2011; Shih et al., 2008; Zeltzer et al., 1999). Since the harsh treatment has been shown

to negatively affect the neurocognitive development in children(Mulhern et al., 2005; Packer et al., 2006; Ribi et al., 2005), future studies should focus on identification of novel targeted approaches to work in combination with the current gold-standard therapies. Unlike the subgroup plasticity observed in high-grade gliomas in response to therapy(Pietsch et al., 2014; Sottoriva et al., 2013), subgroup affiliation of MB remains stable at relapse(Ramaswamy et al., 2013), further supporting the distinct cell of origin of each MB subtype. This in turn is suggestive that understanding molecular mechanisms for each subgroup would be essential in designing targeted therapies. A study profiling 23 patient matched primary and recurrent samples revealed a consistent upregulation of *MYC* genes and mutations in *TP53* driving recurrence of SHH tumors(Zhukova et al., 2013). However, the paucity of patient MB samples collected at relapse has hindered the functional understanding of molecular mechanisms driving therapy failure in Group 3 and 4 MB, subgroups with the highest rates of recurrence. The matter is further complicated by the fact that patients with Group 3 and 4 MB present with inoperable metastatic spread at recurrence unlike the local recurrences observed in SHH patients(Ramaswamy et al., 2013).

1.5 Developmental origins of MB

Mounting experimental evidence has contributed to the notion that each MB subgroup arises from a distinct progenitor population in the course of normal development. The genetic and epigenetic alterations acquired in the process of transformation in turn contribute to the tumors identity and clinical outcome. The gene expression profile of WNT tumors resembles closely the transcriptional profile of dorsal brain stem

progenitors(Gibson et al., 2010), while SHH tumors are derived from the granule neuron precursor cells (GNCPs)(Schuller et al., 2008; Wechsler-Reya and Scott, 1999; Wefers et al., 2014; Yang et al., 2008). Although, cell of origin remains to be experimentally elucidated for Group 3 and Group 4 tumors, the alterations in stem cell maintenance, differential and neurogenesis pathways suggest an early neural stem cell as a potential cell of origin(Perreault et al., 2014; Wefers et al., 2014).

1.6 Cancer stem cell (CSC) hypothesis

Although the term "stem cell" received its current definition in the late 1800s(Ramalho-Santos and Willenbring, 2007) it was not until the seminal work by Dr. James Till, Dr. Ernest McCulloch and colleagues in the 1960s that provided first definitive evidence of adult stem cells(McCulloch et al., 1965; Siminovitch et al., 1963; Till and McCulloch, 1961). Through their adaptation of an *in vivo* spleen colony formation assay, where donor bone marrow cells (BMCs) were transplanted into a pre-irradiated recipient animal following the qualitative and quantitative analysis of colonies formed on the host's spleen, they were able to functionally describe and characterize adult stem cells. They first alluded to the fact that stem cell studies must be based on functional assays and defined the following properties of the cells capable of forming colonies in the recipient: (i) extensive proliferative capacity; (ii) giving rise to cells capable of differentiation and (iii) ability to self-renew. Following their work, adult stem cells have been shown to be present in blood, skin and small intestines, all three associated with a high cell turnover and putative rare population of cells responsible for generating differentiated cells. In a review by Potten and Loeffler, an updated functional definition of stem cells was proposed as undifferentiated

cells with (i) extensive proliferation capacity; (ii) ability to self-renew; (iii) potential to produce differentiated functional progenitors; (iv) ability to regenerate tissue post injury and (v) flexibility in the use of those abilities(Potten and Loeffler, 1990). Interestingly, the existence of adult stem cells was thought to be limited to tissues with inherently high turnover rates up until early 1990s. However, with the development of increasingly enhanced culturing techniques, adult stem cells were discovered in more static tissues including breast(Al-Hajj et al., 2003), brain(Reynolds and Weiss, 1992) and lungs(Kajstura et al., 2011).

1.5.1 Conceptualization of CSCs

Following an observation of phenotypic similarities between embryonic and cancer cells by Joseph Claude Anselme Recamier and Robert Remak in mid-1800s, the first putative notion of stem cells having the ability to give rise to cancers was postulated, termed embryonal rest theory of cancer. Formalized by Franco Durante and Julius Cohnheim the embryonal rest theory of cancer suggests that a small collection of persistent, undifferentiated embryonic tissue was the key to cancer initiation(Cohnheim, 1875). In the later half of the 19th century, the de-differentiation theory of cancer was brought into focus, acting as a substitute for the embryonal rest theory of cancer(Rippert, 1904). Unlike the embryonal rest theory, the dedifferentiation theory proposed that changes in the mature cells give rise to cancer due to the comparative properties of differentiated and cancer cells. A strong support for de-differentiation theory came from the observation made by Rudolf Virchow, who proposed that embryonic tissue in teratocarcinoma arose from chronic inflammation of connective tissue(Virchow, 1863). Other studies in the early 1900s

suggesting that cancers could be caused by chemicals, infectious parasites, and loss of inhibitory influences of the body on tissues, were considered supporting of the de-differentiation hypothesis(Paget, 1853; Rippert, 1904). It was not until 1980s when the role of stem cells in cancer was brought back into the spot light through studies of teratocarcinoma and leukemia.

1.5.2 Teratocarcinoma

Teratocarcinomas are malignant cancers originating from germinal cells. During the analysis of cellular composition of teratocarcinomas, Barry Pierce and colleagues have demonstrated the similarities in the cellular composition between the malignant and normal tissue, as both contained differentiated cells, progenitor cells and stem cells. Although over 90% of cells comprising teratocarcinomas were differentiated cells, the malignant cells were exclusively found in structures resembling early embryoid bodies(Pierce and Dixon, 1959). More importantly, it was later demonstrated that it was the cells found in embryoid bodies that had the potential to be propagated *in vitro* and ability to initiate tumors upon transplantation(Illmensee, 1978; Mintz and Illmensee, 1975) Further experiments by Leroy Stevens demonstrated that teratocarcinomas could arise from normal cells including early mouse embryo cells and testicular germ cells when transplanted from their natural site into abnormal tissues(Stevens, 1970). In the complementary experiments by Mintz and Illmensee, they found that when the stem cells isolated from teratocarcinomas were injected into the blastocyst of a normally developing embryo, they were able to give rise to normal tissue(Stevens, 1964). Together the studies on teratocarcinomas have contributed to the notion of malignant tissue having similar cellular hierarchy as normal tissue but that

tumours were arising from maturation arrest of the stem cells found in normal tissues and not by dedifferentiation. Although originally thought to be limited to teratocarcinomas, conceptualization of stem cell driven tumorigenesis was further developed from studies done on leukemia.

1.5.3 Identification of CSCs in brain tumors

It has been suggested that cancer stem cells (CSCs) are endowed with conventional chemotherapy and radiation resistance, along with tumor-initiating and metastatic properties that are correlative with increased tumor recurrence and poor clinical outcome(Allen and Weiss, 2010). In stark contrast, non-CSCs are thought to be therapy-sensitive and lack any self-renewal capacity(Nguyen et al., 2012). Studies involving human acute myeloid leukemia (AML) by Bonnet and Dick in 1997 provided the first compelling evidence of the existence of CSCs(Bonnet and Dick, 1997). The existence of CSCs in solid tumors was reported in 2003 by Al Hajj who demonstrated the presence of CSCs in breast cancer(Al-Hajj et al., 2003). Currently, CSCs have been proven to exist in various solid tumors including colon, lung, prostate, pancreatic, brain, head and neck and liver among others. Current anti-cancer therapies have a tendency to kill bulk tumor, rather than specifically target the intrinsically resistant CSCs that proliferate following completion of standard therapies. Interestingly, experiments with lung cancer cells have suggested that lung-CSCs rely on both symmetric and asymmetric cellular division, whereas non-CSCs undergo symmetric division(Serrano et al., 2011). With symmetric cell division, each CSC generates either two CSC progeny or two differentiated cells. Conversely, asymmetric division involves each CSC producing a differentiated progeny, along with a CSC. Despite

their reliance on both types of cellular division, CSCs employ symmetric division particularly when subjected to cellular stress, such as chemotherapy(Liu et al., 2013), thus increasing the number of highly proliferative cells capable of repopulating the bulk tumor. Whether tumors emerge from de-differentiation of a normal cell, or rather a transformation event of a normal stem cell or progenitor cell is largely elusive to researchers in the field. With significant tumor heterogeneity, a multipotent cell of origin is highly plausible, particularly due to the presence of several lineage phenotypes with distinct gene expression profiles and cell surface markers. Whether a CSC originates from a transformed stem cell or a de-differentiated, a more profound, functional definition of a cancer stem cell allows for a more accurate description of their role in driving tumour progression.

The discovery of brain tumor stem cells was made on the heels of work in breast cancer(Al-Hajj et al., 2003) and brain tumors were among the first solid tumors in which cells responsible for tumor initiation were identified(Singh et al., 2004). Since the identification of normal neural stem cells (NSC) in mice and humans(Reynolds and Weiss, 1992), several groups focused on whether NSC enrichment conditions could be used to identify a similar population in brain tumors. Hence, human brain tumors were grown in serum-free media with neural specific growth factors, which led to the identification of small cell populations with clonogenic, self-renewing and multi-lineage differentiation potential(Galli et al., 2004; Hemmati et al., 2003; Ignatova et al., 2002; Singh et al., 2004). Utilizing prospective cell sorting through magnetic beads or fluorophore conjugated antibodies, CD133 was the first protein that marked a cancer stem cell-like population in both pediatric and adult brain

tumors(Singh et al., 2003) $CD133^+$ brain tumor cells gave rise to self-renewing colonies (termed neurospheres) *in vitro* and carried higher tumorigenic potential than $CD133^-$ cells when engrafted intracranially in immune-deficient mice. Tumors derived from $CD133^+$ cells were heterogeneous and a phenocopy of the patient's original tumor, suggesting the presence of cellular hierarchy originating from $CD133^+$ cell fraction(Singh et al., 2004). In efforts to further characterize brain tumor stem cells, additional markers such as CD15(Read et al., 2009; Son et al., 2009; Ward et al., 2009), integrin alpha 6(Lathia et al., 2010), L1CAM(Bao et al., 2008), ephrin family of receptors (EphA2, EphA3, EphB2)(Binda et al., 2012; Day et al., 2013; Nakada et al., 2010), as well as neural stem/precursor markers such as Nestin, Sox2(Alonso et al., 2011; Vanner et al., 2014), BMI1(Hemmati et al., 2003) and Notch were subsequently identified. Although further characterization and purification of the brain tumor stem cell compartment is required, current knowledge already suggests that brain tumor stem cells play an important role in not only tumor initiation, but also tumor maintenance and therapy resistance. In the adult malignant brain tumor, glioblastoma, the brain tumor stem cells seem to be localized to the perivascular niche, allowing these cell populations to maintain tumor growth through access to the host vasculature. More significantly, brain tumor stem cells, marked especially by the expression of CD133, have been demonstrated to be resistant to radiation(Bao et al., 2006) and chemotherapy(Beier et al., 2012). Hence, brain tumor stem cells can then also be seen as the source of therapy resistance and disease relapse observed in malignant brain tumors. The collective role that brain tumor stem cells have been shown to play in initiating and maintaining the tumor and allowing the tumor to escape therapy makes them a

significant biological target for therapeutic development, making *in vitro* and *in vivo* brain tumor stem cell models pertinent platforms for future drug discovery.

1.7 Summary of intent

The concept of MB arising from development gone awry, has made it a great candidate to be studied in the context of cancer stem cell hypothesis. The main idea that was explored in this thesis is the presence of a small population of CSCs that is able to evade therapy, maintain tumor growth and drive tumor recurrence[33–35]. Although, tumor initiating cells have been isolated from the newly diagnosed, treatment-naive tumors[29,41–44], the failure of therapy is indicative of the ability of CSCs to undergo clonal evolution in response to therapy. Thus, further understanding of the dynamic nature of CSCs in response to therapy is necessary for the development of new targeted therapies. The inherently increased self-renewal potential of CSCs has identified genes and pathways driving this phenotypic attribute as promising targets for therapeutic intervention. **We hypothesize that a subset of genes regulating self-renewal may identify the treatment refractory population of MB cells that are causative of tumor relapse and can provide potential therapeutic targets for patients diagnosed with Group 3 MB.** Our specific experimental aims are designed to determine the nature of treatment refractory MB CSCs as well as further elucidating role of genes regulating self-renewal in MB pathogenesis.

i. *To establish a therapy-adapted patient derived xenograft mouse model of Group 3 MB.* (Chapter 2)

ii. *To investigate whether genes responsible for stem cell self-renewal are identifying the treatment refractory cell population and are driving tumor relapse.* (Chapter 2)

iii. *To investigate the therapeutic potential of targeting a key self-renewal regulator, BMI1, in the context of recurrent Group 3 MB.* (Chapter 4)

Collectively, the work of this thesis has provided insights into molecular mechanisms driving MB relapse, as well as pre-clinical data suggestive of therapeutic value of targeting genes governing self-renewal in Group 3 MB.

Chapter 2: Stem cell longevity factor BPIFB4 is a driver of medulloblastoma recurrence

This chapter is an original article that is currently in submission to *Nature*.

Bakhshinyan, D., A.A. Adile, C. Venugopal, J. Liu, M. Singh, N. McFarlane, M.K. Subapanditha, M.A. Qazi, P. Vora, M. Kameda-Smith, N. Savage, K.L. Desmond, N. Tatari, D. Tran, M. Seyfrid, K. Hope, N.A. Bock, G. Bader, S.K. Singh (2019). "Stem cell longevity factor BPIFB4 is a driver of medulloblastoma recurrence." ***Nature***

This work represents the primary focus of my PhD thesis. To overcome the paucity of MB samples collected at relapse, we set out to develop a patient-derived xenograft (PDX) mouse-adapted therapy model. In addition to having a distinct advantage of generating human, treatment-refractory MB recurrence for each patient profiled, this model allowed for comprehensive and dynamic profiling of MB cells through functional stem cell and self-renewal assays. However, the biggest novelty of this work lies in its potential to identify drivers of MB progression as cells undergo therapy. Comparative gene expression analysis of MB cells collected throughout therapy revealed upregulation at relapse of a *gene never before characterized in the setting of cancer*, BPIFB4. Despite the absence of modalities capable of targeting BPIFB4 itself, a small molecule inhibitor targeting endothelial nitric oxide synthase (eNOS), a downstream substrate of BPIFB4, impeded the growth of several MB patient-derived lines at low nanomolar concentrations. The development of a model that can recapitulate both disease progression and its response to therapy holds great

promise to mitigate the rarity of matched primary and recurrent MB samples and guide the development of next-generation targeted therapeutic agents.

Stem cell longevity factor BPIFB4 is a driver of medulloblastoma recurrence

Authors: David Bakhshinyan[1,2], Ashley A. Adile[1,2], Chitra Venugopal[1,3], Jeff Liu[4], Mohini Singh[1,2], Nicole McFarlane[1,3], Minomi K. Subapanditha[1], Maleeha A. Qazi[1,2], Parvez Vora[1,3], Michelle Kameda-Smith[1,3], Neil Savage[1,2], Kim L. Desmond[5] Nazanin Tatari, Damian Tran[1], Mathieu Seyfrid[1], Kristin Hope[1], Nicholas A. Bock[5] PhD, Gary D. Bader[4] PhD, Sheila K. Singh*[1,2,3] MD, PhD

[1]McMaster Stem Cell and Cancer Research Institute, McMaster University, Hamilton, ON, Canada

Departments of [2]Biochemistry and Biomedical Sciences and [3]Surgery, Faculty of Health Sciences, McMaster University, Hamilton, ON, Canada

[4]The Donnelly Centre, University of Toronto, Toronto, ON, Canada

[5]Department of Psychology, Neuroscience and Behaviour, McMaster University, Hamilton, ON, Canada

***CORRESPONDING AUTHOR**

Sheila K. Singh, MD, PhD, FRCS(C)

Associate Professor of Pediatric Neurosurgery,

Department of Surgery, McMaster Children's Hospital,

Scientist, McMaster Stem Cell & Cancer Research Institute

MDCL 5027, 1280 Main Street West, Hamilton, ON, L8S 4K1, Canada

T: 905-521-2100 x75237 F: 905-521-992 Email: ssingh@mcmaster.ca

Medulloblastoma (MB) represents one of the leading causes of morbidity and mortality in childhood cancer. Over the past decade, genomic profiling of primary MB characterized molecular heterogeneity within MB cohorts and led to subsequent stratification of MB into four consensus subgroups, each distinct in prognosis and predicted therapeutic response(Cavalli et al., 2017; Schwalbe et al., 2017). However, virtually all MB patients who relapse after conventional therapy succumb to their disease, irrespective of subgroup. The paucity of MB samples collected at relapse has hindered the functional understanding of molecular mechanisms that drive therapy failure. In this study, we developed a patient-derived xenograft (PDX) mouse-adapted therapy model that has a distinct advantage of generating human, treatment-refractory MB recurrence. This model allowed for comprehensive and dynamic profiling of MB cells at engraftment, after radiation, after chemoradiotherapy and at relapse, through functional stem cell self-renewal assays and transcriptomic analysis. Comparative gene expression analysis of MB cells collected throughout therapy revealed highly significant upregulation at relapse of a gene never before characterized in the setting of cancer, bactericidal/permeability-increasing fold-containing-family-B-member-4 (BPIFB4). shRNA-mediated knockdown of BPIFB4 led to markedly decreased proliferation, self-renewal and longevity of MB cells, as well as extended survival and reduced tumor burden *in vivo*. Furthermore, a small molecule inhibitor targeting endothelial nitric oxide synthase (eNOS), a downstream substrate of BPIFB4(Villa et al., 2015), impeded the growth of several MB patient-derived lines at low nanomolar concentrations. For the first time, we describe the role

of BPIFB4 as a potent regulator of self-renewal and specific driver of MB relapse. The development of a model that recapitulates both disease progression and its response to therapy holds great promise to mitigate the rarity of matched primary and recurrent MB samples and guide the development of next-generation targeted therapeutic agents.

Of the four core medulloblastoma (MB) subgroups, patients with Group 3 medulloblastoma (G3 MB) experience the highest frequency of metastatic dissemination (~45%) and subsequently the worst clinical prognosis(Ramaswamy et al., 2013). Although 5-year overall survival for standard risk MB has reached 70-80%, tumor recurrence still remains the most adverse event in MB pathogenesis. Only 6% of relapsed patients have an overall survival (OS) exceeding 5 years, with standard clinical care focusing on palliation rather than therapeutic intervention.

The clonal evolution of tumor cells in response to conventional cytotoxic therapies has become one of the biggest hurdles in designing therapies for patients with tumor recurrence(Greaves and Maley, 2012; Morrissy et al., 2016). As majority of the studies focus on MB at diagnosis, understanding of MB at recurrence remains limited. Our novel patient-derived xenograft (PDX) mouse-adapted therapy model incorporates radio and chemotherapy, the two treatment modalities that exert selective pressure to mimic the clonal evolution of MB in patients (Fig. 1a). Mice xenografted with representative primary human G3 MB lines HD-MB03 and D425 were treated with craniospinal irradiation and a combination of chemotherapy drugs administered to pediatric MB patients, which consists of cisplatin, vincristine and cyclophosphamide. Following treatment, xenografted mice

demonstrated an initial response to treatment as indicated by reduced local and metastatic tumor burden (Fig. 1b, c; Supplementary Fig. 1a-c). Although, the combined therapy regimen improved the overall survival in both HD-MB03 and D425 cohorts (n=8) by 19 and 8.5 days respectively, all treated mice succumbed to subsequent tumor recurrence (Fig. 1d; Supplementary Fig. 1d). Most intriguing was the continual increase in phenotypic traits of proliferation and self-renewal, through the stages of therapy in human MB cells isolated from both local (brains) and metastatic (spines) compartments (Fig. 1e-h; Supplementary Fig. 1e-h). Since the ability of a cancer cell to undergo self-renewal is one of the key pillars of the cancer stem cell (CSC) hypothesis(Greaves and Maley, 2012), we performed a limiting dilution assay to identify any changes in the frequency of self-renewing cells in samples isolated from brains and spines at each stage of therapy. A major increase in incidence of self-renewing cells was observed in samples extracted from brains (HD-MB03: 1/132 at engraftment and 1/37 at relapse), compared to a more modest increase in frequency of self-renewing cells isolated from spines (HD-MB03: 1/147 at engraftment and 1/100 at relapse). This data suggests self-renewal is not a phenotypic trait required by cells with the potential for leptomeningeal metastasis (Fig. 1i, j; Supplementary Fig. 1i, j), further highlighting the bicompartmental nature of the disease(Wu et al., 2012) and the need for development of therapies specific to metastatic cells. Studies profiling CSCs have shown increased resistance to chemoradiotherapy(Bao et al., 2006; Nakai et al., 2009) when compared to more differentiated tumor cells. To ensure that our model was able to select for the cells capable of evading therapy, we measured the response of MB cells isolated at relapse to *in vitro* re-treatment with radiation, cisplatin and vincristine. In all three cases,

we observed an increased tolerance of cells collected at relapse to each of the treatment modalities (Fig. 1k-m; Supplementary Fig.1k-m).

The utility of our PDX mouse-adapted therapy model lies in its ability to generate a comprehensive gene expression comparison between treatment-naïve and recurrent MB to identify driver genes of therapy evasion and subsequent relapse. The initial gene expression profiling of MB cells isolated from brains and spines (Fig. 2a, b; Supplementary Fig. 2a, b, 3; Supplementary Table 1) and subsequent pathway analysis (Fig. 2c, d; Supplementary Fig. 4; Extended Table 1, 2) revealed selective pressures exerted by either chemotherapy or radiation distinctly alter the underlying pathways driving MB cell growth. With very few pathways overlapping between each stage of therapy, our model of MB therapy has for the first time captured the dynamic nature of tumor cells as they are subjected to radiation and chemotherapy. In accordance with previously published reports(Hill et al., 2015), pathway analysis revealed upregulation of Myc-target genes in samples isolated at relapse (Supplementary Fig 2e, f). In addition to validating genes that have been previously described as modulators of CSCs such as proteins belonging to the family of Inhibitors of DNA (ID)(Lasorella et al., 2014; Snyder et al., 2013) (Supplementary Fig 5a-d), our differential expression analysis identified genes yet to be described in the context of cancer. Most intriguing was the observation of consistently high degree of overexpression of *BPIFB4* in samples collected post-therapy in both datasets (Supplementary Table 1; Supplementary Fig 3).

To determine the clinical significance of BPIFB4 upregulation at MB recurrence, we profiled BPIFB4 mRNA expression in a collection of 19 MB samples representing the

four consensus molecular subtypes (WNT n=4; SHH n=6; Gr3 n=3, Gr4 n=6; Supplementary Table 4; Supplementary Fig. 5e, f). Although there was no correlation between high levels of BPIFB4 and the more aggressive subtypes of MB, the profiling of five patient matched primary and recurrent samples revealed a consistent upregulation of BPIFB4 at relapse (Fig. 3a), further validating our model of MB recurrence. Similar to our findings in primary MB patient samples, MB cell lines representative of recurrent disease had higher levels of BPIFB4 mRNA and protein, when compared to their matched treatment-naïve counterparts and healthy human neural stem cells (hNSCs) (Fig. 3b; Supplementary Fig. 5g). Probing a large dataset of published primary MB samples(Cavalli et al., 2017) confirmed a lack of significant upregulation of *BPIFB4* in G3 MB subgroup (Supplementary Fig. 5h), patients with higher expression of BPIFB4 mRNA had worse OS if left untreated (Supplementary Fig. 5i). To investigate whether BPIFB4 may contribute to the aggressive phenotype of MB, we undertook functional studies using two different shRNAs targeting BPIFB4 in both treatment-naïve and recurrent MB cell lines (Supplementary Fig. 5j). In all five MB cell lines tested, D425, D425-Re, HD-MB03, HD-MB03-Re and SU_MB002, we observed a dramatic decrease in proliferation (Fig. 3c) and self-renewal (Fig. 3d). The apparent morphological changes of cells with BPIFB4 KD into a more differentiated phenotype were validated by an increased expression of neuron-specific class III ß-tubulin (TUJ1), a marker of differentiated neuron(Artero Castro et al., 2019) (Supplementary Fig. 6a). Since BPIFB4 was first identified as a cell longevity factor, we tested the effects of BPIFB4 KD on the cell cycle. Interestingly, the reduced proliferation rate was not attributed to the differential distribution of cells within stages of

cell cycle (Supplementary Fig. 6b), but instead to an increasingly higher rate of cells undergoing apoptosis, as indicated by the AnnexinV assay (Fig. 3e). Furthermore, BPIFB4 KD in three recurrent MB lines led to a decreased fraction of self-renewing cells (Fig. 3f) and eventual abrogation of self-renewal after three passages *in vitro* (Fig. 3g), further validating its role in regulating the longevity of MB cells. We next undertook intracranial xenotransplantation of recurrent MB cells that were stably transduced with BPIFB4 KD lentivector and evaluated its effects on tumorigenicity. In all three cohorts (D425-Re, HD-MB03-Re and SU_MB002), BPIFB4 inhibition resulted in prolonged survival (Fig. 3h) and reduced tumor burden in both brains (Fig. 3i, Supplementary Fig. 6c) and spines (Fig. 3i, Supplementary Fig. 6d).

The very small body of existing literature on BPIFB4 suggested its role in the activation of endothelial nitric oxide synthase (eNOS) and subsequent production of nitric oxide (NO)(Villa et al., 2015). Profiling cells with NO reporter probe, DAF-FM, we observed an increased levels of NO in recurrent MB cells when compared to their treatment naïve counterparts (Fig. 4a). Although hNSCs were also observed to have high levels of endogenous NO, its production is distinctively driven by neuronal nitric oxide synthase (nNOS)(Bredt et al., 1990). Furthermore, elevated expression of eNOS but not nNOS is a significant predictor of survival in MB patients (Supplementary Fig. 7a, b). Unlike BPIFB4, eNOS can be targeted using small molecule inhibitors. Notably, a reversible eNOS inhibitor, N^5(1-Iminoethyl)-L-ornithine (L-NIO), was ineffective in reducing growth of MB cell lines (Supplementary Fig. 7c), while an irreversible inhibitor, diphenyleneidodonium chloride (DPI), was potent at low nanomolar concentrations (Fig.

4b). When compared to recurrent MB samples, the inhibitory concentration of DPI was found to be 3-10-fold higher in hNSCs, providing a therapeutic window for treating patients at relapse. Functionally, DPI-directed irreversible eNOS inhibition of MB cells showed reduced levels of endogenous NO in those cells (Supplementary Fig. 7d), with comparable effects on MB cell proliferation (Fig. 4c) and self-renewal (Fig. 4d) to BPIFB4 inhibition. As prolonged NO exposure has been linked to chemoradiotherapy resistance(Pervin et al., 2007), we tested the effects of DPI treatment on sensitization to chemoradiotherapy. DPI pre-treated HD-MB03 and HD-MB03-Re showed a greater response to treatment with irradiation and a combination of cisplatin and vincristine, when compared to DMSO pre-treated counterparts. (Fig. 4e). Furthermore, the sensitivity to DPI treatment was higher in the BPIFB4 KD setting, suggesting an additive effect. (Supplementary Fig. 7e). Our initial *in vitro* findings of eNOS targeting were further validated by *in vivo* administration of DPI to mice xenografted with recurrent MB, which resulted in prolonged survival (Fig. 4f). With several ongoing Phase Ib/II clinical trials testing efficacy of competitive NOS inhibitors in combination with chemotherapy drugs for aggressive solid tumors (NCT02834403; NCT03236935), we provide evidence for the potential of eNOS inhibitors as a novel treatment paradigm for patients with recurrent MB.

The data collected from gene expression and functional profiling of human MB cells undergoing therapy has for the first time characterized the role of a longevity-associated factor, BPIFB4, in maintaining a stem cell-like state of MB cells. Reduced levels of BPIFB4 mRNA in recurrent MB cells were sufficient to diminish their aggressiveness *in vitro* and *in vivo*. Furthermore, preliminary studies targeting eNOS using a selective

small molecule inhibitor lead to increased survival of mice xenografted with recurrent MB. In combination with functional effects of *BPIFB4* KD, the finding of consistent upregulation of *BPIFB4* mRNA levels in all recurrent patient samples profiled and the *in vivo* efficacy of a small molecule eNOS inhibitor may suggest the potential for a unique therapeutic option for patients with MB relapse, irrespective of molecular stratification at diagnosis.

ONLINE METHODS:

The experiments were not randomized, and investigators were not blinded to allocation during experiments and outcome assessment.

Human Medulloblastoma (MB) cell cultures. MB cell lines were cultured in NeuroCult Complete (NCC) media: NeuroCult™ NS-A Basal Medium supplemented with 50mL NeuroCult™ Supplement (STEMCELL™ Technologies), 20ng/mL EGF, 10ng/mL FGF, 0.1% heparin and 1% penicillin-streptomycin for a minimum of 48 hours prior to experiments. SU_MB002 was derived at recurrence from a patient who received only chemotherapy and displayed expression markers of Group 3 MB(Facchino et al., 2010). HD-MB03 was isolated from a 3-year old male patient with metastasized Group 3 MB(Milde et al., 2012). D425-Med(He et al., 1991) (D425) was propagated in Dubecco's Modified Eagle Medium (DMEM) high glucose (Life Technologies) supplemented with 1% penicillin–streptomycin, and 20% FBS. Human fetal neural stem cells (hNSCs) were isolated using a previously described protocol(Venugopal et al., 2012b) and cultured in NCC media.

Intracranial xenografting of MB and *in vivo* treatment protocol. All *in vivo* studies were performed according to McMaster University Animal Research Ethics Board (AREB) approved-protocols. Intracranial injections were performed as previously described(Singh et al., 2004). Cell numbers sufficient to generate a measurable tumor burden was previously determined and are as follows: D425 – $1x10^4$, HD-MB03 – $1x10^6$ and SU_MB002 – $5x10^5$. NOD SCID mice were anaesthetized using isofluorane gas (5% induction, 2.5% maintenance) and 10µL of cells were injected into the frontal lobe using a 50µL Hamilton

syringe, in a non-randomized, non-blinded fashion. The mice designated to receive treatment were subjected to 2Gy of craniospinal irradiation using GammaCell 3000 irradiator 14 days post-engraftment. The mice were irradiated in the specially designed cerrobend shield that allowed negation of full body radiation effects, while exposing the cranium and upper portion of the spine to the full dose of radiation. Following radiation, mice were allowed to recover for a week prior to treatment with cisplatin (2.5mg/kg), vincristine (0.4mg/kg) and a day later with cyclophosphamide (75mg/kg). Mice were closely monitored and changes in tumor burden and survival were recorded.

For the *in vivo* knockdown studies mice were intracranially xenografted with $1.5x10^4$ cells transduced with either shCTRL or shBPIFB4-2 lentiviral vectors. The number of mice allocated per experimental group was determined using the following formula: $N = 1 + 2C(s/d)^2$, where N is the number of mice per treatment arm, C=7.85 (significance level of 5% with a power of 80%), s is standard deviation and d is the difference to be detected.

To assess tumor volume, mice were sacrificed when the control group reached endpoint. For survival studies, treated or control mice were sacrificed when they reached endpoint. Upon reaching endpoint, brains and spines were harvested, formalin-fixed, and paraffin-embedded for hematoxylin and eosin (H&E) and CoxIV staining. Images were captured using an Aperio Slide Scanner and analyzed using ImageScope v11.1.2.760 software (Aperio). COXIV positivity was determined by Positive Pixel Algorithm v9 using ImageScope v11.1.2.760 software (Aperio).

Magnetic Resonance Imaging. 3D magnetic resonance imaging as performed on a 7T Bruker Ascend 300WB vertical bore with the MicWB40 probe (Bruker Biospin). The image volume was acquired with 150µm isotropic voxels, with a field-of-view (FOV) of 25 x 25 x 20mm. Magnetization transfer weighted images were acquired according to the protocol in Watanabe *et al*(Watanabe et al., 2010). The saturation pulse was applied once per repetition time (TR), with a Gaussian shape, pulse width: 12ms, nominal flip angle 523° (max pulse amplitude 6.8µT), offset frequency 2500Hz. Image acquisition was performed with a spoiled gradient echo with TR: 23ms, TE: 3ms, and excitation angle: 5°. The scan time for a single 3D image was 8 minutes and 28 seconds. Eight averages were performed for a total imaging time of 1 hour 7 minutes 11 seconds. Tumor-bearing animals were imaged at multiple timepoints after injection (in increments of weeks) to establish engraftment and progression after treatment. For MRI, animals were induced with 5% isoflurane in 1L/min O_2 in an induction chamber and maintained during imaging with 1 - 2% isoflurane delivered *via* a nose cone. Anesthetized mice were placed on a custom plastic sled, secured with foam and Transpore tape (3M), and loaded head up into the vertical wide-bore spectrometer. Rectal temperature and breath rate were monitored with a Biopac acquisition system (MP36E-CE, Biopac Systems Inc, RRID:SCR_014829). The temperature of water circulating through the gradient was set to 35°C at the cooling unit (BCU20, Bruker Biospin), which reliably maintained animal internal temperature at 37°C. Isoflurane levels were manually adjusted to maintain stable respiration rate of 70 breaths per minute.

Flow cytometric analysis: To isolate human MB cells from mouse tissue, xenograft

samples were cultured as previously described(Venugopal et al., 2012a) and sorted based on human TRA-1-85 marker using MoFlo XDP cell sorter (Beckman Coulter). MB tumorspheres were mechanically dissociated and resuspended in PBS+2mM EDTA (Invitrogen) prior to staining with human anti-TRA-1-85 (1:10, Miltenyi Biotec, REA476) antibody or matched isotype control. Cells were incubated for 15 minutes at room temperature and run on a MoFlo XDP cell sorter. Dead cells were excluded based on the viability dye 7AAD (1:10, Beckman Coulter), and compensation values were determined using IgG CompBeads (BD Biosciences). Regions of TRA-1-85 positivity and negativity were established based on isotype control.

For assessing changes in cell cycle, propidium iodide-based Coulter DNA Prep Kit (Beckman Coulter, #6607055) was used. No deviation from manufacturer's instructions were introduced. To assess the extent of apoptosis, MB cells were dissociated, and single cell suspension was resuspended in 100µL of Annexin V Binding Buffer (BioLegend) with 2µL of 7AAD and 1µL anti-Annexin V antibody (1:100, Life Technologies, #A23204). Samples were incubated at room temperature for 15 minutes and spun at 1100rpm for 3 minutes. Cells were resuspended in 300µL of with Annexin V Binding Buffer and profiled using MoFlo XDP cell sorter.

Cell proliferation assay. Single cell suspension of MB cells was sorted into 96-well plate at a density of 1,000 cells/well in 200µL of NCC with 6 technical replicates per sample. After 4 days, 20µL of PrestoBlue® Cell Viability Reagent (Life Technologies) was added to each well approximately 4 hours prior to the readout timepoint. Fluorescence was measured using FLUOstar Omega Microplate reader (BMG Labtech) at excitation and

emission wavelengths of 540–570nm respectively. Readings were analyzed using Omega software.

Self-renewal and *in vitro* limiting dilution assay. Single cell suspension of MB cells was sorted into 96-well plate at a density of 200 cells/well (500 cells/well in case of KD experiments) in 200µL of NCC with 6 technical replicates per samples. Self-renewal was evaluated by counting the number of spheres (clusters equal to or more than 7 cells) formed in each well after 4 days. For *in vitro* limiting dilution analysis, viable cells were sorted in quadruplicates into 96-well plate, using Moflo XDP at cell densities ranging from 1,000 cells/well to 1 cell/well in 200µL of NCC. The number of wells without any spheres or colonies after 4 days were scored and the fraction of negative wells was plotted against the number of cells per well. The number of cells corresponding to the fraction of negative wells equal to 0.37, is the dilution with 1 self-renewing unit(Tropepe et al., 1999).

***In vitro* dose response curves of cisplatin, vincristine, diphenyleneidodonium chloride (DPI)**

and N^5(1-Iminoethyl)-L-ornithine (L-NIO): $1x10^3$ cells were plated in a 96-well plate in quadruplicates at a volume of 200µL/well with two-fold dilutions of cisplatin or DPI from concentrations of 20µM to 39nM. In the case of vincristine and L-NIO, the concentrations tested ranged from 200nM to 39pM and 500µM to 31.25µM, respectively. Highest volume of DMSO was used as negative control. After 72 hours, proliferation was measured as described in "cell proliferation assay" and IC_{50} values determined by plotting percent cell viability versus $\log_{10}$ transformed concentration of inhibitors. Throughout the manuscript, IC_{50} value refers to the concentration of drug that was effective in reducing viability of cell culture by 50%. IC_{80} values were calculated using the following formula:

$IC_{(F)} = [(100-F)/F]^{1/HS} \times IC_{50}$ (where F = percent reduction of proliferation, HS = Hill Slope).

***In vitro* irradiation of MB cells:** Cells were plated at a density of $2.5x10^5$ cells/well into 6-well tissue culture treated plate in triplicates and were irradiated with a single dose of 2Gy using Faxitron RX-650. After 72 hours, cell viability was assessed by mixing 10µL of cell suspension with 10µL 0.4% Trypan Blue solution (Life Technologies), and the cell counts generated by Countess II FL Automated Cell Counter (Life Technologies) were plotted.

RNA-Sequencing analysis: Gene expression data was obtained from RNA-Sequenced samples as raw counts. The counts data was then normalized using edgeR with CPM (counts-per-million) and filtered by TMM (trimmed mean of M-values) method. TMM kept the genes with CPM greater than or equal to 2 in at least 3 samples as determined by comparing sample densities. Filtered CPM data was transformed by log2-transformation and subjected to batch-correction using the package "Removing Unwanted Variation (RUV)". We used the bottom 75% and low-expressing genes for calculating correction factors by the RUV algorithm. The batch-corrected values were used for detecting differentially expressed (DE) genes by generalized linear model Likelihood Ratio Test (glmLRT) in edgeR comparing each treatment groups to control and engraft samples.

Pathway analysis: Rank files were generated from the p-values and fold change in the comparisons and pathway analysis (GSEA, Broad Institute) were performed. Significant pathways were visualized in Cytoscape (v3.6.1) using the Enrichment Map App (v3.1.0) with p-value < 0.001, FDR q-value < 0.1, and Jaccard > 0.25 for shared genes. Pathway

clusters were organized and labeled by the AutoAnnotate App (v1.2) in Cytoscape.

Microarray analysis: The raw data files were combined and processed by the BioConductor package "lumi". In short, expression data was first normalized by the quantile method and then filtered by detection FDR values. Only probes with detection FDR value < 0.05 in at least 2 samples were included in the analysis. In the case where multiple probes were designed for one gene (duplicates), only the probe with the highest standard deviation was chosen. Out of 47323 probes on the Illumina HT-12 microarray representing 22864 unique genes, 15281 probes/genes passed the FDR filter and duplicate-removal. After quantile normalization, Multidimensional scaling (MDS) plots were used to assess the difference between treatment groups in Brain and Spine. The normalized and log2-transformed intensity values of microarray data were used to calculate differential expression by the BioConductor package "limma". Bayesian moderated t-statistics tests (ModT-test) was performed to determine DE genes and the T values from ModT-tests were used as ranking scores to generate Rank files for Gene Set Enrichment Analysis (GSEA).

Patient data: Human MB samples and clinical data were obtained from consenting patients, as approved by the Research Ethics Board (REB) at Hamilton Health Sciences. To identify the molecular subtype of each sample, RNA from patient tumor samples was isolated using a Total RNA isolation kit (Norgen) and submitted for NanoString nCounter profiling at Farncombe Metagenomics Facility (McMaster University). The custom CodeSet was designed using previously characterized genes for each of the core MB subgroups: WNT – *WIF1*, *TNC*, *GAD1*, *DKK2*, *EMX2*; SHH - *PDLIM3*, *EYA1*, *HHIP*, *ATOH1*, *SFRP1*; Group 3 – *IMPG2*, *GABRA5*, *EGFL11*, *NRL*, *MAB21L2*; Group 4 –

KCNA1, *EOMES2*, *KHDRBS2*, *RBM24*, *UNC5D*, *OAS1* and 6 housekeeping genes – *ACTB*, *TBP*, *LDHA*, *POLR2A*, *GAPDH*, *HPRT1*. The subgroup assignment was determined as previously described.(Northcott et al., 2012b)

RT-qPCR: $2.5x10^5$ cells were collected and total RNA was extracted using a Total RNA isolation kit (Norgen). Complimentary DNA (cDNA) was synthesized using qScript cDNA SuperMix (Bio-Rad) and a C1000 Thermo Cycler (Bio-Rad) with the following cycle settings: 4min at 25°C, 30min at 42°C, 5min at 85°C, hold at 4°C. RT-qPCR was performed using Perfecta SybrGreen (Quanta Biosciences) and CFX96 instrument (Bio-Rad). CFX Manager 3.0 software was used for quantification of gene expression and were normalized to 28SrRNA. The following primers were used to measure mRNA levels of *BPIFB4* (FWD: 5'-AGATCCTTGAGTCCGAGGGAA-3', REV: 5'-TGCGAGGATGCCATCAGC-3'), *ID1* (FWD: 5'-AATCATGAAAGTCGCCAGTG-3', REV: 5'-ATGTCGTAGAGCAGCACGTTT-3'), *ID2* (FWD: 5'-ATGAAAGCCTTCAGTCCCGT-3', REV: 5'-TTCCATCTTGCTCACCTTCTT-3'), *ID3* (FWD: 5'-TCATCTCCAACGACAAAAGG-3', REV: 5'-ACCAGGTTTAGTCTCCAGGAA-3'), and *28SrRNA* (FWD: 5'-AAGCAGGAGGTGTCAGAAA-3', REV: 5'-AAAACTAACCTGTCTCACG-3').

Lentiviral knockdown studies: pGFP-C-shLenti vectors expressing shRNA targeting human BPIFB4 (shBPIFB4-1 5'-TTATCCTCGGCTGGTCATTGAGCGATGTG-3'; shBPIFB4-2 5'-ACAGTGGCTATCGCAGTGCCGAGAATGCA-3') and the control vector (shCRTL 5'- ATCAGTTGCTCAGATACTCAGC-3') were purchased from OriGene (#TL305949 and #TR30023). Lentiviral pLKO.1 vectors expressing shRNA

targeting human ID1, (shID1.1 5'-CGGCTGTTACTCACGCCTCAA-3'; shID1.2 5'-GCAGGTAAACGTGCTGCTCTA-3'), ID2 (shID2.1 5'-GAGCCTGCTATACAACATGAA-3'), ID3 (shID3.1 5'-CATCGACTACATTCTCGACCT-3'; shID3.2 5'-GCCCACTTGACTTCACCAAAT-3'), and the control vector (shGFP 5'-ACAACAGCCACAACGTCTATA-3'), were gifts from Dr. Jason Moffat. Stable cell lines with KD were generated by transduction, and subsequent selection with puromycin. The extent of KD was validated by RT-qPCR as previously described.

Western immunoblotting: Total denatured protein (50μg) was separated by 1% sodium dodecyl sulphate-polyacrylamide gel electrophoresis and transferred onto polyvinylidene fluoride (PVDF) membrane. Western blots were probed with human anti-BPIFB4 antibody (1:2500, Abcam #ab168171, 61kDa) and anti-GapDH antibody (1:50000, Abcam #ab8245, 37kDa) followed by secondary antibody, horseradish peroxidase conjugated goat anti-mouse IgG (1:20000, Bio-Rad #1721011). The bands were visualized using a Luminata^{TM} Forte Western HRP Substrate (Millipore) and ChemiDoc^{TM} MP imaging system. Western immunoblots were quantified with Image J software, and protein levels normalized to the loading control are provided in the respective figures.

Immunofluorescence assay: D425, D425-Re, HD-MB03 and HD-MB03-Re transduced with shBPIFB4-1, shBPIFB4-2 and shCTRL vectors were cultured for 14 days. Following cell expansion, $1.5x10^4$ cells were plated onto poly-L-ornithine (Sigma) and laminin (Corning) coated round glass coverslips, placed in wells of a 24-well plate in 300μL of NCC media. Cells were fixed using 4% paraformaldehyde after 12 hours. Samples were washed using 1X TRIS-buffered saline (TBS) and incubated with blocking solution (1% BSA, 0.2% Triton 100X and 5% goat serum in

1X TBS) for 45 minutes at room temperature followed by a 3 hour incubation in primary antibody, chicken anti-human TUJ1 (1:500, Neuromics #MO15013) at room temperature. Cells were then washed in 1X TBS and incubated with secondary antibody, Alexa Flour 488 donkey anti-chicken IgG (1:400, Life technologies #A-11039), for 2 hours at room temperature. Cells were then washed with 1X TBS and counterstained with prolong gold anti-fade mountant with DAPI (Life technologies). Images were acquired using Olympus IX81 microscope and Volocity® software (Quorum Technologies).

***In vivo* treatment of mice with DPI:** Mice xenografted with $1.0x10^4$ D425-Re and HD-MB03-Re cells were treated with 2 doses/week with 100µg/kg of DPI for 2 weeks. The number of mice allocated per experimental group was determined using the following formula: $N = 1 + 2C(s/d)^2$, where N is the number of mice per treatment arm, C=7.85 (significance level of 5% with a power of 80%), s is standard deviation and d is the difference to be detected.

Measuring levels of nitric oxide (NO): Cellular levels of NO were measured by addition of 1.5µM DAF-FM diacetate to cell cultures as previously described.(Kojima et al., 1999) The levels of GFP fluorescence were evaluated 1 hour post-treatment with DAF-FM and no exogenous L-arginine was added throughout the assay. Samples designated as control were treated with equal volume of DMSO.

Statistical analysis: At least three technical or experimental replicates from each experiment were compiled. Data represent mean±SD with *n* values listed in figure legends. GraphPad Prism™ was used to plot all bar graphs and statistical analyses including student's t-test or 2-way ANOVA, $p<0.05$ was considered significant. All Kaplan-Meier survival plots were plotted with GraphPad Prism™ and long-rank (Mantel-Cox) test was

performed for comparison of median survival, $p<0.05$ was considered significant. For *in silico* analyses all associated statistical tests were performed in R using the coxPH package.

Reporting summary: Further information on research design is available in the Nature Research Reporting Summary linked to this paper.

Data Availability: Data generated in preparation of the manuscript is readily available upon request from the corresponding author.

Supplementary Information is linked to the online version of the paper at www.nature.com/nature

Acknowledgements: D.B. was supported by the Frederick Banting and Charles Best Canada Graduate Scholarships Doctoral Award. **A.A.A**. was supported by Brain Tumor Foundation of Canada research studentship. **G.D.B.** was supported by NIH grant P41 GM103504**S.K.S.** holds Canada Research Chair award, and operating grants from Canadian Institutes of Health Research (CIHR, #MOP-130317), Stem Cell Network, the Ontario Institute for Cancer Research Cancer Stem Cell Program, the Canadian Cancer Society Research Institute, the Cancer Research Society, the Brain Tumor Foundation of Canada, and generous donations from the Box Run Foundation and Team Kelsey Foundation.

Author Contributions: D.B.: Conception and design, Collection and/or assembly of data, Data analysis and interpretation, Manuscript writing, Final approval of manuscript. **A.A.A., C.V.**: Conception and design, Collection and/or assembly of data, Manuscript writing, Final approval of manuscript. **J.F.**: Bioinformatics analysis of microarray and RNA-Seq datasets, Final approval of manuscript. **M.S.**, **N.M.**, **M.K.S.**, **M.A.Q.**, **P.V.**, **M.M.K.S.**, **N.S.**, **K.L.D.**, **N.T.**: Collection of data. **D.T., M.S., K.H., N.A.B.**, **G.B.**: Data analysis and interpretation, Final approval of manuscript: **S.K.S.**: Conception and design, Data analysis and interpretation, Manuscript writing, Final approval of manuscript.

Competing Financial Interests: The authors declare no competing financial interests.

Correspondence and requests for materials should be addressed to ssingh@mcmaster.ca

REFERENCES:

1 Cavalli, F. M. G. *et al.* Intertumoral Heterogeneity within Medulloblastoma Subgroups. *Cancer Cell* **31**, 737-754 e736, doi:10.1016/j.ccell.2017.05.005 (2017).
2 Schwalbe, E. C. *et al.* Novel molecular subgroups for clinical classification and outcome prediction in childhood medulloblastoma: a cohort study. *Lancet Oncol* **18**, 958-971, doi:10.1016/S1470-2045(17)30243-7 (2017).
3 Villa, F. *et al.* Genetic Analysis Reveals a Longevity-Associated Protein Modulating Endothelial Function and Angiogenesis. *Circ Res* **117**, 333-345, doi:10.1161/CIRCRESAHA.117.305875 (2015).
4 Ramaswamy, V. *et al.* Recurrence patterns across medulloblastoma subgroups: an integrated clinical and molecular analysis. *Lancet Oncol* **14**, 1200-1207, doi:10.1016/S1470-2045(13)70449-2 (2013).
5 Greaves, M. & Maley, C. C. Clonal evolution in cancer. *Nature* **481**, 306-313, doi:10.1038/nature10762 (2012).
6 Morrissy, A. S. *et al.* Divergent clonal selection dominates medulloblastoma at recurrence. *Nature* **529**, 351-357, doi:10.1038/nature16478 (2016).
7 Kawauchi, D. *et al.* A mouse model of the most aggressive subgroup of human medulloblastoma. *Cancer Cell* **21**, 168-180, doi:10.1016/j.ccr.2011.12.023 (2012).
8 Wu, X. *et al.* Clonal selection drives genetic divergence of metastatic medulloblastoma. *Nature* **482**, 529-533, doi:10.1038/nature10825 (2012).
9 Bao, S. *et al.* Glioma stem cells promote radioresistance by preferential activation of the DNA damage response. *Nature* **444**, 756-760, doi:10.1038/nature05236 (2006).
10 Nakai, E. *et al.* Enhanced MDR1 expression and chemoresistance of cancer stem cells derived from glioblastoma. *Cancer Invest* **27**, 901-908, doi:10.3109/07357900801946679 (2009).
11 Hill, R. M. *et al.* Combined MYC and P53 defects emerge at medulloblastoma relapse and define rapidly progressive, therapeutically targetable disease. *Cancer Cell* **27**, 72-84, doi:10.1016/j.ccell.2014.11.002 (2015).
12 Lasorella, A., Benezra, R. & Iavarone, A. The ID proteins: master regulators of cancer stem cells and tumor aggressiveness. *Nat Rev Cancer* **14**, 77-91, doi:10.1038/nrc3638 (2014).
13 Snyder, A. D. *et al.* Expression pattern of id proteins in medulloblastoma. *Pathol Oncol Res* **19**, 437-446, doi:10.1007/s12253-012-9599-4 (2013).
14 Artero Castro, A. *et al.* Generation of gene-corrected human induced pluripotent stem cell lines derived from retinitis pigmentosa patient with Ser331Cysfs*5 mutation in MERTK. *Stem Cell Res* **34**, 101341, doi:10.1016/j.scr.2018.11.003 (2019).

15 Bredt, D. S., Hwang, P. M. & Snyder, S. H. Localization of nitric oxide synthase indicating a neural role for nitric oxide. *Nature* **347**, 768-770, doi:10.1038/347768a0 (1990).
16 Pervin, S., Singh, R., Hernandez, E., Wu, G. & Chaudhuri, G. Nitric oxide in physiologic concentrations targets the translational machinery to increase the proliferation of human breast cancer cells: involvement of mammalian target of rapamycin/eIF4E pathway. *Cancer Res* **67**, 289-299, doi:10.1158/0008-5472.CAN-05-4623 (2007).
17 Facchino, S., Abdouh, M., Chatoo, W. & Bernier, G. BMI1 confers radioresistance to normal and cancerous neural stem cells through recruitment of the DNA damage response machinery. *J Neurosci* **30**, 10096-10111, doi:10.1523/JNEUROSCI.1634-10.2010 (2010).
18 Milde, T. *et al.* HD-MB03 is a novel Group 3 medulloblastoma model demonstrating sensitivity to histone deacetylase inhibitor treatment. *J Neurooncol* **110**, 335-348, doi:10.1007/s11060-012-0978-1 (2012).
19 He, X. M. *et al.* Differentiation characteristics of newly established medulloblastoma cell lines (D384 Med, D425 Med, and D458 Med) and their transplantable xenografts. *Lab Invest* **64**, 833-843 (1991).
20 Venugopal, C. *et al.* GBM secretome induces transient transformation of human neural precursor cells. *J Neurooncol* **109**, 457-466, doi:10.1007/s11060-012-0917-1 (2012).
21 Singh, S. K. *et al.* Identification of human brain tumor initiating cells. *Nature* **432**, 396-401, doi:10.1038/nature03128 (2004).
22 Watanabe, T., Frahm, J. & Michaelis, T. Myelin mapping in the living mouse brain using manganese-enhanced magnetization transfer MRI. *Neuroimage* **49**, 1200-1204, doi:10.1016/j.neuroimage.2009.09.050 (2010).
23 Venugopal, C., McFarlane, N. M., Nolte, S., Manoranjan, B. & Singh, S. K. Processing of primary brain tumor tissue for stem cell assays and flow sorting. *J Vis Exp*, doi:10.3791/4111 (2012).
24 Tropepe, V. *et al.* Distinct neural stem cells proliferate in response to EGF and FGF in the developing mouse telencephalon. *Dev Biol* **208**, 166-188, doi:10.1006/dbio.1998.9192 (1999).
25 Northcott, P. A. *et al.* Rapid, reliable, and reproducible molecular sub-grouping of clinical medulloblastoma samples. *Acta Neuropathol* **123**, 615-626, doi:10.1007/s00401-011-0899-7 (2012).
26 Kojima, H. *et al.* Fluorescent Indicators for Imaging Nitric Oxide Production. *Angew Chem Int Ed Engl* **38**, 3209-3212 (1999).

Figure 1

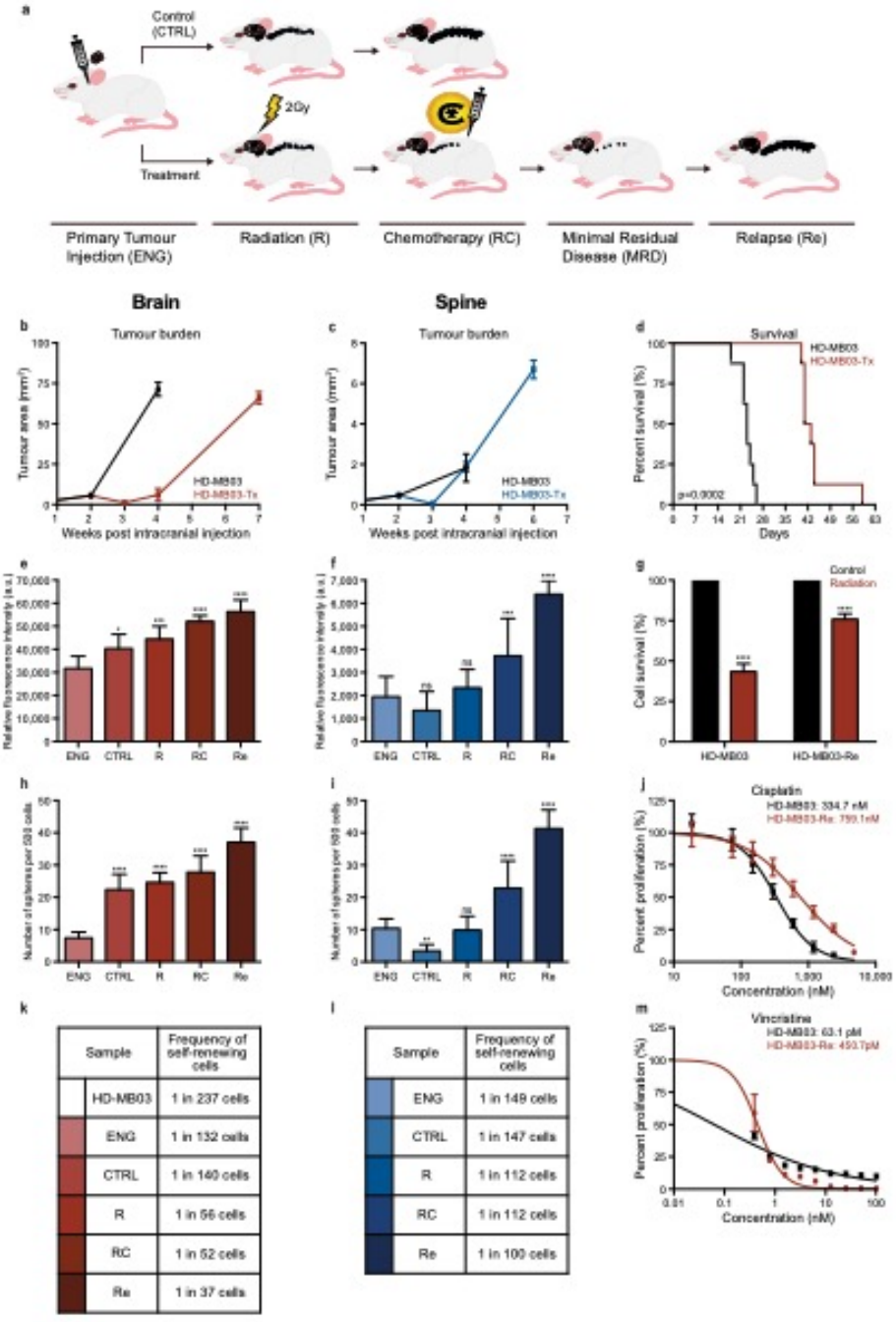

Sample	Frequency of self-renewing cells
HD-MB03	1 in 237 cells
ENG	1 in 132 cells
CTRL	1 in 140 cells
R	1 in 56 cells
RC	1 in 52 cells
Re	1 in 37 cells

Sample	Frequency of self-renewing cells
ENG	1 in 149 cells
CTRL	1 in 147 cells
R	1 in 112 cells
RC	1 in 112 cells
Re	1 in 100 cells

Figure 1: Functional profiling of HD-MB03 cells through *in vivo* chemoradiotherapy. (a) Schematic representation of the novel PDX mouse-adapted therapy model using patient-derived human Group 3 medulloblastoma. Changes in tumor burden in **(b)** brains and **(c)** spines of xenografted mice through therapy (n=3/timepoint). **(d)** Kaplan-Meier curve demonstrating survival benefit of mice undergoing *in vivo* chemoradiotherapy (n=8/treatment arm). Proliferation assay on cells isolated from **(e)** brains and **(g)** spines of mice undergoing *in vivo* chemoradiotherapy (n=3/timepoint). Changes in self-renewing potential of cells isolated from **(f)** brains and **(h)** spines of mice undergoing *in vivo* chemoradiotherapy (n=3/timepoint). Fraction of self-renewing cells in cultures derived from **(i)** brains and **(j)** spines of mice undergoing *in vivo* chemoradiotherapy (n=3/timepoint). Changes in sensitivity of recurrent HD-MB03 cells to *in vitro* treatment **(k)** radiation, **(n)** cisplatin and **(m)** vincristine. Bars represent mean of at least three technical replicates. *$p \leq 0.05$, **$p \leq 0.001$, ***$p \leq 0.0001$; ****$p \leq 0.00001$; unpaired t-test or one-way ANOVA with Sidak's method for multiple comparisons.

Figure 2

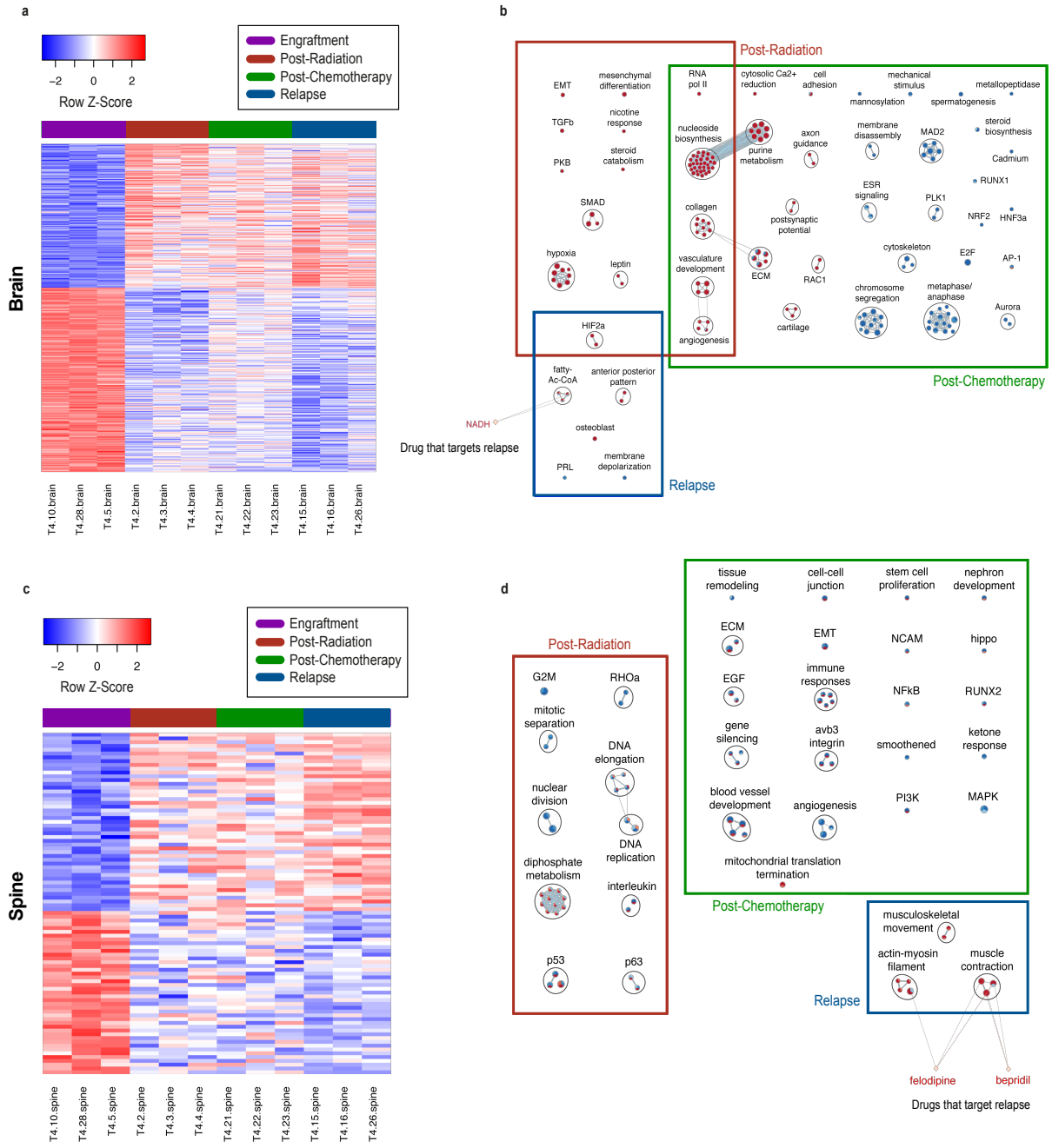
a
Row Z-Score
−2
0
2
Engraftment
Post-Radiation
Post-Chemotherapy
Relapse
Brain
T4.10.brain
T4.28.brain
T4.5.brain
T4.2.brain
T4.3.brain
T4.4.brain
T4.21.brain
T4.22.brain
T4.23.brain
T4.15.brain
T4.16.brain
T4.26.brain
b
Post-Radiation
EMT
mesenchymal differentiation
TGFb
nicotine response
PKB
steroid catabolism
SMAD
hypoxia
leptin
RNA pol II
cytosolic Ca2+ reduction
cell adhesion
mechanical stimulus
mannosylation
spermatogenesis
metallopeptidase
nucleoside biosynthesis
purine metabolism
axon guidance
membrane disassembly
MAD2
steroid biosynthesis
Cadmium
RUNX1
ESR signaling
PLK1
NRF2
HNF3a
collagen
postsynaptic potential
vasculature development
ECM
RAC1
cytoskeleton
E2F
AP-1
chromosome segregation
metaphase/ anaphase
Aurora
angiogenesis
cartilage
Post-Chemotherapy
HIF2a
fatty-Ac-CoA
anterior posterior pattern
NADH
osteoblast
PRL
membrane depolarization
Drug that targets relapse
Relapse
c
Row Z-Score
−2
0
2
Engraftment
Post-Radiation
Post-Chemotherapy
Relapse
Spine
T4.10.spine
T4.28.spine
T4.5.spine
T4.2.spine
T4.3.spine
T4.4.spine
T4.21.spine
T4.22.spine
T4.23.spine
T4.15.spine
T4.16.spine
T4.26.spine
d
Post-Radiation
G2M
RHOa
mitotic separation
DNA elongation
nuclear division
DNA replication
diphosphate metabolism
interleukin
p53
p63
tissue remodeling
cell-cell junction
stem cell proliferation
nephron development
ECM
EMT
NCAM
hippo
EGF
immune responses
NFkB
RUNX2
gene silencing
avb3 integrin
smoothened
ketone response
blood vessel development
angiogenesis
PI3K
MAPK
mitochondrial translation termination
Post-Chemotherapy
musculoskeletal movement
actin-myosin filament
muscle contraction
Relapse
felodipine
bepridil
Drugs that target relapse

Figure 2: RNA-seq analysis of HD-MB03 cells undergoing *in vivo* chemoradiotherapy treatment. A heat map of differentially expressed genes in cells isolated from **(a)** brains and **(b)** spines through the course of *in vivo* treatment. Differential expression profiles were used to generate pathway maps representative of significantly dysregulated pathways in **(c)** brain and **(d)** spine samples.

Figure 3

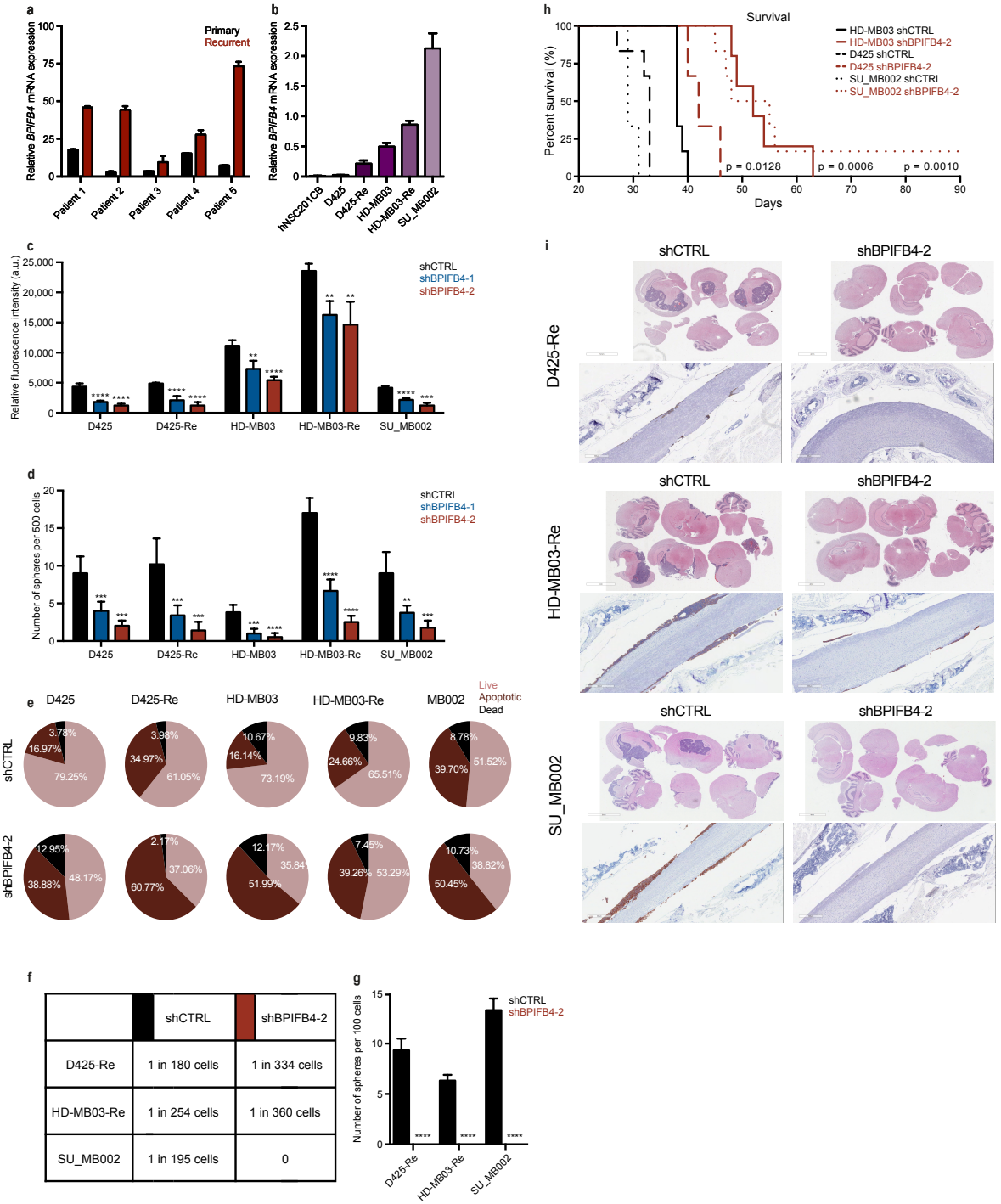
a
Relative BPIFB4 mRNA expression
Primary
Recurrent
Patient 1
Patient 2
Patient 3
Patient 4
Patient 5
b
Relative BPIFB4 mRNA expression
hNSC201CB
D425
D425-Re
HD-MB03
HD-MB03-Re
SU_MB002
h
Survival
Percent survival (%)
Days
HD-MB03 shCTRL
HD-MB03 shBPIFB4-2
D425 shCTRL
D425 shBPIFB4-2
SU_MB002 shCTRL
SU_MB002 shBPIFB4-2
p = 0.0128
p = 0.0006
p = 0.0010
c
Relative fluorescence intensity (a.u.)
shCTRL
shBPIFB4-1
shBPIFB4-2
D425
D425-Re
HD-MB03
HD-MB03-Re
SU_MB002
i
shCTRL
shBPIFB4-2
D425-Re
HD-MB03-Re
SU_MB002
d
Number of spheres per 500 cells
shCTRL
shBPIFB4-1
shBPIFB4-2
D425
D425-Re
HD-MB03
HD-MB03-Re
SU_MB002
e
D425
D425-Re
HD-MB03
HD-MB03-Re
MB002
Live
Apoptotic
Dead
shCTRL
shBPIFB4-2
3.78%
16.97%
79.25%
3.96%
34.97%
61.05%
10.67%
16.14%
73.19%
9.83%
24.66%
65.51%
8.78%
39.70%
51.52%
12.95%
38.88%
48.17%
2.17%
37.06%
60.77%
12.17%
35.84%
51.99%
7.45%
39.26%
53.29%
10.73%
38.82%
50.45%
f
shCTRL
shBPIFB4-2
D425-Re
1 in 180 cells
1 in 334 cells
HD-MB03-Re
1 in 254 cells
1 in 360 cells
SU_MB002
1 in 195 cells
0
g
Number of spheres per 100 cells
shCTRL
shBPIFB4-2
D425-Re
HD-MB03-Re
SU_MB002

Figure 3: Effects of BPIFB4 KD in MB cell lines. (a) BPIFB4 mRNA levels in matched primary and recurrent patient samples. **(b)** Relative BPIFB4 mRNA expression levels in hNSCs and five MB cell lines. Changes in **(c)** proliferation, **(d)** self-renewal, **(e)** fraction of cells undergoing apoptosis, and **(f)** frequency of self-renewing cells in MB cell cultures post lentivector mediated KD of BPIFB4. **(g)** Diminished self-renewal capacity after third *in vitro* passage of three recurrent MB lines with BPIFB4 KD. **(h)** Kaplan-Meier curves demonstrating extended mouse survival in MB cells with BPIFB4 KD (n=6/cohort). **(i)** Representative IHC brain and spine sections stained with H&E and human-COXIV staining respectively. Bars represent mean of at least three technical replicates. *$p \leq 0.05$, **$p \leq 0.001$, ***$p \leq 0.0001$; ****$p \leq 0.00001$; unpaired t-test or one-way ANOVA with Sidak's method for multiple comparisons.

Figure 4

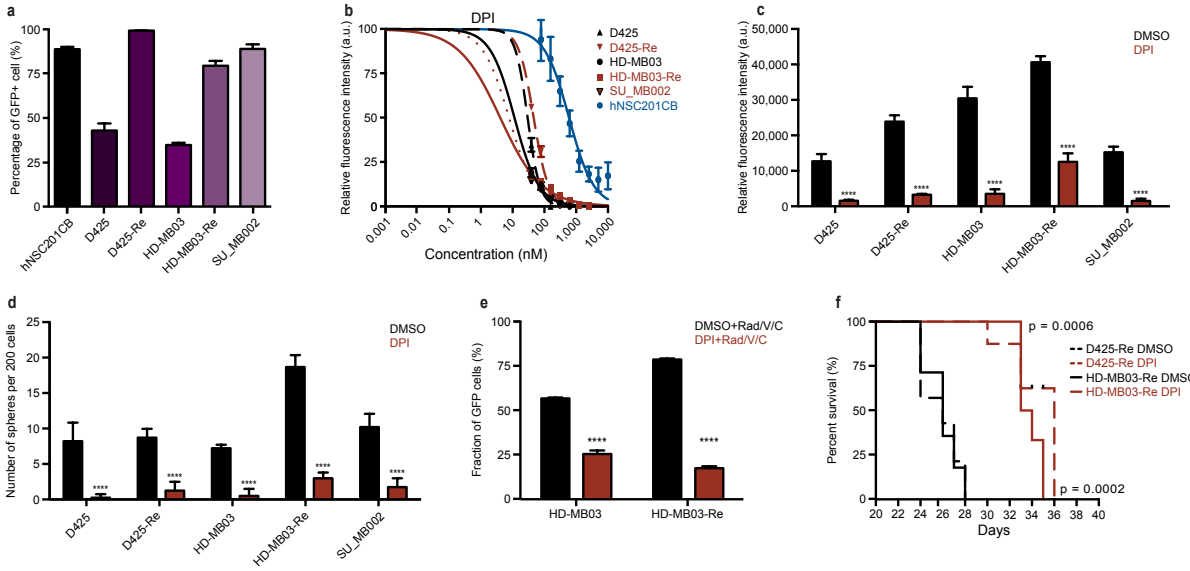
a
Percentage of GFP+ cell (%)
hNSC201CB
D425
D425-Re
HD-MB03
HD-MB03-Re
SU_MB002
b
DPI
Relative fluorescence intensity (a.u.)
Concentration (nM)
D425
D425-Re
HD-MB03
HD-MB03-Re
SU_MB002
hNSC201CB
c
Relative fluorescence intensity (a.u.)
DMSO
DPI
d
Number of spheres per 200 cells
DMSO
DPI
e
Fraction of GFP cells (%)
DMSO+Rad/V/C
DPI+Rad/V/C
HD-MB03
HD-MB03-Re
f
Percent survival (%)
p = 0.0006
p = 0.0002
D425-Re DMSO
D425-Re DPI
HD-MB03-Re DMSO
HD-MB03-Re DPI
Days

Figure 4: Irreversible small molecule targeting of eNOS reduces MB proliferation *in vitro* and *in vivo*. (a) Increased levels of NO in recurrent MB cells as indicated by an increased percentage of GFP+ cells in response to treatment with NO probe. **(b)** IC_{50} curves of DPI in hNSCs and five medulloblastoma lines. Changes in **(c)** proliferation and **(d)** self-renewal of MB cells treated with DPI at concentrations equivalent to IC_{80} for the respective cell line. **(e)** Enhanced efficacy of *in vitro* chemoradiotherapy after treatment of MB cells with DPI. **(f)** Kaplan-Meier curves demonstrating extended mouse survival in MB cells with BPIFB4 KD (n=6/cohort). Bars represent mean of at least three technical replicates. ****$p \leq 0.00001$; unpaired t-test.

Supplementary Figure 1

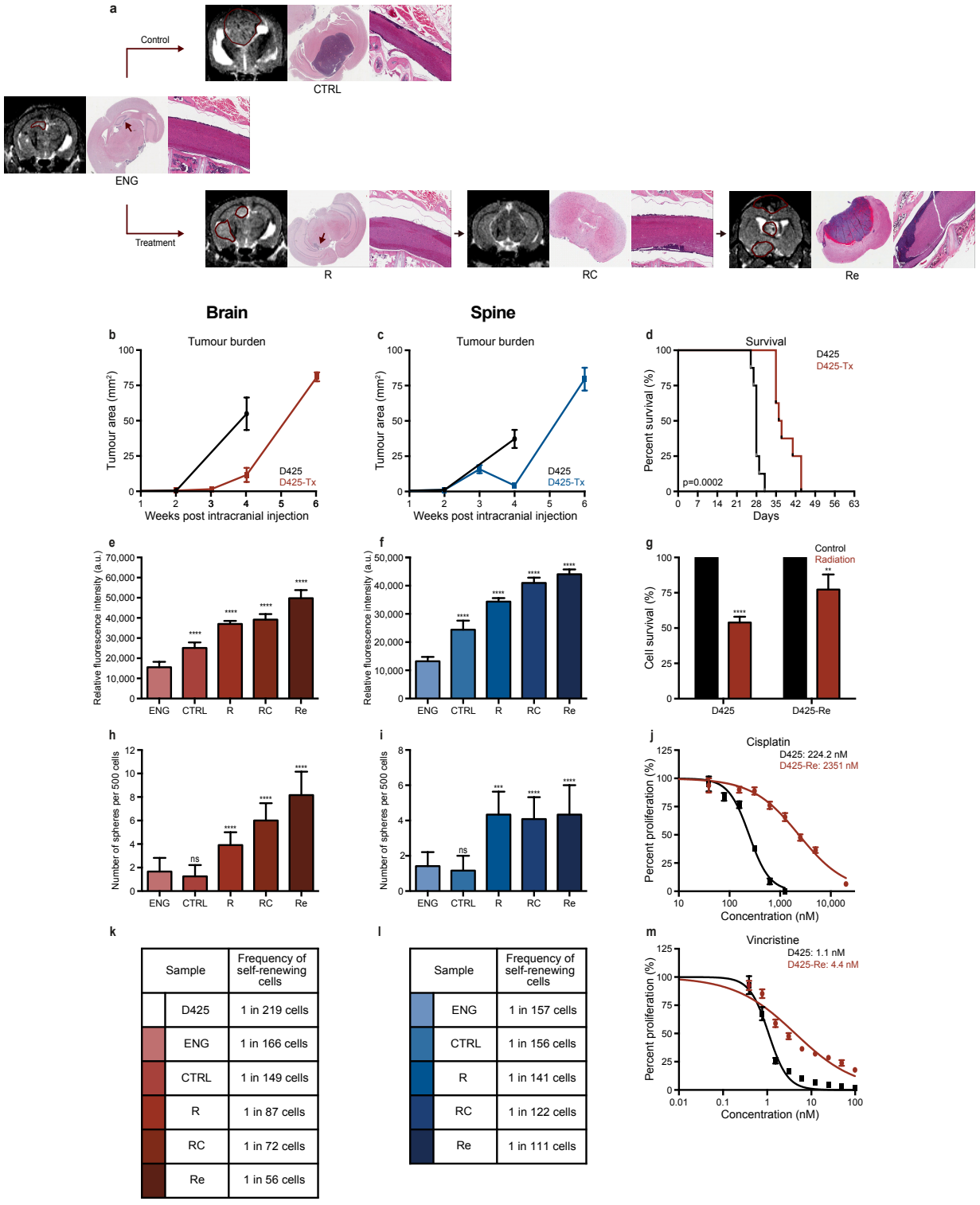

k

Sample	Frequency of self-renewing cells
D425	1 in 219 cells
ENG	1 in 166 cells
CTRL	1 in 149 cells
R	1 in 87 cells
RC	1 in 72 cells
Re	1 in 56 cells

l

Sample	Frequency of self-renewing cells
ENG	1 in 157 cells
CTRL	1 in 156 cells
R	1 in 141 cells
RC	1 in 122 cells
Re	1 in 111 cells

Supplementary Figure 1: Functional profiling of D425 cells through *in vivo* chemoradiotherapy. (a) Schematic representation of the novel PDX mouse-adapted therapy model using patient derived human Group 3 medulloblastoma. Brains and spines collected at engraftment (ENG), post radiation (R), post radiation and chemotherapy (RC) and at relapse (Re) were processed and stained with H&E. Representative MRI images showing brain tumor burden in mice undergoing in vivo chemoradiotherapy. Quantified changes in tumor burden in **(b)** brains and **(c)** spines of xenografted mice through therapy (n=3/timepoint). **(d)** Kaplan-Meier curve demonstrating survival benefit of mice undergoing *in vivo* chemoradiotherapy (n=8/treatment arm). Proliferation assay on cells isolated from **(e)** brains and **(f)** spines of mice undergoing *in vivo* chemoradiotherapy (n=3/timepoint). Changes in self-renewing potential of cells isolated from **(g)** brains and **(h)** spines of mice undergoing *in vivo* chemoradiotherapy (n=3/timepoint). Fraction of self-renewing cells in cultures derived from **(i)** brains and **(j)** spines of mice undergoing *in vivo* chemoradiotherapy (n=3/timepoint). Changes in sensitivity of recurrent D425 cells to *in vitro* treatment **(k)** radiation, **(l)** cisplatin and **(m)** vincristine. Bars represent mean of at least three technical replicates. *$p \leq 0.05$, **$p \leq 0.001$, ***$p \leq 0.0001$; ****$p \leq 0.00001$; unpaired t-test or one-way ANOVA with Sidak's method for multiple comparisons.

Supplementary Figure 2

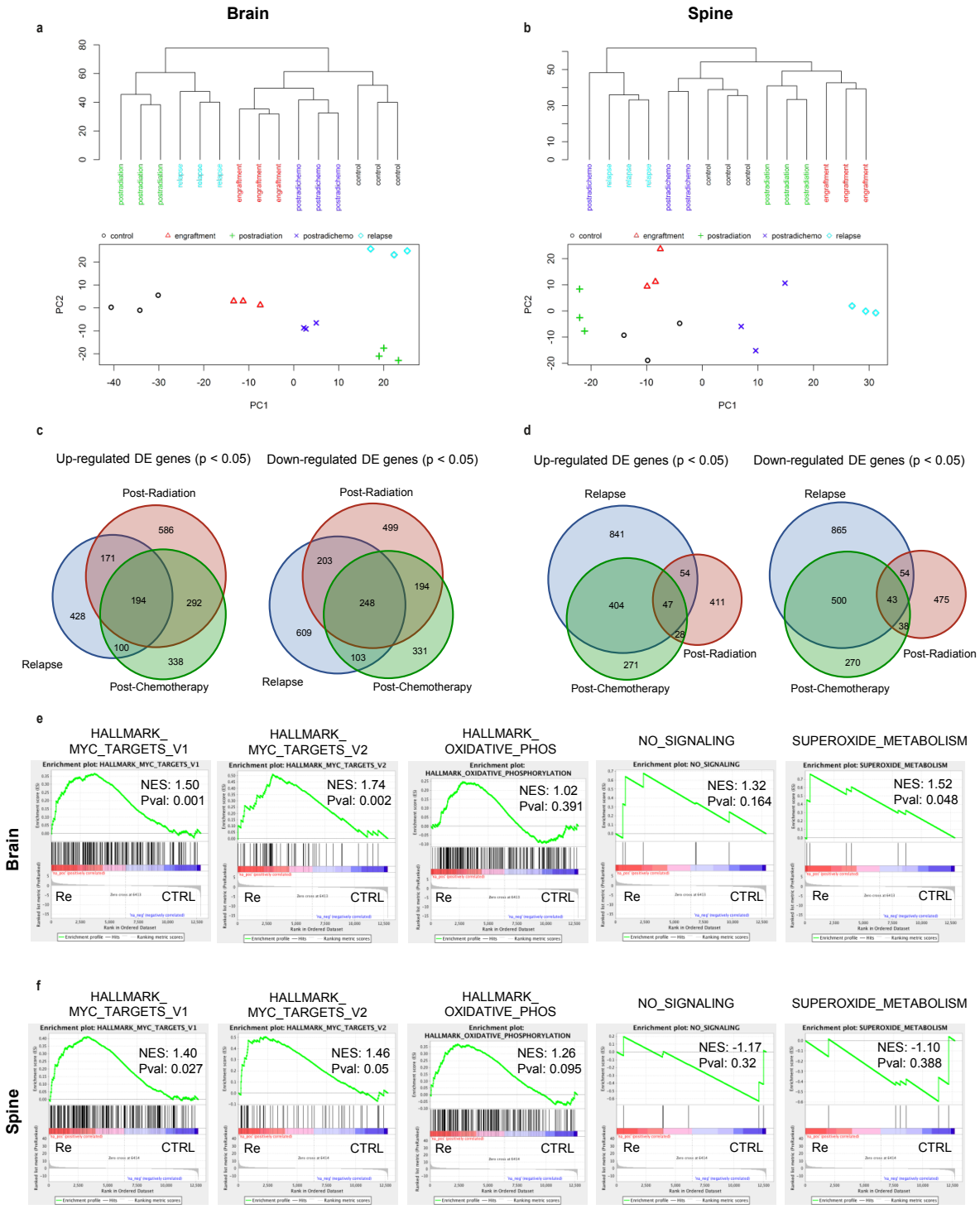

Supplementary Figure 2: Technical validation and pathway analysis of RNA-seq data. Principal component analysis (PCA) of HD-MB03 cells collected from **(a)** brains and **(b)** spines though *in vivo* chemoradiotherapy. Venn diagrams representing the number of differentially expressed genes of cells isolated from **(c)** brain and **(d)** spines at each stage of therapy, compared to the engraftment timepoint.

Supplementary Table 1: Differential gene expression analysis generated from RNA-seq profiling. LogFC values of top 20 up- and down- regulated genes in HD-MB03 cells isolated from **(a)** brains and **(b)** spines of mice undergoing *in vivo* chemoradiotherapy.

Supplementary Table 1

	Brain				Spine			
	Gene	Post-Rad vs. Engraft	Post-Chemo vs. Engraft	Relapse vs. Engraft	Gene	Post-Rad vs. Engraft	Post-Chemo vs. Engraft	Relapse vs. Engraft
Up-regulated genes	BPIFB4	9.76	6.90	3.27	SRL	0.91	3.11	5.46
	CHRNB4	5.17	3.96	4.34	CREG2	3.47	3.16	2.79
	THEM5	5.72	3.73	2.34	HBE1	2.07	1.62	2.65
	DLX2	4.09	3.63	3.17	C2orf82	1.48	2.06	2.20
	MT3	4.78	2.47	2.35	RINL	1.35	1.21	1.64
	LRRC17	3.87	2.47	2.28	ARHGAP27	1.56	1.04	1.24
	SLC44A5	3.69	2.14	2.37	NEURL1B	0.93	0.88	1.49
	ARHGEF4	1.63	3.04	3.45	SLC25A45	1.11	1.01	1.17
	IL6R	3.45	2.87	1.73	TNNC2	0.62	0.59	2.07
	SOX8	3.13	1.65	3.21	THNSL2	1.16	0.96	1.06
	FEZF1-AS1	2.35	1.74	3.76	ALPK2	0.83	1.01	1.31
	INHBB	3.49	2.14	1.97	CDHR1	1.30	0.62	1.16
	EPHB1	3.70	2.51	1.24	IQCH-AS1	0.92	0.88	1.24
	SEMA6B	2.67	2.07	2.51	FABP3	0.78	0.98	1.22
	SLC8A3	2.77	1.86	2.53	RTBDN	0.89	1.20	0.88
	RIPPLY2	2.41	1.70	2.59	SNTB1	0.87	0.79	1.12
	SNTB1	2.07	2.00	2.60	FAM179A	0.87	0.70	1.19
	TMEM200A	3.01	2.18	1.38	DDIT4L	0.78	0.54	1.32
	DLX1	2.58	2.20	1.67	SPOCK1	0.60	0.66	1.34
	DRAXIN	2.56	1.74	2.11	MACROD1	0.57	0.94	1.10
Down-regulated genes	ACTC1	-3.41	-9.80	-7.48	RP11-555J4.4	-1.47	-1.20	-1.45
	CCDC136	-2.86	-3.43	-3.23	LINC00085	-0.61	-0.80	-1.38
	CACNA1H	-4.05	-2.75	-2.58	ADRA2C	-0.86	-0.58	-1.32
	KLHDC8A	-2.91	-2.17	-3.02	TPK1	-0.70	-0.50	-1.08
	VWA5B1	-3.17	-1.47	-2.81	ARHGAP6	-0.74	-0.64	-0.88
	CCDC175	-2.05	-1.92	-2.66	PLAGL1	-0.41	-0.89	-0.83
	KLHL32	-2.25	-1.37	-2.01	ARHGEF18	-0.59	-0.51	-0.71
	RP11-413P11.1	-0.98	-1.44	-2.89	HSPA5	-0.34	-0.60	-0.86
	KCNV2	-2.38	-1.46	-1.46	SHOX2	-0.61	-0.52	-0.67
	ALPL	-2.03	-1.44	-1.83	RP5-991G20.1	-0.56	-0.45	-0.73
	DOC2B	-2.65	-1.31	-1.30	CDH2	-0.50	-0.51	-0.73
	SYT2	-1.79	-1.47	-1.87	TLN2	-0.29	-0.48	-0.82
	ANO9	-1.76	-1.46	-1.81	DNAJB1	-0.46	-0.81	-0.32
	PAPLN	-2.09	-1.66	-1.19	PKD1P6	-0.46	-0.35	-0.55
	GREB1	-1.44	-1.11	-2.32	RP11-395G23.3	-0.53	-0.41	-0.40
	GYLTL1B	-2.84	-0.60	-1.40	NBPF1	-0.46	-0.36	-0.42
	SRL	-2.37	-1.12	-1.25	MROH6	-0.29	-0.58	-0.35
	NMU	-1.24	-1.42	-2.06	DNAJC3	-0.28	-0.45	-0.47
	FRMD3	-2.07	-1.56	-1.02	HERPUD1	-0.30	-0.29	-0.59
	SALL1	-1.95	-1.63	-1.02	PLCB4	-0.38	-0.36	-0.40

Supplementary Figure 3

a **Brain**

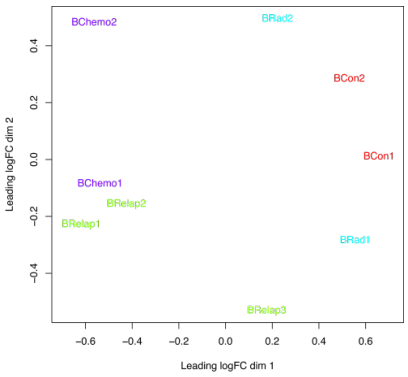

	Post-Radiation		Post-Chemotherapy		Relapse	
	Gene	logFC	Gene	logFC	Gene	logFC
Up-regulated genes	BPIFB4	1.10	BPIFB4	2.77	BPIFB4	2.67
	ID3	1.06	ID3	2.67	ID1	2.17
	ID1	0.96	ID1	2.28	HIST2H2AA4	1.46
	ID2	0.72	ID2	1.95	SAMD11	1.43
	NOL6	0.71	CYR61	1.82	PROM1	1.27
	SAMD11	0.67	CLDN1	1.46	BOLA1	1.20
	CRABP2	0.59	EFEMP1	1.46	H2AFJ	1.12
	PROM1	0.59	AEN	1.46	TIMM23	1.05
	MAP2K2	0.58	SERPINE2	1.40	NSUN2	1.05
	CAMK1D	0.57	C2orf80	1.28	PSMB10	1.03
Down-regulated genes	BEX1	-0.75	CACNA1G	-1.40	RPS4XP21	-1.20
	PFKFB4	-0.77	CDK5R1	-1.40	MFAP3L	-1.20
	RPL36AP39	-0.77	PPM1M	-1.43	SPTBN1	-1.27
	RPL7P8	-0.77	PRDM1	-1.44	RP11-83J16.1	-1.27
	RPL7P59	-0.78	SNORD3D	-1.48	RP11-745A24.1	-1.28
	RCVRN	-0.80	LINC00599	-1.51	KATNBL1	-1.37
	SCG3	-1.04	ERN1	-1.59	TAF1D	-1.40
	RPL7P24	-1.23	HSP90AA2P	-1.70	SNORA70	-1.44
	PRND	-1.47	SGIP1	-1.71	PDE6H	-1.55
	GDF15	-10.73	PRPH2	-1.77	RPL36AP39	-1.83

b **Spine**

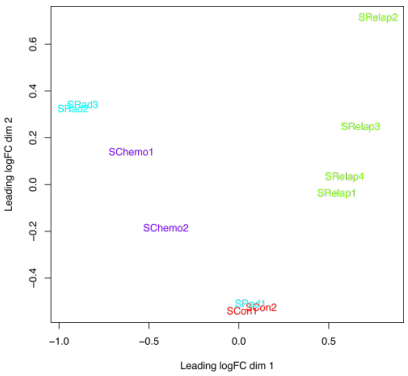

	Post-Radiation		Post-Chemotherapy		Relapse	
	Gene	logFC	Gene	logFC	Gene	logFC
Up-regulated genes	BCO1	1.97	BPIFB4	2.36	TEX19	2.56
	KRT18P31	1.82	ID3	1.99	HIST1H2BD	2.03
	KRT18P55	1.81	ID1	1.83	HIST1H2BE	1.98
	GSTA2	1.62	PRRX2	1.71	ALDOC	1.78
	NEFH	1.52	BMP7	1.59	BEX2	1.74
	CTSV	1.48	IGFBP3	1.58	HELZ2	1.62
	KRT18P13	1.45	TAGLN	1.57	KLF11	1.56
	KCNF1	1.43	KCNF1	1.55	RAB3IL1	1.55
	ID2	1.36	ACTA2	1.46	BEX4	1.53
	ACAT2	1.36	KRT18P55	1.43	CEBPB	1.50
Down-regulated genes	PRDM1	-1.68	INSM2	-1.40	HIBCH	-1.35
	SYP	-1.71	BRSK1	-1.40	LARP6	-1.41
	GNGT1	-1.73	FCAR	-1.42	CTXN1	-1.44
	RAB26	-1.88	SSTR2	-1.43	CTC-512J14.7	-1.44
	COX15	-1.89	ZNF483	-1.44	ST6GALNAC5	-1.53
	INSM2	-2.18	SHROOM4	-1.46	HNRNPA1P35	-1.58
	PDC	-2.21	XRCC2	-1.53	SYP	-1.60
	IFI44	-2.58	POU4F2	-1.54	FAM19A4	-1.65
	PRND	-2.60	SEMA3E	-1.54	INSM2	-2.06
	FAM57B	-2.92	FAM19A4	-1.59	TFPI2	-2.45

Supplementary Figure 3: Differential gene expression analysis generated from gene microarray. PCA and logFC values of top 10 up- and down- regulated genes in D425 cells collected from **(a)** brain and **(b)** spines through therapy.

Supplementary Figure 4

a

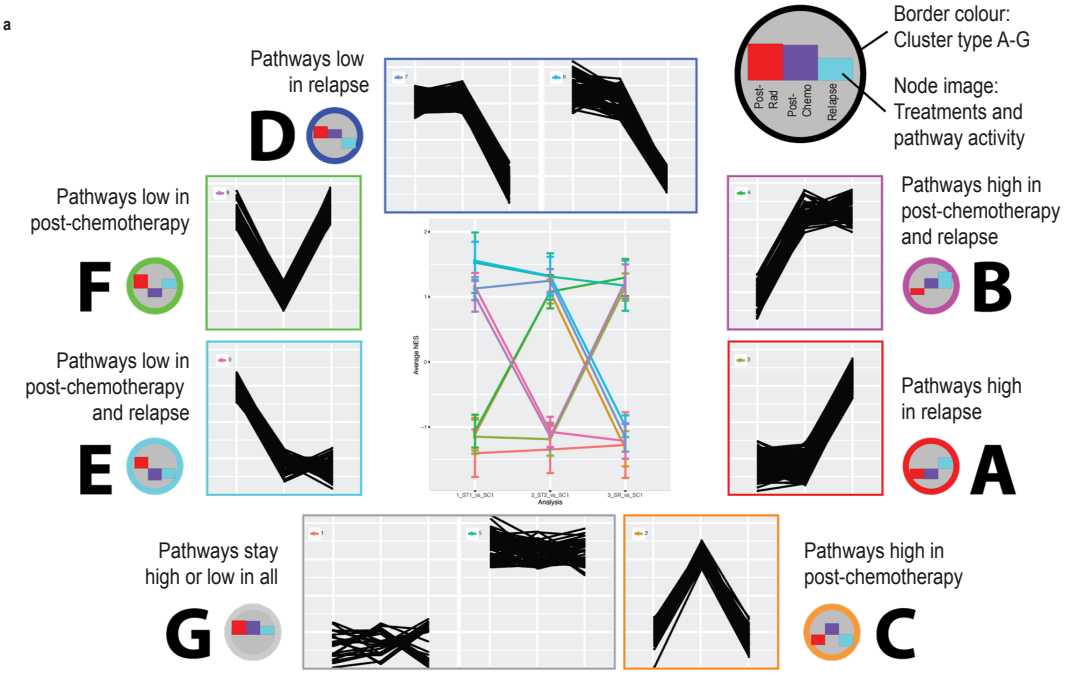

b

	Brain		Spine	
Cluster type	Number	Percentage (%)	Number	Percentage (%)
A	25	6.30	194	22.80
B	219	55.16	65	7.64
C	18	4.53	57	6.70
D	20	5.04	305	35.84
E	37	9.32	55	6.46
F	43	10.83	65	7.64
G	35	8.82	110	12.93

c

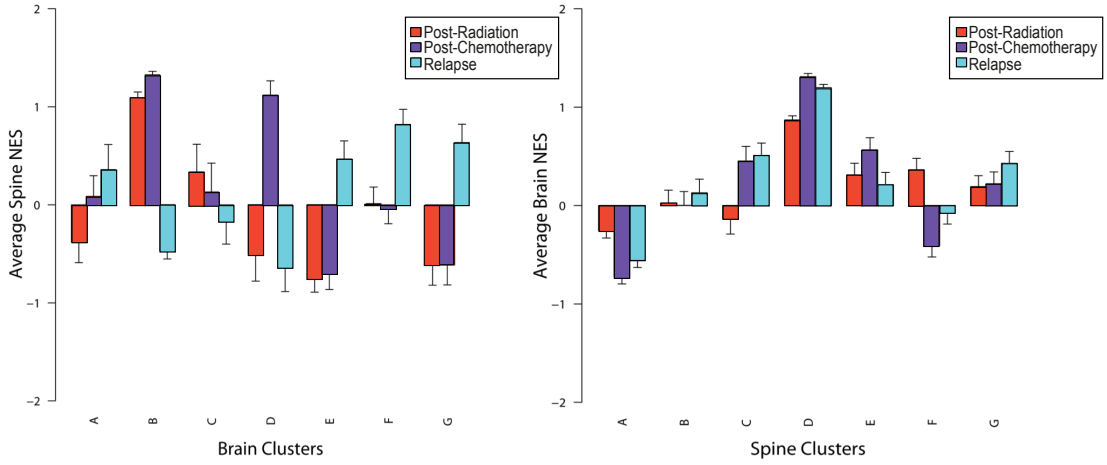

Supplementary Figure 4: Separation of pathways by pattern of change. (**a, b**) Clustering of pathways activated after radiation, chemotherapy and at relapse; pathways with z-value differences greater than 2.33 ($p < 0.01$) were used for clustering. **(c)** Distinct patterns of change in pathway clusters identified in brain and spine samples.

Extended Table 1: Clusters of top 4 pathways (by p-value) with NES in the D425 brain samples.

Extended Data 1

Pathways in Brain	Cluster	Post-Rad	Post-Chemo	Relapse	p_diff
ACTIVATION OF RRNA EXPRESSION BY ERCC6 (CSB) AND EHMT2 (G9A)-REACTOME	A	-0.84	-0.67	2.35	1.33E-04
HDMS DEMETHYLATE HISTONES-REACTOME	A	-0.72	-1.14	1.60	1.63E-04
NONHOMOLOGOUS END-JOINING (NHEJ)-REACTOME	A	-0.89	-0.93	1.73	2.04E-04
POSITIVE EPIGENETIC REGULATION OF RRNA EXPRESSION-REACTOME	A	-0.76	-0.83	2.03	2.15E-04
PROTEIN-DNA COMPLEX SUBUNIT ORGANIZATION-GOBP	B	-0.91	1.79	2.00	1.10E-04
PROGRAMMED CELL DEATH-GOBP	B	-0.97	1.32	1.02	1.18E-04
REGULATION OF GENE EXPRESSION, EPIGENETIC-GOBP	B	-0.90	1.11	1.69	1.23E-04
NUCLEOSOME ASSEMBLY-GOBP	B	-0.87	1.39	1.92	1.29E-04
NEGATIVE REGULATION OF CELLULAR COMPONENT MOVEMENT-GOBP	C	-1.20	1.17	-0.99	1.13E-03
NEGATIVE REGULATION OF CELL MORPHOGENESIS INVOLVED IN DIFFERENTIATION-GOBP	C	-0.84	1.32	-1.08	1.94E-03
PIGMENTATION-GOBP	C	-1.57	0.83	-1.03	2.18E-03
INTRASPECIES INTERACTION BETWEEN ORGANISMS-GOBP	C	-1.38	1.14	-1.18	2.89E-03
SELENOAMINO ACID METABOLISM-REACTOME	D	1.71	1.20	-0.85	4.19E-04
EUKARYOTIC TRANSLATION ELONGATION-REACTOME	D	1.28	1.07	-1.23	5.12E-04
PROTEIN TARGETING TO MEMBRANE-GOBP	D	1.16	1.25	-1.17	5.29E-04
P73 TRANSCRIPTION FACTOR NETWORK-NCI-NATURE CURATED DATA	D	1.09	1.48	-0.97	1.29E-03
POSITIVE REGULATION OF AXON EXTENSION-GOBP	E	0.96	-1.83	-1.58	1.42E-04
UPTAKE AND ACTIONS OF BACTERIAL TOXINS-REACTOME	E	1.02	-1.62	-0.77	4.42E-04
POSITIVE REGULATION OF DEVELOPMENTAL GROWTH-GOBP	E	0.89	-1.68	-1.17	5.52E-04
GABA-B_RECEPTOR_II_SIGNALING-PANTHER PATHWAY	E	1.10	-1.51	-0.87	7.49E-04
CELLULAR RESPONSE TO UNFOLDED PROTEIN-GOBP	F	1.55	-0.95	0.95	1.21E-04
ANTIMICROBIAL HUMORAL RESPONSE-GOBP	F	0.41	-1.07	1.77	1.76E-04
ANTIBACTERIAL HUMORAL RESPONSE-GOBP	F	0.41	-1.06	1.75	2.15E-04
POSITIVE REGULATION OF GENE EXPRESSION, EPIGENETIC-GOBP	F	0.89	-1.05	1.69	2.16E-04
ACID SECRETION-GOBP	G	-0.83	-1.96	-1.40	1.54E-03
SIGNAL RELEASE FROM SYNAPSE-GOBP	G	-0.67	-1.68	-1.23	1.65E-03
SYNAPTIC TRANSMISSION-GOBP	G	-0.91	-1.51	-1.22	1.87E-03
TRANS-SYNAPTIC SIGNALING-GOBP	G	-0.92	-1.53	-1.24	1.90E-03

Extended Table 2: Clusters of top 4 pathways (by p-value) with NES in the D425 spine samples.

Extended Data 2

Pathways in Spine	Cluster	Post-Rad	Post-Chemo	Relapse	p_diff
REGULATION OF INTERLEUKIN-4 PRODUCTION-GOBP	A	-1.24	-1.21	1.63	1.26E-04
CELLULAR RESPONSE TO CARBOHYDRATE STIMULUS-GOBP	A	-1.83	-1.38	1.02	1.36E-04
VESICLE ORGANIZATION-GOBP	A	-1.17	-1.13	1.27	1.46E-04
MUSCLE CONTRACTION-REACTOME	A	-1.32	-1.11	1.22	1.57E-04
NEGATIVE REGULATION OF CELL ACTIVATION-GOBP	B	-0.99	1.14	1.66	1.01E-04
REGULATION OF RHODOPSIN MEDIATED SIGNALING PATHWAY-GOBP	B	-1.74	1.17	0.98	1.23E-04
CELLULAR RESPONSE TO TOPOLOGICALLY INCORRECT PROTEIN-GOBP	B	-0.97	0.98	1.65	1.51E-04
ACTIVATION OF RRNA EXPRESSION BY ERCC6 (CSB) AND EHMT2 (G9A)-REACTOME	B	-0.95	1.31	1.79	1.83E-04
NUCLEAR-TRANSCRIBED MRNA CATABOLIC PROCESS, NONSENSE-MEDIATED DECAY-GOBP	C	-0.89	1.41	-1.18	1.31E-04
ASSOCIATION OF TRIC CCT WITH TARGET PROTEINS DURING BIOSYNTHESIS-REACTOME	C	-0.98	0.96	-1.78	1.55E-04
PROSTACYCLIN SIGNALLING THROUGH PROSTACYCLIN RECEPTOR-REACTOME	C	-1.30	1.13	-1.69	1.59E-04
THROMBIN SIGNALLING THROUGH PROTEINASE ACTIVATED RECEPTORS (PARS)-REACTOME	C	-1.11	1.17	-1.59	1.69E-04
TRANSCRIPTION FROM RNA POLYMERASE II PROMOTER-GOBP	D	1.51	1.35	-0.94	1.00E-04
HYDROGEN ION TRANSMEMBRANE TRANSPORT-GOBP	D	1.06	1.69	-1.13	1.01E-04
POSITIVE REGULATION OF CYTOKINESIS-GOBP	D	1.74	1.37	-1.06	1.03E-04
NUCLEUS ORGANIZATION-GOBP	D	2.11	1.41	-0.90	1.03E-04
RESPONSE TO IONIZING RADIATION-GOBP	E	1.31	-1.29	-1.08	1.44E-04
CELLULAR CARBOHYDRATE CATABOLIC PROCESS-GOBP	E	1.17	-0.99	-1.64	1.67E-04
AXON GUIDANCE-REACTOME DATABASE ID RELEASE 56	E	0.90	-1.17	-1.42	1.94E-04
G2 DNA DAMAGE CHECKPOINT-GOBP	E	1.31	-1.42	-1.10	2.41E-04
LEARNING-GOBP	F	0.69	-1.52	1.27	1.42E-04
CYTOSKELETON ORGANIZATION-GOBP	F	1.47	-0.92	1.00	2.23E-04
ACYLGLYCEROL BIOSYNTHETIC PROCESS-GOBP	F	0.92	-1.52	1.26	2.44E-04
PLC-GAMMA1 SIGNALLING-REACTOME	F	1.11	-1.11	1.63	2.78E-04
FATTY ACID METABOLIC PROCESS-GOBP	G	0.89	0.76	1.61	6.42E-04
COPI-DEPENDENT GOLGI-TO-ER RETROGRADE TRAFFIC-REACTOME	G	1.75	1.07	0.76	6.92E-04
MICROTUBULE-BASED PROCESS-GOBP	G	1.91	0.94	0.86	7.96E-04
NEGATIVE REGULATION OF CATALYTIC ACTIVITY-GOBP	G	1.51	1.46	0.91	8.68E-04

Supplementary Figure 5

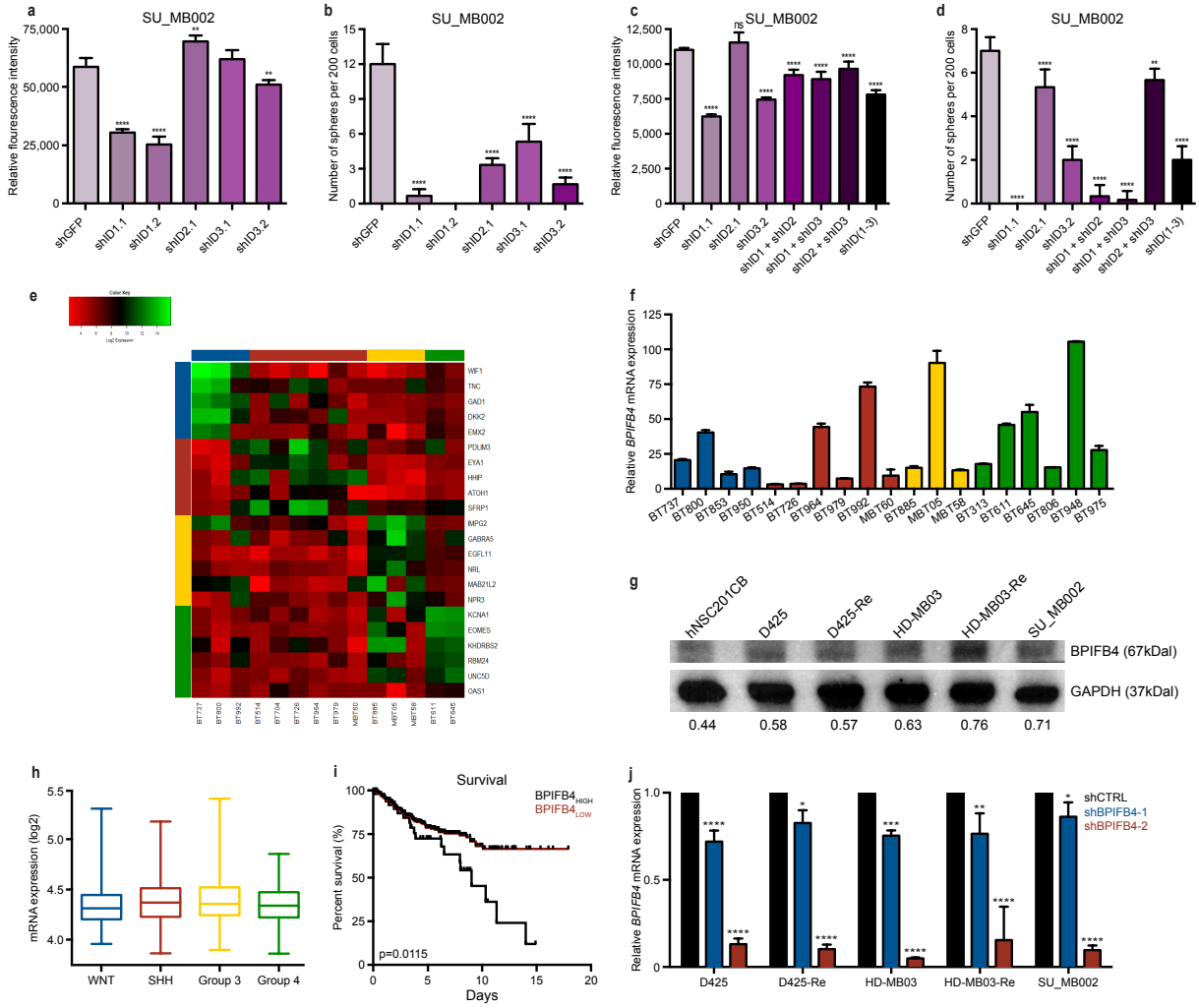

Supplementary Figure 5: Validation of genes identified from comparative gene expression profiling of samples isolated through *in vitro* chemoradiotherapy. Changes in **(a)** proliferation and **(b)** self-renewal in SU_MB002 post lentivector mediated KD of ID1, ID2 and ID3 in SU_MB002 alone and in **(c, d)** combinations. **(e)** Subgroup affiliation of patient MB samples based expression of subgroup specific genes on NanoString nCounter platform. **(f)** Relative mRNA expression of BPIFB4 across 19 patient MB tissues. **(g)** BPIFB4 protein levels across five MB cell lines and hNSCs. **(h)** mRNA expression of BPIFB4 across 643 MB samples described in *et al*. **(i)** Kaplan-Meir curve demonstrating decreased overall survival in patients (n=384) with relative mRNA expression of BPFIB4 over 4.6 (RMA-Normalized). **(j)** Validation of BPIFB4 KD across five MB cell lines. Bars represent mean of at least three technical replicates. *$p \leq 0.05$, **$p \leq 0.001$, ***$p \leq 0.0001$; ****$p \leq 0.00001$; unpaired t-test or one-way ANOVA with Sidak's method for multiple comparisons.

Supplementary Table 2: Demographic and clinical data of 19 MB samples curated at McMaster Children's Hospital. M – Male, F – Female, OS – Overall survival, PFS – progression free survival

Supplementary Table 2

Subgroup	Sample	Age at diagnosis	Sex	Primary/Recurent	Pathology variant	OS (years)	PFS (years)	Status
WNT	BT737	6Y	M	Primary	N/A	3.5	3	Alive
	BT800	11Y	F	Primary	Desmoplastic	3.25	2.5	Alive
	BT853	5Y 6M	F	Primary	Anaplastic	3.25	2.5	Alive
	BT950	8Y	M	Primary	Anaplastic	2	1.5	Alive
SHH	BT514	8Y	F	Primary	Anaplastic	5.5	2	Alive
	BT726	1Y 11M	M	Primary	Desmoplastic	4	1	Alive
	BT964	11Y	F	Recurrent of BT514	Classic	2	1.5	Alive
	BT979	4M 25D	M	Primary	Anaplastic	0.25	0.17	Dead
	BT992	6M 5D	M	Recurrent of BT979	Anaplastic	0.25	0.17	Dead
	MBT60	5Y 2M	M	Recurrent of BT726	Desmoplastic	4	3	Alive
Group 3	BT885	2Y 4M	F	Primary	Desmoplastic	2.75	2	Alive
	MBT05	10M	F	Primary	Desmoplastic	1.33	0.83	Alive
	MBT58	3Y 11M	M	Primary	Desmoplastic	0.67	0.17	Alive
Group 4	BT313	16Y	M	Primary	Desmoplastic	4.5	2.17	Dead
	BT611	18Y	M	Recurrent of BT313	Desmoplastic	4.75	2.6	Dead
	BT645	10M	M	Primary	Desmoplastic	4.75	4	Alive
	BT806	3Y 11M/M	M	Primary	Desmoplastic	3.25	2.5	Alive
	BT948	10Y	M	Primary	Classic	2	1.5	Alive
	BT975	5Y 4M	M	Recurrent of BT806	Classic	3.25	1.6	Alive

Supplementary Figure 6

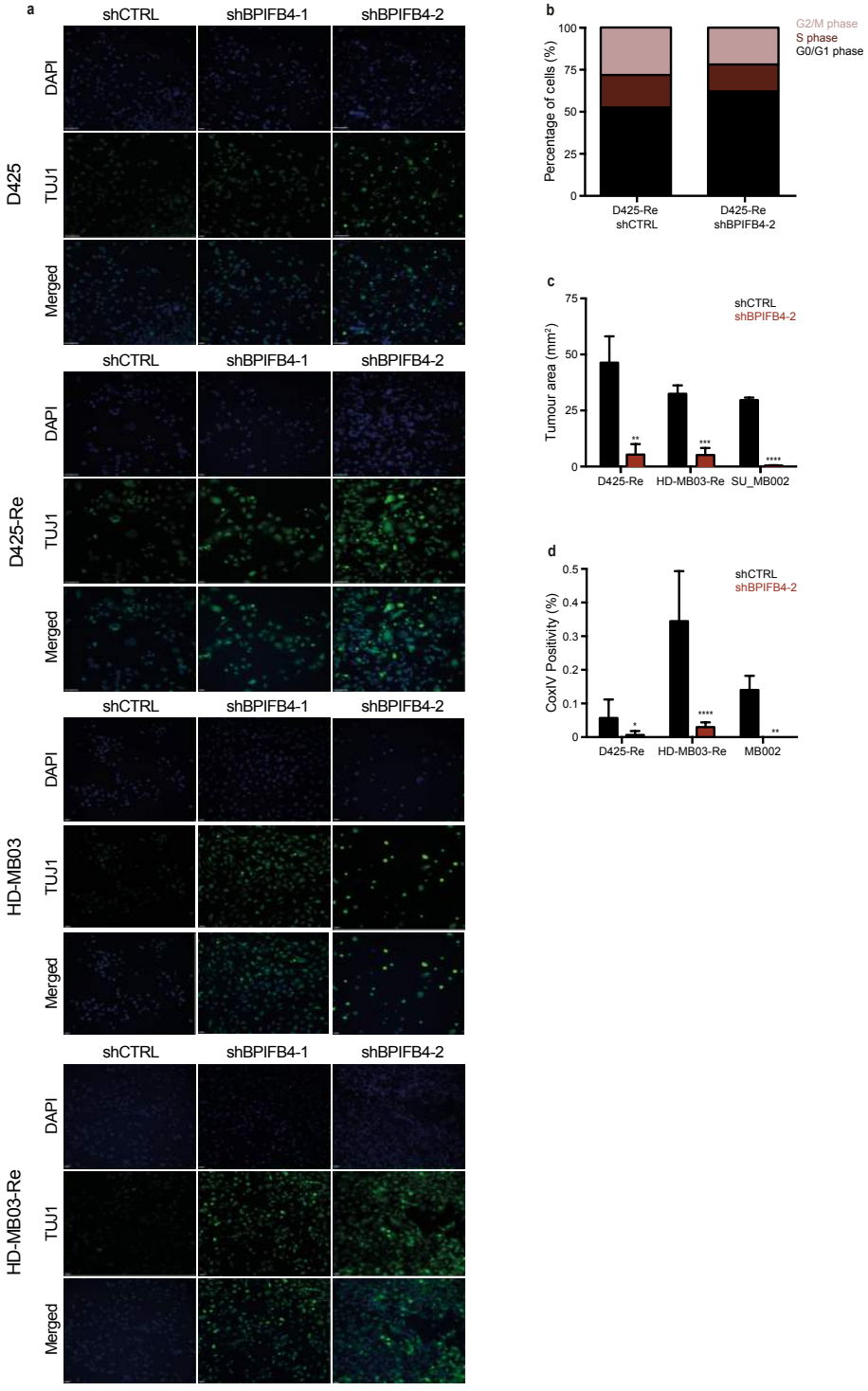

Supplementary Figure 6: Functional profiling of cells post BPIFB4 KD. (a) Increased expression of neuronal differentiation marker, TUJ1 after BPIFB4 KD. **(b)** Changes in percentage of MB cells in G0/G1, S, and G2/M phases of cell cycle post BPIFB4 KD. Quantified tumor burden in **(c)** brains and **(d)** spines of mice xenografted with recurrent MB cells transduced with control or BPIFB4 KD lentivectors as indicated by measured tumor area or positivity of CoxIV staining respectively. Bars represent mean of at least three technical replicates. *$p \leq 0.05$, **$p \leq 0.001$, ***$p \leq 0.0001$; ****$p \leq 0.00001$; unpaired t-test.

Supplementary Figure 7

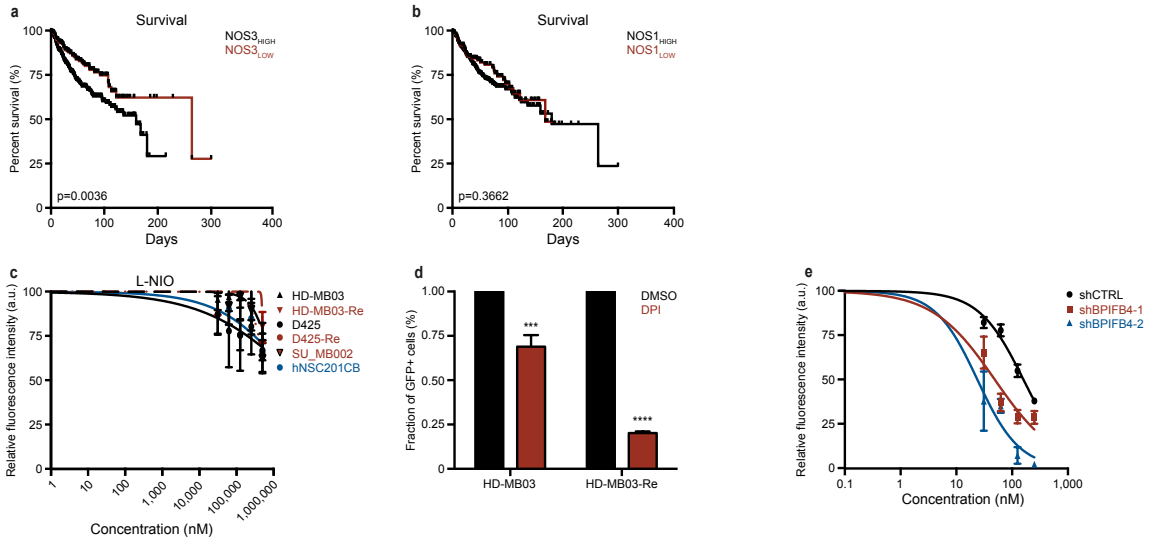

Supplementary Figure 7: Selectivity of DPI in recurrent MB. Kaplan-Meir curves demonstrating **(a)** decreased overall survival in patients with relative mRNA expression of eNOS over 5.4 (RMA-Normalized) and **(b)** no survival disadvantage in patients with relative mRNA expression of nNOS over 5.08 (RMA-Normalized). **(c)** IC_{50} curves of L-NIO in hNSCs and five medulloblastoma lines. **(d)** Reduced levels NO in HD-MB03 and HD-MB03-Re cells after 72-hour treatment with DPI as indicated by a reduced percentage of GFP+ cells in response to treatment with NO probe. **(e)** Increased sensitivity of MB cells to DPI treatment after transduction with BPIFB4 KD lentivector.

Chapter 3: BMI1: a path to targeting cancer stem cells

This chapter is an original published article presented in its published format in *Oncogene* available at https://touchoncology.com/bmi1-a-path-to-targeting-cancer-stem-cells/

Bakhshinyan, D., A. A. Adile, C. Venugopal, S. K. Singh (2017). "BMI1: a path to targeting cancer stem cells." ***European Oncology and Haematology***

In this work, I aimed to provide a comprehensive overview of literature pertaining the basic biology of polycomb repressive complexes 1 and 2 with an emphasis on their role in regulating self-renewal in normal and cancer stem cells. The main focus of the review was a key subunit of polycomb repressive complex 1 (PRC1), BMI1, a major driver of self-renewal and metastatic potential across multiple cancer types. In addition to the discussion of BMI1 mechanism of action, clinical implications of dysregulated BMI1 expression are examined within the review article. Finally, insights on several potential therapeutic modalities for targeting BMI1 and their promise for translation into clinic are described. The review further contributes to the objective my thesis work exploring implications and therapeutic interventions for the aberrant self-renewal in medulloblastoma cells.

Bmi1: a path to targeting cancer stem cells

David Bakhshinyan[1,2] Hon. BSc, Ashley A. Adile[1,2], Chitra Venugopal[1,3] PhD, Sheila K. Singh*[1,2,3] MD, PhD

[1]McMaster Stem Cell and Cancer Research Institute, McMaster University, Hamilton, ON, L8S4L8, Canada

[2]Department of Biochemistry and Biomedical Sciences, Faculty of Health Sciences, McMaster University, Hamilton, ON, L8S4L8, Canada

[3]Department of Surgery, Faculty of Health Sciences, McMaster University, Hamilton, ON, L8S4L8, Canada

***CORRESPONDING AUTHOR**

Sheila K. Singh, MD, PhD, FRCS(C)

Associate Professor of Pediatric Neurosurgery,

Department of Surgery, McMaster Children's Hospital,

Scientist, McMaster Stem Cell & Cancer Research Institute

MDCL 5027, 1280 Main Street West, Hamilton, ON, L8S 4K1, Canada

T: 905-521-2100 x75237 F: 905-521-992 Email: ssingh@mcmaster.ca

Abstract:

The Polycomb group (PcG) genes encode for proteins comprising two multiprotein complexes, Polycomb repressive complex 1 (PRC1) and Polycomb repressive complex 2 (PRC2). Although the initial discovery of PcG genes was made in *Drosophila* as transcriptional repressors of Homeotic (*HOX*) genes, Polycomb repressive complexes have been since implicated in regulating a wide range of cellular processes, including differentiation and self-renewal in normal and cancer stem cells. Bmi1, a subunit of PRC1, has been long implicated in driving self-renewal, the key property of stem cells. Subsequent studies showing upregulation of Bmi1 in several cancers correlated with increased aggressiveness, radioresistance and metastatic potential, provided rationale for development of targeted therapies against Bmi1. Although Bmi1 activity can be reduced through transcriptional, post-transcriptional and post-translational regulation, to date the most promising approach has been through small molecule inhibitors targeting Bmi1 activity. The post-translational targeting of Bmi1 in colorectal carcinoma, lung adenocarcinoma, multiple myeloma and medulloblastoma have led to significant reduction of self-renewal capacity of cancer stem cells, leading to slower tumor progression and reduced extent of metastatic spread. Further value of Bmi1 targeting in cancer can be established through trials evaluating the combinatorial effect of Bmi1 inhibition with current "gold standard" therapies.

Key words

Polycomb group (PcG) genes; BMI1; MEL18; cancer stem cells (CSCs); self-renewal.

Polycomb Group Proteins: Overview

Since the discovery of the Polycomb group (PcG) gene family in *Drosophila* as repressors of Homeotic (*HOX*) genes, PcG protein**s** have been implicated in a range of processes from chromosome X inactivation to stem cell plasticity and differentiation. PcG proteins execute their function through transcriptional repression of the promoter region of a target gene. Although PcG proteins function as two major multiprotein complexes - Polycomb Repressive Complex 1 (PRC1) and Polycomb Repressive Complex 2 (PRC2) - the existence of several context specific subcomplexes has been postulated(Otte and Kwaks, 2003). PRC2 initiates gene silencing through the activity of histone deacetylase, and histone methyltransferases that can methylate lysine 9 and 27 residues on histone H3 and lysine 26 on histone H1(Cao et al., 2002; Czermin et al., 2002; Kuzmichev et al., 2004; Muller et al., 2002; van der Vlag and Otte, 1999). The stable gene repression is then maintained by PRC1 through recognition of tri-methylated H3K27 (H3K27me3)(Czermin et al., 2002). The canonical repression pathway is initiated through trimethylation of H3K27 on the promoter of target gene by PRC2 subunit EZH1 or its paralog EZH2[2-4]. The H3K27me3 mark is readily recognized by PRC1 through chromatin binding ability of its subunit CBX. The repression is further maintained through ubiquitination of lysine 119 residue on histone H2A (H2AK119ub) by RING1, a subunit of PRC1, or chromatin condensation(Fischle et al., 2003; Min et al., 2003; Wang et al., 2004). Promoters of the polycomb target genes have been generally characterized as CpG-rich DNA sequences that are lacking other epigenetic marks(Gao et al., 2012; Jermann et al., 2014; Ku et al., 2008; Lynch et al., 2012; Mendenhall et al., 2010). However, several other models of context

dependent PRC2 recruitment mechanisms, including Polycomb Response Elements (PREs)(Bengani et al., 2013; Cuddapah et al., 2012; Sing et al., 2009; Woo et al., 2010) and ncRNAs(Aguilo et al., 2011; Brockdorff, 2013; Karapetyan et al., 2013; Peschansky and Wahlestedt, 2014) have been investigated.

PcG Genes and Self-renewal:

Over the years, in addition to *HOX* genes, numerous targets of PcG repression have been identified, with one of the examples being *CDKN2A* locus (Figure 1). Encoding for $p16^{INK4A}$ and $p14^{ARF}$ tumor-suppressor proteins, gene products of CDKN2A locus act as important mediators of the cell cycle(Sharpless and Sherr, 2015). The $p16^{INK4A}$ prevents phosphorylation of retinoblastoma protein (RB) through inhibition of cyclin D-dependent CDK4 and CDK6, which allows hypophosphorylated RB to sequester E2F transcription factor and prevent activation of genes required for DNA replication(Serrano et al., 1993). On the other hand, $p14^{ARF}$ interacts with MDM2 E3 ubiquitin ligase, preventing p53 polyubiquitination and subsequent p53 activation(Kamijo et al., 1998; Kamijo et al., 1997; Pomerantz et al., 1998; Zhang et al., 1998). The repression of CDKN2A by PcG proteins in stem cells(Sharpless and DePinho, 2007; Signer and Morrison, 2013) or its frequent deletion in cancer cells(Bignell et al., 2010; Chandler and Peters, 2013) facilitates increased self-renewal and proliferation and has been implicated in neoplastic transformations. A meta-analysis of 11 studies quantifying CDKN2A methylation in 3440 colorectal cancer patients have identified hypermethylation in 23% of tumors. Furthermore, CDKN2A promoter hypermethylation was shown to correlate with poor patient overall survival(Xing et al., 2013) In juvenile myelomonocytic leukemia (JMML), hypermethylation of

CDKN2A was observed in 35% of the patients and correlated with poor outcome(Sakaguchi et al., 2015), similarly to the patients diagnosed with non-small cell lung cancer (NSCLC), hypermethylation of p16 promoter was also associated with worse outcome(Bradly et al., 2012). The notion of slowing down the replication of cancer cells, a major hallmark of tumor biology, has been of great interest, and the efforts have escalated tremendously with the conceptualization and discovery of cancer stem cells (CSCs). The first compelling evidence of cancer cells possessing stem-like properties came from the work of Bonnet and Dick in mouse models of acute myeloid leukemia (AML)(Bonnet and Dick, 1997). Since then, CSCs have been identified and characterized in breast(Al-Hajj et al., 2003), brain(Singh et al., 2004), colon(Barker et al., 2007), and lung(Ho et al., 2007; Salcido et al., 2010) cancers, among others. Due to their ability to evade chemoradiotherapy along with tumor-initiating and metastatic properties, CSCs have been implicated in driving treatment failure, tumor recurrence and poor clinical outcome(Allen and Weiss, 2010). Although CSC populations identified in various cancer types have intrinsically different gene expression patterns, they all share the unique ability to self-renew, unlike the more differentiated cancer cells. This difference confers one of the major limitations of current therapy modalities, as they are effective against bulk tumor consisting of highly proliferative cells, while sparing the intrinsically resistant, slow-dividing CSCs. The increasing evidence connecting self-renewal and therapeutic resistance of CSCs presents a strong rationale for developing of novel therapeutic modalities as a treatment option for many aggressive malignancies. In this review, we discuss the involvement of PRC1

subunits, Bmi1 and Mel18, in regulation of self-renewal in cancer and their potential for therapeutic targeting.

Clinical implications of Bmi1 in cancer:

Bmi1, a 37kDa subunit of PRC1, was first identified as a key component in the activation region of Moloney murine leukemia virus(Alkema et al., 1993). The target gene suppression by PRC1 is primarily achieved through H2A119ub by RING1B E3 ligase, the catalytic activity of which is dramatically reduced in the absence of Bmi1. However, to date no specific enzymatic activity of Bmi1 has been reported(Cao et al., 2005), making it a challenge to target for therapeutic intervention. In early 2000s, Bmi1 was implicated in self-renewal of hematopoietic and neural stem cell populations and driving the proliferation of early cerebellar progenitors(Lessard and Sauvageau, 2003; Molofsky et al., 2003; Park et al., 2003). Further experimental evidence of importance of PcG gene in stem cells came from the study of Bmi1-deficient mice that suffered from continuous loss of hematopoietic cells and cerebellar neurons(van der Lugt et al., 1994). PRC1 complex was further implicated in maintaining proper function of hematopoietic stem cells through interaction between Mph1/Rae28 with Bmi1(Ohta et al., 2002). The oncogenic potential of Bmi1 became evident through investigation of lymphomagenesis in mouse models. Haupt *et al* have demonstrated that in collaboration with c-Myc, Bmi1 contributed to lymphomagenesis in T and B cell lineages(Haupt et al., 1993). The PRC1-mediated transcriptional repression of CDKN2A locus during lymphomagenesis leads to maintenance of proliferative capacity and undifferentiated state(Itahana et al., 2003; Jacobs et al., 1999), and has since been implicated in progression and poor prognosis in a number

of hematologic malignancies(Hosen et al., 2007; Lessard and Sauvageau, 2003). Similarly to normal stem cells, Bmi1 was implicated in maintenance of self-renewal in leukemic stem and progenitor cells(Schuringa and Vellenga, 2010). Intriguingly, there is some evidence that Bmi1 can exert its oncogenic properties even in CDKN2A-deficient models(Bruggeman et al., 2007), suggesting the existence of other gene targets repressed during tumorigenesis. In addition to hematologic malignancies(Hosen et al., 2007; Merkerova et al., 2007), elevated levels of Bmi1 have been shown in colorectal carcinoma, non-small cell lung carcinoma(Vrzalikova et al., 2008), breast carcinoma(Guo et al., 2011; Honig et al., 2010), glioblastoma (GBM)(Abdouh et al., 2009), medulloblastoma(Leung et al., 2004), and prostate cancer(Glinsky, 2007). Clinically, increased Bmi1 expression levels have been shown to correlate with poor patient prognosis in several aggressive cancer types, including colorectal carcinoma(Li et al., 2010), GBM(Cenci et al., 2012), and medulloblastoma(Manoranjan et al., 2013). The maintenance of self-renewal potential by Bmi1 contributes to the aggressive cancer phenotype by allowing CSCs to evade chemoradiotherapy regimens and drive tumor recurrence. Further contributions of Bmi1 to cancer cell survival through therapy has come from its role in promoting DNA damage repair. Both Bmi1 and Ring1B are recruited to the DNA double-strand breaks (DSB) to facilitate unbiquitination of γH2AX(Ismail et al., 2010). The continuous localization of Bmi1 to DSB breaks is highly dependent on functionally intact ataxia-telangiectasia mutated (ATM), in addition to ATM- and Rad-3-Related (ATR) kinases(Ginjala et al., 2011; Marechal and Zou, 2013). Moreover, Bmi1-driven enhancement of DNA DSB repair allows cancer stem cells to negate the detrimental effects of radiation and persist post

therapy. For example, in GBM, a highly malignant adult brain tumor, CD133 expressing brain tumor initiating cells (BTICs)(Singh et al., 2004) were shown to have the capacity of escaping radiation through activation of DNA DSB repair mechanisms(Facchino et al., 2010). However, the loss of Bmi1-assisted DNA DSB repair increases the sensitivity of CSCs to ionizing radiation and promotes accumulation of cells in G_2/M phase of the cell cycle. Aside from driving self-renewal and resistance to radiotherapy, Bmi1 has been implicated in promoting epithelial-mesenchymal transition (EMT), a signaling program frequently associated with cancer invasion and metastatic potential(Singh and Settleman, 2010), through cooperation with Twist 1 in head and neck carcinomas(Yang et al., 2010). By modulating SNAIL activity, Bmi1 is able to promote EMT through repression of *PTEN* and subsequent activation of AKT pathway(Song et al., 2009). The apparent role of Bmi1 in maintaining a stem cell-like state and an invasive phenotype along with its clinical significance in multiple tumor types has prompted investigation into avenues of reducing Bmi1 levels as a potential therapeutic modality.

Therapeutic targeting of Bmi1:

The extensive research on Bmi1 function in numerous malignancies has created a large amount of empirical data, correlating reduced Bmi1 expression levels with less proliferative, more therapy-sensitive and less tumorigenic phenotype of cancer cells. The development of small molecule inhibitors against Bmi1 might create an opportunity for designing therapies that not only target the highly proliferative cancer cells, but also the slowly dividing, therapy-evading CSCs. Additionally, Bmi1 targeting within cancer stem cells can allow for modulation of two key tumor suppressor pathways driven by Rb and

p53. In its turn, the combinatorial approach might allow for de-escalation of existing chemoradiotherapy protocols and minimize the associated toxicity and side effects. Decreased Bmi1 activity can be achieved through transcriptional, post-transcriptional or post-translational regulation(Cao et al., 2011). In breast cancer cells, broad spectrum histone deacetylase (HDAC) inhibitors have been shown to inhibit expression of Bmi1 and the activity of PRC1 complex as measured through a decrease of H1AK119ub(Bommi et al., 2010; Jung et al., 2010). However, HDAC inhibitor-mediated reduction of Bmi1 expression is unlikely to be useful as a targeted therapy against cancer cells, and thus is likely to be associated with toxicity and side effects. In a recent publication by Kaneta et al, researchers have isolated and identified a series of naturally occurring compounds targeting Bmi1 promoter activity. The most active compound, wallichoside was shown to decrease Bmi1 protein levels in colon carcinoma cells and reduced self-renewing capacity of human hepatocellular carcinoma cells(Kaneta et al., 2017). However, further *in vivo* studies in human-mouse xenograft models are warranted to generate better understanding of the compounds therapeutic value. Additionally, molecules targeting Bmi1 transcript have been shown to hold a promising therapeutic potential in reducing oncogenic potential of prostate cancer stem cells(Bansal et al., 2016) and hepatocellular carcinoma(Bartucci et al., 2017). Another potential way to modulate protein function, localization and half-life is through post-translational modifications(Cao et al., 2011). Targeting Bmi1 post-translationally, using small molecule inhibitors can present a more clinically relevant therapy modality with its potential to be selective for CSCs. The first experimental evidence demonstrating the imminent value of targeting Bmi1 through post-translational

modification, came from the study conducted by Voncken *et al*(Voncken et al., 1999) in 1999 where researchers observed fluctuating phosphorylation levels of Bmi1 through its progression in the cell cycle. In G_1/S phase, hypophosphorylated Bmi1 is present in the chromatin-bound state, whereas the phosphorylation of Bmi1 in the G_2/M phase reduces its chromatin association. Mechanistic insight into kinases involved in post-translational modification of Bmi1 came from the yeast two-hybrid interaction assay, which identified MAPKAP kinase 3pK as a regulator of Bmi1 chromatin association, among other PcG proteins(Voncken et al., 2005). In recent years, small molecule inhibitors developed by PTC Therapeutics (NJ), were designed to promote phosphorylation of Bmi1 have been tested in colorectal carcinomas(Kreso et al., 2014), lung adenocarcinomas(Yong et al., 2016), multiple myeloma (MM)(Bolomsky et al., 2016), prostate cancer(Bansal et al., 2016) and medulloblastoma (unpublished data). In all cases, small molecule inhibitor resulted in decreased Bmi1 protein levels and reduced activity of the PRC1 complex. More importantly, diminished Bmi1 levels reduced the self-renewal capacity of cancer stem cells, which in turn correlated with lowered tumorigenic potential *in vitro* and *in vivo*. In keeping with the original observations, cells treated with a Bmi1 inhibitor became more apoptotic(Bansal et al., 2016; Bolomsky et al., 2016; Kreso et al., 2014; Yong et al., 2016) and underwent cell cycle arrest at G_0 phase(Kreso et al., 2014; Yong et al., 2016). Collectively, these studies have provided a strong rationale for including Bmi1 targeted therapy in the treatment strategies for patients presenting with malignancies displaying elevated Bmi1 expression. Currently, the lead compound developed by PTC Therapeutics, PTC-596, is being examined in a Phase I clinical trial (ClinicalTrials.gov Identifier

NCT02404480) for recurrent solid malignancies in adults. Another example of post-translational regulation of Bmi1 is through beta-transducin repeat containing protein (βTrCP) mediated ubiquitination and subsequent degradation of Bmi1. In their work Sahasrabuddhe *et al*, were able to demonstrate that wild-type Bmi1 is readily recognized and bound to by βTrCP, a subunit of SCF (SKP1-cullin F-box) E3-ubiquitin ligase and is destined for ubiquitin-proteasome mediated degradation(Sahasrabuddhe et al., 2011). Development of therapies increasing the extent of Bmi1 ubiquitination might present an avenue to continuously reduce Bmi1 protein levels within the cell and thus ensure un-inhibited transcription of *CDKN2A* locus.

In addition to development small molecules directly affecting Bmi1 transcription or protein levels, novel compounds modulating Bmi1 through inhibition of proteins that contribute to normal regulation of Bmi1 have been tested. Polo-like kinase 1 (PLK1) is overexpressed in several cancer subtypes, correlates with poor patient outcomes and has been shown to play an important role in driving tumor cell growth(Strebhardt, 2010; Strebhardt and Ullrich, 2006). In breast cancer, small molecule inhibition of PLK1 resulted in marked induction of cellular senescence. Further experimentation revealed that downregulation of PLK1 activity caused upregulation of miR-200c and miR-141 which in turn post-transcriptionally inhibited expression of Bmi1(Dimri et al., 2015).

Negating Bmi1 effects by upregulation of Mel18:

Despite the highly similar amino acid sequences and functional redundancy between Bmi1 and its paralog Mel-18(van Lohuizen et al., 1991), the two proteins differ in their regulation of PRC1 complex. Both Bmi1-PRC1 complex and Mel18-PRC1 target

genes with high levels H3K27me3 and contribute to the canonical PcG-mediated gene repression(Gao et al., 2012). However, *in vitro* studies in MCF7 cells indicated that Mel-18-PRC1 complexes have reduced ubiquitination activity compared to Bmi1-PRC1 complexes(Cao et al., 2005; Qian et al., 2010). It has also been postulated that increased levels of Mel-18 allows it to outcompete Bmi1 for integration into PRC1 and thus reduce the extent of PRC1 mediated gene repression(Koppens and van Lohuizen, 2016). Interestingly, the expression pattern of *Bmi1* and *Mel-18* varies in adult tissues suggesting regulation of distinct cellular programs(Gao et al., 2012; Lessard et al., 1998). In contrast to *Bmi1*, expression levels of *Mel-18* escalate during differentiation of HSCs(Lessard et al., 1998; Park et al., 2003; Schuringa and Vellenga, 2010), suggesting that while Bmi1 is essential in preserving HSCs, Mel18 ensures proper differentiation(Kajiume et al., 2009; Oguro et al., 2010). Further functional differences between Bmi1 and Mel18 extend to their role in cancer cells. Unlike Bmi1, that is often upregulated in aggressive cancers, Mel18 is often downregulated(Guo et al., 2007b; Lu et al., 2010; Riis et al., 2012; Tao et al., 2014; Wang et al., 2011; Wang et al., 2009; Zhang et al., 2010) suggesting a tumor suppressive role. Studies in human fibroblasts identified Mel-18 contribution to transcriptional regulation of *Bmi1* through modulation of c-Myc levels. The Mel-18-driven downregulation of c-Myc during cellular senescence reduces its binding to the Bmi1 promoter and thus stalls Bmi1 gene expression(Guo et al., 2007a; Guo et al., 2007b; Kanno et al., 1995; Tetsu et al., 1998). Several other pathways modulated by Mel-18 include Wnt signalling, E-cadherin, and angiogenesis(Guo et al., 2010; Lee et al., 2014; Park et al., 2011). From a therapeutic perspective, Mel-18 presents an intriguing possibility to negate

Bmi1 activity through Mel-18 agonists. The increased levels of Mel-18 will allow for formation of more Mel-18-PRC1 complexes that have opposing effects to Bmi1-PRC1 complexes and thus will reduce the extent to which Bmi1 is able to contribute to therapy evasion and self-renewal ability of cancer stem cells.

Concluding remarks:

A combinatorial approach of targeting the bulk tumor population, along with the cancer stem cell fraction can potentially not only lead to de-escalation of current treatment protocols, but also address the root cause of tumor recurrence. However, since Bmi1 is ubiquitously expressed throughout the human body, the effects of Bmi1 targeting must be carefully and methodically evaluated. In the pre-clinical models investigating the efficacy of Bmi1 targeting with small molecule inhibitors for treatment of childhood medulloblastoma, our lab has shown a higher sensitivity of tumor cells to the Bmi1 inhibitor, relative to neural stem cells (unpublished data). These results highlight the importance of further elucidating different Bmi1 roles and its regulation in cancer cells, when compared to normal cells. The increasing evidence demonstrating Bmi1-driven therapy evasion and tumor recurrence warrants routine profiling of Bmi1 levels in oncologic patients, in order to identify patients who have the potential to benefit from combining Bmi1 targeted therapies with today's gold standard chemoradiotherapies. Moreover, the relationship between Bmi1 and Mel-18 requires further investigation as indirect modulation of Bmi1 levels by Mel-18 can create new therapeutic avenues for minimizing oncogenic effects of Bmi1.

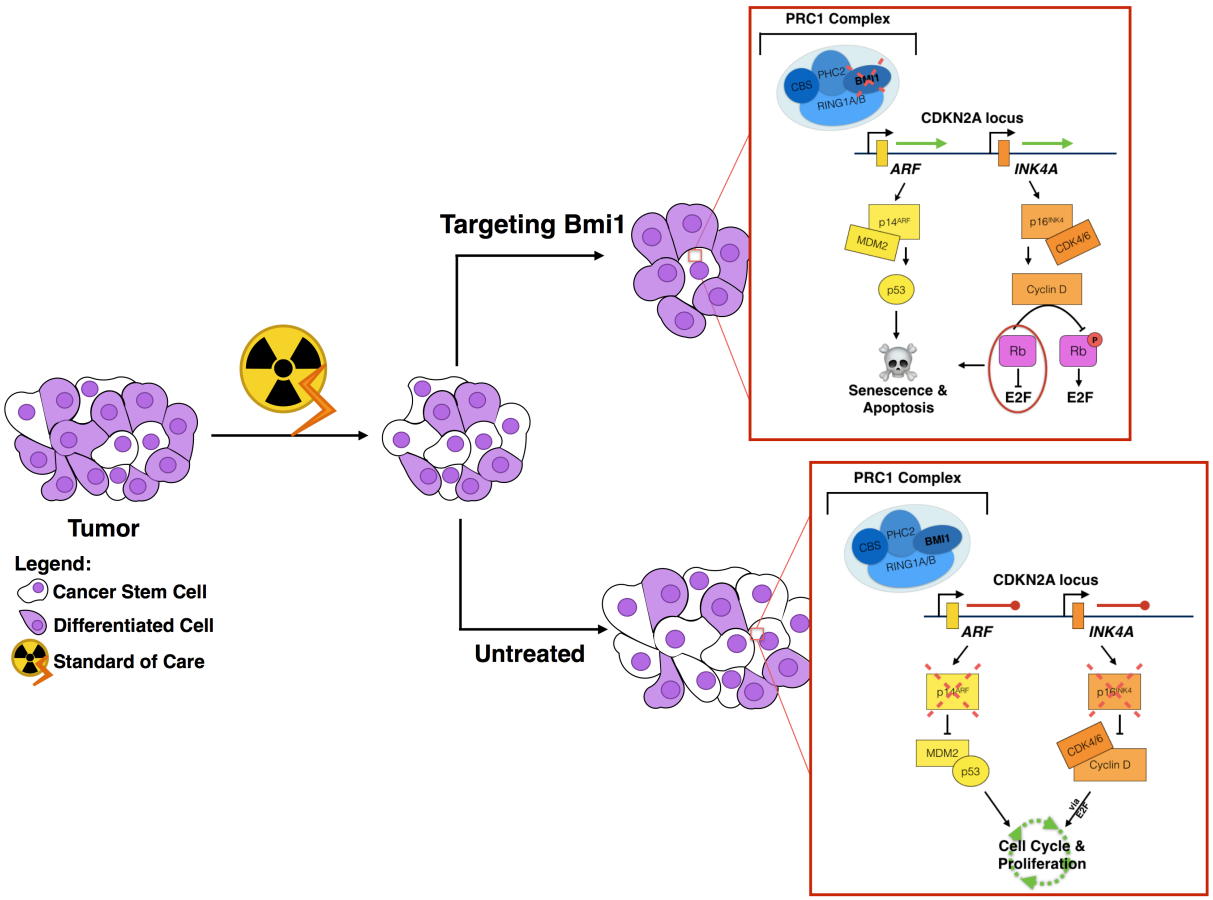

Figure 1: Role of Bmi1 in driving self-renewal of cancer stem cells. Cancer stem cells (CSCs) are endowed with the intrinsic ability to escape the best chemoradiotherapy regimens. Without targeted therapies against CSCs, slowly dividing cells left behind post-therapy will proliferate and drive tumor recurrence and metastatic spread. Within CSCs, Bmi1 directed self-renewal and proliferation is accomplished through transcriptional repression of the *CDKN2A* locus encoding for $p16^{INK4A}$ and $p14^{ARF}$. However, in the absence of Bmi1, p16-mediated inhibition of RB phosphorylation and p14-mediated prevention of p53 polyubiquitination contribute to reduced activation of genes required for DNA replication and cell cycle progression. Through targeted therapies against Bmi1, it is possible to limit proliferation and self-renewal of the rare population of cells responsible for treatment failure and tumor recurrence.

References:

1 Otte, A. P. & Kwaks, T. H. Gene repression by Polycomb group protein complexes: a distinct complex for every occasion? *Current opinion in genetics & development* **13**, 448-454 (2003).
2 Cao, R. *et al.* Role of histone H3 lysine 27 methylation in Polycomb-group silencing. *Science* **298**, 1039-1043, doi:10.1126/science.1076997 (2002).
3 Czermin, B. *et al.* Drosophila enhancer of Zeste/ESC complexes have a histone H3 methyltransferase activity that marks chromosomal Polycomb sites. *Cell* **111**, 185-196 (2002).
4 Muller, J. *et al.* Histone methyltransferase activity of a Drosophila Polycomb group repressor complex. *Cell* **111**, 197-208 (2002).
5 Kuzmichev, A., Jenuwein, T., Tempst, P. & Reinberg, D. Different EZH2-containing complexes target methylation of histone H1 or nucleosomal histone H3. *Mol Cell* **14**, 183-193 (2004).
6 van der Vlag, J. & Otte, A. P. Transcriptional repression mediated by the human polycomb-group protein EED involves histone deacetylation. *Nat Genet* **23**, 474-478, doi:10.1038/70602 (1999).
7 Min, G., Zhou, G., Schapira, M., Sun, T. T. & Kong, X. P. Structural basis of urothelial permeability barrier function as revealed by Cryo-EM studies of the 16 nm uroplakin particle. *J Cell Sci* **116**, 4087-4094, doi:10.1242/jcs.00811 (2003).
8 Fischle, W. *et al.* Molecular basis for the discrimination of repressive methyl-lysine marks in histone H3 by Polycomb and HP1 chromodomains. *Genes Dev* **17**, 1870-1881, doi:10.1101/gad.1110503 (2003).
9 Wang, H. *et al.* Role of histone H2A ubiquitination in Polycomb silencing. *Nature* **431**, 873-878, doi:10.1038/nature02985 (2004).
10 Ku, M. *et al.* Genomewide analysis of PRC1 and PRC2 occupancy identifies two classes of bivalent domains. *PLoS Genet* **4**, e1000242, doi:10.1371/journal.pgen.1000242 (2008).
11 Lynch, M. D. *et al.* An interspecies analysis reveals a key role for unmethylated CpG dinucleotides in vertebrate Polycomb complex recruitment. *EMBO J* **31**, 317-329, doi:10.1038/emboj.2011.399 (2012).
12 Gao, Z. *et al.* PCGF homologs, CBX proteins, and RYBP define functionally distinct PRC1 family complexes. *Mol Cell* **45**, 344-356, doi:10.1016/j.molcel.2012.01.002 (2012).
13 Jermann, P., Hoerner, L., Burger, L. & Schubeler, D. Short sequences can efficiently recruit histone H3 lysine 27 trimethylation in the absence of enhancer activity and DNA methylation. *Proc Natl Acad Sci U S A* **111**, E3415-3421, doi:10.1073/pnas.1400672111 (2014).
14 Mendenhall, E. M. *et al.* GC-rich sequence elements recruit PRC2 in mammalian ES cells. *PLoS Genet* **6**, e1001244, doi:10.1371/journal.pgen.1001244 (2010).
15 Bengani, H. *et al.* Identification and Validation of a Putative Polycomb Responsive Element in the Human Genome. *PLoS One* **8**, e67217, doi:10.1371/journal.pone.0067217 (2013).

16 Woo, C. J., Kharchenko, P. V., Daheron, L., Park, P. J. & Kingston, R. E. A region of the human HOXD cluster that confers polycomb-group responsiveness. *Cell* **140**, 99-110, doi:10.1016/j.cell.2009.12.022 (2010).
17 Sing, A. *et al.* A vertebrate Polycomb response element governs segmentation of the posterior hindbrain. *Cell* **138**, 885-897, doi:10.1016/j.cell.2009.08.020 (2009).
18 Cuddapah, S. *et al.* A novel human polycomb binding site acts as a functional polycomb response element in Drosophila. *PLoS One* **7**, e36365, doi:10.1371/journal.pone.0036365 (2012).
19 Aguilo, F., Zhou, M. M. & Walsh, M. J. Long noncoding RNA, polycomb, and the ghosts haunting INK4b-ARF-INK4a expression. *Cancer Res* **71**, 5365-5369, doi:10.1158/0008-5472.CAN-10-4379 (2011).
20 Brockdorff, N. Noncoding RNA and Polycomb recruitment. *RNA* **19**, 429-442, doi:10.1261/rna.037598.112 (2013).
21 Karapetyan, A. R., Buiting, C., Kuiper, R. A. & Coolen, M. W. Regulatory Roles for Long ncRNA and mRNA. *Cancers (Basel)* **5**, 462-490, doi:10.3390/cancers5020462 (2013).
22 Peschansky, V. J. & Wahlestedt, C. Non-coding RNAs as direct and indirect modulators of epigenetic regulation. *Epigenetics* **9**, 3-12, doi:10.4161/epi.27473 (2014).
23 Sharpless, N. E. & Sherr, C. J. Forging a signature of in vivo senescence. *Nat Rev Cancer* **15**, 397-408, doi:10.1038/nrc3960 (2015).
24 Serrano, M., Hannon, G. J. & Beach, D. A new regulatory motif in cell-cycle control causing specific inhibition of cyclin D/CDK4. *Nature* **366**, 704-707, doi:10.1038/366704a0 (1993).
25 Kamijo, T. *et al.* Tumor suppression at the mouse INK4a locus mediated by the alternative reading frame product p19ARF. *Cell* **91**, 649-659 (1997).
26 Pomerantz, J. *et al.* The Ink4a tumor suppressor gene product, p19Arf, interacts with MDM2 and neutralizes MDM2's inhibition of p53. *Cell* **92**, 713-723 (1998).
27 Zhang, Y., Xiong, Y. & Yarbrough, W. G. ARF promotes MDM2 degradation and stabilizes p53: ARF-INK4a locus deletion impairs both the Rb and p53 tumor suppression pathways. *Cell* **92**, 725-734 (1998).
28 Kamijo, T. *et al.* Functional and physical interactions of the ARF tumor suppressor with p53 and Mdm2. *Proc Natl Acad Sci U S A* **95**, 8292-8297 (1998).
29 Sharpless, N. E. & DePinho, R. A. How stem cells age and why this makes us grow old. *Nat Rev Mol Cell Biol* **8**, 703-713, doi:10.1038/nrm2241 (2007).
30 Signer, R. A. & Morrison, S. J. Mechanisms that regulate stem cell aging and life span. *Cell Stem Cell* **12**, 152-165, doi:10.1016/j.stem.2013.01.001 (2013).
31 Chandler, H. & Peters, G. Stressing the cell cycle in senescence and aging. *Curr Opin Cell Biol* **25**, 765-771, doi:10.1016/j.ceb.2013.07.005 (2013).
32 Bignell, G. R. *et al.* Signatures of mutation and selection in the cancer genome. *Nature* **463**, 893-898, doi:10.1038/nature08768 (2010).
33 Xing, X. *et al.* The prognostic value of CDKN2A hypermethylation in colorectal cancer: a meta-analysis. *Br J Cancer* **108**, 2542-2548, doi:10.1038/bjc.2013.251 (2013).

34 Sakaguchi, H. *et al.* Aberrant DNA Methylation Is Associated with a Poor Outcome in Juvenile Myelomonocytic Leukemia. *PLoS One* **10**, e0145394, doi:10.1371/journal.pone.0145394 (2015).
35 Bradly, D. P. *et al.* CDKN2A (p16) promoter hypermethylation influences the outcome in young lung cancer patients. *Diagn Mol Pathol* **21**, 207-213, doi:10.1097/PDM.0b013e31825554b2 (2012).
36 Bonnet, D. & Dick, J. E. Human acute myeloid leukemia is organized as a hierarchy that originates from a primitive hematopoietic cell. *Nat Med* **3**, 730-737 (1997).
37 Al-Hajj, M., Wicha, M. S., Benito-Hernandez, A., Morrison, S. J. & Clarke, M. F. Prospective identification of tumorigenic breast cancer cells. *Proc Natl Acad Sci U S A* **100**, 3983-3988, doi:10.1073/pnas.0530291100 (2003).
38 Singh, S. K. *et al.* Identification of human brain tumor initiating cells. *Nature* **432**, 396-401, doi:10.1038/nature03128 (2004).
39 Barker, N. *et al.* Identification of stem cells in small intestine and colon by marker gene Lgr5. *Nature* **449**, 1003-1007, doi:10.1038/nature06196 (2007).
40 Ho, M. M., Ng, A. V., Lam, S. & Hung, J. Y. Side population in human lung cancer cell lines and tumors is enriched with stem-like cancer cells. *Cancer Res* **67**, 4827-4833, doi:10.1158/0008-5472.CAN-06-3557 (2007).
41 Salcido, C. D., Larochelle, A., Taylor, B. J., Dunbar, C. E. & Varticovski, L. Molecular characterisation of side population cells with cancer stem cell-like characteristics in small-cell lung cancer. *Br J Cancer* **102**, 1636-1644, doi:10.1038/sj.bjc.6605668 (2010).
42 Allen, K. E. & Weiss, G. J. Resistance may not be futile: microRNA biomarkers for chemoresistance and potential therapeutics. *Mol Cancer Ther* **9**, 3126-3136, doi:10.1158/1535-7163.MCT-10-0397 (2010).
43 Alkema, M. J., Wiegant, J., Raap, A. K., Berns, A. & van Lohuizen, M. Characterization and chromosomal localization of the human proto-oncogene BMI-1. *Hum Mol Genet* **2**, 1597-1603 (1993).
44 Cao, R., Tsukada, Y. & Zhang, Y. Role of Bmi-1 and Ring1A in H2A ubiquitylation and Hox gene silencing. *Mol Cell* **20**, 845-854, doi:10.1016/j.molcel.2005.12.002 (2005).
45 Lessard, J. & Sauvageau, G. Bmi-1 determines the proliferative capacity of normal and leukaemic stem cells. *Nature* **423**, 255-260, doi:10.1038/nature01572 (2003).
46 Park, I. K. *et al.* Bmi-1 is required for maintenance of adult self-renewing haematopoietic stem cells. *Nature* **423**, 302-305, doi:10.1038/nature01587 (2003).
47 Molofsky, A. V. *et al.* Bmi-1 dependence distinguishes neural stem cell self-renewal from progenitor proliferation. *Nature* **425**, 962-967, doi:10.1038/nature02060 (2003).
48 van der Lugt, N. M. *et al.* Posterior transformation, neurological abnormalities, and severe hematopoietic defects in mice with a targeted deletion of the bmi-1 proto-oncogene. *Genes Dev* **8**, 757-769 (1994).

49 Ohta, H. *et al.* Polycomb group gene rae28 is required for sustaining activity of hematopoietic stem cells. *J Exp Med* **195**, 759-770 (2002).
50 Haupt, Y., Bath, M. L., Harris, A. W. & Adams, J. M. bmi-1 transgene induces lymphomas and collaborates with myc in tumorigenesis. *Oncogene* **8**, 3161-3164 (1993).
51 Jacobs, J. J. *et al.* Bmi-1 collaborates with c-Myc in tumorigenesis by inhibiting c-Myc-induced apoptosis via INK4a/ARF. *Genes Dev* **13**, 2678-2690 (1999).
52 Itahana, K. *et al.* Control of the replicative life span of human fibroblasts by p16 and the polycomb protein Bmi-1. *Mol Cell Biol* **23**, 389-401 (2003).
53 Hosen, N. *et al.* Bmi-1-green fluorescent protein-knock-in mice reveal the dynamic regulation of bmi-1 expression in normal and leukemic hematopoietic cells. *Stem Cells* **25**, 1635-1644, doi:10.1634/stemcells.2006-0229 (2007).
54 Schuringa, J. J. & Vellenga, E. Role of the polycomb group gene BMI1 in normal and leukemic hematopoietic stem and progenitor cells. *Curr Opin Hematol* **17**, 294-299, doi:10.1097/MOH.0b013e328338c439 (2010).
55 Bruggeman, S. W. *et al.* Bmi1 controls tumor development in an Ink4a/Arf-independent manner in a mouse model for glioma. *Cancer Cell* **12**, 328-341, doi:10.1016/j.ccr.2007.08.032 (2007).
56 Merkerova, M., Bruchova, H., Kracmarova, A., Klamova, H. & Brdicka, R. Bmi-1 over-expression plays a secondary role in chronic myeloid leukemia transformation. *Leuk Lymphoma* **48**, 793-801, doi:10.1080/10428190601186002 (2007).
57 Vrzalikova, K. *et al.* Prognostic value of Bmi-1 oncoprotein expression in NSCLC patients: a tissue microarray study. *J Cancer Res Clin Oncol* **134**, 1037-1042, doi:10.1007/s00432-008-0361-y (2008).
58 Honig, A. *et al.* Overexpression of polycomb protein BMI-1 in human specimens of breast, ovarian, endometrial and cervical cancer. *Anticancer Res* **30**, 1559-1564 (2010).
59 Guo, B. H. *et al.* Bmi-1 promotes invasion and metastasis, and its elevated expression is correlated with an advanced stage of breast cancer. *Mol Cancer* **10**, 10, doi:10.1186/1476-4598-10-10 (2011).
60 Abdouh, M. *et al.* BMI1 sustains human glioblastoma multiforme stem cell renewal. *J Neurosci* **29**, 8884-8896, doi:10.1523/JNEUROSCI.0968-09.2009 (2009).
61 Leung, C. *et al.* Bmi1 is essential for cerebellar development and is overexpressed in human medulloblastomas. *Nature* **428**, 337-341, doi:10.1038/nature02385 (2004).
62 Glinsky, G. V. Stem cell origin of death-from-cancer phenotypes of human prostate and breast cancers. *Stem Cell Rev* **3**, 79-93 (2007).
63 Li, D. W. *et al.* Expression level of Bmi-1 oncoprotein is associated with progression and prognosis in colon cancer. *J Cancer Res Clin Oncol* **136**, 997-1006, doi:10.1007/s00432-009-0745-7 (2010).

64 Cenci, T. *et al.* Prognostic relevance of c-Myc and BMI1 expression in patients with glioblastoma. *Am J Clin Pathol* **138**, 390-396, doi:10.1309/AJCPRXHNJQLO09QA (2012).
65 Manoranjan, B. *et al.* FoxG1 interacts with Bmi1 to regulate self-renewal and tumorigenicity of medulloblastoma stem cells. *Stem Cells* **31**, 1266-1277, doi:10.1002/stem.1401 (2013).
66 Ismail, I. H., Andrin, C., McDonald, D. & Hendzel, M. J. BMI1-mediated histone ubiquitylation promotes DNA double-strand break repair. *J Cell Biol* **191**, 45-60, doi:10.1083/jcb.201003034 (2010).
67 Marechal, A. & Zou, L. DNA damage sensing by the ATM and ATR kinases. *Cold Spring Harb Perspect Biol* **5**, doi:10.1101/cshperspect.a012716 (2013).
68 Ginjala, V. *et al.* BMI1 is recruited to DNA breaks and contributes to DNA damage-induced H2A ubiquitination and repair. *Mol Cell Biol* **31**, 1972-1982, doi:10.1128/MCB.00981-10 (2011).
69 Facchino, S., Abdouh, M., Chatoo, W. & Bernier, G. BMI1 confers radioresistance to normal and cancerous neural stem cells through recruitment of the DNA damage response machinery. *J Neurosci* **30**, 10096-10111, doi:10.1523/JNEUROSCI.1634-10.2010 (2010).
70 Singh, A. & Settleman, J. EMT, cancer stem cells and drug resistance: an emerging axis of evil in the war on cancer. *Oncogene* **29**, 4741-4751, doi:10.1038/onc.2010.215 (2010).
71 Yang, M. H. *et al.* Bmi1 is essential in Twist1-induced epithelial-mesenchymal transition. *Nat Cell Biol* **12**, 982-992, doi:10.1038/ncb2099 (2010).
72 Song, L. B. *et al.* The polycomb group protein Bmi-1 represses the tumor suppressor PTEN and induces epithelial-mesenchymal transition in human nasopharyngeal epithelial cells. *J Clin Invest* **119**, 3626-3636, doi:10.1172/JCI39374 (2009).
73 Cao, L. *et al.* BMI1 as a novel target for drug discovery in cancer. *J Cell Biochem* **112**, 2729-2741, doi:10.1002/jcb.23234 (2011).
74 Bommi, P. V., Dimri, M., Sahasrabuddhe, A. A., Khandekar, J. & Dimri, G. P. The polycomb group protein BMI1 is a transcriptional target of HDAC inhibitors. *Cell Cycle* **9**, 2663-2673, doi:10.4161/cc.9.13.12147 (2010).
75 Jung, J. W. *et al.* Histone deacetylase controls adult stem cell aging by balancing the expression of polycomb genes and jumonji domain containing 3. *Cell Mol Life Sci* **67**, 1165-1176, doi:10.1007/s00018-009-0242-9 (2010).
76 Kaneta, Y. *et al.* Identification of BMI1 Promoter Inhibitors from Beaumontia murtonii and Eugenia operculata. *J Nat Prod* **80**, 1853-1859, doi:10.1021/acs.jnatprod.7b00138 (2017).
77 Bansal, N. *et al.* BMI-1 Targeting Interferes with Patient-Derived Tumor-Initiating Cell Survival and Tumor Growth in Prostate Cancer. *Clin Cancer Res* **22**, 6176-6191, doi:10.1158/1078-0432.CCR-15-3107 (2016).
78 Bartucci, M. *et al.* Synthesis and Characterization of Novel BMI1 Inhibitors Targeting Cellular Self-Renewal in Hepatocellular Carcinoma. *Target Oncol*, doi:10.1007/s11523-017-0501-x (2017).

79 Voncken, J. W. *et al.* Chromatin-association of the Polycomb group protein BMI1 is cell cycle-regulated and correlates with its phosphorylation status. *J Cell Sci* **112 (Pt 24)**, 4627-4639 (1999).
80 Voncken, J. W. *et al.* MAPKAP kinase 3pK phosphorylates and regulates chromatin association of the polycomb group protein Bmi1. *J Biol Chem* **280**, 5178-5187, doi:10.1074/jbc.M407155200 (2005).
81 Kreso, A. *et al.* Self-renewal as a therapeutic target in human colorectal cancer. *Nat Med* **20**, 29-36, doi:10.1038/nm.3418 (2014).
82 Yong, K. J. *et al.* Targeted BMI1 inhibition impairs tumor growth in lung adenocarcinomas with low CEBPalpha expression. *Sci Transl Med* **8**, 350ra104, doi:10.1126/scitranslmed.aad6066 (2016).
83 Bolomsky, A., Schlangen, K., Schreiner, W., Zojer, N. & Ludwig, H. Targeting of BMI-1 with PTC-209 shows potent anti-myeloma activity and impairs the tumor microenvironment. *J Hematol Oncol* **9**, 17, doi:10.1186/s13045-016-0247-4 (2016).
84 Sahasrabuddhe, A. A., Dimri, M., Bommi, P. V. & Dimri, G. P. betaTrCP regulates BMI1 protein turnover via ubiquitination and degradation. *Cell Cycle* **10**, 1322-1330, doi:10.4161/cc.10.8.15372 (2011).
85 Strebhardt, K. Multifaceted polo-like kinases: drug targets and antitargets for cancer therapy. *Nat Rev Drug Discov* **9**, 643-660, doi:10.1038/nrd3184 (2010).
86 Strebhardt, K. & Ullrich, A. Targeting polo-like kinase 1 for cancer therapy. *Nat Rev Cancer* **6**, 321-330, doi:10.1038/nrc1841 (2006).
87 Dimri, M., Cho, J. H., Kang, M. & Dimri, G. P. PLK1 inhibition down-regulates polycomb group protein BMI1 via modulation of the miR-200c/141 cluster. *J Biol Chem* **290**, 3033-3044, doi:10.1074/jbc.M114.615179 (2015).
88 van Lohuizen, M., Frasch, M., Wientjens, E. & Berns, A. Sequence similarity between the mammalian bmi-1 proto-oncogene and the Drosophila regulatory genes Psc and Su(z)2. *Nature* **353**, 353-355, doi:10.1038/353353a0 (1991).
89 Qian, T., Lee, J. Y., Park, J. H., Kim, H. J. & Kong, G. Id1 enhances RING1b E3 ubiquitin ligase activity through the Mel-18/Bmi-1 polycomb group complex. *Oncogene* **29**, 5818-5827, doi:10.1038/onc.2010.317 (2010).
90 Koppens, M. & van Lohuizen, M. Context-dependent actions of Polycomb repressors in cancer. *Oncogene* **35**, 1341-1352, doi:10.1038/onc.2015.195 (2016).
91 Lessard, J., Baban, S. & Sauvageau, G. Stage-specific expression of polycomb group genes in human bone marrow cells. *Blood* **91**, 1216-1224 (1998).
92 Kajiume, T. *et al.* Reciprocal expression of Bmi1 and Mel-18 is associated with functioning of primitive hematopoietic cells. *Exp Hematol* **37**, 857-866 e852, doi:10.1016/j.exphem.2009.04.011 (2009).
93 Oguro, H. *et al.* Poised lineage specification in multipotential hematopoietic stem and progenitor cells by the polycomb protein Bmi1. *Cell Stem Cell* **6**, 279-286, doi:10.1016/j.stem.2010.01.005 (2010).
94 Wang, W. *et al.* Analysis of Mel-18 expression in prostate cancer tissues and correlation with clinicopathologic features. *Urol Oncol* **29**, 244-251, doi:10.1016/j.urolonc.2009.02.004 (2011).

95 Wang, W. *et al.* The novel tumor-suppressor Mel-18 in prostate cancer: its functional polymorphism, expression and clinical significance. *Int J Cancer* **125**, 2836-2843, doi:10.1002/ijc.24721 (2009).
96 Guo, W. J. *et al.* Mel-18 acts as a tumor suppressor by repressing Bmi-1 expression and down-regulating Akt activity in breast cancer cells. *Cancer Res* **67**, 5083-5089, doi:10.1158/0008-5472.CAN-06-4368 (2007).
97 Tao, J. *et al.* Expression and clinicopathological significance of Mel-18 mRNA in colorectal cancer. *Tumor Biol* **35**, 9619-9625, doi:10.1007/s13277-014-2220-6 (2014).
98 Riis, M. L. *et al.* Molecular profiles of pre- and postoperative breast cancer tumors reveal differentially expressed genes. *ISRN Oncol* **2012**, 450267, doi:10.5402/2012/450267 (2012).
99 Zhang, X. W. *et al.* BMI1 and Mel-18 oppositely regulate carcinogenesis and progression of gastric cancer. *Mol Cancer* **9**, 40, doi:10.1186/1476-4598-9-40 (2010).
100 Lu, Y. W., Li, J. & Guo, W. J. Expression and clinicopathological significance of Mel-18 and Bmi-1 mRNA in gastric carcinoma. *J Exp Clin Cancer Res* **29**, 143, doi:10.1186/1756-9966-29-143 (2010).
101 Tetsu, O. *et al.* mel-18 negatively regulates cell cycle progression upon B cell antigen receptor stimulation through a cascade leading to c-myc/cdc25. *Immunity* **9**, 439-448 (1998).
102 Guo, W. J., Datta, S., Band, V. & Dimri, G. P. Mel-18, a polycomb group protein, regulates cell proliferation and senescence via transcriptional repression of Bmi-1 and c-Myc oncoproteins. *Mol Biol Cell* **18**, 536-546, doi:10.1091/mbc.E06-05-0447 (2007).
103 Kanno, M., Hasegawa, M., Ishida, A., Isono, K. & Taniguchi, M. mel-18, a Polycomb group-related mammalian gene, encodes a transcriptional negative regulator with tumor suppressive activity. *EMBO J* **14**, 5672-5678 (1995).
104 Lee, J. Y. *et al.* Loss of the polycomb protein Mel-18 enhances the epithelial-mesenchymal transition by ZEB1 and ZEB2 expression through the downregulation of miR-205 in breast cancer. *Oncogene* **33**, 1325-1335, doi:10.1038/onc.2013.53 (2014).
105 Guo, B. H. *et al.* Low expression of Mel-18 predicts poor prognosis in patients with breast cancer. *Ann Oncol* **21**, 2361-2369, doi:10.1093/annonc/mdq241 (2010).
106 Park, J. H. *et al.* Loss of Mel-18 induces tumor angiogenesis through enhancing the activity and expression of HIF-1alpha mediated by the PTEN/PI3K/Akt pathway. *Oncogene* **30**, 4578-4589, doi:10.1038/onc.2011.174 (2011).

Chapter 4: BMI1 is a therapeutic target in recurrent medulloblastoma

This chapter is an original published article presented in its published format in *Oncogene* available at https://www.nature.com/articles/s41388-018-0549-9

Bakhshinyan, D., C. Venugopal, A. A. Adile, N. Garg, B. Manoranjan, R. Hallett, X. Wang, S. Mahendram, P. Vora, T. Vijayakumar, M. Subapanditha, M. Singh, M. M. Kameda-Smith, M. Qazi, N. McFarlane, A. Mann, O. A. Ajani, B. Yarascavitch, V. Ramaswamy, H. Farooq, S. Morrissy, L. Cao, N. Sydorenko, R. Baiazitov, W. Du, J. Sheedy, M. Weetall, Y. C. Moon, C. S. Lee, J. M. Kwiecien, K. H. Delaney, B. Doble, Y. J. Cho, S. Mitra, D. Kaplan, M. D. Taylor, T. W. Davis and S. K. Singh (2018). "BMI1 is a therapeutic target in recurrent medulloblastoma." *Oncogene*. doi:10.1038/s41388-018-0549-9

In this manuscript, we used stem cell assays, patient-derived human-mouse xenograft (PDX) models, and genomic and bioinformatic profiling of recurrent human MB lines and patient-derived samples to elucidate the role of BMI1 in driving recurrent MB. Through a collaborative industry partnership, we obtained access to BMI1 small molecule inhibitors, PTC-028 that was used for *in vitro, ex vivo* and *in vivo* treatment of recurrent patient-derived MB stem cells, and PTC-596 that was used for *in vivo* studies. *In vivo* self-renewal deficits in MB cells caused by post-translational targeting of BMI1, led to significant reduction in tumor burden, extent of spinal metastases and tumor initiation ability of recurrent MB cells upon re-transplantation of PTC-028 treated cells into secondary

recipient mouse brains. Although, both mouse and human neural stem cells (NSCs) express BMI1 and are mildly sensitive to BMI1 inhibitors, no significant toxicity was observed in either mouse or human NSCs upon PTC-028 treatment, at doses relevant for MB cells. This study provided extensive evidence of an efficacious therapy for relapsed and treatment-refractory, metastatic and recurrent solid malignancy through post-translational inhibition of BMI1.

BMI1 is a therapeutic target in recurrent medulloblastoma

David Bakhshinyan[1,2] Hon BSc, Chitra Venugopal[1,3] PhD, Ashley A. Adile[1,2] Hon BSc, Neha Garg[1,3] PhD, Branavan Manoranjan[1,2,4] Hon BHSc, Robin Hallett[5] PhD, Xin Wang[6,7] Hon BHSc, Sujeivan Mahendram[1,3] MSc, Parvez Vora[1,3] PhD, Thusyanth Vijayakumar[1,2] BHSc, Minomi Subapanditha[1,3] BSc, Mohini Singh[1,2] BSc, Michelle Masayo Kameda-Smith[1,2,3] MBChB, Maleeha Qazi[1,2] BSc, Nicole McFarlane[1,3], Aneet Mann[1] Hon BHSc, Olufemi A. Ajani[3] MD, Blake Yarascavitch[3] MD, Vijay Ramaswamy[6,8] PhD, Hamza Farooq[6,7] MSc, Sorana Morrissy[8] PhD, Liangxian Cao[10] PhD, Nadiya Sydorenko[10] PhD, Ramil Baiazitov[10] PhD, Wu Du[10] PhD, Josephine Sheedy[10] PhD, Marla Weetall[10] PhD, Young-Choon Moon[10] PhD, Chang-Sun Lee[10] PhD, Jacek M. Kwiecien[11,12] JM, DVM, MSC, PhD, Kathleen H. Delaney[11] KH, DVM, Brad Doble[1,2] PhD, Yoon-Jae Cho[13, 14] MD PhD, Siddhartha Mitra[13,14] MD PhD, David Kaplan[5,15] PhD, Michael D. Taylor[7,9] MD PhD, Thomas W. Davis[10] PhD, and Sheila K. Singh*[1,2,3,4] MD, PhD

[1]McMaster Stem Cell and Cancer Research Institute, McMaster University, Hamilton, ON, L8S 4L8, Canada

Departments of [2]Biochemistry and Biomedical Sciences and [3]Surgery, Faculty of Health Sciences, McMaster University, Hamilton, ON, L8S 4L8, Canada

[4]Michael G. DeGroote School of Medicine, McMaster University, Hamilton, ON, L8S 4L8, Canada

[5]Cell Biology Program, The Hospital for Sick Children, University of Toronto, Toronto, ON, M5S 1A1, Canada

[6]Developmental & Stem Cell Biology Program, The Hospital for Sick Children, University of Toronto, Toronto, ON, M5S 1A1, Canada

[7]Department of Laboratory Medicine and Pathobiology, University of Toronto, Toronto, ON, M5S 1A1, Canada

[8]Division of Haematology/Oncology, Hospital for Sick Children, Toronto, ON, M5G 1X8, Canada

[9]Division of Neurosurgery, Hospital for Sick Children, Toronto, ON, M5G 1X8, Canada

[10]PTC Therapeutics, 100 Corporate Court, South Plainfield, NJ, 07080-2400, USA

[11]Department of Pathology and Molecular Medicine, McMaster University, Hamilton, ON, L8S 4L8, Canada

[12]Department of Clinical Pathomorphology, Medical University of Lublin, Poland

[13]Department of Neurology and Neurological Sciences, Stanford University School of Medicine, Stanford, CA, 94305, USA

[14]Department of Neurosurgery, Stanford University School of Medicine, Stanford, CA, 94305, USA

[15]Department of Molecular Genetics, University of Toronto, Toronto, ON, M5G 1X8, Canada

***CORRESPONDING AUTHOR**

Sheila K. Singh, MD, PhD, FRCS(C)

Associate Professor of Pediatric Neurosurgery,

Department of Surgery, McMaster Children's Hospital,

Scientist, McMaster Stem Cell & Cancer Research Institute

MDCL 5027, 1280 Main Street West, Hamilton, ON, L8S 4K1, Canada

T: 905-521-2100 x75237 F: 905-521-992 Email: ssingh@mcmaster.ca

ABSTRACT:

Medulloblastoma (MB) is the most frequent malignant pediatric brain tumor, representing 20% of newly diagnosed childhood central nervous system malignancies. Although, advances in multimodal therapy yielded a 5-year survivorship of 80%, MB still accounts for the leading cause of childhood cancer mortality. In this work, we describe the epigenetic regulator BMI1 as a novel therapeutic target for the treatment of recurrent human Group 3 MB, a childhood brain tumor for which there is virtually no treatment option beyond palliation. Current clinical trials for recurrent MB patients based on genomic profiles of primary, treatment-naïve tumors will provide limited clinical benefit since recurrent metastatic MBs are highly genetically divergent from their primary tumor. Using a small molecule inhibitor against BMI1, PTC-028, we were able to demonstrate complete ablation of self-renewal of MB stem cells *in vitro*. When administered to mice xenografted with patient tumors, we observed significant reduction in tumor burden in both local and metastatic compartments and subsequent increased survival, without neurotoxicity. Strikingly, serial *in vivo* re-transplantation assays demonstrated a marked reduction in tumor initiation ability of recurrent MB cells upon re-transplantation of PTC-028 treated cells into secondary recipient mouse brains. As Group 3 MB is often metastatic and uniformly fatal at recurrence, with no current or planned trials of targeted therapy, an efficacious targeted agent would be rapidly transitioned to clinical trials.

INTRODUCTION:

Medulloblastoma (MB) is the most frequent malignant pediatric brain tumor, representing 20% of newly diagnosed childhood central nervous system malignancies. Although, advances in multimodal therapy yielded a 5-year survivorship of 80%, MB still accounts for the leading cause of childhood cancer mortality(Ellison, 2010; Huse and Holland, 2010). Treatment-induced morbidity and long-term clinical sequelae leading to poor quality of life is common in surviving children(Taylor et al., 2012). Limited ability of clinico-pathological parameters in predicting treatment response have propelled the use of genomic platforms to re-conceptualize MB into four major molecular subgroups; each distinct in terms of prognosis and predicted therapeutic response(Cavalli et al., 2017; Cho et al., 2011a; Kool et al., 2008; Northcott et al., 2011; Pomeroy et al., 2002; Schwalbe et al., 2017; Thompson et al., 2006). Metastatic disease characterized by leptomeningeal spread and dissemination *via* cerebrospinal fluid is seen in up to 40% of patients at the time of diagnosis and at recurrence in Group 3 and 4 patients and leads to the worst clinical outcome with a 5-year survivorship of approximately 50% of patients with Group 3 MB(Taylor et al., 2012). The salvage rate of recurrent MB is even more dismal at less than 10%, irrespective of the treatment modality used(Ramaswamy et al., 2013). Consequently, current treatment for MB patients who present with recurrent metastatic lesions is limited to palliative care, and the development of novel therapeutics for these patients is further encumbered by rare clinical opportunities in which specimens may be obtained from relapsed patients.

Stemness factors have been shown to contribute to treatment failure and relapse, irrespective of whether these determinants are present in the bulk tumor or rare clonal cells(Reya et al., 2001). BMI1, the epigenetic regulator of fate determination and proliferation, has been implicated in the maintenance of stemness in a number of normal and malignant cell populations(Sauvageau and Sauvageau, 2010; Sparmann and van Lohuizen, 2006). BMI1 functions as a component of the Polycomb Repressive Complex 1 (PRC1), to repress the *Ink4a/Arf* and *p21* loci(Alkema et al., 1993). Recent studies implicated BMI1 in the pathogenesis of brain tumors such as glioma(Bruggeman et al., 2007; Gargiulo et al., 2013) and MB(Leung et al., 2004; Wang et al., 2012), with recent work identifying BMI1 as a novel therapeutic target in solid tumors(Kreso et al., 2014; Yong et al., 2016). Intriguingly, an 11-gene stemness signature representing a conserved BMI1-regulated transcriptional network has been shown to reliably predict poor treatment response, recurrence, metastatic potential, and death in eleven cancer models, including MB(Glinsky et al., 2005). The marked propensity for metastatic dissemination uniformly seen in a wide range of organs suggests the presence of a conserved BMI1-driven pathway engaged in clonal cell populations that is amenable to therapeutic targeting.

In this manuscript, we describe BMI1 as a novel therapeutic target for treatment of recurrent human Group 3 medulloblastoma. Using a small molecule inhibitor targeting BMI1, PTC-028, we significantly reduced stem cell properties of recurrent Group 3 MB lines *in vitro* and *in vivo*. Further experiments revealed that at the doses relevant to MB cells, BMI1 inhibitor spared the self-renewal properties of human neural stem cells while effectively targeting MB cells. As future MB subgroup-specific clinical trials will most

likely begin with relapsed patients, therapeutic targets identified from the comparative analyses between primary and matched-recurrent tumors offer the greatest clinical yield and may be readily translated to patient bedside.

RESULTS:

Increased BMI1 expression predicts MB recurrence and poor patient survival

Since prior work has identified a BMI1-driven gene signature (Glinsky signature) that predicts metastasis and tumor progression across eleven cancer subtypes(Glinsky et al., 2005), we decided to probe for this signature in a publicly available MB genomics database. We found elevated levels of the BMI1 driven gene signature were associated with both reduced relapse-free and overall survival (Figure 1a). In a multivariable analysis that included subtype, age, and metastasis (M)-status, only the BMI1 signature was an independent predictor of overall survival, although subtype and M-status also trended with outcome (Figure 1b). Due to the pivotal role of BMI1 in tumor pathogenesis, we sought to explore the role of this pathway in the context of MB recurrence. We compiled curated databases (BROAD Molecular Signatures Database V5.0) pertaining to BMI1 and its associated Polycomb group complex into a new BMI1-driven signature (Supplementary Table 1), and undertook preliminary gene set enrichment analysis of a cohort of twelve matched primary and recurrent patients MBs(Wang et al., 2015). Gene expression profile of a human MB primary-recurrent dataset revealed spinal metastases to significantly enrich for BMI1 pathway genes (Figure 1c).

Since upregulation of BMI1 has been shown to confer radioresistance in brain tumor cells(Facchino et al., 2010), we set out to investigate the effects of *in vitro* chemoradiotherapy on MB cells, by designing a two-week *in vitro* chemoradiotherapy treatment plan, resembling the existing COG (Children's Oncology Group) protocol ACNS0332 used for treatment of newly diagnosed high-risk MBs (Supplementary Figure

1a). Primary MB cell line, D425, was used to optimize radiation and chemotherapy dosages (Supplementary Figure 1b-d). When cells were harvested post-treatment to assess BMI1 levels, we found both BMI1 transcript and protein expression levels were significantly enhanced in treated cells (Figure 1d-e). mRNA expression of other stem cell markers such as *CD133*, *FOXG*1 *FUT4*, and *SOX2* and was also increased after chemoradiotherapy (Supplementary Figure 1e). To investigate the *in vivo* significance of upregulation of BMI1 in recurrent MB, we undertook intracranial xenografting of a therapy-naïve Group 3 MB cell line (D425) into NOD SCID mice, followed by treatment with standard chemoradiotherapy. Despite the fact that untreated mice formed larger tumors and treated mice presented an expected decrease in tumor size (Figure 1f, left panels), we observed a marked increase in BMI1 levels in treatment-refractory tumor cells (Figure 1f, right panels, Supplementary Figure 1f).

Targeting BMI1 using small molecule inhibitors

PTC-028 was established through lead identification and chemical modification of PTC-209, a small molecule BMI1 inhibitor (PTC Therapeutics) that showed efficacy in targeting self-renewal of colorectal cancer-initiating cells(Kreso et al., 2014). It was found that changing the 2-amino-thiazole middle ring contained within PTC-209 to a 2-amino-pyrazine provided analogs with potency increased by 2-3 orders of magnitude. Furthermore, the replacement of the imidazolopyridine (or imidazolopyrimidine) right flank with benzimidazole provided analogs with increased oral bioavailability. Introduction of fluorination on the benzimidazole led to the discovery of PTC-028 (Supplementary Figure 2a). The IC_{50} of PTC-028 in normal hNSCs (human neural stem cells) was found to

be 6.7μM (Hill Slope = -1.512), which was higher than IC_{50} values determined in the two recurrent MB lines (SU_MB002 = 1.6μM, Hill Slope = -1.109; D458 = 4.5μM; Hill Slope = -1.001) (Figure 2a).

The BMI1 inhibitors of this class cause hyper-phosphorylation and subsequent degradation of BMI1 protein as measured by both Western blot analysis (Figure 2b and Supplementary Figure 2b). The canonical PRC1 mediated target gene repression is achieved through ubiquitination of Lysine 119 residue of histone 2A (uH2AK119)(Wang et al., 2004). Using PTC-028 we were able to demonstrate the selective reduction of PRC1 activity through the reduction of global Lys119 ubiquitinated H2A levels in SU_MB002 and D458 cells but not in hNSCs (Figure 2b). In order to test the specificity of the inhibitor to BMI1, we treated SU_MB002 cells with bortezomib, a reversible proteasome inhibitor with and without PTC-028. It was intriguing to observe that even in the presence of bortezomib, treatment of MB cells with PTC-028 resulted in marked reduction of BMI1 protein levels (Supplementary Figure 2c).

The modified inhibitor, PTC-028 was tested in our model systems of recurrent MB and normal hNSCs. Similar to our *BMI1* knockdown (KD) studies (Supplementary Figure 3), *in vitro* treatment with PTC-028 reduced the proliferative capacity and self-renewal, as measured by the decrease in number and frequency of spheres formed in recurrent Group 3 MB cell lines SU_MB002 (Figure 2c-e) and D458 (Figure 2f-h). To further understand the mechanism of reduction in cell proliferative capacity after treatment with BMI1 small molecule inhibitor, we undertook cell cycle studies of treated MB cells. Treatment of MB cells with PTC-028 for 72 hours led to significant reduction of the cell populations in the

S-phases in both SU_MB002 and D458 (Figure 2i). Since BMI1 has the ability to activate cell cycle by repressing the expression of several cell cycle regulators including *p16Ink4*, *p21* and *HOXA9*, we analyzed the mRNA expression levels of these genes in MB cells that were treated with PTC-028. The *in vitro* treatment with PTC-028 and subsequent BMI1 degradation, resulted in an increased expression of all three genes in both recurrent MB lines, SU_MB002 (Figure 2j) and D458 (Figure 2k), indicating the release from the BMI1-mediated repression.

PTC-028 spares human neural stem cells, while inhibiting growth of MB

BMI1 plays a crucial role in regulating self-renewal of both hNSCs and MB stem cells. Previous experiments indicated that PTC-209 spares primary human hematopoietic stem cells while targeting colorectal cancer-initiating cells(Kreso et al., 2014), suggesting a potential therapeutic window for BMI1-targeted therapies. Similar to the *in vitro* studies done in MB cells, we treated hNSCs with PTC-028 at a previously established therapeutically effective dose for MB cells. Functionally, although treatment of hNSCs with high dose of PTC-028 led to a decrease in proliferative potential (Supplementary Figure 4a, d) their ability to self-renew was spared (Supplementary Figure 4b, c, e, f). Unlike MB cells, PTC-028 treated hNSCs were able to remain a fraction of cells in S-phase of the cell cycle, despite an evident increase in cells undergoing apoptosis (Supplementary Figure 4g).

To rule out cytotoxic effects on hNSCs after treatment with PTC-028, we performed a mixing experiment of recurrent MB cells, SU_MB002 or D458 tagged with GFP and non-GFP-expressing hNSCs (Figure 3a). Cell populations were mixed at a ratio of 1:1 and then

treated with either DMSO or PTC-028, at a dose equivalent to IC_{80} for SU_MB002 (5.45μM) or D458 (17.9μM) for 72 hours. After 72 hours, cells were analyzed using flow cytometry to assess the differential activity of PTC-028 in MB cells and hNSCs. Although doses of BMI1 inhibitor used were comparable or higher than the IC_{50} values calculated for hNSCs, BMI1 inhibition resulted in reduced percentage of live MB cells while sparing unlabeled hNSCs (Figure 3b-c). The initial results were confirmed by performing a reverse experiment, mixing GFP-labelled hNSCs and unlabeled MB cells. When treated with DMSO, MB cells were able to propagate unhindered and constitute a vast majority of the analyzed cell population, however, when treated with PTC-028, the growth of MB cells was inhibited, allowing for expansion of hNSCs (Supplementary Figure 4h). A similar experiment was performed employing the frequently used chemotherapeutic agent, cisplatin. Unlike PTC-028, treatment with cisplatin (IC_{50}: SU_MB002 - 614.4nM, Hill Slope = -0.7628; hNSCs - 416.2nM, Hill Slope = -4.925) resulted in continuous expansion of GFP-positive MB cells and inhibited growth of hNSCs (Figure 3d-e). This data suggests that in contrast to conventional chemotherapy drug used for treatment of MB, BMI1 inhibitor treatment spares hNSCs, which can potentially translate into a reduced neurotoxicity in patients.

BMI1 inhibitor treatment selectively reduces expression of target genes driving tumor growth and aggressiveness in MB cells, with minimal effect on hNSC target gene expression

To further understand the mechanisms by which PTC-028 affects MB, we have undertaken a gene expression profiling of PTC-028 treated D425, D458 and hNSCs. We

found that both MB samples displayed a larger number of differentially expressed genes when compared to NSCs (Supplementary Fig 5a), underscoring enhanced drug activity in MB samples compared to NSCs. Gene expression enrichment analysis (GSEA) using two BMI1 signatures present within the MSigDB C6 oncogenic signatures revealed downregulation of BMI1 signaling in response to PTC-028 in MB samples compared to DMSO treated control samples (Figure 4a). We annotated enrichment maps from GSEA run with the MSigDB C2 based on broad agreement between the enriched gene sets, revealing PTC-028 induced increase in expression gene sets associated with TLR signaling and broad decrease in expression of gene sets associated with RNA metabolism, cell cycle, translation, and glucose metabolism (Supplementary Figure 5b). In addition to this broad level analysis, we completed GSEA with the MSigDB hallmark gene set, which revealed robust downregulation of MYC signaling, oxidative phosphorylation and glycolysis (Figure 4b and Supplementary Table 2). As expected, these changes were not significant in NSCs (Supplementary Figure 5c). To test whether these changes were relevant to MB patients we completed survival analysis using the leading edge genes from the enriched hallmark gene sets as a signature indicating activity of the relevant pathway. In all cases, increased signaling activity was associated with lower survival in MB patients (Figure 4c). Taken together, our data suggests that BMI1 inhibitors reduce the aggressive and metastatic behavior of MB by downregulating key oncogenic pathways such as Myc, whose high expression often reflects a classic Group 3 MB with metastases at diagnosis(Taylor et al., 2012).

***In vivo* therapeutic targeting of BMI1**

Having established the role of BMI1 inhibitor *in vitro*, we set out to test the ability of PTC-028 to inhibit growth of human MB through both *ex vivo* and *in vivo* studies. Initial efficacy of the BMI1 inhibitor in animal models was validated though experiments measuring bioavailability and pharmacokinetics of PTC-028. Pharmacokinetic analysis following oral dosing of 10 mg/kg PTC-028 in 0.5% hydroxypropyl methyl cellulose (HPMC) suspension demonstrated that PTC-028 is orally bioavailable (Supplementary Figure 6). Tissue analysis taken from this study at 6 and 16 hours post-dose demonstrated that PTC-028 is taken up into tissues, including the brain, at comparable levels to those observed in the plasma (Supplementary Table 3). Pharmacodynamic analysis was conducted in nude mice bearing established subcutaneous HT1080 fibrosarcoma flank tumors. Tumor growth was reduced in mice treated with 10mg/kg PTC-028 either once a day for ten days or twice a day for four days (Supplementary Figure 6b). After 10 days, BMI1 levels were significantly reduced (Supplementary Figure 6c) in the treated group. The initial bioavailability study for MB brain tumor xenografts revealed that the highest amount of PTC-028 after 4-hour post oral gavage is in plasma and in MB tumors (Supplementary Figure 6d). Furthermore, after completion of 6-dose (3 doses/week on alternating days for 2 weeks) treatment regimen with PTC-028, there was no significant weight loss (Supplementary Figure 6e) and no cytotoxicity observed in brains, lungs, heart, kidneys and liver when comparing control and PTC-028 treated mice (Supplementary Figure 7). Histological analysis of the brain from control and PTC-028- treated mice revealed large masses of large, pleomorphic tumor cells in the subarachnoid space and in the ventricles compressing the brain tissue and also scattered intracerebral masses

throughout the brain. Often, at the edge of a tumor mass there was an active infiltration of the adjacent brain tissue by individual or small clusters of cancer cells. Although cells with karyorrhectic nucleus and shrunken hyper-eosinophilic cytoplasm were rarely scattered in the masses of control mice, such cells were numerous in the tumor masses of PTC-028 treated mice. Cell death was not observed in the brain tissue adjacent to tumor masses in control and PTC-028 treated mice. To investigate whether PTC-028 has an effect on murine BMI1, we compared BMI1 levels in DMSO and PTC-028 treated mouse NSCs (Supplementary Figure 6f). Owing to the fact that hNSCs have higher IC_{50} values for PTC-028, we used high doses of the inhibitor for treatment of mNSCs. Similar to human MB cells, we observed a reduction in BMI1 protein levels post treatment with PTC-028, further confirming specificity of the drug to BMI1 in both human and mouse cells.

Since BMI1 is highly overexpressed in recurrent MB lines, we used D458 and SU_MB002 for *in vivo* studies. These cells are refractory to conventional chemoradiotherapy, but as they express high levels of BMI1, we hypothesized that the BMI1 inhibitor, PTC-028 would effectively target these cells, with the added advantage of excellent bioavailability through oral administration. The initial intracranial injections of PTC-028 or DMSO *ex vivo* treated D458 cells in varying cell numbers, ranging from 10,000 to 500,000 cells/mouse, resulted in a 60-80% reduction in tumor burden across all dilutions (Supplementary Figure 8a-b). Next, we initiated the two-week *in vivo* treatment protocol by administering either PTC-028 (10mg/kg dose, three times a week) or vehicle into NOD SCID mice intracranially xenografted with recurrent MB cells. Mice treated with PTC-028 showed a reduction in intracranial tumor burden and decreased metastatic leptomeningeal

dissemination to spines in both recurrent MB lines, SU_MB002 (Figure 5a-b) and D458 (Supplementary Figure 8c-d). Furthermore, mice engrafted with two recurrent cell lines and treated with PTC-028 also exhibited significant increase in survival (Figure 5c and Supplementary Figure 8e). The immunohistochemical staining of brain sections from both PTC-028 and vehicle treated mice revealed a reduction in BMI1 levels in the remaining tumor cells post treatment with PTC-028, further validating the on-target activity of the inhibitor (Figure 5d). Strikingly, through serial *in vivo* re-transplantation assays, we observed a marked reduction in tumor initiation ability of recurrent MB cells upon re-transplantation of PTC-028 treated cells into secondary recipient mouse brains (Figure 5e). These data illustrate the great potential of BMI1 inhibitors in effectively targeting treatment refractory disease in patients with recurrent and metastatic MB.

DISCUSSION:

Current clinical trials for recurrent MB patients who no longer tolerate or respond to risk-adapted therapy are based on the genomic profiles of primary, treatment-naïve tumors(Ramaswamy et al., 2013). These approaches are poised to be of limited clinical benefit for patients since recurrent Group 3 and 4 MBs, which often present as metastases, are highly genetically divergent from their primary tumor(Wu et al., 2012). The experimental approach taken in our study aimed at evaluating the therapeutic efficacy of novel small molecule inhibitor in models representative of recurrent Group 3 MB, and therefore should have immediate clinical implications for recurrent childhood MB, a tumor that is uniformly fatal and treated with palliation alone.

Our results establish BMI1 as a necessary factor that enables cells to adapt to current therapies and drive recurrence based on phenotypic differences in stemness. Primary MB cells that survived the *in vitro* and *in vivo* chemoradiotherapy protocols were found to be highly enriched in BMI1. Although the question of whether BMI1 expression is induced or cells with increased BMI1 expression are selected for through the course of chemoradiotherapy remains to be answered, it is evident that population of cells with high BMI1 expression contribute to tumor recurrence and represent a potential therapeutic target. Additional support for BMI1 in driving recurrence was observed using our prognostic BMI1 signature, which not only enriched for those patients most likely to relapse and succumb to their disease but also offered a phenotypic platform for assessing the efficiency at which candidate molecules impaired the self-renewal of primary and matched-recurrent MB cells (Figure 1). The maintenance of self-renewal potential by BMI1

and its role in promoting DNA damage repair enables the BTICs to evade chemoradiotherapy regiments and drive tumor recurrence. The continuous recruitment of BMI1 to the DNA double-strand breaks (DSBs) and subsequent promotion of DNA repair allows cells to contravene the effects of ionizing radiation and persist post-therapy(Ismail et al., 2010). Studies on CD133+ GBM cancer stem cells demonstrated that loss of BMI1-directed DNA DSB repair activity can re-sensitize the seemingly radiation resistant population of cells to radiotherapy and induce replicative senescence. PTC-028 selectively inhibited a conserved BMI1-regulated transcriptional network that maintained MB self-renewal (Figure 4), leading to notable abrogation of spinal metastases (Figure 5). Similar results were observed following short-term *ex vivo* treatment, which suggests MB cells are reliant on BMI1 to sustain tumor progression, clonal maintenance and metastatic dissemination (Supplementary Figure 8).

An important consideration is the effect of PTC-028 on normal human neural stem cells. In addition to hematopoietic and skeletal defects, $BMI1^{-/-}$ mice develop clinical manifestations of cerebellar disease such as progressive ataxic gait, balance disorders, tremors, and behavioral abnormalities(Leung et al., 2004). Histologically, the cerebellar cytoarchitecture in these mice contain a marked reduction in the cellularity of the granule and molecular layers suggesting a decrease in the mitotically active granule neuron precursor (GNP) population. We observed no changes in the self-renewal or proliferative capacity of post-natal human neural stem cells treated with PTC-028, indicating our therapeutic dose would have no noticeable effects on the normal central nervous system (Figure 3 and Supplementary Figure 4). Of note, in our work we transiently lowered BMI1

levels in xenografts and cell culture, whereas previous transgenic mouse studies analyzed the effects of complete BMI1 knockout during development and beyond, which may account for the observed differences. Given the detrimental neurocognitive effects of high-dose radiation in Group 3 MB patients our finding that PTC-028 does not impair the function of normal human neural stem cells provides further support for targeted inhibition of BMI1 as a high-yield therapeutic with limited effects on quality-of-life in both primary and recurrent Group 3 MB.

Changes in risk-adapted therapy for childhood MB resulted in a significant survival advantage over the past 20 years. The establishment of a robust molecular classification has paved the way for a more personalized treatment scheme. While, targeted therapies according to this molecular framework are currently underway for primary MB (NCT01878617), similar approaches have yet to be applied for the treatment of recurrent Group 3 MB. The failure of current cancer therapeutics, especially for Group 3 MB, may be attributed to a number of determinants such as clonal expansion based on cellular and genomic diversity(Wu et al., 2012), properties of stemness such as self-renewal(Pei et al., 2012), and the inability to effectively identify targets that act on multiple pathways of functional significance(Bandopadhayay et al., 2014). Our study describes the application of an inhibitor targeting BMI1, a chromatin modifier and epigenetic regulator of stemness, to a metastatic treatment-refractory pediatric brain tumor thought to be driven by a stem cell population. Through inhibiting a conserved BMI1-regulated transcriptional network, we reproducibly eradicated metastatic clones in two recurrent Group 3 MB patient lines; preclinical data that may drastically alter the treatment of tumors that are uniformly fatal

with conventional approaches. By considering cancer as a disease in which heterogeneous cell populations are carried forward from ontogeny into primary oncology and distal recurrence/metastasis, our therapeutic paradigm may be generally applied to several solid tumor malignancies. Emerging studies continue to conceptualize cancer as a disease driven by determinants of stemness(Chen et al., 2012) for which greater effort should be taken to target these phenotypic traits, as they may be the most influential processes in regulating tumor maintenance and relapse(Venugopal et al., 2015). Such approaches will yield immediate clinical impact as those patients who currently succumb to their illness often present with tumor recurrence and metastasis.

MATERIALS AND METHODS:

Cell Cultures

SU_MB002 was a kind gift from Dr. Yoon-Jae Cho that was derived at recurrence from a patient who received only chemotherapy and display expression markers of Group 3 MB(Facchino et al., 2010). SU_MB002 cells were propagated in NeuroCult Complete (NCC): NeuroCult^{TM} NS-A Basal Medium (Stemcell^{TM} technology #05750) supplemented with 50mL NeuroCult^{TM} Supplement, 20ng/mL EGF, 10ng/mL FGF, 0.1% heparin and 1% penicillin-streptomycin. Commercially available cell lines representing primary, therapy-naïve (D425) and recurrent (D458) Group 3 MB cell lines(He et al., 1991) were propagated in DMEM high glucose (Life Technologies# 11965-118) supplemented with 1% penicillin–streptomycin, and 20% FBS, but cultured in NCC for 48hours prior to experiments. Human fetal neural stem cells (hNSCs) were isolated using a previously described protocol(Venugopal et al., 2012b) and cultured in NeuroCult Complete medium. Mouse neural stem cells were isolated from E14 CD1 embryos and cultured *in vitro* using mouse specific NeuroCult Complete medium for 72 hours prior to experimentation.

In vitro chemoradiotherapy

Cells plated at a density of $1x10^6$ cells/mL were treated with a single dose of 2Gy radiation (Faxitron RX-650) and incubated for a week. Following incubation, cells were treated with a single dose of 200nM cisplatin and 2nM vincristine and incubated for an additional week. The doses were chosen based on IC_{50} values calculated using D425. At the third week, cells were analyzed by RT-qPCR and Western immunoblotting for BMI1 mRNA and protein levels respectively.

Real-time Quantitative PCR (RT-qPCR)

Total RNA was extracted using a Norgen Total RNA isolation kit and quantified using the NanoDrop Spectrophotometer ND-1000. Complementary DNA was synthesized from 1μg RNA by using qScript cDNA Super Mix (Quanta Biosciences) and a C1000 Thermo Cycler (Bio-Rad) with the following cycle parameters: 4min at 25°C, 30min at 42°C, 5min at 85°C, hold at 4°C. RT-qPCR was performed by using Perfecta SybrGreen (Quanta Biosciences) and CFX96 instrument (Bio-Rad). CFX Manager 3.0 software was used for quantification of gene expression and levels were normalized to GapDH, b-Actin or b2 microglobulin expression. Primers are listed in Supplementary Table 4.

Western immunoblotting (WB)

Denatured total protein (10μg) was separated using 10% sodium dodecyl sulphate–polyacrylamide gel electrophoresis and transferred to polyvinylidene fluoride membrane. Western blots were probed with anti-human BMI1 antibody (EMD Millipore, #05-637, 40kDA), anti-ubiquityl-histone 2A (Lys 119) antibody (Cell Signaling #8240, 23kDa), anti-histone 2A antibody (Cell Signaling #12349, 14kDa), anti-GapDH antibody (Abcam #ab8245, 37kDa) and anti-b-tubulin antibody (Abcam #ab6046, 50kDa). The secondary antibody was horseradish peroxidase conjugated goat anti-mouse IgG (Bio-Rad #1721011) or goat anti-rabbit IgG (Sigma #A0545). The bands were visualized using an Luminata^{TM} Forte Western HRP Substrate (Millipore) and chemicdoc. Western immunoblots were quantified with Image J software, and protein levels normalized to the loading control are provided in the respective figures.

Analoging effort to generate improved BMI1 inhibitor: PTC-028

PTC-028 (Fig. S2A) was discovered as a result of further optimization of PTC-209[3]. It was found that changing the thiazole middle core (such as in PTC-209) to a pyrazine middle core (such as in PTC-028) provided analogs with potency increased 2-3 orders of magnitude. Furthermore, the replacement of the imidazolopyridine (or imidazolopyrimidine) right flank with benzimidazole provided analogs with greatly increased oral bioavailability.

Synthesis of PTC-028

Compound A: 4-Trifluoromethylaniline (4.83g, 30mmol) and 2,6-dichloropyrazine (4.5g, 30mmol) were dissolved in DMF (50mL) and cooled to -78°C. To this solution was added 2.5M solution of sodium tert-pentoxide in THF (40mL, 100mmol). The reaction was gradually warmed to RT and reaction was completed as showed by LC-MS. Aqueous work up followed by chromatography gave the title compound as dark solid (7.08g) in 86% yield.

Compound B: To a MW tube was added Compound A (546mg, 2mmol), 1,2-difluoro-4,5-diaminobenzene (560mg, 4mmol), Pd2dba3 (100 mg, 0.1 mmol), X-Phos (100mg, 0.2mmol) and K3PO4 (1.27g, 6mmol) and DME (10mL). The mixture was heated under MW at 120°C for 1h. Reaction was completed as showed by LC-MS. Aqueous work up followed by chromatography (30% - 100% EtOAc/hexcane followed by 0% - 10% MeOH/EtOAc) gave the title compound as dark solid (627mg, 83% yield).

PTC-028: To the solution of Compound B (76mg, 0.2mmol) in MeCN (2mL) was added acetyl chloride (21mL, 0.3mmol). The reaction was stirred at RT for 10min, then heated by MW at 180°C for 10min. The reaction mixture was diluted with EtOAc and washed with NaHCO3 followed by brine. The ester layer was concentrated and purified by

chromatography to give the tile compound (32mg, 35% yield). 1H NMR (CDCl3, 500 MHz) d: 8.31 (1H, s), 8.13 (1H, s), 7.73 (2H, d, J = 8.6), 7.56 (2H, d, J = 8.6 Hz), 7.52 (1H, m), 7.31 (1H, m), 3.03 (2H, q, J = 7.5 Hz), 2.68 (3H, s), M+1, 406.

Treatment of MB cells with BMI1 inhibitor

1000 cells were plated in a 96-well plate in quadruplicates at a volume of 200µL/well with two-fold dilutions of BMI1 inhibitor from a starting concentration of 20µM and ending at 39nM. DMSO was used as a control. Three days after treatment, Presto Blue assay was performed as described in the cell proliferation assay. By plotting percent (%) cell viability versus log dilutions of the inhibitors, IC_{50} value was determined. Throughout the manuscript, IC_{50} concentration refers to the concentration of BMI1 inhibitor at which cell proliferation was reduced by 50%. IC_{80} values were calculated using the following formula:

$IC_{(F)} = [(100-F)/F]^{1/HS} \times IC_{50}$ (Where F = percent reduction of proliferation, HS = Hill Slope).

Cell sorting and analysis using flow cytometry

Tumorspheres were enzymatically dissociated to single cells with Liberase/Blendzyme (Roche). Intracellular staining was performed using BD Cytofix/CytopermTM fixation/permeabilisation kit (BD Biosciences) and dead cells excluded using LIVE/DEAD® Fixable Near-IR Dead Cell Stain Kit (Invitrogen). The viability dye 7AAD was used to exclude dead cells for surface staining and sorting. BD™ CompBeads were used to establish compensation values where required.

Cell proliferation assay

Single cells were plated in 96-well plates, at a density of 1,000 cells/200µL per well in quadruplicate for each sample and incubated for four days. 20µL of Presto Blue (Life technologies), a fluorescent cell metabolism indicator, was added to each well approximately 4 hours prior to the readout time point. Fluorescence was measured using FLUOstar Omega Fluorescence 556 Microplate reader (BMG LABTECH) at excitation and emission wavelengths of 540–570 nm respectively. Readings were analyzed by Omega software.

***In vitro* limiting dilution analysis and self-renewal assay**

For *in vitro* limiting dilution analysis, cells were sorted in quadruplicates into 96 well plate using Moflo XDP at the cell densities raging from 1000cells/well to 1cell/well. Unlike SU_MB002, D458 cells do not readily form spheres in culture hence we performed colony forming assay, where the cells were embedded into 0.35% soft agar, promptly after the sort. The number of wells without any spheres/colonies after 4 days were scored and fraction of negative wells was plotted against the number of cells per well. The number of cells with the fraction of negative wells equal to 0.37 is the dilution with 1 self-renewing unit(Tropepe et al., 1999). Self-renewal assay was performed by counting the number of spheres formed in the wells containing 200cells/well.

Cell cycle analysis:

The cell cycle analyses on D458 and SU_MB002 cells after PTC-028 treatment or lentiviral mediated KD of BMI1 were performed using APC BrdU Flow Kit (BD Biosciences #552598). No modifications to the protocol were made.

BMI1 immunohistochemical staining

4mm formalin-fixed paraffin-embedded sections were dewaxed in 5 changes of xylene and brought down to water through graded alcohols. Antigen retrieval or unmasking procedures were applied, if necessary (see below for H.I.E.R). Endogenous peroxidase and biotin activities were blocked respectively, using 3% hydrogen peroxide and avidin/biotin blocking kit (Vector #SP-2001). Serum block was applied for 10min with 10% normal serum from the species where the secondary antibody is made in. Sections were drained and incubated accordingly at room temperature with the appropriate primary antibody using conditions previously optimized(Wang et al., 2012). Sections were incubated for an hour with BMI1 antibody (R&D # MAB33342) at 1:500 dilution. This was followed with a biotin labeled secondary (Vector labs) for 30min and horseradish peroxidase-conjugated ultrastreptavidin labeling reagent (ID labs.) for 30min. After washing well in TBS (Tris-bufferd saline), color development was done with freshly prepared DAB (DAKO #K3468). Finally, sections were counterstained lightly with Mayer's Hematoxylin, dehydrated in alcohols, cleared in xylene and mounted in Permount (Fisher #SP15-500).

H.I.E.R.: Heat Induced Epitope Retrieval refers to microwaving tissue sections in a medium for antigen retrieval. For this antibody we use a Tris-EDTA Buffter at pH 9.0 and the solution and tissue sections are being heated up inside a microwavable pressure cooker. After the pressure is built up inside the cooker (exact time will depend on the actual set-up), boiling is maintained for another 3min with a lower setting. The cooker is then removed from the microwave oven and allowed to cool off on the bench for 20min. Sections are then removed from the hot buffer into warm water and then rinsed in TBS.

The IHC slides were scanned using Aperio ScanScope slide scanner (Aperio Technologies, CA), and the images were analyzed using Positivity Pixel Count 9.0 algorithm within ImageScope software (Aperio Technologies, CA).

Lentiviral KD studies

We obtained lentiviral constructs CS-H1-BMI1shRNA-EF-1-EGFP (shBmi1-1) expressing shRNA targeting BMI1 (5' GAGAAGGAATGGTCCACTT 3') and CS-HI Luc shRNA-EF-1-EGFP expressing the target sequence for Luciferase as a negative control (5'ACGCTGAGTACTTCGAAAT3'), as a kind gift from Professor Atsushi Iwama (Chiba University, Japan). Lentiviral pLKO.1 vectors shBmi1-2 expressing shRNAs targeting human BMI1 (5'CCTAATACTTTCCAGATTGAT3'), and the control vector, shGFP (5'ACAACAGCCACAACGTCTATA3'), were gifts from Dr. Jason Moffat. Stable cell lines with BMI1 KD or over expression were generated by transduction followed by maintenance of cultures with zeocin (shBmi1-1) or puromycin (shBmi1-2) respectively.

Lambda Protein Phosphatase Treatment

Following cell harvest, lysates were supplemented with 1mM MnCl2 and 1X NEBuffer for PMP (50mM HEPES, 100mM NaCl, 2mM DTT, 0.01% Brij 35, pH 7.5). Lysates were either supplemented with 800units of lambda protein phosphatase (NEB, #P0753L) or water (untreated), and incubated at 30°C for 30 minutes.

ELISA assays

HT1080 cells were treated with vehicle control (0.5% DMSO) or compounds at the indicated concentration for 48 hours, and BMI1 protein in the cell lysate was quantified using BMI1 specific sandwich ELISA kits generated by PTC Therapeutics. Tumor tissues

were harvested at dosing day 10 and homogenised in lyses buffer (PBS, 0.5% NP40 and protease inhibitor) by a tissue homogenizer. Total protein concentrations were determined by Bradford method and equivalent protein concentrations were then analysed via ELISA. The capture mouse anti-BMI1, clone F6 was purchased from Millipore (#05-637), while PTC Therapeutics generated the detection rabbit anti-BMI1 antibody.

Microarray analysis

RNA samples from 2 independent MB lines (D425 and D458) and normal human neural stem cells (hNSCs) that were treated with PTC-028 (500nM and 3.5μM for D425 and D458 respectively and 7μM for hNSCs) for 12 hours or DMSO were labelled using Illumina Total Prep-96 RNA Amplification kit (Ambion) as per amplification protocol. 750ng of cRNA generated from these samples were hybridized onto Human HT-12 V4 Beadchips. The BeadChips were incubated at 58°C, with rotation speed 5 for 18 hours for hybridization. The BeadChips were washed and stained as per Illumina protocol and scanned on the iScan (Illumina). The data files were quantified in GenomeStudio Version 2011.1 (Illumina). All samples passed Illumina sample dependent and independent QC Metrics. GSEA analysis was performed using the MySigDB oncogenic signature collection.

Signature analysis

Signatures representing the various GSEA hallmark processes were selected to comprise the leading edge genes from enriched gene sets. The Affymetrix data set described above was used to evaluate the capacity of each signature to predict outcome in MB patients. Briefly, a signature score was $\sum_{i \in R} x_i$ calculated for each patient as

follows: Where *x* is the log2-transformed expression, *R* is the set of genes comprising the Glinsky signature, similar to as described previously(Hallett et al., 2012a; Hallett et al., 2012b).

Gene set enrichment analysis

Gene Set Enrichment Analysis(Subramanian et al., 2005) was used to analyze all publicly annotated BMI1 signature genes in the metastatic compartment of medulloblastoma compared to matched primary samples. All BMI1 pathway gene sets were manually compiled from the Molecular Signatures Database v5.0 curated at the Broad Institute. Using the previously published human primary-metastasis medulloblastoma dataset(Wang et al., 2015), GSEA analysis was performed using gene-set permutations with a FDR cutoff of 3.5% and p-value cutoff of 0.01. Raw Affymetrix CEL files and associated clinical data was downloaded from the broad institute (http://www.broadinstitute.org/pubs/medulloblastoma/cho)(Cho et al., 2011b). Further details are described in the Supplemental Experimental Procedures. Enrichment mapping was completed using Cytoscape (v2.8.2).

Gene expression analysis of CEL files

Raw Affymetrix CEL files were processed using RMA(Irizarry et al., 2003). For the in-house Illumina array, two hundred nanograms from 24 RNA samples were label using Illumina TotalPrep-96 RNA Amplification kit (Ambion), and 750 nanograms of cRNA generated from these samples was used to hybridized onto Human HT-12 v4 beadchips. The mean value for each probe was extracted and normalized using a cubic

spline method. For both Affymetrix and Illumina array data probes were collapsed by Unigene IDs based on highest mean expression.

Intracranial xenografting of MB and *in vivo* treatment protocol

All *in vivo* studies were performed according to McMaster University Animal Research Ethics Board (AREB) approved-protocols. Intracranial injections were performed as previously described(Singh et al., 2004) using each of the following MB samples: SU_MB002 and D458. Briefly, the appropriate number of live cells (determined by Trypan Blue exclusion) were resuspended in 10μL of PBS. NOD SCID mice were anaesthetized using isofluorane gas (5% induction, 2.5% maintenance) and cells were injected into the frontal lobe using a 10μL Hamilton syringe, in a non-randomized, non-blinded fashion. The mice were treated in randomized, non-blinded manner with PTC-028 (12mg/kg) or vehicle orally for 3 times a week for 2 consecutive weeks for a total of 6 doses. The number of animals per treatment arm was determined using the following formulation: $N = 1 + 2C(s/d)$ where n is the number of animals per arm, "C" = 7.85 when significance level is 5% with a power of 80%, "s" is standard deviation, and "d" is the difference to be detected.

For assessing tumor volume, the mice were sacrificed when the control group reached endpoint. For survival studies, treated or control mice were sacrificed when they reached endpoint. Upon reaching endpoint, brains were harvested, formalin-fixed, and paraffin-embedded for hematoxylin and eosin (H&E). Images were captured using an Aperio Slide Scanner and analyzed using ImageScope v11.1.2.760 software (Aperio).

Statistical analysis

At least three technical or experimental replicates from each experiment were compiled. Data represent mean±SD with *n* values listed in figure legends. GraphPad Prism™ was used to plot all bar graphs and statistical analyses including student's t-test or 2-way ANOVA, $p<0.05$ was considered significant. All Kaplan-Meier survival plots were plotted with GraphPad Prism™ and long-rank (Mantel-Cox) test was performed for comparison of median survival, $p<0.05$ was considered significant. For *in silico* analyses all associated statistical tests were performed in R using the coxPH package.

AUTHOR CONTRIBUTIONS

D.B.: Conception and design, Collection and/or assembly of data, Data analysis and interpretation, Manuscript writing, Final approval of manuscript. C.V., A.A.A.: Conception and design, Collection and/or assembly of data, Manuscript writing, Final approval of manuscript. N.G., B.M.: Collection and/or assembly of data, Data analysis and interpretation, Manuscript writing, Final approval of manuscript. R.H., X.W., S.M., P.V., T.V., M.S., M.S., M.M.K-S., M.Q., N.M., A.M.: Data analysis and interpretation, Final approval of manuscript. O.A.A., B.Y.: Provision of study material or patients, Final approval of manuscript. V.R., H.F., S.M.: Collection and/or assembly of data, Data analysis and interpretation. L.C., N.S., R.B., W.D., J.S., M.W., Y-C.M. C-S.L.: Provision of study material or patients, Final approval of manuscript. J.M.K., K.H.D.: Data analysis and interpretation. B.D. Y-J.C., S.M., D.K., M.D.T.: Conception and design, Data analysis and interpretation, Final approval of manuscript. T.W.D.: Provision of study material or patients, Final approval of manuscript.: S.K.S.: Conception and design, Data analysis and interpretation, Manuscript writing, Final approval of manuscript.

ACKNOWLEDGMENTS

S.K.S. is supported by Canada Research Chair award, and operating grants from Canadian Institutes of Health Research (CIHR), Stem Cell Network, the Ontario Institute for Cancer Research Cancer Stem Cell Program, the Canadian Cancer Society Research Institute, the Cancer Research Society, the Brain Tumor Foundation of Canada, and generous donations from the Box Run Foundation, Team Kelsey, and patients and their families.

CONFLICT OF INTEREST

The authors declare no competing financial interests.

REFERENCES:

1. Ellison DW. Childhood medulloblastoma: novel approaches to the classification of a heterogeneous disease. Acta Neuropathol. 2010;120(3):305-16.
2. Huse JT, Holland EC. Targeting brain cancer: advances in the molecular pathology of malignant glioma and medulloblastoma. Nat Rev Cancer. 2010;10(5):319-31.
3. Taylor MD, Northcott PA, Korshunov A, Remke M, Cho YJ, Clifford SC, et al. Molecular subgroups of medulloblastoma: the current consensus. Acta Neuropathol. 2012;123(4):465-72.
4. Cho JH, Wang K, Galas DJ. An integrative approach to inferring biologically meaningful gene modules. BMC Syst Biol. 2011;5:117.
5. Kool M, Koster J, Bunt J, Hasselt NE, Lakeman A, van Sluis P, et al. Integrated genomics identifies five medulloblastoma subtypes with distinct genetic profiles, pathway signatures and clinicopathological features. PLoS One. 2008;3(8):e3088.
6. Northcott PA, Korshunov A, Witt H, Hielscher T, Eberhart CG, Mack S, et al. Medulloblastoma comprises four distinct molecular variants. J Clin Oncol. 2011;29(11):1408-14.
7. Pomeroy SL, Tamayo P, Gaasenbeek M, Sturla LM, Angelo M, McLaughlin ME, et al. Prediction of central nervous system embryonal tumor outcome based on gene expression. Nature. 2002;415(6870):436-42.
8. Thompson MC, Fuller C, Hogg TL, Dalton J, Finkelstein D, Lau CC, et al. Genomics identifies medulloblastoma subgroups that are enriched for specific genetic alterations. J Clin Oncol. 2006;24(12):1924-31.
9. Cavalli FMG, Remke M, Rampasek L, Peacock J, Shih DJH, Luu B, et al. Intertumoral Heterogeneity within Medulloblastoma Subgroups. Cancer Cell. 2017;31(6):737-54 e6.
10. Schwalbe EC, Lindsey JC, Nakjang S, Crosier S, Smith AJ, Hicks D, et al. Novel molecular subgroups for clinical classification and outcome prediction in childhood medulloblastoma: a cohort study. Lancet Oncol. 2017;18(7):958-71.
11. Ramaswamy V, Remke M, Bouffet E, Faria CC, Perreault S, Cho YJ, et al. Recurrence patterns across medulloblastoma subgroups: an integrated clinical and molecular analysis. Lancet Oncol. 2013;14(12):1200-7.
12. Reya T, Morrison SJ, Clarke MF, Weissman IL. Stem cells, cancer, and cancer stem cells. Nature. 2001;414(6859):105-11.
13. Sauvageau M, Sauvageau G. Polycomb group proteins: multi-faceted regulators of somatic stem cells and cancer. Cell Stem Cell. 2010;7(3):299-313.
14. Sparmann A, van Lohuizen M. Polycomb silencers control cell fate, development and cancer. Nat Rev Cancer. 2006;6(11):846-56.
15. Alkema MJ, Wiegant J, Raap AK, Berns A, van Lohuizen M. Characterization and chromosomal localization of the human proto-oncogene BMI-1. Hum Mol Genet. 1993;2(10):1597-603.

16. Bruggeman SW, Hulsman D, Tanger E, Buckle T, Blom M, Zevenhoven J, et al. Bmi1 controls tumor development in an Ink4a/Arf-independent manner in a mouse model for glioma. Cancer Cell. 2007;12(4):328-41.
17. Gargiulo G, Cesaroni M, Serresi M, de Vries N, Hulsman D, Bruggeman SW, et al. In vivo RNAi screen for BMI1 targets identifies TGF-beta/BMP-ER stress pathways as key regulators of neural- and malignant glioma-stem cell homeostasis. Cancer Cell. 2013;23(5):660-76.
18. Leung C, Lingbeek M, Shakhova O, Liu J, Tanger E, Saremaslani P, et al. Bmi1 is essential for cerebellar development and is overexpressed in human medulloblastomas. Nature. 2004;428(6980):337-41.
19. Wang X, Venugopal C, Manoranjan B, McFarlane N, O'Farrell E, Nolte S, et al. Sonic hedgehog regulates Bmi1 in human medulloblastoma brain tumor-initiating cells. Oncogene. 2012;31(2):187-99.
20. Kreso A, van Galen P, Pedley NM, Lima-Fernandes E, Frelin C, Davis T, et al. Self-renewal as a therapeutic target in human colorectal cancer. Nat Med. 2014;20(1):29-36.
21. Yong KJ, Basseres DS, Welner RS, Zhang WC, Yang H, Yan B, et al. Targeted BMI1 inhibition impairs tumor growth in lung adenocarcinomas with low CEBPalpha expression. Sci Transl Med. 2016;8(350):350ra104.
22. Glinsky GV, Berezovska O, Glinskii AB. Microarray analysis identifies a death-from-cancer signature predicting therapy failure in patients with multiple types of cancer. J Clin Invest. 2005;115(6):1503-21.
23. Wang X, Dubuc AM, Ramaswamy V, Mack S, Gendoo DM, Remke M, et al. Medulloblastoma subgroups remain stable across primary and metastatic compartments. Acta Neuropathol. 2015;129(3):449-57.
24. Facchino S, Abdouh M, Chatoo W, Bernier G. BMI1 confers radioresistance to normal and cancerous neural stem cells through recruitment of the DNA damage response machinery. J Neurosci. 2010;30(30):10096-111.
25. Wang H, Wang L, Erdjument-Bromage H, Vidal M, Tempst P, Jones RS, et al. Role of histone H2A ubiquitination in Polycomb silencing. Nature. 2004;431(7010):873-8.
26. Wu X, Northcott PA, Dubuc A, Dupuy AJ, Shih DJ, Witt H, et al. Clonal selection drives genetic divergence of metastatic medulloblastoma. Nature. 2012;482(7386):529-33.
27. Ismail IH, Andrin C, McDonald D, Hendzel MJ. BMI1-mediated histone ubiquitylation promotes DNA double-strand break repair. J Cell Biol. 2010;191(1):45-60.
28. Pei Y, Moore CE, Wang J, Tewari AK, Eroshkin A, Cho YJ, et al. An animal model of MYC-driven medulloblastoma. Cancer Cell. 2012;21(2):155-67.
29. Bandopadhayay P, Bergthold G, Nguyen B, Schubert S, Gholamin S, Tang Y, et al. BET bromodomain inhibition of MYC-amplified medulloblastoma. Clin Cancer Res. 2014;20(4):912-25.

30. Chen J, Li Y, Yu TS, McKay RM, Burns DK, Kernie SG, et al. A restricted cell population propagates glioblastoma growth after chemotherapy. Nature. 2012;488(7412):522-6.
31. Venugopal C, Hallett R, Vora P, Manoranjan B, Mahendram S, Qazi MA, et al. Pyrvinium Targets CD133 in Human Glioblastoma Brain Tumor-Initiating Cells. Clin Cancer Res. 2015;21(23):5324-37.
32. He XM, Wikstrand CJ, Friedman HS, Bigner SH, Pleasure S, Trojanowski JQ, et al. Differentiation characteristics of newly established medulloblastoma cell lines (D384 Med, D425 Med, and D458 Med) and their transplantable xenografts. Lab Invest. 1991;64(6):833-43.
33. Venugopal C, Wang XS, Manoranjan B, McFarlane N, Nolte S, Li M, et al. GBM secretome induces transient transformation of human neural precursor cells. J Neurooncol. 2012;109(3):457-66.
34. Tropepe V, Sibilia M, Ciruna BG, Rossant J, Wagner EF, van der Kooy D. Distinct neural stem cells proliferate in response to EGF and FGF in the developing mouse telencephalon. Dev Biol. 1999;208(1):166-88.
35. Hallett RM, Dvorkin-Gheva A, Bane A, Hassell JA. A gene signature for predicting outcome in patients with basal-like breast cancer. Sci Rep. 2012;2:227.
36. Hallett RM, Pond G, Hassell JA. A target based approach identifies genomic predictors of breast cancer patient response to chemotherapy. BMC Med Genomics. 2012;5:16.
37. Subramanian A, Tamayo P, Mootha VK, Mukherjee S, Ebert BL, Gillette MA, et al. Gene set enrichment analysis: a knowledge-based approach for interpreting genome-wide expression profiles. Proc Natl Acad Sci U S A. 2005;102(43):15545-50.
38. Cho YJ, Tsherniak A, Tamayo P, Santagata S, Ligon A, Greulich H, et al. Integrative genomic analysis of medulloblastoma identifies a molecular subgroup that drives poor clinical outcome. J Clin Oncol. 2011;29(11):1424-30.
39. Irizarry RA, Hobbs B, Collin F, Beazer-Barclay YD, Antonellis KJ, Scherf U, et al. Exploration, normalization, and summaries of high density oligonucleotide array probe level data. Biostatistics. 2003;4(2):249-64.
40. Singh SK, Hawkins C, Clarke ID, Squire JA, Bayani J, Hide T, et al. Identification of human brain tumor initiating cells. Nature. 2004;432(7015):396-401.

Figure 1

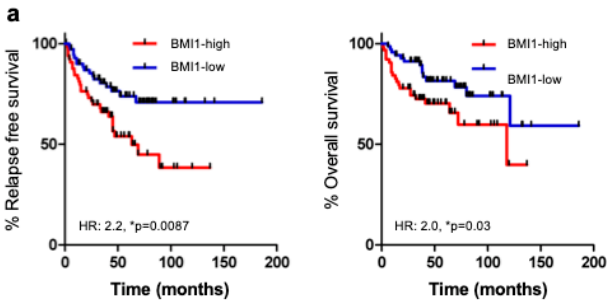

b

Multivariate Cox analysis of Glinsky Signature in Pomeroy dataset (Overall Survival)		
Variable	**Hazard Ratio**	**P value**
Glinsky signature	2.8	0.04
Subtype	1.9	0.08
Age	1.0	0.62
(M)-status	2.1	0.07

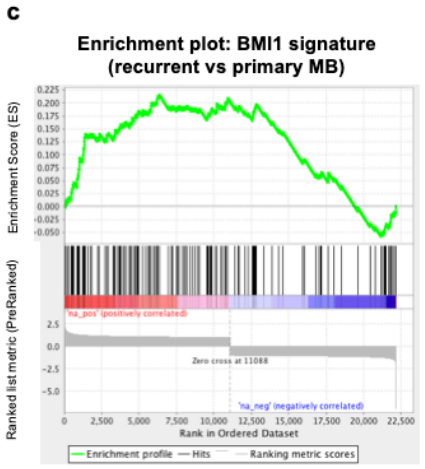

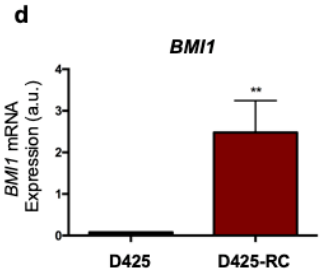

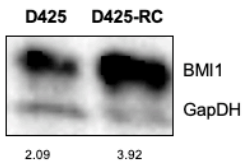

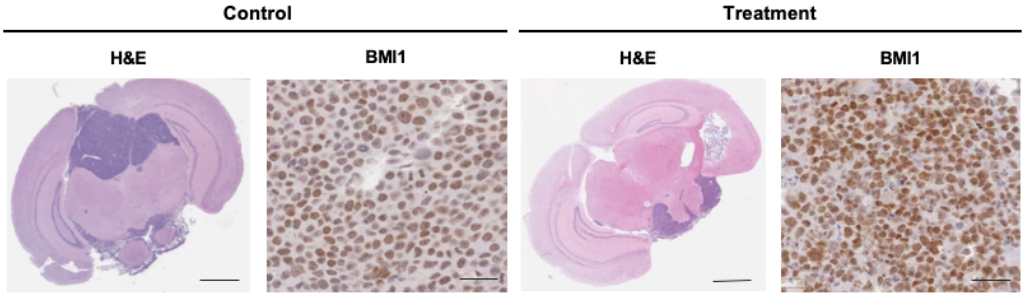

Figure 1: Increased BMI1 expression predicts MB recurrence and poor patient survival. (a) Increased levels of a BMI1 driven gene signature were associated with both reduced relapse-free (HR: 2.2) and overall survival (HR: 2.0). (b) Multivariate analysis evaluating predictive potential of MB subtype, age, metastatic status and BMI1 signature of overall survival in MB. (c) GSEA enrichment plot of genes involved in BMI1 pathway in matched primary versus recurrent MB samples (n=12). Primary Group 3 MB cells (D425) treated with *in vitro* chemoradiotherapy were harvested and profiled for changes in (d) *BMI1* mRNA expression by RT-qPCR and (e) BMI1 protein levels by western immunoblotting. (f) NOD SCID mice were intracranially xenografted with D425 cells line (n=6, $1x10^4$ cells/mice) and treated with 2Gy of craniospinal irradiation in followed by a single cycle of chemotherapy consisting of cisplatin (2.5mg/kg), vincristine (0.4mg/kg) and cyclophosphamide (75mg/kg). Xenografts were fixed, embedded in paraffin, and stained with H&E (scale bar=5000μm) or anti-human BMI1 antibody by immunohistochemistry (scale bar=50μm). Numbers underneath depicted western immunoblots represent band intensity levels of BMI1 protein normalized to the loading control. Bars represent mean of three technical or experimental replicates, mean±SD, two-tailed t-test. (*$p<0.05$, **$p\leq0.001$, ***$p<0.0001$, ****$p<0.00001$). See also Supplementary Figure 1 and Supplementary Table 1.

Figure 2

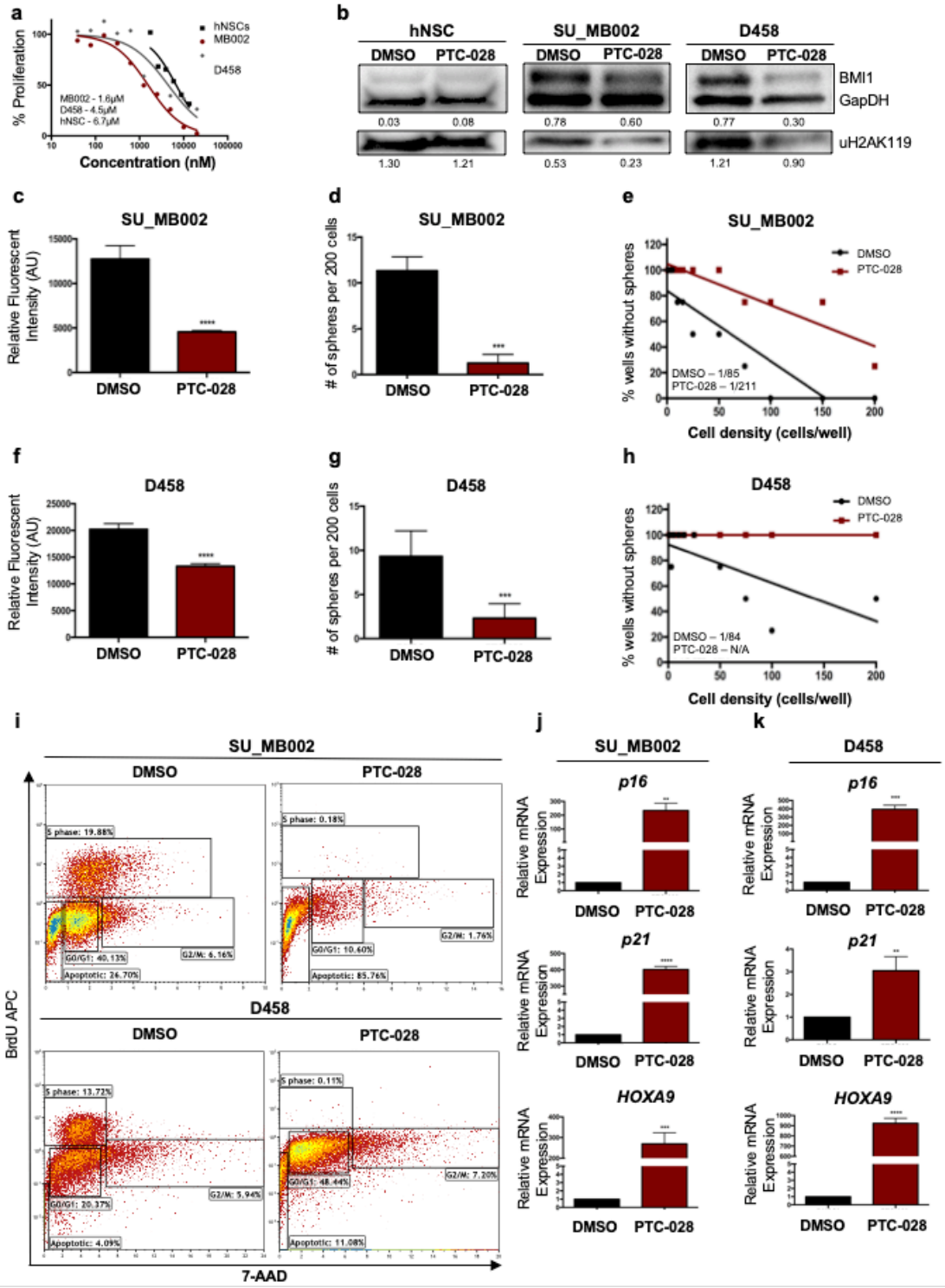
a
% Proliferation
Concentration (nM)
hNSCs
MB002
D458
MB002 - 1.6μM
D458 - 4.5μM
hNSC - 6.7μM
b
hNSC
SU_MB002
D458
DMSO
PTC-028
BMI1
GapDH
uH2AK119
0.03
0.08
0.78
0.60
0.77
0.30
1.30
1.21
0.53
0.23
1.21
0.90
c
SU_MB002
Relative Fluorescent Intensity (AU)
d
SU_MB002
# of spheres per 200 cells
e
SU_MB002
% wells without spheres
Cell density (cells/well)
DMSO – 1/85
PTC-028 – 1/211
f
D458
Relative Fluorescent Intensity (AU)
g
D458
# of spheres per 200 cells
h
D458
% wells without spheres
Cell density (cells/well)
DMSO – 1/84
PTC-028 – N/A
i
SU_MB002
D458
DMSO
PTC-028
BrdU APC
7-AAD
S phase: 19.88%
G0/G1: 40.13%
G2/M: 6.16%
Apoptotic: 26.70%
S phase: 0.18%
G0/G1: 10.60%
G2/M: 1.76%
Apoptotic: 85.76%
S phase: 13.72%
G0/G1: 20.37%
G2/M: 5.94%
Apoptotic: 4.09%
S phase: 0.11%
G0/G1: 48.44%
G2/M: 7.20%
Apoptotic: 11.08%
j
SU_MB002
k
D458
p16
p21
HOXA9
Relative mRNA Expression
DMSO
PTC-028

Figure 2: *In vitro* treatment of recurrent Group 3 MB with PTC-028. (a) Dose response curves generated by treating hNSCs, SU_MB002 and D458 cells with varying concentrations of PTC-028. (b) Reduction of BMI1 and uH2A (Lysine 119) levels in SU_MB002 and D458 after 72-hour treatment with PTC-028 at the respective IC_{50} concentrations (SU_MB002 - 1.6μM; D458 – 4.5μM), but not in hNSCs treated with 17.9 μM PTC-028 (IC_{80} of D458). Small molecule inhibitor-modulated downregulation of BMI1 in both recurrent Group 3 lines resulted in decreased cellular proliferation (c, f) and self-renewal as measured by number of spheres formed (d, g) and limiting dilution assay (e, h) at the respective IC_{80} concentrations: 5.45uM (SU_MB002); 17.9uM (D458)). (i) After 72-hour incubation with PTC-028 (IC_{80}) both SU_MB002 (upper panel) and D458 (lower panel) cells showed significant reduction of treated MB cells in S phase and an increased apoptotic fraction. (j, k) Increase in mRNA levels of *p16*, *p21* and *HOXA9* after treatment with BMI1 inhibitor (IC_{80}). Bars represent mean of three technical or experimental replicates, mean±SD, two-tailed t-test (*$p \leq 0.05$, **$p \leq 0.001$, ***$p \leq 0.0001$; ****$p \leq 0.00001$). See also Supplementary Figure 2 and Supplementary Figure 3.

Figure 3

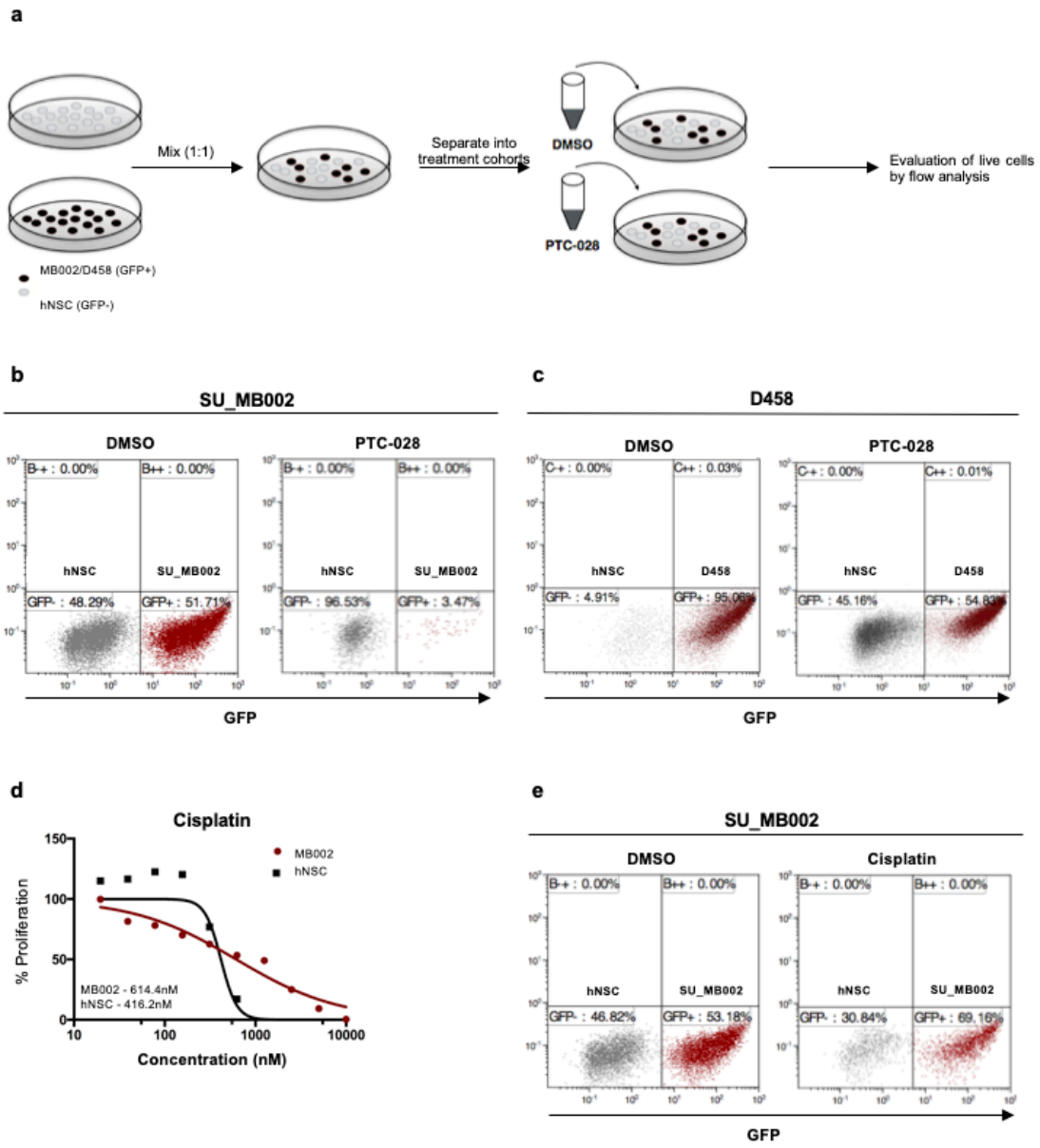
a
Mix (1:1)
Separate into treatment cohorts
DMSO
PTC-028
Evaluation of live cells by flow analysis
MB002/D458 (GFP+)
hNSC (GFP-)
b
SU_MB002
DMSO
PTC-028
B+ : 0.00%
B++ : 0.00%
hNSC
SU_MB002
GFP- : 48.29%
GFP+ : 51.71%
GFP- : 96.53%
GFP+ : 3.47%
GFP
c
D458
DMSO
PTC-028
C+ : 0.00%
C++ : 0.03%
C++ : 0.01%
hNSC
D458
GFP- : 4.91%
GFP- : 45.16%
GFP
d
Cisplatin
MB002
hNSC
% Proliferation
MB002 - 614.4nM
hNSC - 416.2nM
Concentration (nM)
e
SU_MB002
DMSO
Cisplatin
GFP- : 46.82%
GFP+ : 53.18%
GFP- : 30.84%
GFP+ : 69.16%
GFP

Figure 3: BMI1 inhibitors reduce MB cell proliferative capacity when dosed in the nanomolar range, while hNSCs remain resistant to BMI1 inhibitor treatment at doses relevant to MB cells. (a) Recurrent MB lines, SU_MB002 or D458 (GFP-tagged) and human NSCs (non-GFP labelled) were mixed in equal ratios and treated with PTC-028 at IC_{80} of either MB line for 72 hours prior to flow cytometric analysis. (b, c) After 72-hour treatment with PTC-028, hNSCs persisted post-treatment, while percentage of MB cells were eradicated post-therapy. (d) Dose response curves for cisplatin in SU_MB002 and hNSCs. (e) Unlike treatment with BMI1 inhibitor, exposure to cisplatin has resulted in reduction of hNSCs and a continuous expansion of MB cells. See also Supplementary Figure 4.

Figure 4

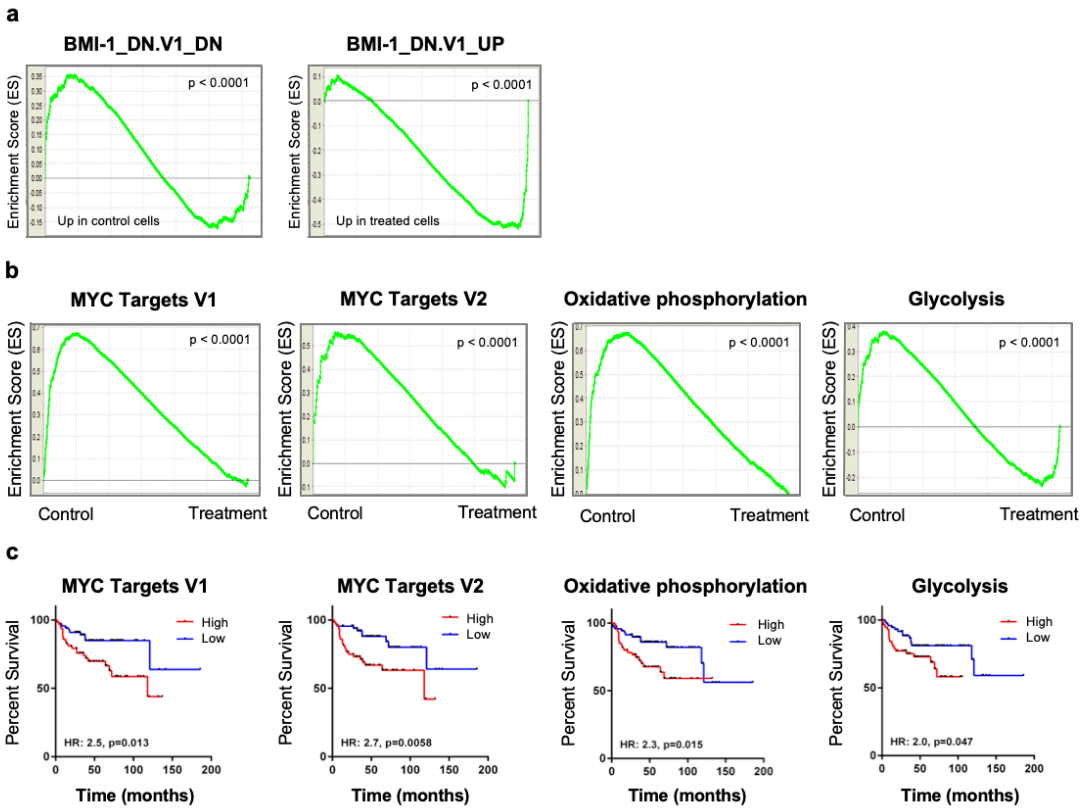
a
BMI-1_DN.V1_DN
BMI-1_DN.V1_UP
Enrichment Score (ES)
p < 0.0001
Up in control cells
Up in treated cells
b
MYC Targets V1
MYC Targets V2
Oxidative phosphorylation
Glycolysis
Control
Treatment
c
Percent Survival
High
Low
HR: 2.5, p=0.013
HR: 2.7, p=0.0058
HR: 2.3, p=0.015
HR: 2.0, p=0.047
Time (months)

Figure 4: BMI1 inhibitor treatment selectively reduces expression of target genes driving tumor growth and aggressiveness in MB cells, with minimal effect on hNSC target gene expression. Matched primary and recurrent MB cell lines (D425 and D458 respectively) and human NSCs were treated with PTC-028 at IC_{80} values calculated for MB cells and IC_{50} values calculated for hNSCs for 12 hours, and gene expression profiling of PTC-028-treated cells was compared with DMSO-treated cells, with technical replicates (n=3 in MB and n=2 in hNSCs). (a) For comparison, two BMI1 signatures present within MSigDB C6 oncogenic database were used (see Material and Methods section). Marked downregulation of BMI1 signaling was observed in MB samples treated with PTC-028 when compared to DMSO treated cells. (b) Myc targets, oxidative phosphorylation and glycolysis processes were significantly downregulated upon PTC-028 treatment and (c) used as a survival signature to probe the Pomeroy dataset. See also Supplementary Figure 5 and Supplementary Table 2.

Figure 5

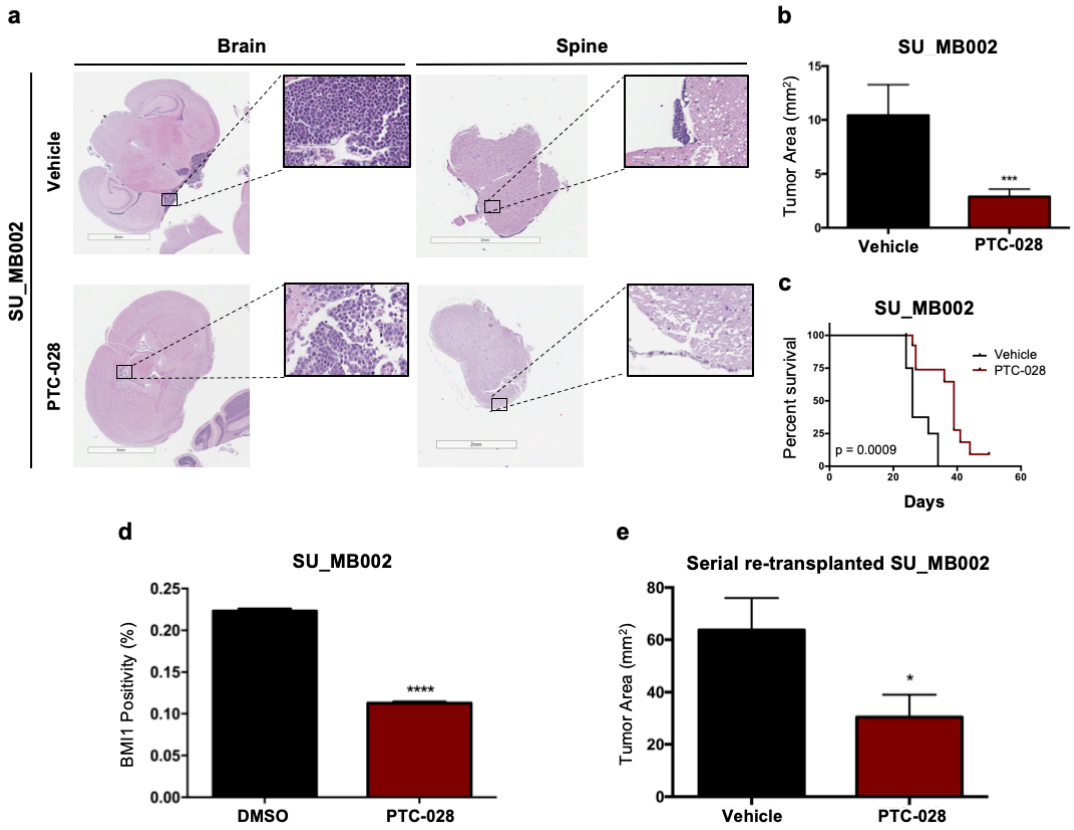
a
Brain
Spine
SU_MB002
Vehicle
PTC-028
b
SU_MB002
Tumor Area (mm²)
***
Vehicle
PTC-028
c
SU_MB002
Percent survival
Vehicle
PTC-028
p = 0.0009
Days
d
SU_MB002
BMI1 Positivity (%)
****
DMSO
PTC-028
e
Serial re-transplanted SU_MB002
Tumor Area (mm²)
*
Vehicle
PTC-028

Figure 5: Therapeutic targeting of BMI1 in MB using *in vivo* approach. NOD SCID mice (n=5/cohort for tumor size; n=10/cohort for survival studies) were intracranially injected with 50,000 viable cells from patient derived recurrent MB cell line, SU_MB002. After one week, mice were treated with 10mg/kg body weight of either PTC-028 or vehicle control for two weeks, three times a week. At the end of the third week, mice were sacrificed for tumor volume analysis, and the remaining mice were monitored for their survival. (a) Representative H&E sections of the brains (a, left panel) and spines (a, right panel). (b) Reduction in tumor burden after PTC-028 treatment. (c) A significant survival benefit is observed with PTC-028 treatment (mean survival = 39 days) compared to control treatment (mean survival 26 days), p=0.0009. (d) Brain sections stained for human BMI1 by IHC revealed a marked decrease in BMI1 protein in the tumor cells remaining post treatment with PTC-028. (e) Reduction in tumor burden in mice serially xenotransplanted with *in vivo* PTC-028-treated SU_MB002 cells. Bars represent mean of three technical replicates, mean±SD, two-tailed t-test (*$p \leq 0.05$, **$p \leq 0.001$, ***$p \leq 0.0001$; ****$p \leq 0.00001$).

Supplementary Figure 1

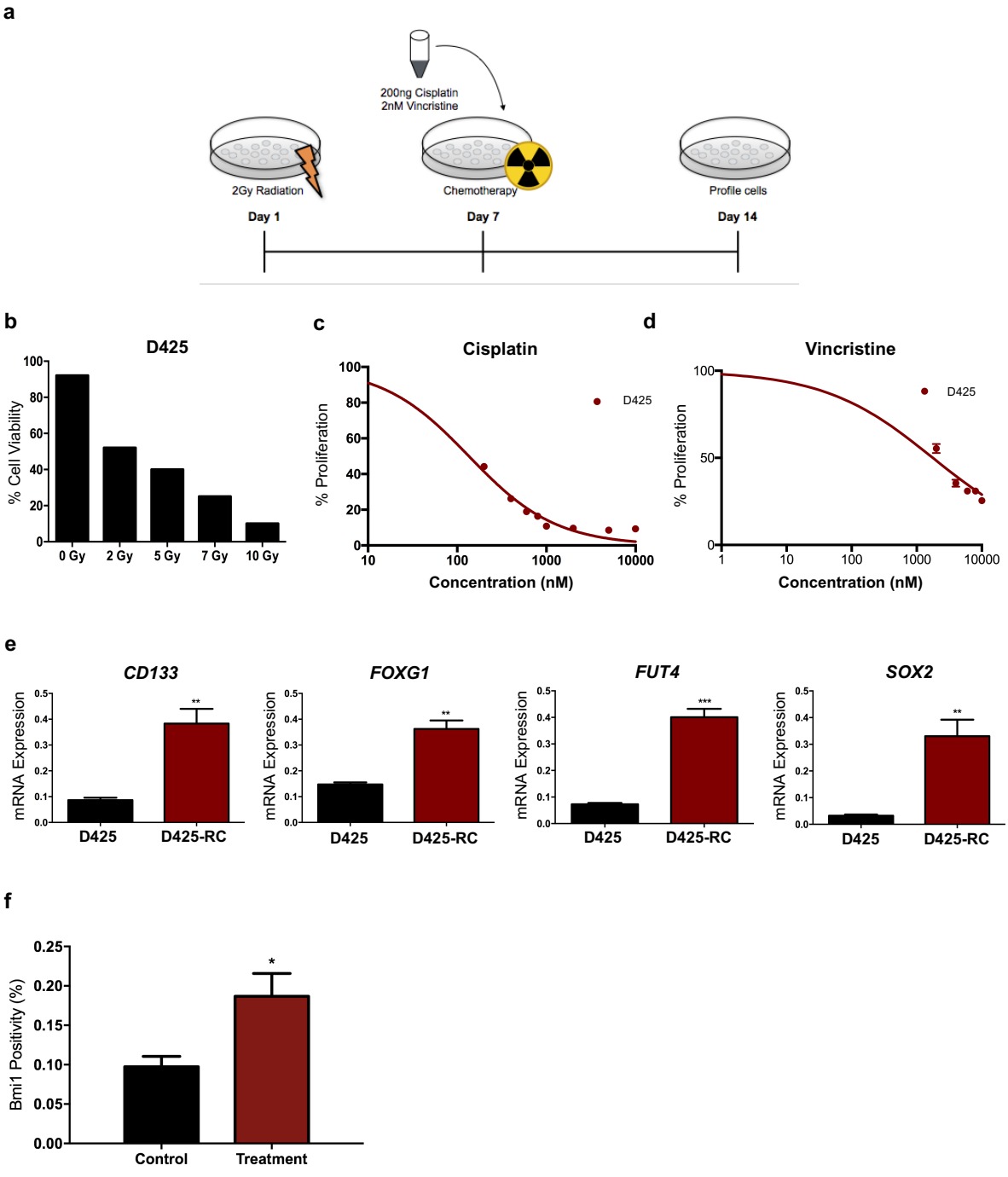

Supplementary Figure 1, related to Figure 1: *In vitro* chemoradiotherapy treatment of primary MB. (a) A schematic timeline of *in vitro* chemoradiotherapy treatment protocol. (b) Changes in cell viability as measured by Trypan blue assay after $1x10^6$ D425 cells were treated with radiation doses ranging from 2Gy to 10Gy. 50% cell viability was observed with 2Gy dosage and hence was chosen for further *in vitro* chemoradiotherapy studies. 1000cells/well of primary MBs were treated with varying concentrations of (c) cisplatin or (d) vincristine in a 96 well plate for 4 days. IC_{50} curves were generated by Presto Blue assay with four technical replicates. IC_{50} values for cisplatin and vincristine were 200nM and 2nM respectively. (e) An increase in mRNA expression levels of additional stem cell markers including *CD133*, *FOXG1*, *FUT4* and *SOX2* in D425 after *in vitro* chemoradiotherapy treatment protocol (D425-RC) compared to control untreated cells (D425). (f) Increase in BMI1 positivity in MB xenografts after treatment with *in vivo* chemoradiotherapy. Bars represent mean of three technical replicates, mean±SD, two-tailed t-test (*$p \leq 0.05$, **$p \leq 0.001$, ***$p \leq 0.0001$; ****$p \leq 0.00001$).

Supplementary Figure 2

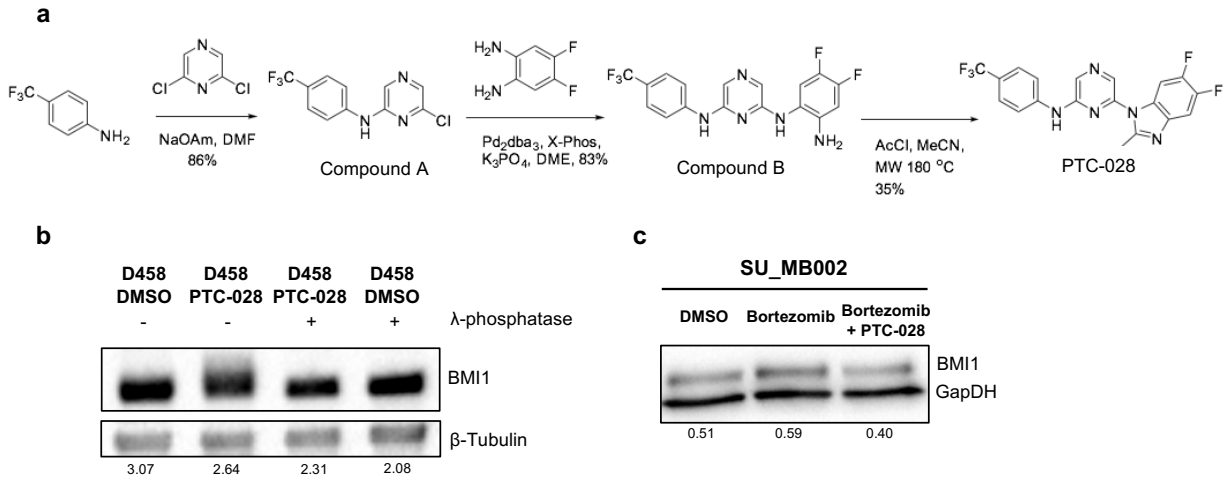

Supplementary Figure 2, related to Figure 2: PTC-028 mechanism of action. (a) A step-wise outline of PTC-028 ($C_{19}H_{12}N_5F_5$) synthesis. See supplementary Materials and Methods section for complete description. (b) D458 cells were treated with IC_{50} of PTC-028 for 20 hours, after which cell lysates were assessed for BMI1 by western immunoblotting with and without λ-phosphatase. The supershift was diminished by λ-phosphatase treatment, thus confirming hyperphosphorylation of BMI1. (c) Changes in BMI1 levels in SU_MB002 levels in response to treatment with bortezomib, a reversible proteasome inhibitor, alone and in combination with PTC-028. Even in the presence of bortezomib, there is a decrease in BMI1 protein levels after BMI1 inhibitor treatment, further suggesting specificity of PTC-028. Numbers underneath the depicted western blots represent levels of BMI1 protein relative to the loading control (β-tubulin or GapDH).

Supplementary Figure 3

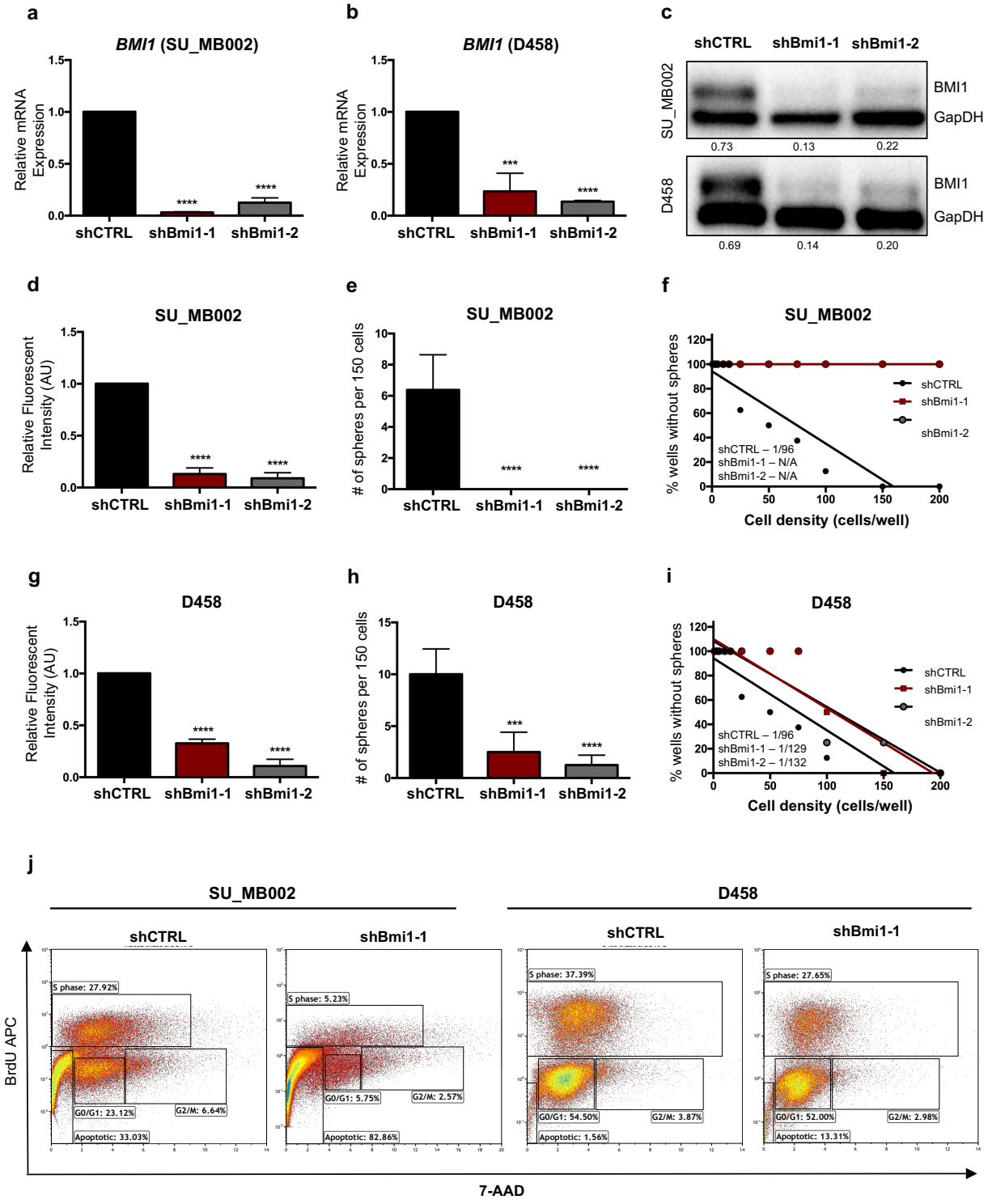

Supplementary Figure 3, related to Figure 2: Functional effects of BMI1 KD in recurrent MB. (a-b) Validation of reduction in *BMI1* mRNA and (c) protein levels post lentiviral KD in SU_MB002 and D458. Numbers underneath the depicted western blot represent levels of BMI1 protein relative to the loading control (GapDH). Downregulation of BMI1 in both recurrent Group 3 lines resulted in decreased (d, g) proliferation and self-renewal as measured by (e, h) number of spheres formed and (f, i) limiting dilution assay. (j) Changes in cell cycle post shRNA-mediated knockdown of BMI1 in SU_MB002 and D458 cells. See Materials and Methods section for detailed experimental procedures. Bars represent mean of three technical replicates, mean±SD, two-tailed t-test (*$p \leq 0.05$, **$p \leq 0.001$, ***$p \leq 0.0001$; ****$p \leq 0.00001$).

Supplementary Figure 4

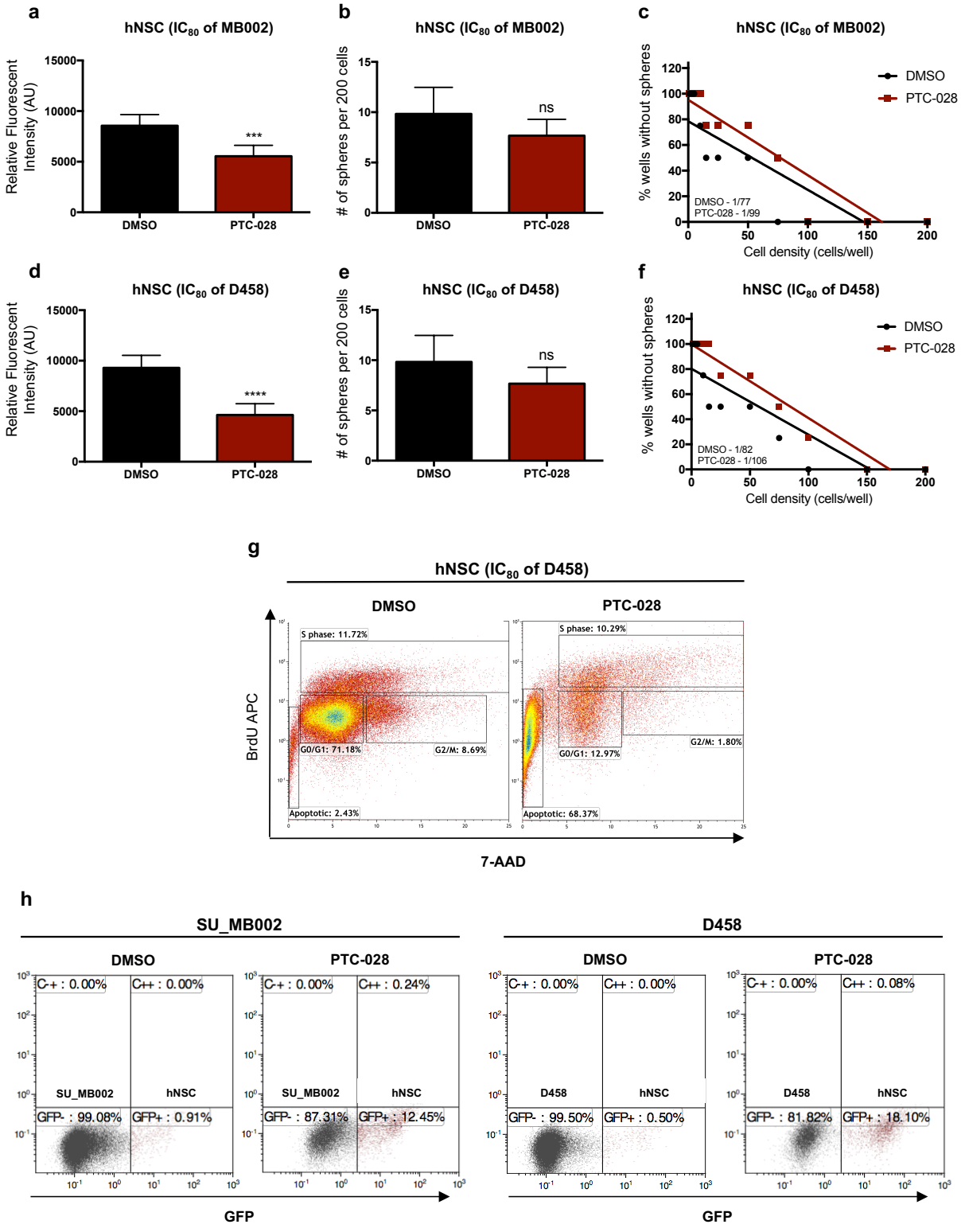

Supplementary Figure 4 related to Figure 3: *In vitro* effects of PTC-028 on hNSC.

Functional changes in hNSCs treated with PTC-028 were investigated by (a, d) proliferation assay, (b, e) sphere formation assay, and (c, f) limiting dilution assay. (g) Cell cycle analysis using BrdU incorporation of hNSC after treatment with 17.9μM of PTC-028. (h) GFP-labelled hNSCs were mixed with recurrent MB lines, SU_MB002 and D458 in 1:1 ratio and subjected to treatment with PTC-028 or DMSO. The percentage of GFP+ cells was evaluated by flow cytometry after 72 hours. Bars represent mean of three technical replicates, mean±SD, two-tailed t-test (*$p \leq 0.05$, **$p \leq 0.001$, ***$p \leq 0.0001$; ****$p \leq 0.00001$).

Supplementary Figure 5

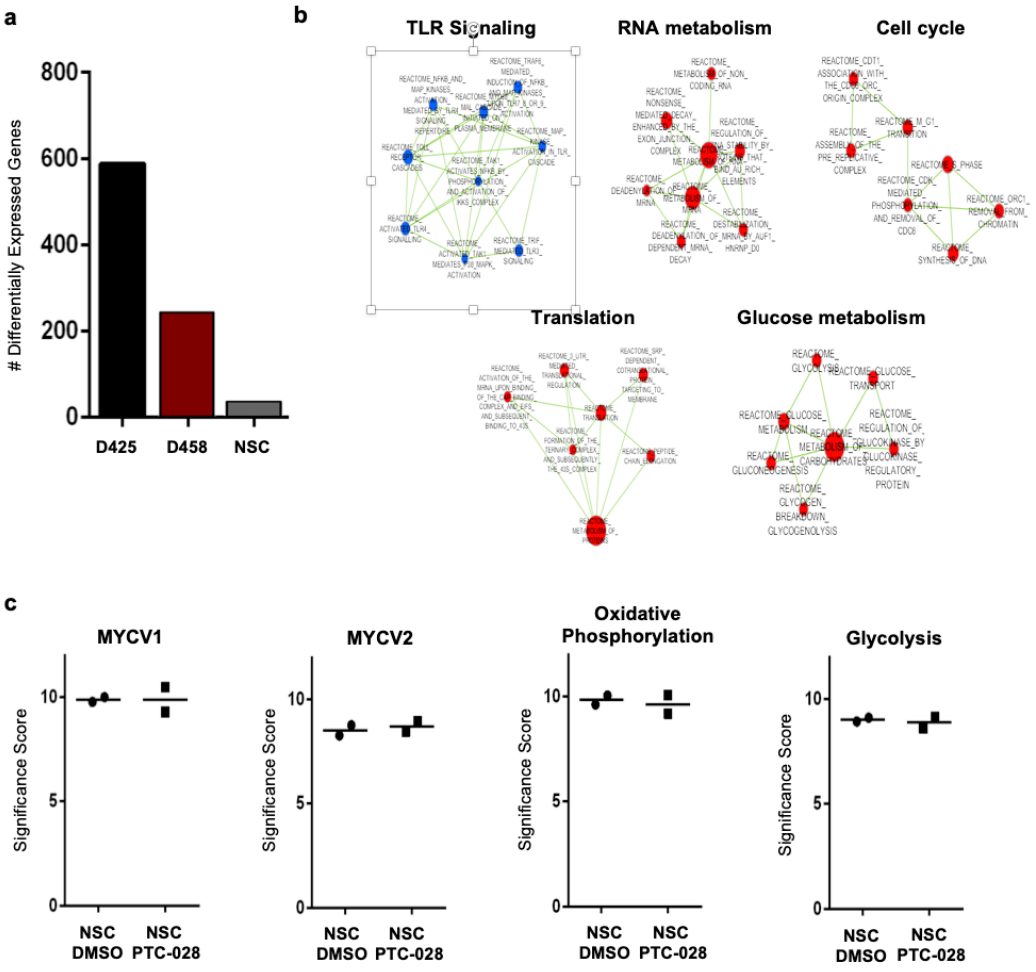

Supplementary Figure 5, related to Figure 4: Annotated enrichment maps for GSEA with C2 MSigDB of PTC-028 treated D425 & D458 cells and effects of PTC-028 on hNSCs. (a) Number of differentially expressed genes in the PTC-028 treated cell lines. (b) Blue indicates processes induced, whereas red indicates those inhibited by PTC-028. For details about procedure, see supplemental experimental procedures section on Microarray analysis. (c) Signature scores in PTC-028 treated hNSC cells with for leading genes selected from relevant gene sets. Overall, there are no significant changes in the MYC driven pathways, oxidative phosphorylation or glycolysis upon treatment with PTC-028, suggesting NSCs are spared. Experimental details are outlined in the Materials and Methods section on Microarray analysis.

Supplementary Figure 6

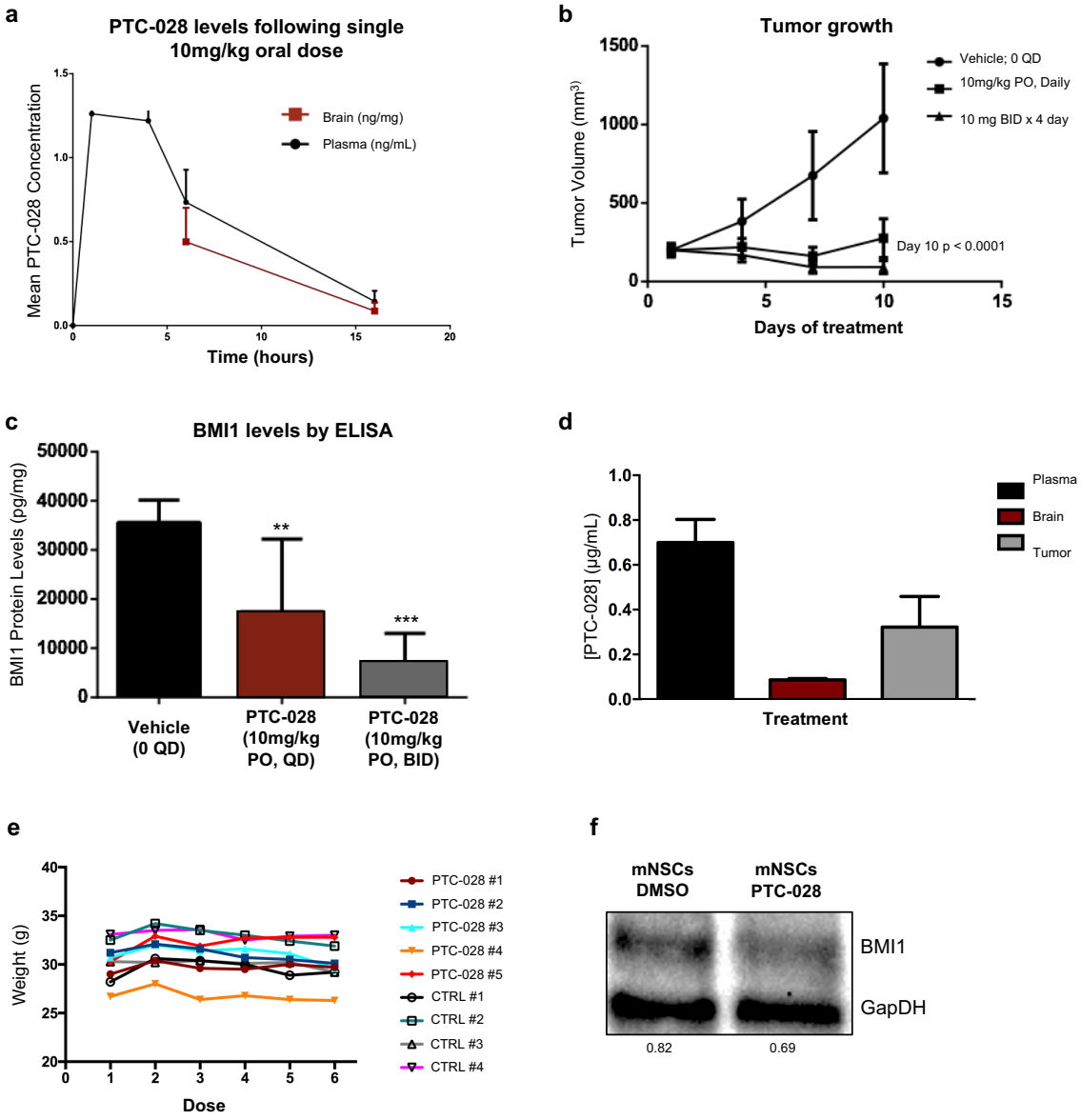

Supplementary Figure 6, related to Figure 5: Tumor growth kinetics of pharmacodynamics study. (a) Mean exposures in tissues taken from C57 BL mice dosed orally with an HPMC suspension of 10mg/kg of PTC-028 (n=3). (b) Mice bearing established HT1080 tumors in the flank were dosed with the indicated regimens for 10 days prior to harvest. (c) BMI1 protein level was measured by ELISA in the control and treatment group of mice engrafted with HT1080 tumors. PTC-028 significantly reduced tumor BMI1 protein levels. (d) The initial bioavailability analysis of PTC-028 4 hours post oral dosing was performed and identified the highest presence of the inhibitor in the plasma and xenografted SU_MB002 tumor, compared to the normal brain tissue. (e) Changes in weight in NOD SCID mice xenotransplanted with SU_MB002 cells and *in vivo* treated with either vehicle or PTC-028. (f) Changes in BMI1 protein level in mouse NSCs treated with PTC-028 in comparison with DMSO treatment. Bars represent mean of three technical replicates, mean±SD, two-tailed t-test (*$p \leq 0.05$, **$p \leq 0.001$, ***$p \leq 0.0001$; ****$p \leq 0.00001$).

Supplementary Figure 7

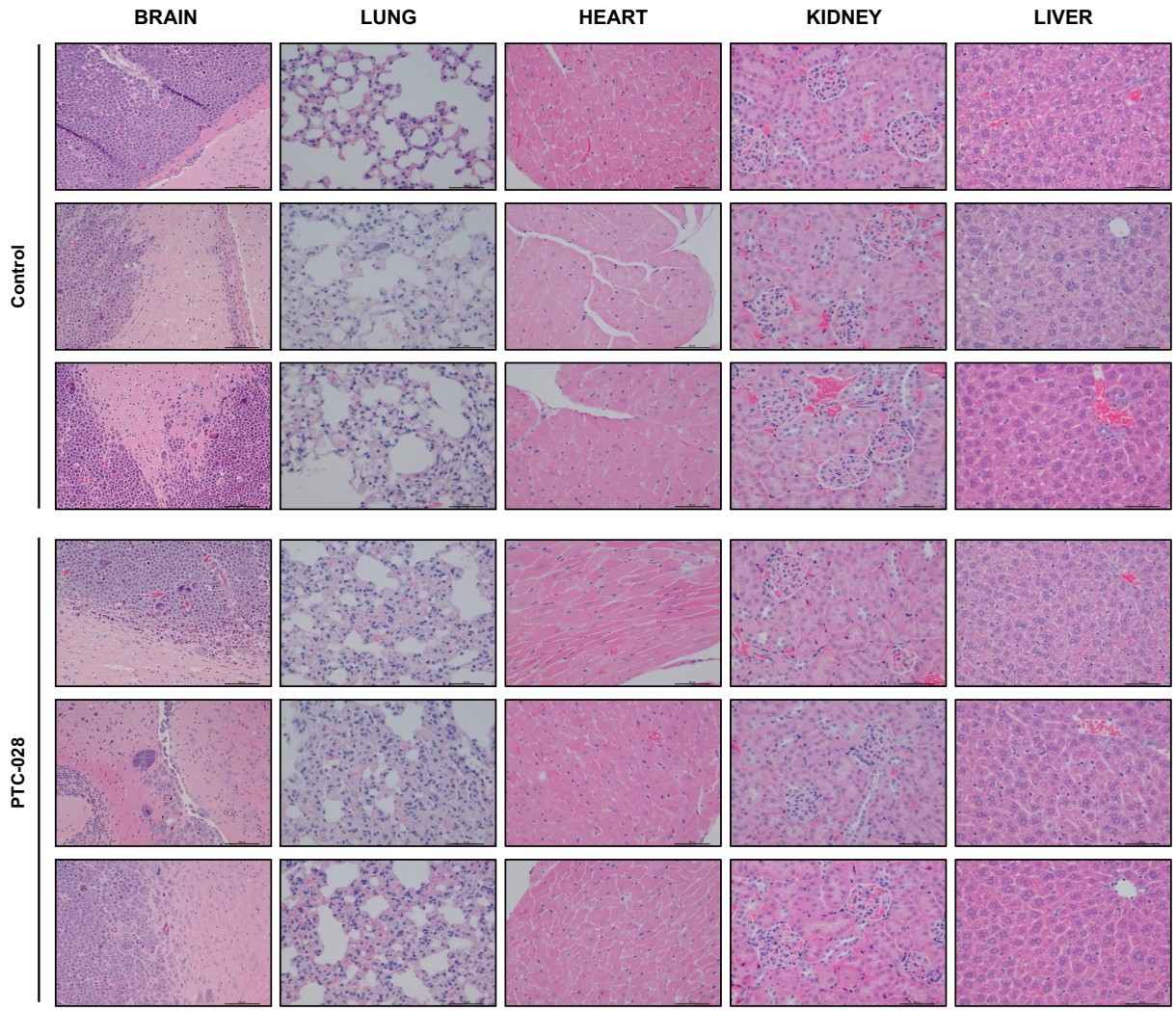

Supplementary Figure 7, related to Figure 5: Investigation of *in vivo* cytotoxicity of PTC-028. Brain, lungs, liver, kidney and heart collected from either control or PTC-028 treated NOD SCID mice (n=3/cohort) were harvested 4 hours after the last oral dose of BMI1 inhibitor. The organs were then paraffin embedded and H&E stained. The pathological investigation revealed that none of the organs exhibited signs of inhibitor related cytotoxicity.

Supplementary Figure 8

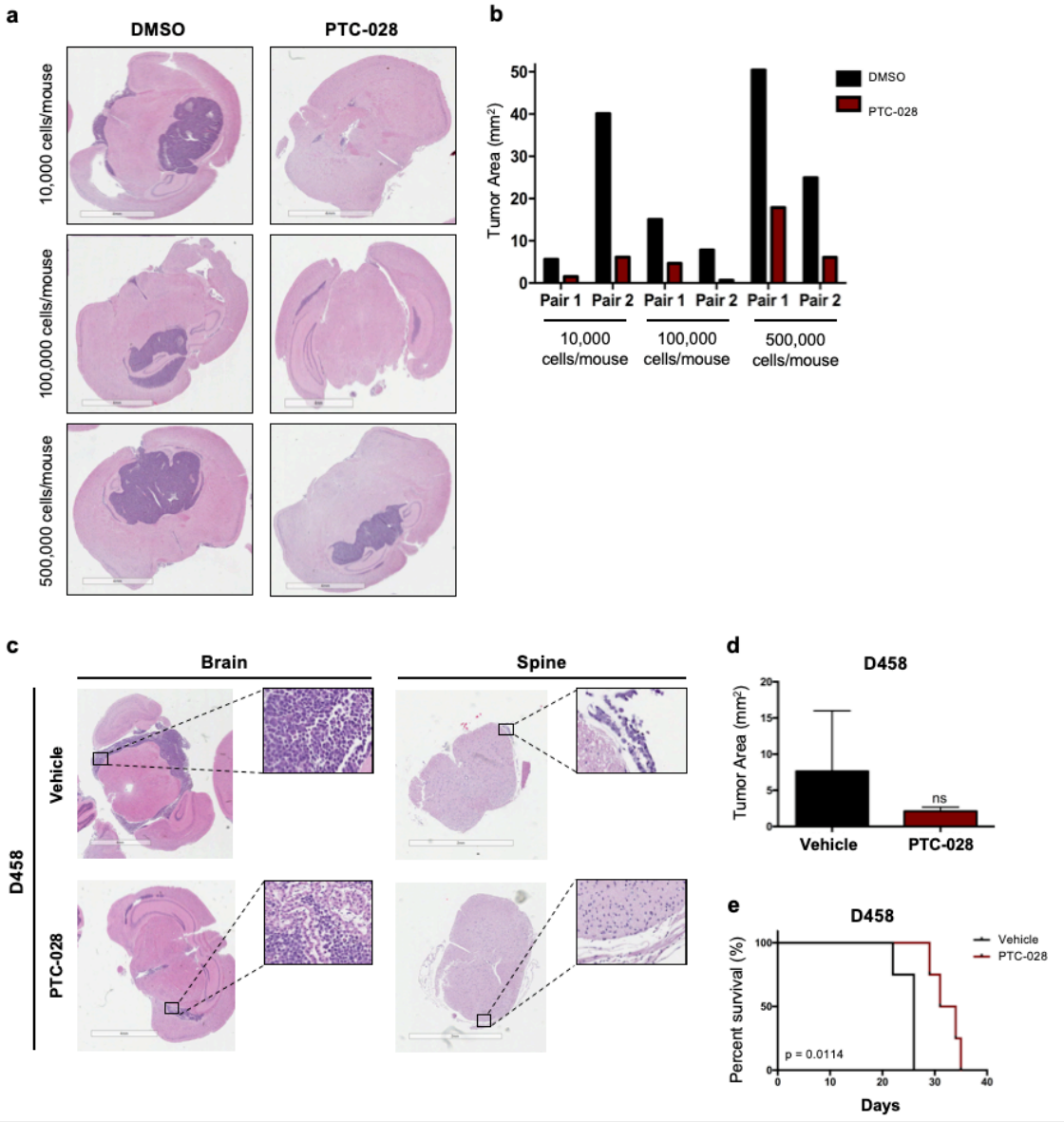

Supplementary Figure 8 related to Figure 5: *Ex vivo* and *in vivo* treatment of D458 with PTC-028. D458 cells were treated *ex vivo* with IC_{80} dose of PTC-028 or DMSO for 72hrs and three different concentrations of viable cells (n=2/group) were injected into immunocompromised mice. (a) Representative H&E stained brains sections showing a reduction of tumor burden in mice injected with PTC-028 pre-treated D458 cells in comparison to the DMSO treated counterparts. (b) Quantification of tumor burden in brains extracted from both treatment and control mice, reveals a consistent reduction of tumor area in mice injected with *ex vivo* treated MB cells when compared to the control animals. NOD SCID mice (n=3/cohort for tumor size and n=5/cohort for survival studies) were intracranially injected (frontal lobe) with 100,000 viable D458 cells. After one week, mice were treated with 10mg/kg body weight of either PTC-028 or control (vehicle) for two weeks, three times a week. Vehicle composition is 0.5% HPMC and 0.1% Tween-80 in water, used to make a dosing suspension. At the end of third week, mice were sacrificed (n=3/cohort) for tumor volume analysis, and the remaining mice (n=5/cohort) were monitored for their survival. (c) Representative H&E sections of the brains (left panels) and spines (right panels) show a reduction in intracranial and spinal leptomeningeal tumor burden in BMI1-inhibitor-treated mice. (d) Quantified tumor burden in mice treated with PTC-028 or vehicle solution. (e) A significant survival benefit was observed post PTC-028 treatment (mean survival = 32.5 days) compared to vehicle treatment (mean survival = 26 days). (*$p \leq 0.05$, **$p \leq 0.001$, ***$p \leq 0.0001$; ****$p \leq 0.00001$).

Supplementary Table 1, related to Figure 1: **Gene set enrichment analysis.** The gene sets are compiled from the various experiments that the authors conducted by overexpressing or downregulating BMI1 in a relevant MB cell line. The first gene sets (BMI1_UP/DN) were done using gene expression platforms(Wiederschain et al., 2007). The second dataset is from gene expression compiled using Ewing sarcoma database(Douglas et al., 2008), which was also done using overexpression and knockdown studies. The other database MORF_BMI1 is a computed gene list generated by Broad that is manually annotated (http://www.broadinstitute.org/gsea/msigdb/cards/MORF_BMI1.html).

Supplementary Table 1

PROBE	RANK IN GENE LIST	RANK METRIC SCORE	RUNNING ES	CORE ENRICHMENT
TIMP3	319	1.526909471	0.00859461	Yes
CCDC80	464	1.441977024	0.02382295	Yes
CLDN1	471	1.440531135	0.045270447	Yes
JUN	817	1.336823106	0.0498233	Yes
KCNN3	844	1.33036375	0.06870532	Yes
ITGB8	864	1.327391624	0.0878591	Yes
CAV1	942	1.310061812	0.10412859	Yes
MYOF	1077	1.287487268	0.117479935	Yes
PLAUR	1089	1.285038233	0.13635695	Yes
ITGA3	1235	1.264169693	0.14885926	Yes
EDN1	1244	1.262978673	0.16753936	Yes
ITGA4	1292	1.256255865	0.18435435	Yes
P4HA2	1294	1.256166458	0.2032483	Yes
NAV2	1473	1.235645413	0.21382816	Yes
AXL	1647	1.216268063	0.224342	Yes
PAPPA	1712	1.209403038	0.23968177	Yes
F2RL1	2141	1.181477666	0.23813887	Yes
ADM	2181	1.179061174	0.2541518	Yes
CRISPLD2	2311	1.170999765	0.26597297	Yes
GADD45A	2455	1.1641711	0.27705806	Yes
ABLIM3	2456	1.164101839	0.2946092	Yes
NTM	2488	1.162315249	0.31073144	Yes
COL5A1	3041	1.137333512	0.30291516	Yes
BMP5	3640	1.115989566	0.29269674	Yes
MICALL1	3948	1.107487798	0.29551044	Yes
LRRC8A	4128	1.102346897	0.30403534	Yes
MICAL2	4179	1.101064205	0.31837484	Yes
RHOD	4459	1.094270825	0.32225555	Yes
PLAT	4540	1.092440605	0.3351083	Yes
CPA4	4727	1.088276863	0.34310448	Yes
CCND1	5448	1.07380724	0.32673275	No
GAL	5960	1.064958453	0.31967947	No
SAFB2	6726	1.053223252	0.30096227	No
FOSL1	7111	1.047781825	0.2993935	No
MICB	7562	1.041966915	0.29475227	No
IL7R	7882	1.037695527	0.29597104	No
BMP1	8454	1.030182362	0.28567997	No
MICA	8459	1.030100703	0.30102986	No
S100A2	8490	1.029672027	0.31519747	No
MAP1B	8693	1.027355313	0.32155156	No
PODXL	10942	1.001457214	0.23498625	No
ADAM19	12131	-1.01197052	0.19651721	No
TPM1	12939	-1.021246552	0.1754185	No
DNMT3B	15746	-1.058716059	0.06448131	No
INHBA	15945	-1.061628938	0.07153305	No
SDC3	16190	-1.065614939	0.07656456	No
FAM43A	16561	-1.071532726	0.075987026	No
MMP7	17611	-1.091545463	0.045003917	No
NET1	17725	-1.093794465	0.056384675	No
KRT75	17865	-1.096819997	0.066635214	No
LFNG	18187	-1.104279399	0.0687674	No
BCL7A	18701	-1.117247581	0.06241203	No
NAV1	19980	-1.160081744	0.022105876	No
TEK	21801	-1.355123758	-0.039771214	No
CDK6	21910	-1.402357221	-0.023512144	No
PTHLH	22163	-2.3273592	1.81E-04	No

Supplementary Table 2, related to Figure 4: Gene signature of PTC-028 treated MB cells. GSEA analysis of PTC-028 treated D425 and D458 cells using the hallmark MSigDB gene sets. (a) Pathways inhibited post treatment with PTC-028 and (b) pathways induced in response to PTC-028 treatment.

Supplementary Table 2

a

PTC-028 inhibited	NES	NOM p-val	FDR q-val
HALLMARK_MYC_TARGETS_V1	2.7376404	0	0
HALLMARK_OXIDATIVE_PHOSPHORYLATION	2.7342591	0	0
HALLMARK_BILE_ACID_METABOLISM	2.0218518	0	0
HALLMARK_FATTY_ACID_METABOLISM	1.9542177	0	0
HALLMARK_MYC_TARGETS_V2	1.941926	0	0

b

PTC-028 induced	NES	NOM p-val	FDR q-val
HALLMARK_APOPTOSIS	-2.2167857	0	0
HALLMARK_TNFA_SIGNALING_VIA_NFKB	-2.1283877	0	0.005294118
HALLMARK_MYOGENESIS	-2.0295672	0	0.003529412
HALLMARK_MITOTIC_SPINDLE	-1.9644133	0	0.002647059
HALLMARK_IL6_JAK_STAT3_SIGNALING	-1.8592203	0	0.004117647

Supplementary Table 3, related to Fig. 5: Pharmaceutical properties of PTC-028.

Supplementary Table 3

PTC-028	
Structure	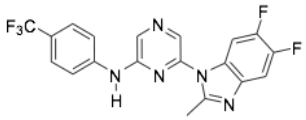
EC_{50}, nM (HT1080 ELISA)	24
Mouse microsome metabolism, % loss, 1h	13%
Caco-2 (10^{-6} cm/sec)	0.9
Plasma exposure, µg/mL	0.7*
Muscle exposure, µg/g	1.8*
Brain exposure, µg/g	0.5*

*PK: mouse, PO, 10 mg/kg, HPMC, 6h

Supplementary Table 4: Primer sequences used for RT-qPCR experiments. GapDH, β2-microglobilin (β2M) or β-actin were used as housekeeping controls.

Supplementary Table 4

Gene	Forward Sequence	Reverse Sequence
BMI1	5'–GGAGGAGGTGAATGATAAAAGAT–3'	5'–AGGTTCCTCCTCATACATGACA–3'
SOX2	5'–TCAGGAGTTGTCAAGGCAGAGAAG–3'	5'–GCCGCCGCCGATGATTGTTATTAT–3'
p16	5'–CAGGTGGGTAGAGGGTCTGC–3'	5'–GCCAGGAGGAGGTCTGTGATT–3'
p21	5'–TGTCACTGTCTTGTACCCTTG–3'	5'–GGCGTTTGGAGTGGTAGAA–3'
FUT4	5'–ACAATTACAAAGTGCCAGCCACCG–3'	5'–TGTGGAATCCCGGTAACACCAAGA–3'
CD133	5'–GTGTCCTGGGGCTGCTGTTTA–3'	5'–CCATTTTCCTTCTGTCGCTGG–3'
FOXG1	5'–GCCACAATCTGTCCCTCAAC–3'	5'–GACGGGTCCAGCATCCAGTA–3'
HOXA9	5'–CCTGACTGACTATGCTTGTGG–3'	5'–CTTGTCTCCGCCGCTCTCAT–3'
GAPDH	5'–TGCACCACCAACTGCTTAGC–3'	5'–GGCATGGACTGTGGTCATGAG–3'
β2M	5'–TCTCTGCTGGATGACGTGAG–3'	5'–TAGCTGTGCTCGCGCTACT–3'
β-Actin	5'–TATCCCTGTACGCCTCT–3'	5'–AGGTCTTTGCGGATGT–3'

SUPPLEMENTARY REFERENCES:

1. Wiederschain D, Chen L, Johnson B, Bettano K, Jackson D, Taraszka J, et al. Contribution of polycomb homologues Bmi-1 and Mel-18 to medulloblastoma pathogenesis. Mol Cell Biol. 2007;27(13):4968-79.
2. Douglas D, Hsu JH, Hung L, Cooper A, Abdueva D, van Doorninck J, et al. BMI-1 promotes ewing sarcoma tumorigenicity independent of CDKN2A repression. Cancer Res. 2008;68(16):6507-15.

Chapter 5: Identification of druggable targets to work in combination with BMI1 inhibitors.

Preamble:

This chapter contains excerpts from the following first-authored book chapter:

Bakhshinyan D., A.A. Adile, M.A. Qazi, M. Singh, M.M. Kameda-Smith, N. Yelle, C. Chokshi, C. Venugopal, S.K. Singh (2016). "Introduction to Cancer Stem Cells: Past, Present and Future" ***Methods in Molecular Biology***

Our initial work studying post-translational targeting of BMI1 using small molecule inhibitors showed a remarkable decrease in cell proliferation and self-renewal *in vitro* (Chapter 5, Figure 2), as well as reduction of local and spinal metastatic disease in recurrent MB (Chapter 5, Figure 5). However, mice treated with PTC-028 still succumbed to the disease post-BMI1 inhibition, suggestive of either incomplete elimination of BMI1 expressing cells or emergence of new clonal population driving therapy failure. Furthermore, we have developed a combinatorial *in vivo* model, in which we treated with standard chemoradiotherapy together with PTC-028 analog, PTC-596 (Figure 1a). PTC-596 has been tested in pre-clinical models of glioblastoma (Jin et al., 2017) and its efficacy is currently being tested in ongoing Phase 1 clinical trials for adult patients with advanced solid cancers (ClinicalTrials.gov Identifier: NCT02404480) and pediatric brain tumors (ClinicalTrials.gov Identifier: NCT03605550). The combinatorial treatment resulted in an

even greater survival benefit and tumor burden reduction for both concurrently and sequentially treated PDX mouse cohorts, than either of the modalities alone (Fig. 1b-d). Although both concurrent and sequential administration of PTC-596 lead to a similar extent of survival, at the endpoint of control mice, the observed tumor burden was significantly lower in sequentially treated animals. One possible explanation is the fact that upfront treatment with chemoradiotherapy has been shown to induce expression of BMI1 in majority of the cells (Chapter 5, Figure 1) and hence increase the target population susceptible to BMI1 inhibition. Nevertheless, mice still succumbed to the disease even after combinatorial treatment, highlighting the main obstacle in treating a constantly evolving tumor and the need to investigate potential polytherapy that can work in combination with BMI1 targeting. Through utilization of DNA barcoding and CRISPR-Cas9 screening technologies, we set to identify the clonal dynamics and putative sensitizers to chemoradiotherapy and BMI1 inhibition. The identified targets will represent the novel candidates for development of polytherapy targeting multiple self-renewing populations in recurrent MB in combination with small molecules targeting BMI1.

5.1 DNA Barcoding

Concept of cellular heterogeneity is displayed in both normal and cancer systems, with the presence of distinct cellular subpopulations. Intratumoral heterogeneity (ITH) at the cellular, genetic and functional level has been shown to occur to a startling degree in many cancers, and is increasingly appreciated as a key determinant of treatment failure and disease recurrence (Burrell et al., 2013; Meacham and Morrison, 2013; Swanton, 2015). Pioneering work using lentivector-mediated clonal tracking (Jin et al., 2017) of

hematopoietic stem cells by John Dick, demonstrated distinct clonal contribution of various cell populations to bone marrow engraftment in mice (Mazurier et al., 2004). Resolution of clonal tracking was further improved by pairing cellular barcoding with sequence-based detection system, thus offering higher sensitivity for identification of major and minor clones (Gerrits et al., 2010). The application of cellular DNA barcoding technology has helped researchers to start appreciating the complexity tumoral heterogeneity and gain insights into temporal tumor evolution and how tumor cells respond to therapy. Through utilization of DNA barcoding technology in studies of acute lymphoblastic leukemia (ALL) (Turke et al., 2010), colorectal cancer(Kreso et al., 2013; Nolan-Stevaux et al., 2013) and breast cancer (Navin et al., 2011), researchers were able to postulate that even when a presumably clonal population is transplanted *in vivo* the tumor growth is driven by a rare, pre-existing clonal cell subpopulation. However, in other studies by Connie Eaves' group, they demonstrated that multiple clonal populations in breast cancer can be detected and a constant flux in clonal composition was observed (Nguyen et al., 2014). Together these studies have highlighted polyclonality as an intrinsic property of tumor populations allowing for continuous adaptive potential under multiple environmental factors including chemo- and radiotherapies. Identification of clonal subpopulations responsible for driving tumor recurrence allows for development of novel therapeutic approaches that selectively targets treatment-refractory clones.

In collaboration with Dr. Jason Moffat, we set out to optimize and implement DNA barcoding technology in the setting of recurrent MB as it undergoes treatment with chemoradiotherapy and small molecule-mediated targeting of BMI1 separately and in

combination (Figure 2). To commence the *in vivo* DNA barcoding tracking, puromycin dose response curves and doubling time of SU_MB002 cells were evaluated (Figure 3a, b). The collected data along with the estimated viral titer (Figure 3c) were used to deduce optimal lentivector transduction and selection of successfully "barcoded" cells. Following *in vitro* expansion, the barcoded SU_MB002 cells were intracranially xenografted into immunocompromised mice. Mice were subsequently separated into 4 treatment cohorts for treatment with (i) control vehicle, CTRL; (ii) chemoradiotherapy, SoC; (iii) BMI1 inhibitor; and (iv) SoC+BMI1 inhibitor (Figure 2). Brains and spines from 5 mice/cohort were collected and used for extraction of genomic DNA (gDNA) for sequencing and downstream bioinformatics analysis to determine clonal composition following each treatment modality. The obtained data will be used to determine the clonal composition of the cells driving tumor progression after each treatment strategy and whether the same polytherapy might be efficacious for each cohort.

5.2 CRISPR-Cas9 Screening

The ability to target genomic locations in normal and cancer cells paves the way to evaluate the roles of specific genes in cancer involved in cancer development and resistance. Studies involving highly specific site-specific DNA manipulations in eukaryotic cells have been made easier after the development of Zinc Finger Nucleases (ZFNs) (Bibikova et al., 2003; Porteus and Baltimore, 2003), TALE domains in transcription activator-like effector nucleases (TALENs) (Boch et al., 2009) and CRISPR/Cas (clustered regularly interspaced palindromic repeats/CRISPR-associated) technology. Originally discovered as part of adaptive immunity in select bacteria and archaea, CRISPR allows

these organisms to respond to and eliminate invading genetic materials than ZFNs and TALENs (Bolotin et al., 2005; Mojica et al., 2005), and has now been extensively adapted for eukaryotic genome engineering (106). CRISPR allows for the precise manipulation of genetic locations in the mammalian genome, even if these regions are functionally silenced or structurally condensed (Knight et al., 2015). Combined with the precise nature of CRISPR-Cas, the ease of generating large libraries of targeting constructs has poised this genomic editing system to discover novel therapeutic targets in cancer using loss-of-function (LoF) and gain-of-function screens (GoF).

CRISPR sgRNA genome-wide libraries have been developed for *in vitro* screening and, more recently, *in vivo* screening. First-generation CRISPR sgRNA LoF libraries were initially developed to target over 18 000 genes in the human genome, including over 1000 microRNAs (miRNA) (Shalem et al., 2014; Wang et al., 2014). Recently, an improved CRISPR LoF library targeting the human genome was developed by Hart et al., known as the Toronto KnockOut (TKO) library. The second-generation TKO CRISPR library contains ~2000 high-confidence fitness genes and demonstrates that KO of context-dependent fitness genes is linked to pathway-specific genetic vulnerabilities (Hart et al., 2015). Recently, Chen et al. showed that the use of genome-wide CRISPR LoF screens in tumor growth and metastasis *in vivo*, by transplanting a mutant mouse cancer cell line using a genome scale library with ~68000 sgRNAs into immunocompromised mice (Chen et al., 2015).

Using CRISPR sgRNA KO-libraries, we are conducting an *in vitro* genome-wide LoF screen in treatment-refractory SU_MB002 cells. To begin, assays confirming

screening potential of the selected cell line, as well as cellular doubling time and dose response curves of the proposed treatments were performed (Figure 4). After initial optimization, the cells were transduced with a pooled genome-wide LoF CRISPR sgRNA library. Following selection and propagation of transduced Cas9-sgRNA clones, genetic vulnerabilities in the presence or absence of conventional chemoradiotherapy could be identified based on the *in vitro* growth of cancer cells. MB cells will be treated with IC_{20} of radiation, cisplatin, vincristine and PTC-596 every doubling period. Genomic samples of the transduced cells will be collected at different time points and sequenced to identify an absence of particular sgRNA suggesting potential genetic vulnerability (Figure 5). Following validation, these genetic vulnerabilities can be targeted using small-molecule inhibitors or immunotherapeutic biologics.

5.3 Case Study

The future of treatment and management of MB patients lies in combining the cellular and molecular analysis of each individual tumor. Here, I would like to present a case study of an 11yo female patient with recurrent Group 4 MB to demonstrate how a combination of molecular subgrouping and further molecular profiling can help guide next generation of personalized therapies. Initially, we have performed RNA isolation from the obtained frozen tissue specimen and submitted it for gene expression analysis using previously designed 86-gene codeset for NanoString(Northcott et al., 2012b). The results were compared against human neural stem cells (hNSCs), a representative WNT tumor specimen (BT800) and another Group 4 tumor (BT611) (Table 1). As expected there was an obvious increase in MYCN expression, a hallmark of Group 4 MBs. Furthermore, in concordance

with our IHC results (Figure 6) an upregulation of BMI1 was observed in the tumor sample when compared to healthy neural stem cells. Another gene encoding an important protein involved in histone methylation, EZH2, was upregulated in both Group 4 samples. Moreover, the patient matched recurrent sample (S18) showed almost expression of BMI1, similarly to the xenograft sample of recurrent MB (Figure 6). Taken together, the data is strongly suggestive that the patient might be the ideal candidate for treatment with BMI1 inhibitor. Further investigation of clonal dynamics and molecular dissection of mechanisms by which MB cells evade targeted therapies against BMI1 will allow to identify and test synergistic treatments that will enhance the anti-tumoral effects of BMI1 inhibitors.

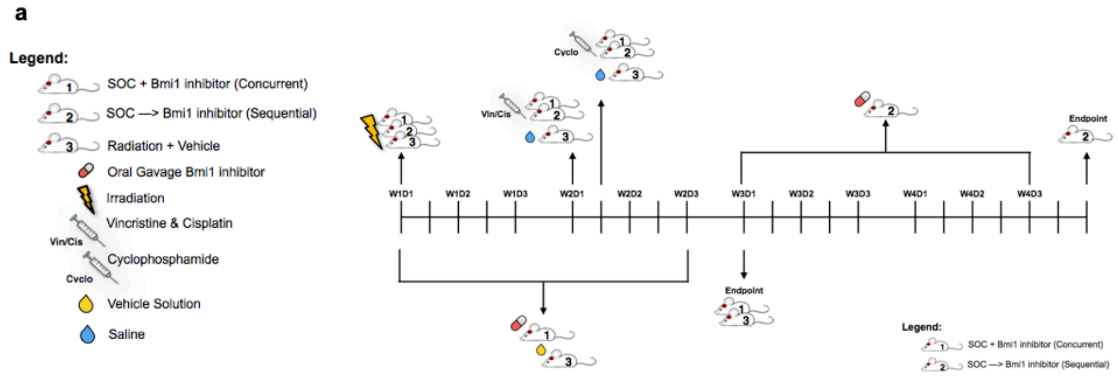
a
Legend:
SOC + Bmi1 inhibitor (Concurrent)
SOC —> Bmi1 inhibitor (Sequential)
Radiation + Vehicle
Oral Gavage Bmi1 inhibitor
Irradiation
Vincristine & Cisplatin
Cyclophosphamide
Vehicle Solution
Saline
Vin/Cis
Cyclo
W1D1
W1D2
W1D3
W2D1
W2D2
W2D3
W3D1
W3D2
W3D3
W4D1
W4D2
W4D3
Endpoint
Endpoint
Legend:
SOC + Bmi1 inhibitor (Concurrent)
SOC —> Bmi1 inhibitor (Sequential)

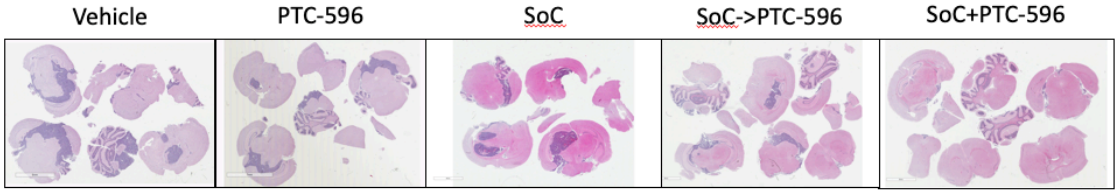
b
Vehicle
PTC-596
SoC
SoC->PTC-596
SoC+PTC-596

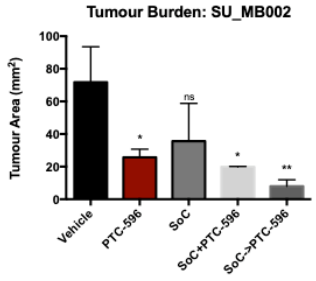
c
Tumour Burden: SU_MB002
Tumour Area (mm²)
100
80
60
40
20
0
ns
*
*
**
Vehicle
PTC-596
SoC
SoC+PTC-596
SoC->PTC-596

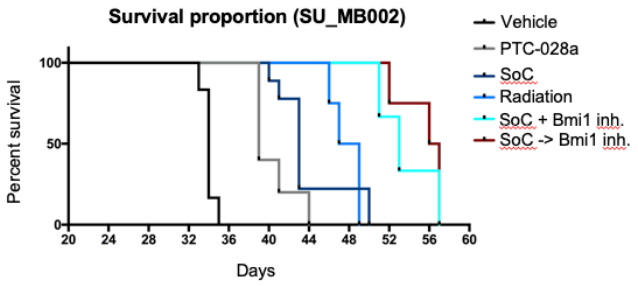
d
Survival proportion (SU_MB002)
Percent survival
100
50
0
20
24
28
32
36
40
44
48
52
56
60
Days
Vehicle
PTC-028a
SoC
Radiation
SoC + Bmi1 inh.
SoC -> Bmi1 inh.

Figure 1: Combining BMI1 inhibition with SoC. BMI1 inhibition in combination with chemoradiotherapy treatment leads to reduced tumorigenesis in MB. (a) SU_MB002 xenografted mice mice are stratified into control and 3 treatment cohorts. For standard of care (SoC), mice initially undergo a cycle of 2Gy craniospinal irradiation followed by treatment with the modified COG A395 chemotherapy regimen of cisplatin and vincristine. PTC-596, BMI1 inhibitor, was administered orally at 10mg/kg 3 times a week for 2 weeks. (b) Representative H&E stained IHC slides demonstrating tumor burden in mice from each cohort at the endpoint of mice treated with vehicle control. (c) Quantified tumor area in mice from each cohort at the endpoint of mice treated with vehicle control. (d) An additional survival benefit was observed by combining small molecule mediated inhibition of BMI1 and chemoradiotherapy. Median survival in CTRL cohort was 33 days, in PTC-596 treated was 40 days, in radiation and SoC treatments was 46 and 47 days respectively and in mice treated with combination of SoC and BMI1 inhibitor concurrently and sequentially was 53 and 56.5 days respectively.

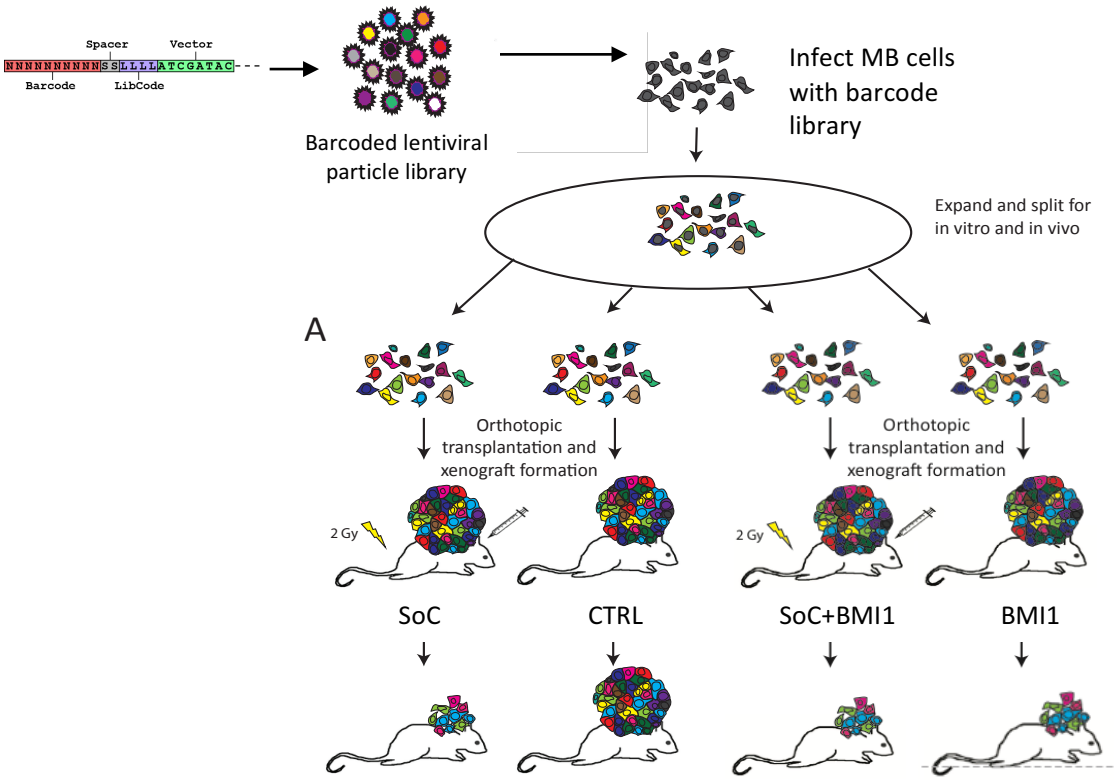
Spacer
Vector
NNNNNNNNNSSLLLLATCGATAC
Barcode
LibCode
Barcoded lentiviral particle library
Infect MB cells with barcode library
Expand and split for in vitro and in vivo
A
Orthotopic transplantation and xenograft formation
Orthotopic transplantation and xenograft formation
2 Gy
2 Gy
SoC
CTRL
SoC+BMI1
BMI1

Figure 2: Tracking MB cells *in vivo* using DNA barcoding. Schematic representation of the proposed DNA barcoding tracking experiment. After transduction and selection, $5x10^5$ barcoded SU_MB002 cells were intracranially xenografted into immunocompromised mice. In all cohorts, mice were allowed to reach endpoint, after-which brains and spines were harvested for gDNA extraction.

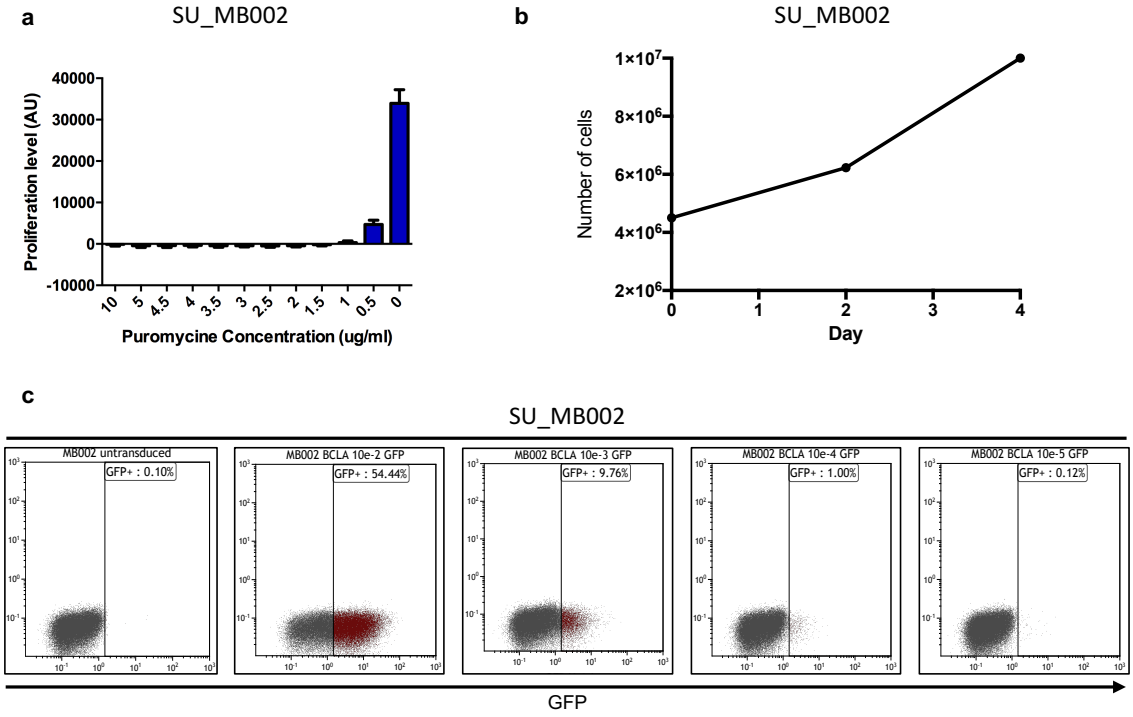
a
SU_MB002
Proliferation level (AU)
40000
30000
20000
10000
0
-10000
10
5
4.5
4
3.5
3
2.5
2
1.5
1
0.5
0
Puromycine Concentration (ug/ml)
b
SU_MB002
Number of cells
1×10^7
8×10^6
6×10^6
4×10^6
2×10^6
0
1
2
3
4
Day
c
SU_MB002
MB002 untransduced
GFP+ : 0.10%
MB002 BCLA 10e-2 GFP
GFP+ : 54.44%
MB002 BCLA 10e-3 GFP
GFP+ : 9.76%
MB002 BCLA 10e-4 GFP
GFP+ : 1.00%
MB002 BCLA 10e-5 GFP
GFP+ : 0.12%
GFP

Figure 3: Preliminary assays using SU_MB002 cells prior to transduction with DNA barcoding library. (a) Puromycin kill curve demonstrating the minimal concentration of puromycin required to kill 100% of the MB cells is 1.5µg/ml. (b) SU_MB002 grew at the observed doubling time of 3.5 days. (c) Evaluation of GFP levels post transduction of SU_MB002 cells with varying concentration of DNA barcoding library.

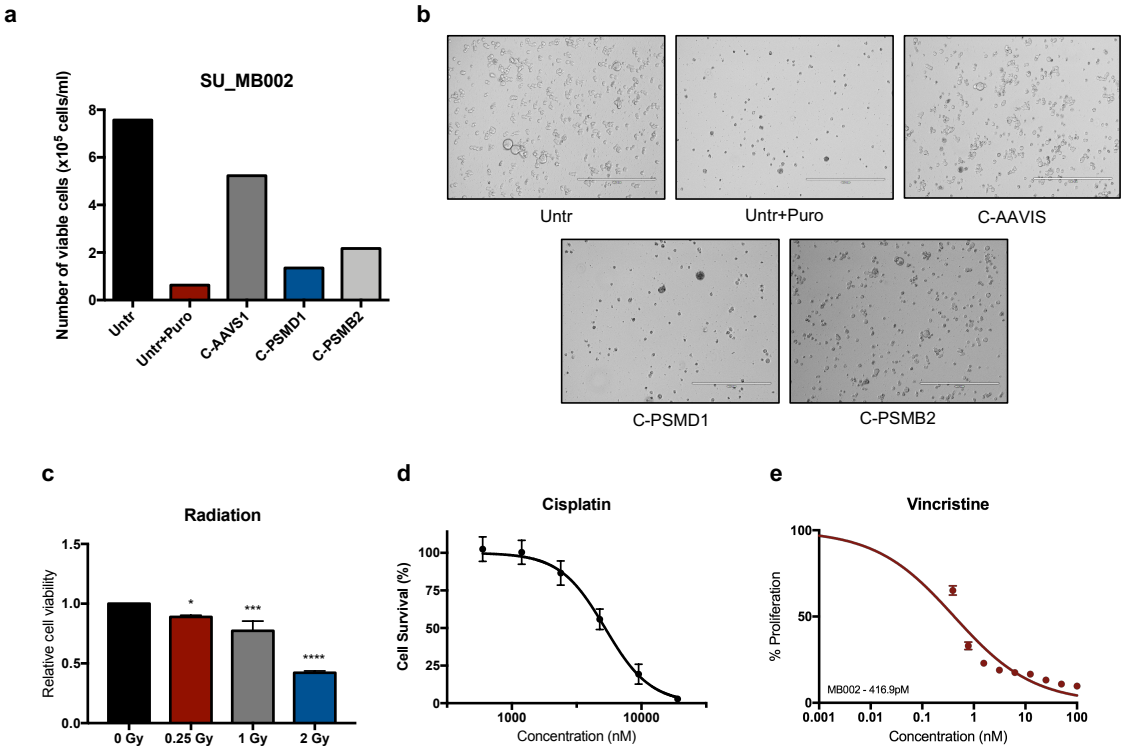
a
SU_MB002
Number of viable cells (x10^5 cells/ml)
Untr
Untr+Puro
C-AAVS1
C-PSMD1
C-PSMB2
b
Untr
Untr+Puro
C-AAVIS
C-PSMD1
C-PSMB2
c
Radiation
Relative cell viability
0 Gy
0.25 Gy
1 Gy
2 Gy
d
Cisplatin
Cell Survival (%)
Concentration (nM)
e
Vincristine
% Proliferation
MB002 - 416.9pM
Concentration (nM)

Figure 4: Assays evaluating the suitability of SU_MB002 for the *in vitro* genome-wide CRISPR-Cas9 screen. (a, b) CRISPR-Cas9 mediated knockout of essential proteasome subunits led to a diminished cellular viability. The dose response curves of (c) radiation, (d) cisplatin and (e) vincristine in SU_MB002 as determined by the change in viability or proliferation.

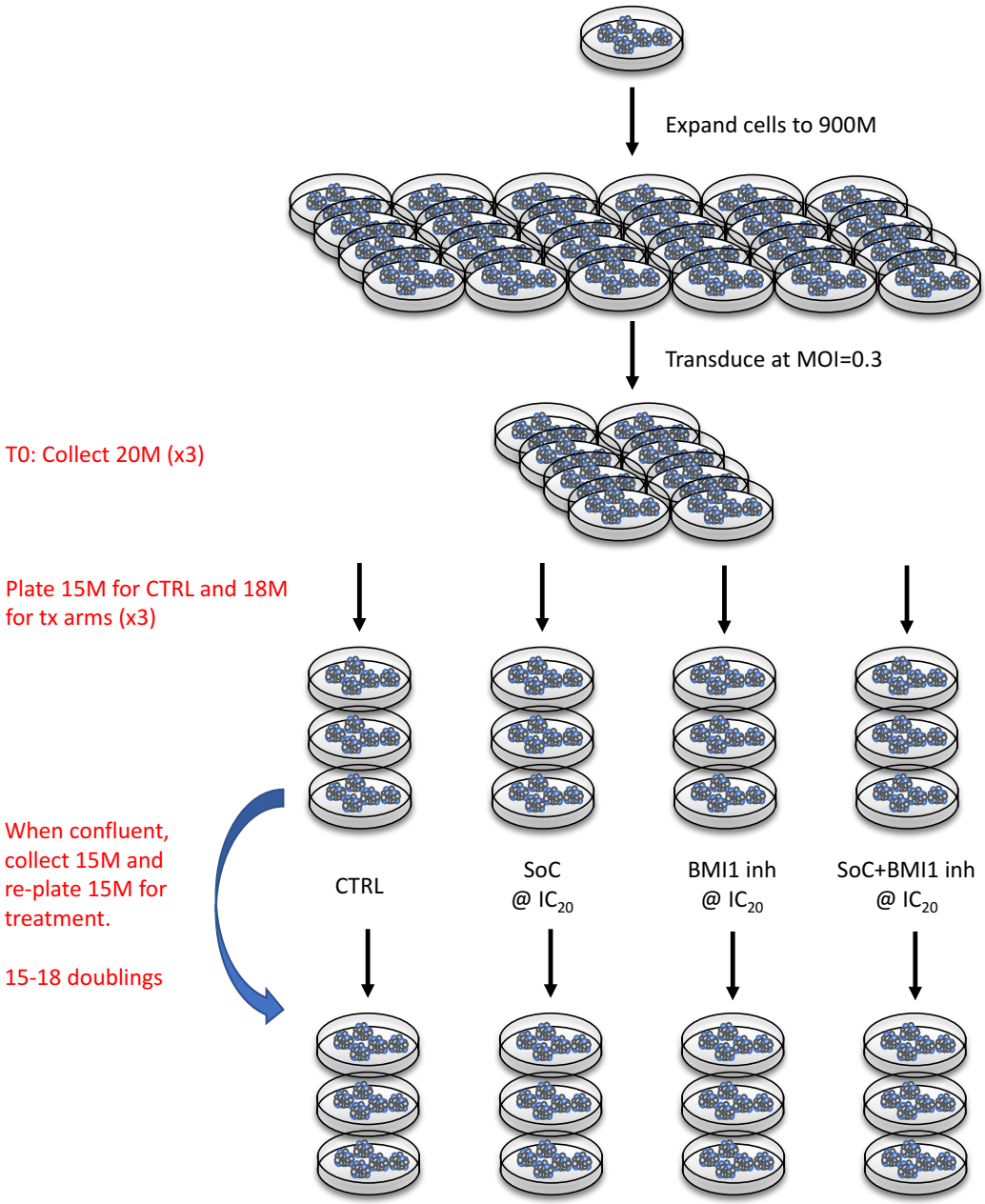
Expand cells to 900M
Transduce at MOI=0.3
T0: Collect 20M (x3)
Plate 15M for CTRL and 18M for tx arms (x3)
When confluent, collect 15M and re-plate 15M for treatment.
15-18 doublings
CTRL
SoC @ IC20
BMI1 inh @ IC20
SoC+BMI1 inh @ IC20

Figure 5: Schematic for the proposed *in vitro* genome-wide CRISPR-Cas9 screen.

Table 1: mRNA counts generated using NanoString nCounter system.

		WNT	Group 4	
GENE:	**hNSC**	**BT800**	**BT611**	**S16**
IMPG2	52.04	6884.58	43.16	16907.77
EGFL11	9.68	18.12	74.55	5131.52
KHDRBS2	13.31	14.59	1114.3	4841.81
EZH2	964.54	541.86	3905.94	4479.14
NOTCH2	1350.6	1679.93	1181	3901.79
Bmi1	645.05	1526.57	3246.78	3514.11
FSTL5	18.15	31.82	262.88	3353.62
MYCN	96.82	2623.98	2569.96	1302.68
IGF2	12.1	19	1135.88	864.98
NRL	18.15	46.85	74.55	800.37
PTCH2	24.2	15.47	353.12	631.54
UNC5D	44.78	19.89	623.85	258.45
EYA1	7.26	11.49	29.43	108.38
GLI1	3.63	16.35	43.16	31.26

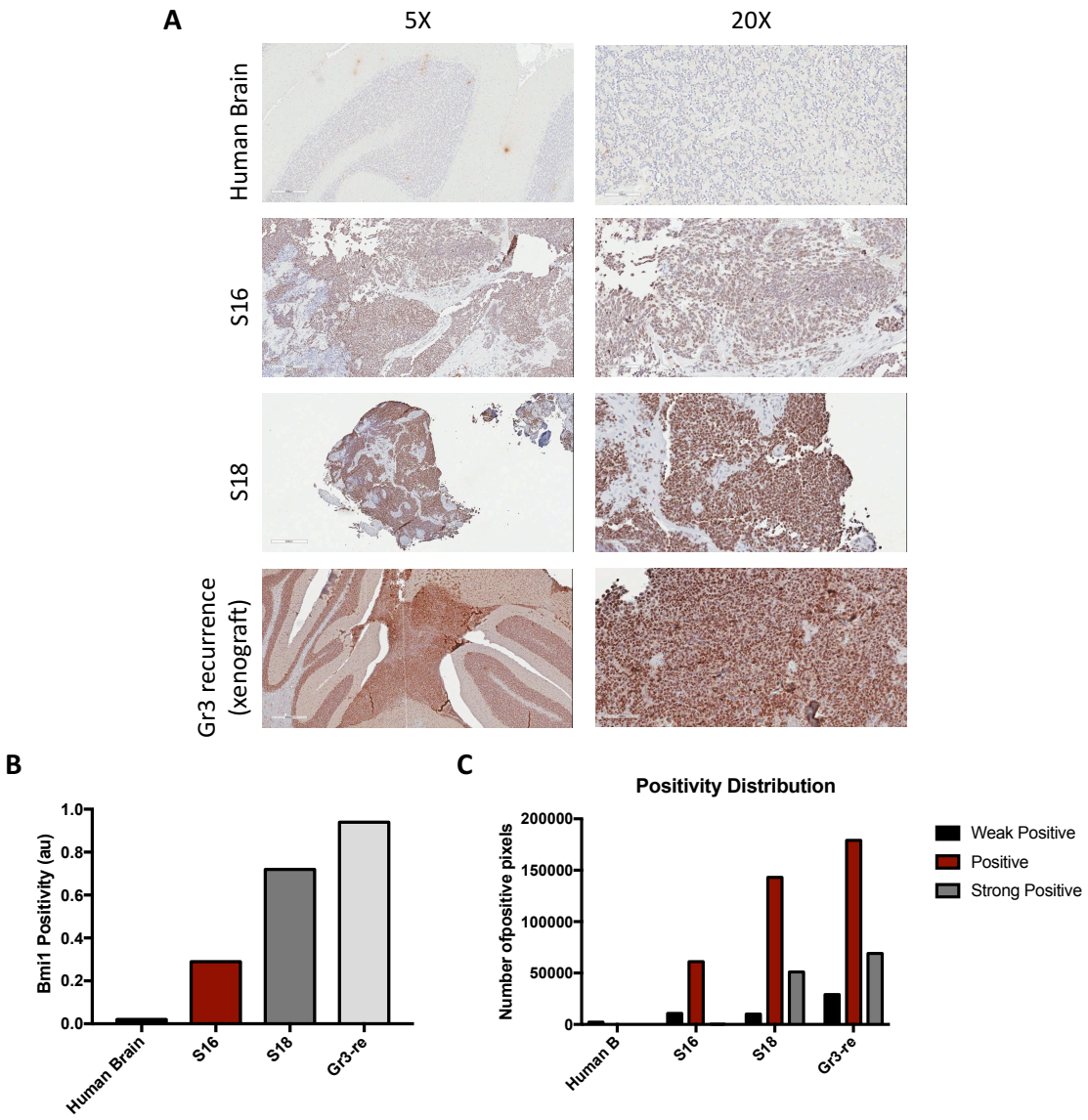
A
5X
20X
Human Brain
S16
S18
Gr3 recurrence (xenograft)
B
Bmi1 Positivity (au)
1.0
0.8
0.6
0.4
0.2
0.0
Human Brain
S16
S18
Gr3-re
C
Positivity Distribution
Number ofpositive pixels
200000
150000
100000
50000
0
Human B
S16
S18
Gr3-re
Weak Positive
Positive
Strong Positive

Figure 6: Immunohistochemical analysis of BMI1 expression in matched primary-recurrent tissue specimen. BMI1 protein levels were profiled in 4 samples by immunohistochemistry using (Ab name: Human BMI-1 Antibody Monoclonal Mouse IgG2A Clone # 384509 R&D, Catalog Number: MAB33342): (i) normal human brain tissue; (ii) S16 sample (Primary); (iii) S18 (Recurrent) sample; and (iv) Group 3 Recurrent MB, generated through therapy adapted PDX mouse model. Images were processed and analyzed with Aperio ImageScope software.

Chapter 6: Discussion

Insights into molecular drivers of MB pathogenesis will continue to guide identification of targeted therapies allowing for selective killing of MB cells while sparing the normal cells of the developing cerebellum. However, due to existence of distinct MB subtypes, each driven by a different set of genes, development of subtype-specific targeted therapies is required. The focus of this thesis has been to identify and characterize molecular drivers of recurrent Group 3 MB, with the specific emphasis on gene regulating self-renewal, as well as investigate their therapeutic potential.

6.1 Targeted therapies for Group 3 MB

Although molecular profiling have not revealed any single pathway driving Group 3 MB progression, a defining feature of this subgroup is an aberrant expression or amplification of *MYC* oncogene((Taylor et al., 2012). Unfortunately, target-specific small molecule inhibitors against MYC remain to be described, inhibitors of epigenetic regulators of *MYC* have shown to decrease viability of Group 3 MB cells(Bandopadhayay et al., 2014; Veo et al., 2019). Treatment of Group 3 MB cells with BET inhibitor, JQ1, decreased expression of *MYC* and subsequently reduced proliferation in MYC-driven MB cells(Bandopadhayay et al., 2014). More recently, a monomethyltrasferase of histone 4 lysine 20, SETD8, has been described as a potential target for *MYC*-driven MB. By performing a combined functional genomic and chemical screen, Veo *et al*, demonstrated that epigenetic probe targeting SETD8, UNC0379 can reduce *in vitro* self-renewal and metastasis in Group 3 MB. However, the efficiency of blood-brain-barrier penetration of this compound remains

to be investigated(Veo et al., 2019). Similarly to other cancers, it is unlikely that targeting one driver gene in a heterogeneous tumor will result in a long-lasting effect, thus it is important to investigate synergistic effects between multiple inhibitors to achieve a global and sustained response. Interestingly, a study combining inhibitors of histone deacetylase (HDAC) with PI3K inhibitors showed a combinatorial effect that prolonged mouse survival *in vivo*(Pei et al., 2016). In our work (Chapters 4 & 5), we showed that following chemoradiotherapy, Group 3 MB cells were susceptible to BMI1 inhibition, however, it was insufficient to fully prevent disease progression. Currently, more work is being conducted to understand molecular mechanisms driving therapy failure and development of combinatorial therapies (Chapter 6). In addition to DNA barcoding and CRISPR screening technology, a large scale chemical screen on therapy resistant cells might provide an insight into potential candidates for further synergistic evaluation. Using FDA-approved libraries might further expedite translation of the findings into clinic. A study conducted by Morfouace et al, have tested a library of FDA-approved compound on treatment naïve Group 3 MB and identified the sensitivity of cells to folate pathway inhibitor, pemetrexed(Morfouace et al., 2016). The combination of pemetrexed, with gemcitabine is currently being tested in a clinical trial (NCT01878617) for newly diagnosed MB.

In the recent years, the therapeutic relevance of treatments has been assessed through the established PDX models of Group 3 MB(Bandopadhayay et al., 2014; Cook Sangar et al., 2017; Morfouace et al., 2016; Pei et al., 2016; Tang et al., 2014). The major benefit of using PDX models is the preservation of molecular and cellular features of the original tumor

unlike the *in vitro* passaged cells lines(Daniel et al., 2009; Zhao et al., 2012). However, the number of samples that can be established into a PDX remains limited, with increased prevalence of PDX lines representative of non-Wnt/Shh MB subtypes. Through generation of a therapy adapted PDX model of Group 3 MB (Chapter 2), we were able to comprehensively profile gene expression patters of cells undergoing therapy. This gene expression profile can be used to identify potential therapeutic targets using computational approaches such as disease-model signature versus compound-variety enriched response (DiSCoVER)(Hanaford et al., 2016). When applied to the model of Group 3 MB, software analysis predicted efficacy of CDK4/6 inhibitor, which were later validated in PDX model of Group 3 MB(Cook Sangar et al., 2017). The major obstacle in translating MB targeting compounds is the blood-brain barrier. Although many compounds have shown their promising efficacy *in vitro* some failed to cross the blood brain barrier and were rendered ineffective. A recent study by Phoenix *et al*, has shown that Wnt MB tumors are able to cause a local disruption in the blood-brain barrier making tumor cells exposed to chemotherapy(Phoenix et al., 2016).

6.2 Targeting nitric oxide pathway for treatment refractory MB

One of the key observations made from profiling gene expression of cells as they undergo therapy (Chapter 2) was the upregulation of genes contributing to cellular levels of nitric oxide (NO). Since its identification in 1987(Ignarro et al., 1987; Palmer et al., 1987), NO has emerged as a molecule of interest in cancer. Currently, the exact role of NO in cancers cells remains unclear, as there are studies suggestive of its tumoricidal(Harada et al., 2004;

Shang et al., 2002) and tumor promoting effects(Cobbs et al., 1995; Reveneau et al., 1999; Thomsen et al., 1994). NO is endogeneously synthesized by a family of nitric oxide synthase (NOS) enzymes: NOS1 (nNOS), NOS2 (iNOS), NOS3 (eNOS). Unlike the inducible NOS (iNOS), nNOS and eNOS are constituently expressed in neurons and endothelial cells respectively(Moncada et al., 1991). Production of NO largely depends on the calcium concentration in the tissue, while the concentration of NO dictates its downstream effects(Ambs et al., 1998; Grisham et al., 1999). While in some cancers, increased levels of NO can contribute to regulation of cell cycle, angiogenesis, invasion and metastasis(Ying and Hofseth, 2007), it can also lead to induction of pro-apoptotic signalling, upregulation of p53 and suppression of DNA synthesis. The dichotomous nature of NO in cancer remains to be a hurdle in developing therapies exploiting NO signalling cascade and thus further tumor type specific studies are required.

A study in 1995 profiling levels of NOS isoforms in brain tumors including medulloblastoma, showed an upregulation of NOS1 and NOS2 isoforms when compared to normal brain tissue(Cobbs et al., 1995). Furthermore, in a cell line model of SHH MB, an upregulation of a calcium channel known as Transient Receptor Potential Cation Channel Subfamily C Member 4 (TRPC4), induced increased NO production and subsequent tumor motility *in vitro*(Wei et al., 2017). Nevertheless, studies on the exact role of NO in MB initiation, progression, metastasis and relapse are limited and should be further investigated using the new generation of genomic tools.

6.3 Concluding remarks

Over the last 25 years, MB therapies have remained largely unchanged and although five-year survival rates have reached 70-80%, there are still patients who are presented with tumor relapse and/or metastatic dissemination and are limited to palliation. In this thesis work, I have presented a therapy-adapted PDX model of the most aggressive MB subgroup used to profile gene expression and functional attributes of MB cells as they undergo therapy. The resulting comprehensive profiling lead to identification of a previously uncharacterized in the setting of cancer gene, BPIFB4, as a potential driver of therapy evasion and tumor relapse. Furthermore, the developed model allows for pre-clinical testing of novel therapeutic agents in combination with the current gold-standard therapy. Finally, by profiling effects of inhibiting a key self-renewal regulator gene, BMI1, I was able to demonstrate its value for treatment of recurrent MB patients. Studies into combinatorial therapy regimens driven by extensive molecular profiling of each patient's tumor will continue to provide new therapies for this devastating disease.

Bibliography:

Abdouh, M., Facchino, S., Chatoo, W., Balasingam, V., Ferreira, J., and Bernier, G. (2009). BMI1 sustains human glioblastoma multiforme stem cell renewal. J Neurosci *29*, 8884-8896.
Aguilo, F., Zhou, M.M., and Walsh, M.J. (2011). Long noncoding RNA, polycomb, and the ghosts haunting INK4b-ARF-INK4a expression. Cancer Res *71*, 5365-5369.
Al-Hajj, M., Wicha, M.S., Benito-Hernandez, A., Morrison, S.J., and Clarke, M.F. (2003). Prospective identification of tumorigenic breast cancer cells. Proc Natl Acad Sci U S A *100*, 3983-3988.
Alimova, I., Venkataraman, S., Harris, P., Marquez, V.E., Northcott, P.A., Dubuc, A., Taylor, M.D., Foreman, N.K., and Vibhakar, R. (2012). Targeting the enhancer of zeste homologue 2 in medulloblastoma. Int J Cancer *131*, 1800-1809.
Alkema, M.J., Wiegant, J., Raap, A.K., Berns, A., and van Lohuizen, M. (1993). Characterization and chromosomal localization of the human proto-oncogene BMI-1. Hum Mol Genet *2*, 1597-1603.
Allen, K.E., and Weiss, G.J. (2010). Resistance may not be futile: microRNA biomarkers for chemoresistance and potential therapeutics. Mol Cancer Ther *9*, 3126-3136.
Alonso, M.M., Diez-Valle, R., Manterola, L., Rubio, A., Liu, D., Cortes-Santiago, N., Urquiza, L., Jauregi, P., Lopez de Munain, A., Sampron, N*., et al.* (2011). Genetic and epigenetic modifications of Sox2 contribute to the invasive phenotype of malignant gliomas. PLoS One *6*, e26740.
Ambs, S., Merriam, W.G., Ogunfusika, M.O., Bennett, W.P., Ishibe, N., Hussain, S.P., Tzeng, E.E., Geller, D.A., Billiar, T.R., and Harris, C.C. (1998). p53 and vascular endothelial growth factor regulate tumor growth of NOS2-expressing human carcinoma cells. Nat Med *4*, 1371-1376.
Artero Castro, A., Long, K., Bassett, A., Machuca, C., Leon, M., Avila-Fernandez, A., Corton, M., Vidal-Puig, T., Ayuso, C., Lukovic, D*., et al.* (2019). Generation of gene-corrected human induced pluripotent stem cell lines derived from retinitis pigmentosa patient with Ser331Cysfs*5 mutation in MERTK. Stem Cell Res *34*, 101341.
Bandopadhayay, P., Bergthold, G., Nguyen, B., Schubert, S., Gholamin, S., Tang, Y., Bolin, S., Schumacher, S.E., Zeid, R., Masoud, S*., et al.* (2014). BET bromodomain inhibition of MYC-amplified medulloblastoma. Clin Cancer Res *20*, 912-925.
Bansal, N., Bartucci, M., Yusuff, S., Davis, S., Flaherty, K., Huselid, E., Patrizii, M., Jones, D., Cao, L., Sydorenko, N*., et al.* (2016). BMI-1 Targeting Interferes with Patient-Derived Tumor-Initiating Cell Survival and Tumor Growth in Prostate Cancer. Clin Cancer Res *22*, 6176-6191.
Bao, S., Wu, Q., Li, Z., Sathornsumetee, S., Wang, H., McLendon, R.E., Hjelmeland, A.B., and Rich, J.N. (2008). Targeting cancer stem cells through L1CAM suppresses glioma growth. Cancer Res *68*, 6043-6048.

Bao, S., Wu, Q., McLendon, R.E., Hao, Y., Shi, Q., Hjelmeland, A.B., Dewhirst, M.W., Bigner, D.D., and Rich, J.N. (2006). Glioma stem cells promote radioresistance by preferential activation of the DNA damage response. Nature *444*, 756-760.
Barker, N., van Es, J.H., Kuipers, J., Kujala, P., van den Born, M., Cozijnsen, M., Haegebarth, A., Korving, J., Begthel, H., Peters, P.J.*, et al.* (2007). Identification of stem cells in small intestine and colon by marker gene Lgr5. Nature *449*, 1003-1007.
Bartucci, M., Hussein, M.S., Huselid, E., Flaherty, K., Patrizii, M., Laddha, S.V., Kui, C., Bigos, R.A., Gilleran, J.A., El Ansary, M.M.S.*, et al.* (2017). Synthesis and Characterization of Novel BMI1 Inhibitors Targeting Cellular Self-Renewal in Hepatocellular Carcinoma. Target Oncol.
Beier, D., Schriefer, B., Brawanski, K., Hau, P., Weis, J., Schulz, J.B., and Beier, C.P. (2012). Efficacy of clinically relevant temozolomide dosing schemes in glioblastoma cancer stem cell lines. J Neurooncol *109*, 45-52.
Bengani, H., Mendiratta, S., Maini, J., Vasanthi, D., Sultana, H., Ghasemi, M., Ahluwalia, J., Ramachandran, S., Mishra, R.K., and Brahmachari, V. (2013). Identification and Validation of a Putative Polycomb Responsive Element in the Human Genome. PLoS One *8*, e67217.
Bibikova, M., Beumer, K., Trautman, J.K., and Carroll, D. (2003). Enhancing gene targeting with designed zinc finger nucleases. Science *300*, 764.
Bignell, G.R., Greenman, C.D., Davies, H., Butler, A.P., Edkins, S., Andrews, J.M., Buck, G., Chen, L., Beare, D., Latimer, C.*, et al.* (2010). Signatures of mutation and selection in the cancer genome. Nature *463*, 893-898.
Binda, E., Visioli, A., Giani, F., Lamorte, G., Copetti, M., Pitter, K.L., Huse, J.T., Cajola, L., Zanetti, N., DiMeco, F.*, et al.* (2012). The EphA2 receptor drives self-renewal and tumorigenicity in stem-like tumor-propagating cells from human glioblastomas. Cancer Cell *22*, 765-780.
Boch, J., Scholze, H., Schornack, S., Landgraf, A., Hahn, S., Kay, S., Lahaye, T., Nickstadt, A., and Bonas, U. (2009). Breaking the code of DNA binding specificity of TAL-type III effectors. Science *326*, 1509-1512.
Bolomsky, A., Schlangen, K., Schreiner, W., Zojer, N., and Ludwig, H. (2016). Targeting of BMI-1 with PTC-209 shows potent anti-myeloma activity and impairs the tumour microenvironment. J Hematol Oncol *9*, 17.
Bolotin, A., Quinquis, B., Sorokin, A., and Ehrlich, S.D. (2005). Clustered regularly interspaced short palindrome repeats (CRISPRs) have spacers of extrachromosomal origin. Microbiology *151*, 2551-2561.
Bommi, P.V., Dimri, M., Sahasrabuddhe, A.A., Khandekar, J., and Dimri, G.P. (2010). The polycomb group protein BMI1 is a transcriptional target of HDAC inhibitors. Cell Cycle *9*, 2663-2673.
Bonnet, D., and Dick, J.E. (1997). Human acute myeloid leukemia is organized as a hierarchy that originates from a primitive hematopoietic cell. Nat Med *3*, 730-737.
Bradly, D.P., Gattuso, P., Pool, M., Basu, S., Liptay, M., Bonomi, P., and Buckingham, L. (2012). CDKN2A (p16) promoter hypermethylation influences the outcome in young lung cancer patients. Diagn Mol Pathol *21*, 207-213.

Bredt, D.S., Hwang, P.M., and Snyder, S.H. (1990). Localization of nitric oxide synthase indicating a neural role for nitric oxide. Nature *347*, 768-770.
Brockdorff, N. (2013). Noncoding RNA and Polycomb recruitment. RNA *19*, 429-442.
Bruggeman, S.W., Hulsman, D., Tanger, E., Buckle, T., Blom, M., Zevenhoven, J., van Tellingen, O., and van Lohuizen, M. (2007). Bmi1 controls tumor development in an Ink4a/Arf-independent manner in a mouse model for glioma. Cancer Cell *12*, 328-341.
Burrell, R.A., McGranahan, N., Bartek, J., and Swanton, C. (2013). The causes and consequences of genetic heterogeneity in cancer evolution. Nature *501*, 338-345.
Cao, L., Bombard, J., Cintron, K., Sheedy, J., Weetall, M.L., and Davis, T.W. (2011). BMI1 as a novel target for drug discovery in cancer. J Cell Biochem *112*, 2729-2741.
Cao, R., Tsukada, Y., and Zhang, Y. (2005). Role of Bmi-1 and Ring1A in H2A ubiquitylation and Hox gene silencing. Mol Cell *20*, 845-854.
Cao, R., Wang, L., Wang, H., Xia, L., Erdjument-Bromage, H., Tempst, P., Jones, R.S., and Zhang, Y. (2002). Role of histone H3 lysine 27 methylation in Polycomb-group silencing. Science *298*, 1039-1043.
Cavalli, F.M.G., Remke, M., Rampasek, L., Peacock, J., Shih, D.J.H., Luu, B., Garzia, L., Torchia, J., Nor, C., Morrissy, A.S.*, et al.* (2017). Intertumoral Heterogeneity within Medulloblastoma Subgroups. Cancer Cell *31*, 737-754 e736.
Cenci, T., Martini, M., Montano, N., D'Alessandris, Q.G., Falchetti, M.L., Annibali, D., Savino, M., Bianchi, F., Pierconti, F., Nasi, S.*, et al.* (2012). Prognostic relevance of c-Myc and BMI1 expression in patients with glioblastoma. Am J Clin Pathol *138*, 390-396.
Chandler, H., and Peters, G. (2013). Stressing the cell cycle in senescence and aging. Curr Opin Cell Biol *25*, 765-771.
Chen, J., Li, Y., Yu, T.S., McKay, R.M., Burns, D.K., Kernie, S.G., and Parada, L.F. (2012). A restricted cell population propagates glioblastoma growth after chemotherapy. Nature *488*, 522-526.
Chen, S., Sanjana, N.E., Zheng, K., Shalem, O., Lee, K., Shi, X., Scott, D.A., Song, J., Pan, J.Q., Weissleder, R.*, et al.* (2015). Genome-wide CRISPR screen in a mouse model of tumor growth and metastasis. Cell *160*, 1246-1260.
Cho, J.H., Wang, K., and Galas, D.J. (2011a). An integrative approach to inferring biologically meaningful gene modules. BMC Syst Biol *5*, 117.
Cho, Y.J., Tsherniak, A., Tamayo, P., Santagata, S., Ligon, A., Greulich, H., Berhoukim, R., Amani, V., Goumnerova, L., Eberhart, C.G.*, et al.* (2011b). Integrative genomic analysis of medulloblastoma identifies a molecular subgroup that drives poor clinical outcome. J Clin Oncol *29*, 1424-1430.
Cobbs, C.S., Brenman, J.E., Aldape, K.D., Bredt, D.S., and Israel, M.A. (1995). Expression of nitric oxide synthase in human central nervous system tumors. Cancer Res *55*, 727-730.
Cohnheim, J. (1875). Congenitales, quergestreiftes muskelsarkon der nireren. Virchows Arch, 65-64.

Cook Sangar, M.L., Genovesi, L.A., Nakamoto, M.W., Davis, M.J., Knobluagh, S.E., Ji, P., Millar, A., Wainwright, B.J., and Olson, J.M. (2017). Inhibition of CDK4/6 by Palbociclib Significantly Extends Survival in Medulloblastoma Patient-Derived Xenograft Mouse Models. Clin Cancer Res *23*, 5802-5813.
Crawford, J.R., MacDonald, T.J., and Packer, R.J. (2007). Medulloblastoma in childhood: new biological advances. Lancet Neurol *6*, 1073-1085.
Cuddapah, S., Roh, T.Y., Cui, K., Jose, C.C., Fuller, M.T., Zhao, K., and Chen, X. (2012). A novel human polycomb binding site acts as a functional polycomb response element in Drosophila. PLoS One *7*, e36365.
Czermin, B., Melfi, R., McCabe, D., Seitz, V., Imhof, A., and Pirrotta, V. (2002). Drosophila enhancer of Zeste/ESC complexes have a histone H3 methyltransferase activity that marks chromosomal Polycomb sites. Cell *111*, 185-196.
Daniel, V.C., Marchionni, L., Hierman, J.S., Rhodes, J.T., Devereux, W.L., Rudin, C.M., Yung, R., Parmigiani, G., Dorsch, M., Peacock, C.D.*, et al.* (2009). A primary xenograft model of small-cell lung cancer reveals irreversible changes in gene expression imposed by culture in vitro. Cancer Res *69*, 3364-3373.
Day, B.W., Stringer, B.W., Al-Ejeh, F., Ting, M.J., Wilson, J., Ensbey, K.S., Jamieson, P.R., Bruce, Z.C., Lim, Y.C., Offenhauser, C.*, et al.* (2013). EphA3 maintains tumorigenicity and is a therapeutic target in glioblastoma multiforme. Cancer Cell *23*, 238-248.
Dimri, M., Cho, J.H., Kang, M., and Dimri, G.P. (2015). PLK1 inhibition down-regulates polycomb group protein BMI1 via modulation of the miR-200c/141 cluster. J Biol Chem *290*, 3033-3044.
Douglas, D., Hsu, J.H., Hung, L., Cooper, A., Abdueva, D., van Doorninck, J., Peng, G., Shimada, H., Triche, T.J., and Lawlor, E.R. (2008). BMI-1 promotes ewing sarcoma tumorigenicity independent of CDKN2A repression. Cancer Res *68*, 6507-6515.
Dubuc, A.M., Remke, M., Korshunov, A., Northcott, P.A., Zhan, S.H., Mendez-Lago, M., Kool, M., Jones, D.T., Unterberger, A., Morrissy, A.S.*, et al.* (2013). Aberrant patterns of H3K4 and H3K27 histone lysine methylation occur across subgroups in medulloblastoma. Acta Neuropathol *125*, 373-384.
Dunkel, I.J., Boyett, J.M., Yates, A., Rosenblum, M., Garvin, J.H., Jr., Bostrom, B.C., Goldman, S., Sender, L.S., Gardner, S.L., Li, H.*, et al.* (1998). High-dose carboplatin, thiotepa, and etoposide with autologous stem-cell rescue for patients with recurrent medulloblastoma. Children's Cancer Group. J Clin Oncol *16*, 222-228.
Ellison, D.W. (2010). Childhood medulloblastoma: novel approaches to the classification of a heterogeneous disease. Acta Neuropathol *120*, 305-316.
Ezzat, S., Kamal, M., El-Khateeb, N., El-Beltagy, M., Taha, H., Refaat, A., Awad, M., Abouelnaga, S., and Zaghloul, M.S. (2016). Pediatric brain tumors in a low/middle income country: does it differ from that in developed world? J Neurooncol *126*, 371-376.
Facchino, S., Abdouh, M., Chatoo, W., and Bernier, G. (2010). BMI1 confers radioresistance to normal and cancerous neural stem cells through recruitment of the DNA damage response machinery. J Neurosci *30*, 10096-10111.

Fattet, S., Haberler, C., Legoix, P., Varlet, P., Lellouch-Tubiana, A., Lair, S., Manie, E., Raquin, M.A., Bours, D., Carpentier, S.*, et al.* (2009). Beta-catenin status in paediatric medulloblastomas: correlation of immunohistochemical expression with mutational status, genetic profiles, and clinical characteristics. J Pathol *218*, 86-94.
Fischle, W., Wang, Y., Jacobs, S.A., Kim, Y., Allis, C.D., and Khorasanizadeh, S. (2003). Molecular basis for the discrimination of repressive methyl-lysine marks in histone H3 by Polycomb and HP1 chromodomains. Genes Dev *17*, 1870-1881.
Fouladi, M., Blaney, S.M., Poussaint, T.Y., Freeman, B.B., 3rd, McLendon, R., Fuller, C., Adesina, A.M., Hancock, M.L., Danks, M.K., Stewart, C.*, et al.* (2006). Phase II study of oxaliplatin in children with recurrent or refractory medulloblastoma, supratentorial primitive neuroectodermal tumors, and atypical teratoid rhabdoid tumors: a pediatric brain tumor consortium study. Cancer *107*, 2291-2297.
Gajjar, A., Chintagumpala, M., Ashley, D., Kellie, S., Kun, L.E., Merchant, T.E., Woo, S., Wheeler, G., Ahern, V., Krasin, M.J.*, et al.* (2006). Risk-adapted craniospinal radiotherapy followed by high-dose chemotherapy and stem-cell rescue in children with newly diagnosed medulloblastoma (St Jude Medulloblastoma-96): long-term results from a prospective, multicentre trial. Lancet Oncol *7*, 813-820.
Galli, R., Binda, E., Orfanelli, U., Cipelletti, B., Gritti, A., De Vitis, S., Fiocco, R., Foroni, C., Dimeco, F., and Vescovi, A. (2004). Isolation and characterization of tumorigenic, stem-like neural precursors from human glioblastoma. Cancer Res *64*, 7011-7021.
Gandola, L., Massimino, M., Cefalo, G., Solero, C., Spreafico, F., Pecori, E., Riva, D., Collini, P., Pignoli, E., Giangaspero, F.*, et al.* (2009). Hyperfractionated accelerated radiotherapy in the Milan strategy for metastatic medulloblastoma. J Clin Oncol *27*, 566-571.
Gao, Z., Zhang, J., Bonasio, R., Strino, F., Sawai, A., Parisi, F., Kluger, Y., and Reinberg, D. (2012). PCGF homologs, CBX proteins, and RYBP define functionally distinct PRC1 family complexes. Mol Cell *45*, 344-356.
Gargiulo, G., Cesaroni, M., Serresi, M., de Vries, N., Hulsman, D., Bruggeman, S.W., Lancini, C., and van Lohuizen, M. (2013). In vivo RNAi screen for BMI1 targets identifies TGF-beta/BMP-ER stress pathways as key regulators of neural- and malignant glioma-stem cell homeostasis. Cancer Cell *23*, 660-676.
Gerrits, A., Dykstra, B., Kalmykowa, O.J., Klauke, K., Verovskaya, E., Broekhuis, M.J., de Haan, G., and Bystrykh, L.V. (2010). Cellular barcoding tool for clonal analysis in the hematopoietic system. Blood *115*, 2610-2618.
Gibson, P., Tong, Y., Robinson, G., Thompson, M.C., Currle, D.S., Eden, C., Kranenburg, T.A., Hogg, T., Poppleton, H., Martin, J.*, et al.* (2010). Subtypes of medulloblastoma have distinct developmental origins. Nature *468*, 1095-1099.
Gilbertson, R.J. (2004). Medulloblastoma: signalling a change in treatment. Lancet Oncol *5*, 209-218.
Ginjala, V., Nacerddine, K., Kulkarni, A., Oza, J., Hill, S.J., Yao, M., Citterio, E., van Lohuizen, M., and Ganesan, S. (2011). BMI1 is recruited to DNA breaks and contributes to DNA damage-induced H2A ubiquitination and repair. Mol Cell Biol *31*, 1972-1982.

Glinsky, G.V. (2007). Stem cell origin of death-from-cancer phenotypes of human prostate and breast cancers. Stem Cell Rev *3*, 79-93.
Glinsky, G.V., Berezovska, O., and Glinskii, A.B. (2005). Microarray analysis identifies a death-from-cancer signature predicting therapy failure in patients with multiple types of cancer. J Clin Invest *115*, 1503-1521.
Greaves, M., and Maley, C.C. (2012). Clonal evolution in cancer. Nature *481*, 306-313.
Grisham, M.B., Jourd'Heuil, D., and Wink, D.A. (1999). Nitric oxide. I. Physiological chemistry of nitric oxide and its metabolites:implications in inflammation. Am J Physiol *276*, G315-321.
Guo, B.H., Feng, Y., Zhang, R., Xu, L.H., Li, M.Z., Kung, H.F., Song, L.B., and Zeng, M.S. (2011). Bmi-1 promotes invasion and metastasis, and its elevated expression is correlated with an advanced stage of breast cancer. Mol Cancer *10*, 10.
Guo, B.H., Zhang, X., Zhang, H.Z., Lin, H.L., Feng, Y., Shao, J.Y., Huang, W.L., Kung, H.F., and Zeng, M.S. (2010). Low expression of Mel-18 predicts poor prognosis in patients with breast cancer. Ann Oncol *21*, 2361-2369.
Guo, W.J., Datta, S., Band, V., and Dimri, G.P. (2007a). Mel-18, a polycomb group protein, regulates cell proliferation and senescence via transcriptional repression of Bmi-1 and c-Myc oncoproteins. Mol Biol Cell *18*, 536-546.
Guo, W.J., Zeng, M.S., Yadav, A., Song, L.B., Guo, B.H., Band, V., and Dimri, G.P. (2007b). Mel-18 acts as a tumor suppressor by repressing Bmi-1 expression and down-regulating Akt activity in breast cancer cells. Cancer Res *67*, 5083-5089.
Gururangan, S., Krauser, J., Watral, M.A., Driscoll, T., Larrier, N., Reardon, D.A., Rich, J.N., Quinn, J.A., Vredenburgh, J.J., Desjardins, A.*, et al.* (2008). Efficacy of high-dose chemotherapy or standard salvage therapy in patients with recurrent medulloblastoma. Neuro Oncol *10*, 745-751.
Hallett, R.M., Dvorkin-Gheva, A., Bane, A., and Hassell, J.A. (2012a). A gene signature for predicting outcome in patients with basal-like breast cancer. Sci Rep *2*, 227.
Hallett, R.M., Pond, G., and Hassell, J.A. (2012b). A target based approach identifies genomic predictors of breast cancer patient response to chemotherapy. BMC Med Genomics *5*, 16.
Hanaford, A.R., Archer, T.C., Price, A., Kahlert, U.D., Maciaczyk, J., Nikkhah, G., Kim, J.W., Ehrenberger, T., Clemons, P.A., Dancik, V.*, et al.* (2016). DiSCoVERing Innovative Therapies for Rare Tumors: Combining Genetically Accurate Disease Models with In Silico Analysis to Identify Novel Therapeutic Targets. Clin Cancer Res *22*, 3903-3914.
Harada, K., Supriatno, Kawaguchi, S., Tomitaro, O., Yoshida, H., and Sato, M. (2004). Overexpression of iNOS gene suppresses the tumorigenicity and metastasis of oral cancer cells. In Vivo *18*, 449-455.
Hart, T., Chandrashekhar, M., Aregger, M., Steinhart, Z., Brown, K.R., MacLeod, G., Mis, M., Zimmermann, M., Fradet-Turcotte, A., Sun, S.*, et al.* (2015). High-Resolution CRISPR Screens Reveal Fitness Genes and Genotype-Specific Cancer Liabilities. Cell *163*, 1515-1526.
Haupt, Y., Bath, M.L., Harris, A.W., and Adams, J.M. (1993). bmi-1 transgene induces lymphomas and collaborates with myc in tumorigenesis. Oncogene *8*, 3161-3164.

He, X.M., Wikstrand, C.J., Friedman, H.S., Bigner, S.H., Pleasure, S., Trojanowski, J.Q., and Bigner, D.D. (1991). Differentiation characteristics of newly established medulloblastoma cell lines (D384 Med, D425 Med, and D458 Med) and their transplantable xenografts. Lab Invest *64*, 833-843.
Hemmati, H.D., Nakano, I., Lazareff, J.A., Masterman-Smith, M., Geschwind, D.H., Bronner-Fraser, M., and Kornblum, H.I. (2003). Cancerous stem cells can arise from pediatric brain tumors. Proc Natl Acad Sci U S A *100*, 15178-15183.
Hill, R.M., Kuijper, S., Lindsey, J.C., Petrie, K., Schwalbe, E.C., Barker, K., Boult, J.K., Williamson, D., Ahmad, Z., Hallsworth, A*., et al.* (2015). Combined MYC and P53 defects emerge at medulloblastoma relapse and define rapidly progressive, therapeutically targetable disease. Cancer Cell *27*, 72-84.
Ho, M.M., Ng, A.V., Lam, S., and Hung, J.Y. (2007). Side population in human lung cancer cell lines and tumors is enriched with stem-like cancer cells. Cancer Res *67*, 4827-4833.
Honig, A., Weidler, C., Hausler, S., Krockenberger, M., Buchholz, S., Koster, F., Segerer, S.E., Dietl, J., and Engel, J.B. (2010). Overexpression of polycomb protein BMI-1 in human specimens of breast, ovarian, endometrial and cervical cancer. Anticancer Res *30*, 1559-1564.
Hosen, N., Yamane, T., Muijtjens, M., Pham, K., Clarke, M.F., and Weissman, I.L. (2007). Bmi-1-green fluorescent protein-knock-in mice reveal the dynamic regulation of bmi-1 expression in normal and leukemic hematopoietic cells. Stem Cells *25*, 1635-1644.
Huse, J.T., and Holland, E.C. (2010). Targeting brain cancer: advances in the molecular pathology of malignant glioma and medulloblastoma. Nat Rev Cancer *10*, 319-331.
Ignarro, L.J., Buga, G.M., Wood, K.S., Byrns, R.E., and Chaudhuri, G. (1987). Endothelium-derived relaxing factor produced and released from artery and vein is nitric oxide. Proc Natl Acad Sci U S A *84*, 9265-9269.
Ignatova, T.N., Kukekov, V.G., Laywell, E.D., Suslov, O.N., Vrionis, F.D., and Steindler, D.A. (2002). Human cortical glial tumors contain neural stem-like cells expressing astroglial and neuronal markers in vitro. Glia *39*, 193-206.
Illmensee, K. (1978). Reversion of malignancy and normalized differentiation of teratocarcinoma cells in chimeric mice. Basic Life Sci *12*, 3-25.
Irizarry, R.A., Hobbs, B., Collin, F., Beazer-Barclay, Y.D., Antonellis, K.J., Scherf, U., and Speed, T.P. (2003). Exploration, normalization, and summaries of high density oligonucleotide array probe level data. Biostatistics *4*, 249-264.
Ismail, I.H., Andrin, C., McDonald, D., and Hendzel, M.J. (2010). BMI1-mediated histone ubiquitylation promotes DNA double-strand break repair. J Cell Biol *191*, 45-60.
Itahana, K., Zou, Y., Itahana, Y., Martinez, J.L., Beausejour, C., Jacobs, J.J., Van Lohuizen, M., Band, V., Campisi, J., and Dimri, G.P. (2003). Control of the replicative life span of human fibroblasts by p16 and the polycomb protein Bmi-1. Mol Cell Biol *23*, 389-401.

Jacobs, J.J., Scheijen, B., Voncken, J.W., Kieboom, K., Berns, A., and van Lohuizen, M. (1999). Bmi-1 collaborates with c-Myc in tumorigenesis by inhibiting c-Myc-induced apoptosis via INK4a/ARF. Genes Dev *13*, 2678-2690.
Jakacki, R.I., Burger, P.C., Zhou, T., Holmes, E.J., Kocak, M., Onar, A., Goldwein, J., Mehta, M., Packer, R.J., Tarbell, N.*, et al.* (2012). Outcome of children with metastatic medulloblastoma treated with carboplatin during craniospinal radiotherapy: a Children's Oncology Group Phase I/II study. J Clin Oncol *30*, 2648-2653.
Jermann, P., Hoerner, L., Burger, L., and Schubeler, D. (2014). Short sequences can efficiently recruit histone H3 lysine 27 trimethylation in the absence of enhancer activity and DNA methylation. Proc Natl Acad Sci U S A *111*, E3415-3421.
Jin, X., Kim, L.J.Y., Wu, Q., Wallace, L.C., Prager, B.C., Sanvoranart, T., Gimple, R.C., Wang, X., Mack, S.C., Miller, T.E.*, et al.* (2017). Targeting glioma stem cells through combined BMI1 and EZH2 inhibition. Nat Med *23*, 1352-1361.
Johnston, D.L., Keene, D., Kostova, M., Strother, D., Lafay-Cousin, L., Fryer, C., Scheinemann, K., Carret, A.S., Fleming, A., Percy, V.*, et al.* (2014). Incidence of medulloblastoma in Canadian children. J Neurooncol *120*, 575-579.
Jung, J.W., Lee, S., Seo, M.S., Park, S.B., Kurtz, A., Kang, S.K., and Kang, K.S. (2010). Histone deacetylase controls adult stem cell aging by balancing the expression of polycomb genes and jumonji domain containing 3. Cell Mol Life Sci *67*, 1165-1176.
Kajiume, T., Ohno, N., Sera, Y., Kawahara, Y., Yuge, L., and Kobayashi, M. (2009). Reciprocal expression of Bmi1 and Mel-18 is associated with functioning of primitive hematopoietic cells. Exp Hematol *37*, 857-866 e852.
Kajstura, J., Rota, M., Hall, S.R., Hosoda, T., D'Amario, D., Sanada, F., Zheng, H., Ogorek, B., Rondon-Clavo, C., Ferreira-Martins, J.*, et al.* (2011). Evidence for human lung stem cells. N Engl J Med *364*, 1795-1806.
Kamijo, T., Weber, J.D., Zambetti, G., Zindy, F., Roussel, M.F., and Sherr, C.J. (1998). Functional and physical interactions of the ARF tumor suppressor with p53 and Mdm2. Proc Natl Acad Sci U S A *95*, 8292-8297.
Kamijo, T., Zindy, F., Roussel, M.F., Quelle, D.E., Downing, J.R., Ashmun, R.A., Grosveld, G., and Sherr, C.J. (1997). Tumor suppression at the mouse INK4a locus mediated by the alternative reading frame product p19ARF. Cell *91*, 649-659.
Kaneta, Y., Arai, M.A., Ishikawa, N., Toume, K., Koyano, T., Kowithayakorn, T., Chiba, T., Iwama, A., and Ishibashi, M. (2017). Identification of BMI1 Promoter Inhibitors from Beaumontia murtonii and Eugenia operculata. J Nat Prod *80*, 1853-1859.
Kanno, M., Hasegawa, M., Ishida, A., Isono, K., and Taniguchi, M. (1995). mel-18, a Polycomb group-related mammalian gene, encodes a transcriptional negative regulator with tumor suppressive activity. EMBO J *14*, 5672-5678.
Karapetyan, A.R., Buiting, C., Kuiper, R.A., and Coolen, M.W. (2013). Regulatory Roles for Long ncRNA and mRNA. Cancers (Basel) *5*, 462-490.
Kawauchi, D., Robinson, G., Uziel, T., Gibson, P., Rehg, J., Gao, C., Finkelstein, D., Qu, C., Pounds, S., Ellison, D.W.*, et al.* (2012). A mouse model of the most aggressive subgroup of human medulloblastoma. Cancer Cell *21*, 168-180.

Khanna, V., Achey, R.L., Ostrom, Q.T., Block-Beach, H., Kruchko, C., Barnholtz-Sloan, J.S., and de Blank, P.M. (2017). Incidence and survival trends for medulloblastomas in the United States from 2001 to 2013. J Neurooncol *135*, 433-441.
Knight, S.C., Xie, L., Deng, W., Guglielmi, B., Witkowsky, L.B., Bosanac, L., Zhang, E.T., El Beheiry, M., Masson, J.B., Dahan, M.*, et al.* (2015). Dynamics of CRISPR-Cas9 genome interrogation in living cells. Science *350*, 823-826.
Kojima, H., Urano, Y., Kikuchi, K., Higuchi, T., Hirata, Y., and Nagano, T. (1999). Fluorescent Indicators for Imaging Nitric Oxide Production. Angew Chem Int Ed Engl *38*, 3209-3212.
Kool, M., Koster, J., Bunt, J., Hasselt, N.E., Lakeman, A., van Sluis, P., Troost, D., Meeteren, N.S., Caron, H.N., Cloos, J.*, et al.* (2008). Integrated genomics identifies five medulloblastoma subtypes with distinct genetic profiles, pathway signatures and clinicopathological features. PLoS One *3*, e3088.
Koppens, M., and van Lohuizen, M. (2016). Context-dependent actions of Polycomb repressors in cancer. Oncogene *35*, 1341-1352.
Korshunov, A., Remke, M., Werft, W., Benner, A., Ryzhova, M., Witt, H., Sturm, D., Wittmann, A., Schottler, A., Felsberg, J.*, et al.* (2010). Adult and pediatric medulloblastomas are genetically distinct and require different algorithms for molecular risk stratification. J Clin Oncol *28*, 3054-3060.
Kreso, A., O'Brien, C.A., van Galen, P., Gan, O.I., Notta, F., Brown, A.M., Ng, K., Ma, J., Wienholds, E., Dunant, C.*, et al.* (2013). Variable clonal repopulation dynamics influence chemotherapy response in colorectal cancer. Science *339*, 543-548.
Kreso, A., van Galen, P., Pedley, N.M., Lima-Fernandes, E., Frelin, C., Davis, T., Cao, L., Baiazitov, R., Du, W., Sydorenko, N.*, et al.* (2014). Self-renewal as a therapeutic target in human colorectal cancer. Nat Med *20*, 29-36.
Ku, M., Koche, R.P., Rheinbay, E., Mendenhall, E.M., Endoh, M., Mikkelsen, T.S., Presser, A., Nusbaum, C., Xie, X., Chi, A.S.*, et al.* (2008). Genomewide analysis of PRC1 and PRC2 occupancy identifies two classes of bivalent domains. PLoS Genet *4*, e1000242.
Kuzmichev, A., Jenuwein, T., Tempst, P., and Reinberg, D. (2004). Different EZH2-containing complexes target methylation of histone H1 or nucleosomal histone H3. Mol Cell *14*, 183-193.
Lasorella, A., Benezra, R., and Iavarone, A. (2014). The ID proteins: master regulators of cancer stem cells and tumour aggressiveness. Nat Rev Cancer *14*, 77-91.
Lathia, J.D., Gallagher, J., Heddleston, J.M., Wang, J., Eyler, C.E., Macswords, J., Wu, Q., Vasanji, A., McLendon, R.E., Hjelmeland, A.B.*, et al.* (2010). Integrin alpha 6 regulates glioblastoma stem cells. Cell Stem Cell *6*, 421-432.
Lee, J.Y., Park, M.K., Park, J.H., Lee, H.J., Shin, D.H., Kang, Y., Lee, C.H., and Kong, G. (2014). Loss of the polycomb protein Mel-18 enhances the epithelial-mesenchymal transition by ZEB1 and ZEB2 expression through the downregulation of miR-205 in breast cancer. Oncogene *33*, 1325-1335.
Lessard, J., Baban, S., and Sauvageau, G. (1998). Stage-specific expression of polycomb group genes in human bone marrow cells. Blood *91*, 1216-1224.

Lessard, J., and Sauvageau, G. (2003). Bmi-1 determines the proliferative capacity of normal and leukaemic stem cells. Nature *423*, 255-260.
Leung, C., Lingbeek, M., Shakhova, O., Liu, J., Tanger, E., Saremaslani, P., Van Lohuizen, M., and Marino, S. (2004). Bmi1 is essential for cerebellar development and is overexpressed in human medulloblastomas. Nature *428*, 337-341.
Li, D.W., Tang, H.M., Fan, J.W., Yan, D.W., Zhou, C.Z., Li, S.X., Wang, X.L., and Peng, Z.H. (2010). Expression level of Bmi-1 oncoprotein is associated with progression and prognosis in colon cancer. J Cancer Res Clin Oncol *136*, 997-1006.
Liu, J., Xiao, Z., Wong, S.K., Tin, V.P., Ho, K.Y., Wang, J., Sham, M.H., and Wong, M.P. (2013). Lung cancer tumorigenicity and drug resistance are maintained through ALDH(hi)CD44(hi) tumor initiating cells. Oncotarget *4*, 1698-1711.
Lu, Y.W., Li, J., and Guo, W.J. (2010). Expression and clinicopathological significance of Mel-18 and Bmi-1 mRNA in gastric carcinoma. J Exp Clin Cancer Res *29*, 143.
Lynch, M.D., Smith, A.J., De Gobbi, M., Flenley, M., Hughes, J.R., Vernimmen, D., Ayyub, H., Sharpe, J.A., Sloane-Stanley, J.A., Sutherland, L.*, et al.* (2012). An interspecies analysis reveals a key role for unmethylated CpG dinucleotides in vertebrate Polycomb complex recruitment. EMBO J *31*, 317-329.
Manoranjan, B., Wang, X., Hallett, R.M., Venugopal, C., Mack, S.C., McFarlane, N., Nolte, S.M., Scheinemann, K., Gunnarsson, T., Hassell, J.A.*, et al.* (2013). FoxG1 interacts with Bmi1 to regulate self-renewal and tumorigenicity of medulloblastoma stem cells. Stem Cells *31*, 1266-1277.
Marechal, A., and Zou, L. (2013). DNA damage sensing by the ATM and ATR kinases. Cold Spring Harb Perspect Biol *5*.
Mazurier, F., Gan, O.I., McKenzie, J.L., Doedens, M., and Dick, J.E. (2004). Lentivector-mediated clonal tracking reveals intrinsic heterogeneity in the human hematopoietic stem cell compartment and culture-induced stem cell impairment. Blood *103*, 545-552.
McCulloch, E.A., Till, J.E., and Siminovitch, L. (1965). The role of independent and dependent stem cells in the control of hemopoietic and immunologic responses. Wistar Inst Symp Monogr *4*, 61-68.
Meacham, C.E., and Morrison, S.J. (2013). Tumour heterogeneity and cancer cell plasticity. Nature *501*, 328-337.
Mendenhall, E.M., Koche, R.P., Truong, T., Zhou, V.W., Issac, B., Chi, A.S., Ku, M., and Bernstein, B.E. (2010). GC-rich sequence elements recruit PRC2 in mammalian ES cells. PLoS Genet *6*, e1001244.
Merkerova, M., Bruchova, H., Kracmarova, A., Klamova, H., and Brdicka, R. (2007). Bmi-1 over-expression plays a secondary role in chronic myeloid leukemia transformation. Leuk Lymphoma *48*, 793-801.
Milde, T., Lodrini, M., Savelyeva, L., Korshunov, A., Kool, M., Brueckner, L.M., Antunes, A.S., Oehme, I., Pekrun, A., Pfister, S.M.*, et al.* (2012). HD-MB03 is a novel Group 3 medulloblastoma model demonstrating sensitivity to histone deacetylase inhibitor treatment. J Neurooncol *110*, 335-348.

Min, G., Zhou, G., Schapira, M., Sun, T.T., and Kong, X.P. (2003). Structural basis of urothelial permeability barrier function as revealed by Cryo-EM studies of the 16 nm uroplakin particle. J Cell Sci *116*, 4087-4094.
Mintz, B., and Illmensee, K. (1975). Normal genetically mosaic mice produced from malignant teratocarcinoma cells. Proc Natl Acad Sci U S A *72*, 3585-3589.
Mojica, F.J., Diez-Villasenor, C., Garcia-Martinez, J., and Soria, E. (2005). Intervening sequences of regularly spaced prokaryotic repeats derive from foreign genetic elements. Journal of molecular evolution *60*, 174-182.
Molofsky, A.V., Pardal, R., Iwashita, T., Park, I.K., Clarke, M.F., and Morrison, S.J. (2003). Bmi-1 dependence distinguishes neural stem cell self-renewal from progenitor proliferation. Nature *425*, 962-967.
Moncada, S., Palmer, R.M., and Higgs, E.A. (1991). Nitric oxide: physiology, pathophysiology, and pharmacology. Pharmacol Rev *43*, 109-142.
Morfouace, M., Nimmervoll, B., Boulos, N., Patel, Y.T., Shelat, A., Freeman, B.B., 3rd, Robinson, G.W., Wright, K., Gajjar, A., Stewart, C.F.*, et al.* (2016). Preclinical studies of 5-fluoro-2'-deoxycytidine and tetrahydrouridine in pediatric brain tumors. J Neurooncol *126*, 225-234.
Morrissy, A.S., Garzia, L., Shih, D.J., Zuyderduyn, S., Huang, X., Skowron, P., Remke, M., Cavalli, F.M., Ramaswamy, V., Lindsay, P.E.*, et al.* (2016). Divergent clonal selection dominates medulloblastoma at recurrence. Nature *529*, 351-357.
Mulhern, R.K., Palmer, S.L., Merchant, T.E., Wallace, D., Kocak, M., Brouwers, P., Krull, K., Chintagumpala, M., Stargatt, R., Ashley, D.M.*, et al.* (2005). Neurocognitive consequences of risk-adapted therapy for childhood medulloblastoma. J Clin Oncol *23*, 5511-5519.
Muller, J., Hart, C.M., Francis, N.J., Vargas, M.L., Sengupta, A., Wild, B., Miller, E.L., O'Connor, M.B., Kingston, R.E., and Simon, J.A. (2002). Histone methyltransferase activity of a Drosophila Polycomb group repressor complex. Cell *111*, 197-208.
Nakada, M., Anderson, E.M., Demuth, T., Nakada, S., Reavie, L.B., Drake, K.L., Hoelzinger, D.B., and Berens, M.E. (2010). The phosphorylation of ephrin-B2 ligand promotes glioma cell migration and invasion. Int J Cancer *126*, 1155-1165.
Nakai, E., Park, K., Yawata, T., Chihara, T., Kumazawa, A., Nakabayashi, H., and Shimizu, K. (2009). Enhanced MDR1 expression and chemoresistance of cancer stem cells derived from glioblastoma. Cancer Invest *27*, 901-908.
Navin, N., Kendall, J., Troge, J., Andrews, P., Rodgers, L., McIndoo, J., Cook, K., Stepansky, A., Levy, D., Esposito, D.*, et al.* (2011). Tumour evolution inferred by single-cell sequencing. Nature *472*, 90-94.
Nguyen, L.V., Cox, C.L., Eirew, P., Knapp, D.J., Pellacani, D., Kannan, N., Carles, A., Moksa, M., Balani, S., Shah, S.*, et al.* (2014). DNA barcoding reveals diverse growth kinetics of human breast tumour subclones in serially passaged xenografts. Nat Commun *5*, 5871.
Nguyen, L.V., Vanner, R., Dirks, P., and Eaves, C.J. (2012). Cancer stem cells: an evolving concept. Nat Rev Cancer *12*, 133-143.

Nolan-Stevaux, O., Tedesco, D., Ragan, S., Makhanov, M., Chenchik, A., Ruefli-Brasse, A., Quon, K., and Kassner, P.D. (2013). Measurement of Cancer Cell Growth Heterogeneity through Lentiviral Barcoding Identifies Clonal Dominance as a Characteristic of In Vivo Tumor Engraftment. PLoS One *8*, e67316.
Northcott, P.A., Jones, D.T., Kool, M., Robinson, G.W., Gilbertson, R.J., Cho, Y.J., Pomeroy, S.L., Korshunov, A., Lichter, P., Taylor, M.D.*, et al.* (2012a). Medulloblastomics: the end of the beginning. Nat Rev Cancer *12*, 818-834.
Northcott, P.A., Korshunov, A., Witt, H., Hielscher, T., Eberhart, C.G., Mack, S., Bouffet, E., Clifford, S.C., Hawkins, C.E., French, P.*, et al.* (2011). Medulloblastoma comprises four distinct molecular variants. J Clin Oncol *29*, 1408-1414.
Northcott, P.A., Shih, D.J., Remke, M., Cho, Y.J., Kool, M., Hawkins, C., Eberhart, C.G., Dubuc, A., Guettouche, T., Cardentey, Y.*, et al.* (2012b). Rapid, reliable, and reproducible molecular sub-grouping of clinical medulloblastoma samples. Acta Neuropathol *123*, 615-626.
Oguro, H., Yuan, J., Ichikawa, H., Ikawa, T., Yamazaki, S., Kawamoto, H., Nakauchi, H., and Iwama, A. (2010). Poised lineage specification in multipotential hematopoietic stem and progenitor cells by the polycomb protein Bmi1. Cell Stem Cell *6*, 279-286.
Ohta, H., Sawada, A., Kim, J.Y., Tokimasa, S., Nishiguchi, S., Humphries, R.K., Hara, J., and Takihara, Y. (2002). Polycomb group gene rae28 is required for sustaining activity of hematopoietic stem cells. J Exp Med *195*, 759-770.
Otte, A.P., and Kwaks, T.H. (2003). Gene repression by Polycomb group protein complexes: a distinct complex for every occasion? Current opinion in genetics & development *13*, 448-454.
Oyharcabal-Bourden, V., Kalifa, C., Gentet, J.C., Frappaz, D., Edan, C., Chastagner, P., Sariban, E., Pagnier, A., Babin, A., Pichon, F.*, et al.* (2005). Standard-risk medulloblastoma treated by adjuvant chemotherapy followed by reduced-dose craniospinal radiation therapy: a French Society of Pediatric Oncology Study. J Clin Oncol *23*, 4726-4734.
Packer, R.J., Gajjar, A., Vezina, G., Rorke-Adams, L., Burger, P.C., Robertson, P.L., Bayer, L., LaFond, D., Donahue, B.R., Marymont, M.H.*, et al.* (2006). Phase III study of craniospinal radiation therapy followed by adjuvant chemotherapy for newly diagnosed average-risk medulloblastoma. J Clin Oncol *24*, 4202-4208.
Paget, J. (1853). Lectures on Surgical Pathology.
Palmer, R.M., Ferrige, A.G., and Moncada, S. (1987). Nitric oxide release accounts for the biological activity of endothelium-derived relaxing factor. Nature *327*, 524-526.
Park, I.K., Qian, D., Kiel, M., Becker, M.W., Pihalja, M., Weissman, I.L., Morrison, S.J., and Clarke, M.F. (2003). Bmi-1 is required for maintenance of adult self-renewing haematopoietic stem cells. Nature *423*, 302-305.
Park, J.H., Lee, J.Y., Shin, D.H., Jang, K.S., Kim, H.J., and Kong, G. (2011). Loss of Mel-18 induces tumor angiogenesis through enhancing the activity and expression of HIF-1alpha mediated by the PTEN/PI3K/Akt pathway. Oncogene *30*, 4578-4589.

Pei, Y., Liu, K.W., Wang, J., Garancher, A., Tao, R., Esparza, L.A., Maier, D.L., Udaka, Y.T., Murad, N., Morrissy, S.*, et al.* (2016). HDAC and PI3K Antagonists Cooperate to Inhibit Growth of MYC-Driven Medulloblastoma. Cancer Cell *29*, 311-323.
Pei, Y., Moore, C.E., Wang, J., Tewari, A.K., Eroshkin, A., Cho, Y.J., Witt, H., Korshunov, A., Read, T.A., Sun, J.L.*, et al.* (2012). An animal model of MYC-driven medulloblastoma. Cancer Cell *21*, 155-167.
Perreault, S., Ramaswamy, V., Achrol, A.S., Chao, K., Liu, T.T., Shih, D., Remke, M., Schubert, S., Bouffet, E., Fisher, P.G.*, et al.* (2014). MRI surrogates for molecular subgroups of medulloblastoma. AJNR Am J Neuroradiol *35*, 1263-1269.
Pervin, S., Singh, R., Hernandez, E., Wu, G., and Chaudhuri, G. (2007). Nitric oxide in physiologic concentrations targets the translational machinery to increase the proliferation of human breast cancer cells: involvement of mammalian target of rapamycin/eIF4E pathway. Cancer Res *67*, 289-299.
Peschansky, V.J., and Wahlestedt, C. (2014). Non-coding RNAs as direct and indirect modulators of epigenetic regulation. Epigenetics *9*, 3-12.
Phoenix, T.N., Patmore, D.M., Boop, S., Boulos, N., Jacus, M.O., Patel, Y.T., Roussel, M.F., Finkelstein, D., Goumnerova, L., Perreault, S.*, et al.* (2016). Medulloblastoma Genotype Dictates Blood Brain Barrier Phenotype. Cancer Cell *29*, 508-522.
Pierce, G.B., and Dixon, F.J., Jr. (1959). Testicular teratomas. I. Demonstration of teratogenesis by metamorphosis of multipotential cells. Cancer *12*, 573-583.
Pietsch, T., Schmidt, R., Remke, M., Korshunov, A., Hovestadt, V., Jones, D.T., Felsberg, J., Kaulich, K., Goschzik, T., Kool, M.*, et al.* (2014). Prognostic significance of clinical, histopathological, and molecular characteristics of medulloblastomas in the prospective HIT2000 multicenter clinical trial cohort. Acta Neuropathol *128*, 137-149.
Pizer, B., Donachie, P.H., Robinson, K., Taylor, R.E., Michalski, A., Punt, J., Ellison, D.W., and Picton, S. (2011). Treatment of recurrent central nervous system primitive neuroectodermal tumours in children and adolescents: results of a Children's Cancer and Leukaemia Group study. Eur J Cancer *47*, 1389-1397.
Pomerantz, J., Schreiber-Agus, N., Liegeois, N.J., Silverman, A., Alland, L., Chin, L., Potes, J., Chen, K., Orlow, I., Lee, H.W.*, et al.* (1998). The Ink4a tumor suppressor gene product, p19Arf, interacts with MDM2 and neutralizes MDM2's inhibition of p53. Cell *92*, 713-723.
Pomeroy, S.L., Tamayo, P., Gaasenbeek, M., Sturla, L.M., Angelo, M., McLaughlin, M.E., Kim, J.Y., Goumnerova, L.C., Black, P.M., Lau, C.*, et al.* (2002). Prediction of central nervous system embryonal tumour outcome based on gene expression. Nature *415*, 436-442.
Porteus, M.H., and Baltimore, D. (2003). Chimeric nucleases stimulate gene targeting in human cells. Science *300*, 763.
Potten, C.S., and Loeffler, M. (1990). Stem cells: attributes, cycles, spirals, pitfalls and uncertainties. Lessons for and from the crypt. Development *110*, 1001-1020.

Qian, T., Lee, J.Y., Park, J.H., Kim, H.J., and Kong, G. (2010). Id1 enhances RING1b E3 ubiquitin ligase activity through the Mel-18/Bmi-1 polycomb group complex. Oncogene *29*, 5818-5827.
Ramalho-Santos, M., and Willenbring, H. (2007). On the origin of the term "stem cell". Cell Stem Cell *1*, 35-38.
Ramaswamy, V., Remke, M., Bouffet, E., Faria, C.C., Perreault, S., Cho, Y.J., Shih, D.J., Luu, B., Dubuc, A.M., Northcott, P.A.*, et al.* (2013). Recurrence patterns across medulloblastoma subgroups: an integrated clinical and molecular analysis. Lancet Oncol *14*, 1200-1207.
Read, T.A., Fogarty, M.P., Markant, S.L., McLendon, R.E., Wei, Z., Ellison, D.W., Febbo, P.G., and Wechsler-Reya, R.J. (2009). Identification of CD15 as a marker for tumor-propagating cells in a mouse model of medulloblastoma. Cancer Cell *15*, 135-147.
Reveneau, S., Arnould, L., Jolimoy, G., Hilpert, S., Lejeune, P., Saint-Giorgio, V., Belichard, C., and Jeannin, J.F. (1999). Nitric oxide synthase in human breast cancer is associated with tumor grade, proliferation rate, and expression of progesterone receptors. Lab Invest *79*, 1215-1225.
Reya, T., Morrison, S.J., Clarke, M.F., and Weissman, I.L. (2001). Stem cells, cancer, and cancer stem cells. Nature *414*, 105-111.
Reynolds, B.A., and Weiss, S. (1992). Generation of neurons and astrocytes from isolated cells of the adult mammalian central nervous system. Science *255*, 1707-1710.
Ribi, K., Relly, C., Landolt, M.A., Alber, F.D., Boltshauser, E., and Grotzer, M.A. (2005). Outcome of medulloblastoma in children: long-term complications and quality of life. Neuropediatrics *36*, 357-365.
Riis, M.L., Luders, T., Markert, E.K., Haakensen, V.D., Nesbakken, A.J., Kristensen, V.N., and Bukholm, I.R. (2012). Molecular profiles of pre- and postoperative breast cancer tumours reveal differentially expressed genes. ISRN Oncol *2012*, 450267.
Rippert, H. (1904). Geschwulstelehre fur Aerzte und Studierende.
Robinson, G., Parker, M., Kranenburg, T.A., Lu, C., Chen, X., Ding, L., Phoenix, T.N., Hedlund, E., Wei, L., Zhu, X.*, et al.* (2012). Novel mutations target distinct subgroups of medulloblastoma. Nature *488*, 43-48.
Sahasrabuddhe, A.A., Dimri, M., Bommi, P.V., and Dimri, G.P. (2011). betaTrCP regulates BMI1 protein turnover via ubiquitination and degradation. Cell Cycle *10*, 1322-1330.
Sakaguchi, H., Muramatsu, H., Okuno, Y., Makishima, H., Xu, Y., Furukawa-Hibi, Y., Wang, X., Narita, A., Yoshida, K., Shiraishi, Y.*, et al.* (2015). Aberrant DNA Methylation Is Associated with a Poor Outcome in Juvenile Myelomonocytic Leukemia. PLoS One *10*, e0145394.
Salcido, C.D., Larochelle, A., Taylor, B.J., Dunbar, C.E., and Varticovski, L. (2010). Molecular characterisation of side population cells with cancer stem cell-like characteristics in small-cell lung cancer. Br J Cancer *102*, 1636-1644.
Sauvageau, M., and Sauvageau, G. (2010). Polycomb group proteins: multi-faceted regulators of somatic stem cells and cancer. Cell Stem Cell *7*, 299-313.

Schuller, U., Heine, V.M., Mao, J., Kho, A.T., Dillon, A.K., Han, Y.G., Huillard, E., Sun, T., Ligon, A.H., Qian, Y.*, et al.* (2008). Acquisition of granule neuron precursor identity is a critical determinant of progenitor cell competence to form Shh-induced medulloblastoma. Cancer Cell *14*, 123-134.
Schuringa, J.J., and Vellenga, E. (2010). Role of the polycomb group gene BMI1 in normal and leukemic hematopoietic stem and progenitor cells. Curr Opin Hematol *17*, 294-299.
Schwalbe, E.C., Lindsey, J.C., Nakjang, S., Crosier, S., Smith, A.J., Hicks, D., Rafiee, G., Hill, R.M., Iliasova, A., Stone, T.*, et al.* (2017). Novel molecular subgroups for clinical classification and outcome prediction in childhood medulloblastoma: a cohort study. Lancet Oncol *18*, 958-971.
Serrano, D., Bleau, A.M., Fernandez-Garcia, I., Fernandez-Marcelo, T., Iniesta, P., Ortiz-de-Solorzano, C., and Calvo, A. (2011). Inhibition of telomerase activity preferentially targets aldehyde dehydrogenase-positive cancer stem-like cells in lung cancer. Mol Cancer *10*, 96.
Serrano, M., Hannon, G.J., and Beach, D. (1993). A new regulatory motif in cell-cycle control causing specific inhibition of cyclin D/CDK4. Nature *366*, 704-707.
Shalem, O., Sanjana, N.E., Hartenian, E., Shi, X., Scott, D.A., Mikkelsen, T.S., Heckl, D., Ebert, B.L., Root, D.E., Doench, J.G.*, et al.* (2014). Genome-scale CRISPR-Cas9 knockout screening in human cells. Science *343*, 84-87.
Shang, Z.J., Li, J.R., and Li, Z.B. (2002). Effects of exogenous nitric oxide on oral squamous cell carcinoma: an in vitro study. J Oral Maxillofac Surg *60*, 905-910; discussion 910-901.
Sharpless, N.E., and DePinho, R.A. (2007). How stem cells age and why this makes us grow old. Nat Rev Mol Cell Biol *8*, 703-713.
Sharpless, N.E., and Sherr, C.J. (2015). Forging a signature of in vivo senescence. Nat Rev Cancer *15*, 397-408.
Shih, C.S., Hale, G.A., Gronewold, L., Tong, X., Laningham, F.H., Gilger, E.A., Srivastava, D.K., Kun, L.E., Gajjar, A., and Fouladi, M. (2008). High-dose chemotherapy with autologous stem cell rescue for children with recurrent malignant brain tumors. Cancer *112*, 1345-1353.
Shih, D.J., Northcott, P.A., Remke, M., Korshunov, A., Ramaswamy, V., Kool, M., Luu, B., Yao, Y., Wang, X., Dubuc, A.M.*, et al.* (2014). Cytogenetic prognostication within medulloblastoma subgroups. J Clin Oncol *32*, 886-896.
Signer, R.A., and Morrison, S.J. (2013). Mechanisms that regulate stem cell aging and life span. Cell Stem Cell *12*, 152-165.
Siminovitch, L., McCulloch, E.A., and Till, J.E. (1963). The Distribution of Colony-Forming Cells among Spleen Colonies. J Cell Physiol *62*, 327-336.
Sing, A., Pannell, D., Karaiskakis, A., Sturgeon, K., Djabali, M., Ellis, J., Lipshitz, H.D., and Cordes, S.P. (2009). A vertebrate Polycomb response element governs segmentation of the posterior hindbrain. Cell *138*, 885-897.
Singh, A., and Settleman, J. (2010). EMT, cancer stem cells and drug resistance: an emerging axis of evil in the war on cancer. Oncogene *29*, 4741-4751.

Singh, S.K., Clarke, I.D., Terasaki, M., Bonn, V.E., Hawkins, C., Squire, J., and Dirks, P.B. (2003). Identification of a cancer stem cell in human brain tumors. Cancer Res *63*, 5821-5828.
Singh, S.K., Hawkins, C., Clarke, I.D., Squire, J.A., Bayani, J., Hide, T., Henkelman, R.M., Cusimano, M.D., and Dirks, P.B. (2004). Identification of human brain tumour initiating cells. Nature *432*, 396-401.
Snyder, A.D., Dulin-Smith, A.N., Houston, R.H., Durban, A.N., Brisbin, B.J., Oostra, T.D., Marshall, J.T., Kahwash, B.M., and Pierson, C.R. (2013). Expression pattern of id proteins in medulloblastoma. Pathol Oncol Res *19*, 437-446.
Son, M.J., Woolard, K., Nam, D.H., Lee, J., and Fine, H.A. (2009). SSEA-1 is an enrichment marker for tumor-initiating cells in human glioblastoma. Cell Stem Cell *4*, 440-452.
Song, L.B., Li, J., Liao, W.T., Feng, Y., Yu, C.P., Hu, L.J., Kong, Q.L., Xu, L.H., Zhang, X., Liu, W.L.*, et al.* (2009). The polycomb group protein Bmi-1 represses the tumor suppressor PTEN and induces epithelial-mesenchymal transition in human nasopharyngeal epithelial cells. J Clin Invest *119*, 3626-3636.
Sottoriva, A., Spiteri, I., Piccirillo, S.G., Touloumis, A., Collins, V.P., Marioni, J.C., Curtis, C., Watts, C., and Tavare, S. (2013). Intratumor heterogeneity in human glioblastoma reflects cancer evolutionary dynamics. Proc Natl Acad Sci U S A *110*, 4009-4014.
Sparmann, A., and van Lohuizen, M. (2006). Polycomb silencers control cell fate, development and cancer. Nat Rev Cancer *6*, 846-856.
Stevens, L.C. (1964). Experimental Production of Testicular Teratomas in Mice. Proc Natl Acad Sci U S A *52*, 654-661.
Stevens, L.C. (1970). The development of transplantable teratocarcinomas from intratesticular grafts of pre- and postimplantation mouse embryos. Dev Biol *21*, 364-382.
Strebhardt, K. (2010). Multifaceted polo-like kinases: drug targets and antitargets for cancer therapy. Nat Rev Drug Discov *9*, 643-660.
Strebhardt, K., and Ullrich, A. (2006). Targeting polo-like kinase 1 for cancer therapy. Nat Rev Cancer *6*, 321-330.
Subramanian, A., Tamayo, P., Mootha, V.K., Mukherjee, S., Ebert, B.L., Gillette, M.A., Paulovich, A., Pomeroy, S.L., Golub, T.R., Lander, E.S.*, et al.* (2005). Gene set enrichment analysis: a knowledge-based approach for interpreting genome-wide expression profiles. Proc Natl Acad Sci U S A *102*, 15545-15550.
Swanton, C. (2015). Cancer evolution constrained by mutation order. The New England journal of medicine *372*, 661-663.
Tang, Y., Gholamin, S., Schubert, S., Willardson, M.I., Lee, A., Bandopadhayay, P., Bergthold, G., Masoud, S., Nguyen, B., Vue, N.*, et al.* (2014). Epigenetic targeting of Hedgehog pathway transcriptional output through BET bromodomain inhibition. Nat Med *20*, 732-740.
Tao, J., Liu, Y.L., Zhang, G., Ma, Y.Y., Cui, B.B., and Yang, Y.M. (2014). Expression and clinicopathological significance of Mel-18 mRNA in colorectal cancer. Tumour Biol *35*, 9619-9625.

Taylor, M.D., Northcott, P.A., Korshunov, A., Remke, M., Cho, Y.J., Clifford, S.C., Eberhart, C.G., Parsons, D.W., Rutkowski, S., Gajjar, A.*, et al.* (2012). Molecular subgroups of medulloblastoma: the current consensus. Acta Neuropathol *123*, 465-472.
Taylor, R.E., Bailey, C.C., Robinson, K.J., Weston, C.L., Walker, D.A., Ellison, D., Ironside, J., Pizer, B.L., and Lashford, L.S. (2005). Outcome for patients with metastatic (M2-3) medulloblastoma treated with SIOP/UKCCSG PNET-3 chemotherapy. Eur J Cancer *41*, 727-734.
Tetsu, O., Ishihara, H., Kanno, R., Kamiyasu, M., Inoue, H., Tokuhisa, T., Taniguchi, M., and Kanno, M. (1998). mel-18 negatively regulates cell cycle progression upon B cell antigen receptor stimulation through a cascade leading to c-myc/cdc25. Immunity *9*, 439-448.
Thompson, M.C., Fuller, C., Hogg, T.L., Dalton, J., Finkelstein, D., Lau, C.C., Chintagumpala, M., Adesina, A., Ashley, D.M., Kellie, S.J.*, et al.* (2006). Genomics identifies medulloblastoma subgroups that are enriched for specific genetic alterations. J Clin Oncol *24*, 1924-1931.
Thomsen, L.L., Lawton, F.G., Knowles, R.G., Beesley, J.E., Riveros-Moreno, V., and Moncada, S. (1994). Nitric oxide synthase activity in human gynecological cancer. Cancer Res *54*, 1352-1354.
Till, J.E., and McCulloch, E.A. (1961). A direct measurement of the radiation sensitivity of normal mouse bone marrow cells. Radiat Res *14*, 213-222.
Tropepe, V., Sibilia, M., Ciruna, B.G., Rossant, J., Wagner, E.F., and van der Kooy, D. (1999). Distinct neural stem cells proliferate in response to EGF and FGF in the developing mouse telencephalon. Dev Biol *208*, 166-188.
Turke, A.B., Zejnullahu, K., Wu, Y.L., Song, Y., Dias-Santagata, D., Lifshits, E., Toschi, L., Rogers, A., Mok, T., Sequist, L.*, et al.* (2010). Preexistence and clonal selection of MET amplification in EGFR mutant NSCLC. Cancer Cell *17*, 77-88.
van der Lugt, N.M., Domen, J., Linders, K., van Roon, M., Robanus-Maandag, E., te Riele, H., van der Valk, M., Deschamps, J., Sofroniew, M., van Lohuizen, M.*, et al.* (1994). Posterior transformation, neurological abnormalities, and severe hematopoietic defects in mice with a targeted deletion of the bmi-1 proto-oncogene. Genes Dev *8*, 757-769.
van der Vlag, J., and Otte, A.P. (1999). Transcriptional repression mediated by the human polycomb-group protein EED involves histone deacetylation. Nat Genet *23*, 474-478.
van Lohuizen, M., Frasch, M., Wientjens, E., and Berns, A. (1991). Sequence similarity between the mammalian bmi-1 proto-oncogene and the Drosophila regulatory genes Psc and Su(z)2. Nature *353*, 353-355.
Vanner, R.J., Remke, M., Gallo, M., Selvadurai, H.J., Coutinho, F., Lee, L., Kushida, M., Head, R., Morrissy, S., Zhu, X.*, et al.* (2014). Quiescent sox2(+) cells drive hierarchical growth and relapse in sonic hedgehog subgroup medulloblastoma. Cancer Cell *26*, 33-47.

Venugopal, C., Hallett, R., Vora, P., Manoranjan, B., Mahendram, S., Qazi, M.A., McFarlane, N., Subapanditha, M., Nolte, S.M., Singh, M.*, et al.* (2015). Pyrvinium Targets CD133 in Human Glioblastoma Brain Tumor-Initiating Cells. Clin Cancer Res *21*, 5324-5337.
Venugopal, C., McFarlane, N.M., Nolte, S., Manoranjan, B., and Singh, S.K. (2012a). Processing of primary brain tumor tissue for stem cell assays and flow sorting. J Vis Exp.
Venugopal, C., Wang, X.S., Manoranjan, B., McFarlane, N., Nolte, S., Li, M., Murty, N., Siu, K.W., and Singh, S.K. (2012b). GBM secretome induces transient transformation of human neural precursor cells. J Neurooncol *109*, 457-466.
Veo, B., Danis, E., Pierce, A., Sola, I., Wang, D., Foreman, N.K., Jin, J., Ma, A., Serkova, N., Venkataraman, S.*, et al.* (2019). Combined functional genomic and chemical screens identify SETD8 as a therapeutic target in MYC-driven medulloblastoma. JCI Insight *4*.
Villa, F., Carrizzo, A., Spinelli, C.C., Ferrario, A., Malovini, A., Maciag, A., Damato, A., Auricchio, A., Spinetti, G., Sangalli, E.*, et al.* (2015). Genetic Analysis Reveals a Longevity-Associated Protein Modulating Endothelial Function and Angiogenesis. Circ Res *117*, 333-345.
Virchow, R. (1863). Dir Krankhoften Geschwulste. Vol II. Onkologie, Pt 1.
Voncken, J.W., Niessen, H., Neufeld, B., Rennefahrt, U., Dahlmans, V., Kubben, N., Holzer, B., Ludwig, S., and Rapp, U.R. (2005). MAPKAP kinase 3pK phosphorylates and regulates chromatin association of the polycomb group protein Bmi1. J Biol Chem *280*, 5178-5187.
Voncken, J.W., Schweizer, D., Aagaard, L., Sattler, L., Jantsch, M.F., and van Lohuizen, M. (1999). Chromatin-association of the Polycomb group protein BMI1 is cell cycle-regulated and correlates with its phosphorylation status. J Cell Sci *112 (Pt 24)*, 4627-4639.
Vrzalikova, K., Skarda, J., Ehrmann, J., Murray, P.G., Fridman, E., Kopolovic, J., Knizetova, P., Hajduch, M., Klein, J., Kolek, V.*, et al.* (2008). Prognostic value of Bmi-1 oncoprotein expression in NSCLC patients: a tissue microarray study. J Cancer Res Clin Oncol *134*, 1037-1042.
Wang, H., Wang, L., Erdjument-Bromage, H., Vidal, M., Tempst, P., Jones, R.S., and Zhang, Y. (2004). Role of histone H2A ubiquitination in Polycomb silencing. Nature *431*, 873-878.
Wang, T., Wei, J.J., Sabatini, D.M., and Lander, E.S. (2014). Genetic screens in human cells using the CRISPR-Cas9 system. Science *343*, 80-84.
Wang, W., Lin, T., Huang, J., Hu, W., Xu, K., and Liu, J. (2011). Analysis of Mel-18 expression in prostate cancer tissues and correlation with clinicopathologic features. Urol Oncol *29*, 244-251.
Wang, W., Yuasa, T., Tsuchiya, N., Ma, Z., Maita, S., Narita, S., Kumazawa, T., Inoue, T., Tsuruta, H., Horikawa, Y.*, et al.* (2009). The novel tumor-suppressor Mel-18 in prostate cancer: its functional polymorphism, expression and clinical significance. Int J Cancer *125*, 2836-2843.

Wang, X., Dubuc, A.M., Ramaswamy, V., Mack, S., Gendoo, D.M., Remke, M., Wu, X., Garzia, L., Luu, B., Cavalli, F.*, et al.* (2015). Medulloblastoma subgroups remain stable across primary and metastatic compartments. Acta Neuropathol *129*, 449-457.
Wang, X., Venugopal, C., Manoranjan, B., McFarlane, N., O'Farrell, E., Nolte, S., Gunnarsson, T., Hollenberg, R., Kwiecien, J., Northcott, P.*, et al.* (2012). Sonic hedgehog regulates Bmi1 in human medulloblastoma brain tumor-initiating cells. Oncogene *31*, 187-199.
Ward, R.J., Lee, L., Graham, K., Satkunendran, T., Yoshikawa, K., Ling, E., Harper, L., Austin, R., Nieuwenhuis, E., Clarke, I.D.*, et al.* (2009). Multipotent CD15+ cancer stem cells in patched-1-deficient mouse medulloblastoma. Cancer Res *69*, 4682-4690.
Watanabe, T., Frahm, J., and Michaelis, T. (2010). Myelin mapping in the living mouse brain using manganese-enhanced magnetization transfer MRI. Neuroimage *49*, 1200-1204.
Wechsler-Reya, R.J., and Scott, M.P. (1999). Control of neuronal precursor proliferation in the cerebellum by Sonic Hedgehog. Neuron *22*, 103-114.
Wefers, A.K., Warmuth-Metz, M., Poschl, J., von Bueren, A.O., Monoranu, C.M., Seelos, K., Peraud, A., Tonn, J.C., Koch, A., Pietsch, T.*, et al.* (2014). Subgroup-specific localization of human medulloblastoma based on pre-operative MRI. Acta Neuropathol *127*, 931-933.
Wei, W.C., Huang, W.C., Lin, Y.P., Becker, E.B.E., Ansorge, O., Flockerzi, V., Conti, D., Cenacchi, G., and Glitsch, M.D. (2017). Functional expression of calcium-permeable canonical transient receptor potential 4-containing channels promotes migration of medulloblastoma cells. J Physiol *595*, 5525-5544.
Wiederschain, D., Chen, L., Johnson, B., Bettano, K., Jackson, D., Taraszka, J., Wang, Y.K., Jones, M.D., Morrissey, M., Deeds, J.*, et al.* (2007). Contribution of polycomb homologues Bmi-1 and Mel-18 to medulloblastoma pathogenesis. Mol Cell Biol *27*, 4968-4979.
Woo, C.J., Kharchenko, P.V., Daheron, L., Park, P.J., and Kingston, R.E. (2010). A region of the human HOXD cluster that confers polycomb-group responsiveness. Cell *140*, 99-110.
Wu, X., Northcott, P.A., Dubuc, A., Dupuy, A.J., Shih, D.J., Witt, H., Croul, S., Bouffet, E., Fults, D.W., Eberhart, C.G.*, et al.* (2012). Clonal selection drives genetic divergence of metastatic medulloblastoma. Nature *482*, 529-533.
Xing, X., Cai, W., Shi, H., Wang, Y., Li, M., Jiao, J., and Chen, M. (2013). The prognostic value of CDKN2A hypermethylation in colorectal cancer: a meta-analysis. Br J Cancer *108*, 2542-2548.
Yang, M.H., Hsu, D.S., Wang, H.W., Wang, H.J., Lan, H.Y., Yang, W.H., Huang, C.H., Kao, S.Y., Tzeng, C.H., Tai, S.K.*, et al.* (2010). Bmi1 is essential in Twist1-induced epithelial-mesenchymal transition. Nat Cell Biol *12*, 982-992.
Yang, Z.J., Ellis, T., Markant, S.L., Read, T.A., Kessler, J.D., Bourboulas, M., Schuller, U., Machold, R., Fishell, G., Rowitch, D.H.*, et al.* (2008). Medulloblastoma can be initiated by deletion of Patched in lineage-restricted progenitors or stem cells. Cancer Cell *14*, 135-145.

Ying, L., and Hofseth, L.J. (2007). An emerging role for endothelial nitric oxide synthase in chronic inflammation and cancer. Cancer Res *67*, 1407-1410.
Yong, K.J., Basseres, D.S., Welner, R.S., Zhang, W.C., Yang, H., Yan, B., Alberich-Jorda, M., Zhang, J., de Figueiredo-Pontes, L.L., Battelli, C.*, et al.* (2016). Targeted BMI1 inhibition impairs tumor growth in lung adenocarcinomas with low CEBPalpha expression. Sci Transl Med *8*, 350ra104.
Zeltzer, P.M., Boyett, J.M., Finlay, J.L., Albright, A.L., Rorke, L.B., Milstein, J.M., Allen, J.C., Stevens, K.R., Stanley, P., Li, H.*, et al.* (1999). Metastasis stage, adjuvant treatment, and residual tumor are prognostic factors for medulloblastoma in children: conclusions from the Children's Cancer Group 921 randomized phase III study. J Clin Oncol *17*, 832-845.
Zhang, X.W., Sheng, Y.P., Li, Q., Qin, W., Lu, Y.W., Cheng, Y.F., Liu, B.Y., Zhang, F.C., Li, J., Dimri, G.P.*, et al.* (2010). BMI1 and Mel-18 oppositely regulate carcinogenesis and progression of gastric cancer. Mol Cancer *9*, 40.
Zhang, Y., Xiong, Y., and Yarbrough, W.G. (1998). ARF promotes MDM2 degradation and stabilizes p53: ARF-INK4a locus deletion impairs both the Rb and p53 tumor suppression pathways. Cell *92*, 725-734.
Zhao, X., Liu, Z., Yu, L., Zhang, Y., Baxter, P., Voicu, H., Gurusiddappa, S., Luan, J., Su, J.M., Leung, H.C.*, et al.* (2012). Global gene expression profiling confirms the molecular fidelity of primary tumor-based orthotopic xenograft mouse models of medulloblastoma. Neuro Oncol *14*, 574-583.
Zhukova, N., Ramaswamy, V., Remke, M., Pfaff, E., Shih, D.J., Martin, D.C., Castelo-Branco, P., Baskin, B., Ray, P.N., Bouffet, E.*, et al.* (2013). Subgroup-specific prognostic implications of TP53 mutation in medulloblastoma. J Clin Oncol *31*, 2927-2935.

Appendix I: Copyright Statements

1. European Oncology & Haematology:

DAVID BAKHSHINYAN <bakhshd@mcmaster.ca>

RE: Permission to reprint material in a PhD Thesis
1 message

Tim Sheldrick <tim.sheldrick@touchmedicalmedia.com> Thu, Mar 7, 2019 at 4:37 AM
To: DAVID BAKHSHINYAN <bakhshd@mcmaster.ca>

Hi David,

Permission granted. Good luck with the thesis!

Regards,

Tim

From: DAVID BAKHSHINYAN [mailto:bakhshd@mcmaster.ca]
Sent: 06 March 2019 22:23
To: tim.sheldrick@touchmedicalmedia.com
Cc: Joanna Brockley <joanna.brockley@touchmedicalmedia.com>
Subject: Permission to reprint material in a PhD Thesis

To Whom It May Concern,

I am completing a PhD thesis at McMaster University entitled “GENES PRESERVING STEM CELL STATE IN MEDULLOBLASTOMA CONTRIBUTE TO THERAPY EVASION AND RELAPSE”. I would like your permission to reprint in full the following journal article in my thesis:

Bakhshinyan, D., A. A. Adile, C. Venugopal, S. K. Singh (2017). "BMI1: a path to targeting cancer stem cells." ***European Oncology and Haematology***

Please note that I am the first author of this work.

I am also requesting that you grant irrevocable, nonexclusive licence to McMaster University to reproduce this material as a part of the thesis. Proper acknowledgement of your copyright of the reprinted material will be given in the thesis.

Sincerely,

David Bakhshinyan

2. Oncogene:

McMaster University

DAVID BAKHSHINYAN <bakhshd@mcmaster.ca>

Permission to reprint material in a PhD Thesis
2 messages

DAVID BAKHSHINYAN <bakhshd@mcmaster.ca> Wed, Mar 6, 2019 at 5:10 PM
To: Journalpermissions@springernature.com

To Whom It May Concern,

I am completing a PhD thesis at McMaster University entitled "GENES PRESERVING STEM CELL STATE IN MEDULLOBLASTOMA CONTRIBUTE TO THERAPY EVASION AND RELAPSE". I would like your permission to reprint in full the following journal article in my thesis:

Bakhshinyan, D., C. Venugopal, A. A. Adile, N. Garg, B. Manoranjan, R. Hallett, X. Wang, S. Mahendram, P. Vora, T. Vijayakumar, M. Subapanditha, M. Singh, M. M. Kameda-Smith, M. Qazi, N. McFarlane, A. Mann, O. A. Ajani, B. Yarascavitch, V. Ramaswamy, H. Farooq, S. Morrissy, L. Cao, N. Sydorenko, R. Baiazitov, W. Du, J. Sheedy, M. Weetall, Y. C. Moon, C. S. Lee, J. M. Kwiecien, K. H. Delaney, B. Doble, Y. J. Cho, S. Mitra, D. Kaplan, M. D. Taylor, T. W. Davis and S. K. Singh (2018). "BMI1 is a therapeutic target in recurrent medulloblastoma." *Oncogene*. doi:10.1038/s41388-018-0549-9

Please note that I am the first author of this work.

I am also requesting that you grant irrevocable, nonexclusive licence to McMaster University to reproduce this material as a part of the thesis. Proper acknowledgement of your copyright of the reprinted material will be given in the thesis.

Sincerely,

David Bakhshinyan
--
David Bakhshinyan, (H)B.Sc.
PhD Candidate.Biochemistry and Biomedical Sciences,
McMaster University
E-mail: bakhshd@mcmaster.ca Phone: +1-416-732-7892

Laboratory of Dr. Sheila K. Singh
Brain Tumour Stem Cell Research Program
Stem Cell and Cancer Research Institute (SCC-RI)
McMaster University, MDCL 5077, 1280 Main St. W.,
Hamilton, ON, Canada L8S 4K1

Journalpermissions <journalpermissions@springernature.com> Fri, Mar 8, 2019 at 11:25 AM
To: DAVID BAKHSHINYAN <bakhshd@mcmaster.ca>

Dear David,

Thank you for contacting Springer Nature. As an author, you have the right to use this manuscript and figures, as per the licence-to-publish you signed:

Ownership of copyright in in original research articles remains with the Author, and provided that, when reproducing the contribution or extracts from it or from the Supplementary Information, the Author acknowledges first and reference publication in the Journal, the Author retains the following non-exclusive rights:

a) To reproduce the contribution in whole or in part in any printed/electronic volume (book or thesis) of which they are the author(s).

b) The author and any academic institution where they work at the time may reproduce the contribution for the purpose of course teaching.

c) To reuse figures or tables created by the Author and contained in the Contribution in oral presentations and other works created by them.

d) To post a copy of the contribution as accepted for publication after peer review (in locked Word processing file, of a PDF version thereof) on the Author's own web site, or the Author's institutional repository, or the Author's funding body's archive, six months after publication of the printed or online edition of the Journal, provided that they also link to the contribution on the publisher's website.

The above use of the term 'Contribution' refers to the author's own version, not the final version as published in the Journal.

Best wishes,

Oda

Oda Siqveland

Rights Executive

SpringerNature

The Campus, 4 Crinan Street, London N1 9XW,

United Kingdom

T +44 (0) 207 014 6851

http://www.nature.com

http://www.springer.com

http://www.palgrave.com

Appendix II: Academic accomplishments

The following are the highlights of academic achievements from September 2013 to March 2019.

PUBLICATIONS (RESEARCH):

Published Refereed Papers (*Equal contribution by authors)

1. Shouksmith AE, Grimard ML, Geletu M, Luchman A, Heaton WL, Araujo ED, Berger-Bevcar A, Gawel JM, **Bakhshinyan D**, Adile AA, Venugopal C, Johns AE, Al-Qaysi O, Lewis AM, O'Hare T, Deininger MD, Singh SK, Weiss S, Fishel M, Gunning PT. (2018). Identification and characterization of AES-135, a nanomolar HDAC inhibitor with potent biological effects in 3D patient-derived tumor spheroids of pancreatic cancer. *Journal of Medicinal Chemistry*

2. **Bakhshinyan D**, Venugopal C, Adile AA, Garg N, Manoranjan B Hallett R, Wang X, Mahendram S, Vijayakumar T, Subapanditha M, Qazi M, Singh M, McFarlane N, Mann A, Vora P, Olufemi A, Yarascavich B, Ramaswamy V, Farooq V, Morissy H, Cao L, Sydorenko, N, Baiazitov R, Sheedy J, Weetall M, Moon YC, Cho YJ, Mitra S, Kaplan D, Taylor M, Davis T, Singh SK. (2018). Bmi1 as a therapeutic target for recurrent medulloblastoma. *Oncogene*

3. Atherton MJ, Stephenson KB, Tzelepis F, **Bakhshinyan D**, Nikota JK, Son HH, Jirovec A, Lefebvre C, Dvorkin-Gheva A, Ashkar AA, Wan Y, Stojdl DF, Belanger EC, Breau RH, Bell JC, Saad F, Sheila SK, Dialo JS, Lichty BD. (2018). Transforming the prostatic tumor microenvironment with oncolytic virotherapy. *Oncoimmunology*

4. **Bakhshinyan D**, Adile AA, Venugopal C, Singh SK. (2017). Bmi1: a path to targeting cancer stem cells *European Oncology & Hematology*

5. Kameda-Smith MM, Manoranjan B, **Bakhshinyan D**, Adile AA, Venugopal C, Singh SK. (2017). Brain tumor initiating cells: with great technology will come greater understanding. *Future Neurology*

6. Singh M, Venugopal C, Tokar T, Brown KR, McFarlane N, **Bakhshinyan D**, Vijayakumar T, Manoranjan B, Mahendram S, Vora P, Qazi M, Dhillon M, Tong A, Durrer K, Murty N, Hallett R, Hassell JA, Kaplan DR, Cutz JC, Jurisica I, Moffat J, Singh SK. (2017). RNAi screen identifies essential regulators of human brain metastasis-initiating cells. *Acta Neuropathologica*

7. Singh, M, **Bakhshinyan D**, Venugopal C, Singh SK. (2017). Preclinical modelling of therapeutics avenues for cancer metastasis to central nervous system. *Frontiers in Oncology*

8. Garg N, **Bakhshinyan D**, Venugopal C, Rosa AD, Vijayakumar T, Manoranjan B,

Hallett R, McFarlane N, Mahendram S, Delaney K, Kwiecien J, Arpin CC, Lai PS, Gomez-Biagi RF, Ali AM, Ajani OA, Hassell JA, Gunning PT, Singh SK. (2016). Targeting STAT3 signaling in CD133+ medulloblastoma stem cells: a novel therapeutic strategy for recurrent group 3 medulloblastoma. *Oncotarget*

9. Chkuaseli T, Newborn LR, **Bakhshinyan D**, White AD. (2015). Protein expression strategies in Tobacco necrosis virus-D. *Virology*

10. Venugopal C, Hallett R, Vora P, Manoranjan B, Qazi MA, McFarlane N, Mahendram S, Nolte SM, Singh M, **Bakhshinyan D**, Garg N, Lach B, Provias JP, Reddy K, Murty NK, Doble BW, Bhatia M, Hassell JA, Singh SK. (2015). Pyrvinium targets CD133 in human glioblastoma brain tumor-initiating cells. *Clinical Cancer Research*

11. Singh M, Garg N, Venugopal C, Hallett RM, Tokar T, McFarlane N, Mahendram S, **Bakhshinyan D**, Manoranjan B, Vora P, Qazi M, Arpin CC, Page B, Haftchenary S, Rosa DA, Lao P-S, Gomez-Biagi RF, Ali AM, Lewis A, Geletu M, Murty NK, Hassell JA, Jurisica I, Gunning PT, Singh SK. (2015). STAT3 pathway regulates lung-derived brain metastasis initiating cell capacity through mIR-21 activation. *Oncotarget*

12. Garg N, Vijayakymar T, **Bakhshinyan D**, Venugopal C, Singh SK. (2015). MicroRNA regulation of brain tumor-initiating cells in central nervous system tumors. *Stem Cells International*

Submitted Refereed Papers (*Equal contribution by authors)

1. **Bakhshinyan D**, Adile AA, Venugopal C, Liu J, Singh M, Qazi MA, Vora P, Kameda-Smith M, Savage N, Desmond KL, Tatari N, Bock N, Bader G, Singh SK. Stem cell longevity factor BPIFB4 is a driver of medulloblastoma recurrence. *Nature Medicine*

2. Workenhe S, **Bakhshinyan D**, Wei J, MacNeill K, Nguyen A, Li D, Wan Y, Wang X, Singh SK, Bramson J, Mossman K. (2018). Therapy-induced necroptosis renders autochthonous mammary tumors susceptible to checkpoint blockade immunotherapy. *Cancer Discovery*

3. Manoranjan B, Venugopal C, **Bakhshinyan D**., Dvorkina, A., Subapanditha M, Kameda-Smith MM, Ashley A. Adile, Savage N, Doble BW, Singh SK. (2018). Context-specific tumor suppressive function of the canonical Wnt pathway in pediatric medulloblastoma highlights a therapeutic strategy for treatment-refractory subgroups. *Cancer Discovery*

4. Park J, de Araujo ED, Tin G, Ahmar S, Wingelhofer B, **Bakhshinyan D**, Geletu M, Berger A, Cumaraswamy AC, Rosa DA, Gomez R, Israelian J, Erogoden F, Ball BP, Armstrong D, Venugopal C, Fekl U, Prosser SR, Moriggl R, Singh SK, Gunning PT. (2018) Cloaking Potent Electrophilic Warheads: Shape, a Stealth Approach. *Nature Chemical Biology*

In Preparation Refereed Papers (*Equal contribution by authors)

5. **Bakhshinyan D**, Venugopal C, Singh SK. Identification of therapy resistant genes in Group 3 MB using DNA barcoding and genome-wide CRISPR screen. *Cancer Cell*

Published Refereed Book Chapters (*Equal contribution by authors)

1. Adile AA, **Bakhshinyan D**, Venugopal C, Singh SK (2018). In vitro assays for screening small molecules. Brain tumor stem cells. Methods & Protocols: Methods in Molecular Biology, Springer

2. Yelle N, **Bakhshinyan D**, Venugopal C, Singh SK (2018). Introduction to Brain Tumor Stem Cells. Brain tumor stem cells. Methods & Protocols: Methods in Molecular Biology, Springer

3. Bobrowski D, Seyfrid M, **Bakhshinyan D**, Venugopal C, Singh S K. (2018). In Vitro Study of BTSCs Self-Renewal. Brain tumor stem cells. Methods & Protocols: Methods in Molecular Biology, Springer

4. **Bakhshinyan D**, Adile AA, Qazi MA, Singh M, Kameda-Smith MM, Yelle N, Chokshi C, Venugopal C, Singh SK. (2017). Introduction to Cancer Stem Cells: Past, Present and Future. In: Methods in Molecular Biology: Cancer Stem Cells: Methods and Protocols. Springer

5. **Bakhshinyan D***, Qazi MA*, Garg N, Venugopal C, McFarlane N, Singh SK. (2015). Isolation and Identification of Neural Stem/Progenitor Cells. In: Principles of Stem Cell Biology and Cancer: Future Applications and Therapeutics. John Wiley & Sons, Ltd.

6. Manoranjan B, Garg N, **Bakhshinyan D**, Singh SK. (2014). *The role of stem cells in pediatric central nervous system malignancies.* In: Stem Cell Biology in Neoplasms of the Central Nervous System, John Wiley & Sons, Ltd.

Scientific Meetings: Published Poster Abstracts (*Presenter)

1. **Bakhshinyan D***, Adile A, Venugopal C, Singh M, Qazi M, Singh S. (2017). Genes preserving stem cell state in Group 3 MB BTICs contribute to therapy evasion and relapse. OICR Translational Research Conference, Kingsbridge, ON

2. **Bakhshinyan D***, Adile A, Venugopal C, Singh M, Qazi M, Singh S. (2017). Genes preserving stem cell state in Group 3 MB BTICs contribute to therapy evasion and relapse. 5th Biennial Conference on Pediatric Society of Neuro-oncology Basic and Translational Research Meeting, San Francisco, CA, USA

3. **Bakhshinyan D***, Adile A, Venugopal C, Singh M, Qazi M, Singh S. (2017). Genes preserving stem cell state in Group 3 MB BTICs contribute to therapy evasion and

relapse. American Association for Cancer Research, Boston, MA, USA, *Cancer Research*

4. **Bakhshinyan D***, Adile A, Venugopal C, Singh M, Qazi M, Manoranjan B, Kameda-Smith M, Singh S. (2017). Genes preserving stem cell state in Group 3 MB BTICs contribute to therapy evasion and relapse. 4th Biennial Conference on Pediatric Society of Neuro-oncology Basic and Translational Research Meeting, New York, NY, USA *J. Neuroonc* 19 (Suppl 6):vi225

5. Qazi M*, Nixon A, **Bakhshinyan D**, Venugopal C, Vora P, Brown K, Subapanditha, Yelle N, Chokshi C, Seyfrid M, Moffat J, Singh S. Clonal dynamics of human glioblastoma in response to chemoradiotherapy. (2017) 22nd Annual Scientific Meeting of the Society for Neuro-Oncology (SNO), San Francisco, CA *J. Neuroonc* 19 (Suppl 6):vi255

6. Singh M, Venugopal C, Tokar T, McFarlane N, **Bakhshinyan D**, Qazi M, Vora P, Murty N, Jurisica I, Singh SK. Abstract CMET-47. Preclinical validation of novel therapeutics targeting BMIC population in human brain metastases. (2017) 22nd Annual Scientific Meeting of the Society for Neuro-Oncology (SNO), San Francisco, CA *J. Neuroonc* 19 (Suppl 6):vi49

7. Manoranjan B*, Venugopal C, Kameda-Smith M, **Bakhshinyan D**, Subapanditha M, Doble BW, Singh SK. Context-specific tumor suppressive function of the canonical Wnt pathway in pediatric medulloblastoma highlights a therapeutic strategy for treatment-refractory subgroups. (2017) 22nd Annual Scientific Meeting of the Society for Neuro-Oncology (SNO), San Francisco, CA *J. Neuroonc* 19 (Suppl 6):vi230

8. Kameda-Smith MM*, Venugopal C, Manoranjan B, **Bakhshinyan D**, Adile A, Hope K, Singh SK. Investigating the role of the RNA binding protein, Musashi, in Group 3 medulloblastoma. (2017) 4th Biennial Conference on Pediatric Society of Neuro-oncology Basic and Translational Research Meeting, New York, NY, USA, *J Neuroonc* 19 (Suppl 4):iv43

9. **Bakhshinyan D***, Vijayakumar T, Venugopal C, Singh M, Qazi M, Mahendram S, Manoranjan B, McFarlane N, Adile A, Singh SK. Abstract 3870. Clonal evolution of medulloblastoma BTICs in response to therapy (2017). American Association for Cancer Research, Washington, D.C., USA, *Cancer Research*

10. Vora P*, Chokshi C, Qazi M, Singh M, Venugopal C, Mahendram S, Adams J, **Bakhshinyan D**, London M, Singh J, Subapanditha M, McFarlane N, Pan J, Bramson J, Sidhu S, Moffat J, Singh SK. Abstract 3758. The efficacy of CD133 BiTEs and CAR-T cells in preclinical model of glioblastoma. American Association for Cancer Research, Washington, D.C., USA, *Cancer Research*

11. Manoranjan B, Venugopal C, Pavlovic Z, Bakhshinyan D, Kameda-Smith M, Subapnditha M, Mahendram, Moffat J, Singh SK. Abstract 5831. Activated Wnt signaling for the treatment of recurrent medulloblastoma American Association for Cancer Research, Washington, D.C., USA, *Cancer Research*

12. Manoranjan B*, Mahendram S, **Bakhshinyan D**, Kameda-Smith M, Venugopal C, Doble BW, Singh SK. Activated Wnt signaling for the therapeutic targeting of treatment-refractory medulloblastoma stem cells. (2016) Canadian Journal of Neurological Sciences. 43(Suppl4):S2-S3. 17th Biennial Canadian Neuro-Oncology Meeting, Toronto, ON, Canada.

13. Singh M*, Venugopal C, McFarlane N, **Bakhshinyan D**, Mahendram S, Brown K, Tong A, Durrer K, Hallett R, Hassell R, Moffat J, Singh S. (2015). Development and application of a novel model of human lung-to-brain metastasis to identify unique metastatic gene signatures.

14. **Bakhshinyan D***, Vijayakumar T, Garg N, Manoranjan B, McFarlane N, Venugopal C, Singh S. (2015). *Discovering the Treatment Refractory BTIC Population in Group 3 Medulloblastoma*. 3rd Biennial Conference on Pediatric Neuro-Oncology Basic and Translational Research

15. Manoranjan B*, Venugopal C, Mahendran S, Moreira S, Hallett R, Vijayakumar T, **Bakhshinyan D**, McFarlane N, Hassell J, Doble B, Singh S. (2015). Activated Wnt Signaling Targets Sox2+ Treatment-Refractory Shh-Dependent Medulloblastoma Stem Cells. 3rd Biennial Conference on Pediatric Neuro-Oncology Basic and Translational Research

16. Vora P*, Qazi M, Venugopal C, Subhapandita M, McFarlane N, **Bakhshinyan D**, Singh S. (2015). Bmi1 Identifies the Treatment Refractory Stem Cells in Human Glioblastoma. 20th Annual Society for Neuro-Oncology Annual Scientific Meeting and Education Day

17. Singh SK*, Manoranjan B, Venugopal C, Vora P, McFarlane N, Garg N, Singh S, Mann A, **Bakhshinyan D**, Mahendran S, Dunn S. (2014). Sox2 Identifies the Treatment Refractory Stem Cell Population in Group 2 Medulloblastoma. 20th International Conference on Brain Tumor Research and Therapy

SCHOLARLY ACTIVITIES:

Scientific Meetings: Podium Oral Presentations (*Presenter)

1. **Bakhshinyan D***, Adile AA, Venugopal C, Singh M, Subapanditha, M, McFarlane N, Sing SK. (2018). *Genes preserving stem cell state in Group 3 MB BTICs contribute to therapy evasion and relapse*. 18th Biennial Canadian Neuro-Oncology meeting, Banff, AB, Canada

2. **Bakhshinyan D***, Adile AA, Venugopal C, Singh M, Subapanditha, M, McFarlane N, Sing SK*. (2017). *Genes preserving stem cell state in Group 3 MB BTICs contribute to therapy evasion and relapse.* Society for Neuro-Oncology, San Francisco, CA, USA

3. **Bakhshinyan D***, Adile AA, Venugopal C, Singh M, Subapanditha, M, McFarlane N, Sing SK. (2017). Clonal evolution of medulloblastoma brain tumor initiating cells through therapy. Faculty of Health Sciences Research Plenary, Hamilton, ON, Canada

4. **Bakhshinyan D*** & Qazi MA*. (2015) *Flow cytometry advancing brain tumor research.* **Keynote presentation** at the industry workshop: Analytical Methods for Profiling of Stem Cell, sponsored by Beckman Coulter. Till & McCulloch Meetingsm Toronto, ON, Canada.

5. **Bakhshinyan D***, Vijayakumar T, Garg N, Manoranjan B, McFarlane N, Venugopal C, Singh SK. (2015) *Clonal evolution of medulloblastoma brain tumor-initiating cells (BTICs) in response to therapy: Discovering the refractory BTIC population.* 3rd Biennial Pediatric Neuro-Oncology Basic and Translational Research Conference, Abstract MB-14, San Diego, CA, USA.

6. **Bakhshinyan D***, Vijayakumar T, Garg N, Manoranjan B, McFarlane N, Venugopal C, Singh SK. (2015) *Clonal evolution of medulloblastoma brain tumor-initiating cells (BTICs) in response to therapy: Discovering the refractory BTIC population.* McMaster University Faculty of Health Sciences Research Plenary, Hamilton, ON, Canada.

Scientific Meetings: Unpublished Poster Abstracts (*Presenter)

1. Kameda-Smith MM*, Venugopal C, Subapanditha M, **Bakhshinyan D**, Adile A, Manoranjan B Hope K, Singh SK. Investigating the role of the RNA binding protein, Musashi, in pediatric medulloblastoma. Keystone DNA and RNA methylation conference, Vancouver, BC, Canada 2018

2. Kameda-Smith MM*, Venugopal C, Manoranjan B, **Bakhshinyan D**, Adile A, Hope K, Singh SK. Investigating the role of the RNA binding protein, Musashi, in pediatric medulloblastoma. Cold Spring Harbour Laboratory Eukaryotic mRNA Processing Conference, Cold Spring Harbour, NY, USA, 2017.

3. Singh M*, Venugopal C, McFarlane N, **Bakhshinyan D**, Mahendram S, Brown K, Tong A, Durrer K, Hallett R, Hassell J, Moffat J, Singh SK. *Development and application of a novel model of human lung-to-brain metastasis to identify unique metastatic gene signatures.* Till & McCulloch Meetings, Abstract No. 22. Toronto, ON, Canada. 2015.

4. **Bakhshinyan D***, Vijayakumar T, Venugopal C, Vora P, Singh M, McFarlane N, Singh, M, Manoranjan B, Qazi M, Singh SK. *Clonal evolution of Medulloblastoma*

brain tumor-initiating cells (BTICs) in response to therapy. Till & McCulloch Meetings, Abstract No. 23. Toronto, ON, Canada. 2015.

5. Garg N*, Hallett R, **Bakhshinyan D**, Vijayakumar T, Mahendram S, Manoranjan B, Venugopal C, McFarlane N, Rosa D, Gunning P, Singh SK. *Potential role of CD133 driven STAT3 pathway in Group 3 medulloblastoma.* Till & McCulloch Meetings, Abstract No. 109. Toronto, ON, Canada. 2015.

6. Manoranjan B*, Mahendram S, **Bakhshinyan D**, Venugopal C, Doble B, Singh SK. *Targeted therapy for treatment refractory medulloblastoma stem cells.* Till & McCulloch Meetings, Abstract No. 110. Toronto, ON, Canada. 2015.

7. Vora P*, Qazi M, Venugopal C, Subhapandita M, Mahendram S, **Bakhshinyan D**, McFarlane N, Singh SK. Till & McCulloch Meetings, Abstract No. 112. Toronto, ON, Canada. 2015.

8. **Bakhshinyan D***, Garg N, Venugopal C, Mann A, Vora P, Singh M, van Ommeren R, McFarlane N, Singh, M, Manoranjan B, Qazi M, Scheinemann K, MacDonald P, Delaney K, Whitton A, Dunn S, Singh SK. *Clonal evolution of Medulloblastoma brain tumor-initiating cells (BTICs) in response to therapy: Discovering the refractory BTIC population.* Till & McCulloch Meetings, Abstract No. 134. Ottawa, ON, Canada. 2014.

9. Manoranjan B*, Mahendram S, Vijaykumar T, **Bakhshinyan D**, Hallet R, Garg N, Venugopal C, McFarlane N, Hassel J, Doble BW, Singh SK. *Activated Wnt signaling targets Sox2+ treatment refractory medullobastomal stem cells*. Till & McCulloch Meetings, Abstract No. 135. Ottawa, ON, Canada. 2014.

10. Garg N*, Singh M, **Bakhshinyan D**, Vora P, Venugopal C, McFarlane N, Manoranjan B, Mahendram S, Gunning P, Singh SK. *Potential role of STAT3 pathway in regulating tumor initiating cells to and within the central nervous system*. Till & McCulloch Meetings, Abstract No. 148. Ottawa, ON, Canada. 2014.

11. **Bakhshinyan D***, Venugopal C, Mann A, Vora P, Singh M, , van Ommeren R, McFarlane N, Singh Manoranjan B, Qazi M, Scheinemann K, MacDonald P, Delaney K, Whitton A, Dunn S, Singh SK. *Clonal evolution of Medulloblastoma brain tumor-initiating cells (BTICs) in response to therapy: Discovering the refractory BTIC population.* Ontario Institute for Cancer Research Cancer Stem Cell Meeting, Abstract No. O2. Toronto, ON, Canada. 2013.

12. **Bakhshinyan D***, Lima-Fernandes E, Wang Y, Barsyte-Lovejoy D, O'Brien A, Arrowsmith C. *Effects of EZH2 inhibition on colon cancer stem cell renewal*. Medical Biophysics Summer Student Poster Day, Toronto, ON, Canada. 2013

AWARDS & ACHIEVEMENTS (RESEARCH):

Brain Tumor Foundation of Canada Travel Award ($500)
Canadian Neuro-Oncology Society
- Selected by CNO committee as one of the top entries in the 2018 abstract competition

Banting Best Canada Graduate Scholarship Doctoral Award ($105,000)
McMaster University, Hamilton, ON
- Awarded to a top 86 doctoral students in Canada

Travel Award to 2015 Till & McCulloch Meetings ($1,000)
Stem Cell Network, Toronto, ON
- Selected by the Till & McCulloch Meetings Steering Committee as one of the top entries in 2015 Abstract Competition

Department of Biochemistry and Biomedical Sciences Travel Award ($500)
McMaster University, Hamilton, ON
- Selected by the Department as one of the top graduate students to receive the award to attend a workshop (3rd Biennial Pediatric Neuro-Oncology Basic and Translational Research Conference)

Stem Cell and Cancer Research Institute Travel Award ($1,000)
McMaster University, Hamilton, ON
- Selected by the Department as one of the top graduate students to receive the award to attend a workshop (3rd Biennial Pediatric Neuro-Oncology Basic and Translational Research Conference)

Travel Award to 2014 Till & McCulloch Meetings ($1,000)
Stem Cell Network, Ottawa, ON
- Selected by the Till & McCulloch Meetings Steering Committee as one of the top entries in 2014 Abstract Competition

Travel Award to 2013 Approaches to Clinical and Translational Research ($1,000)
Stem Cell Network, Ottawa, ON
- Selected by Stem Cell Network Training and Education Committee as one of the top applicants to attend the workshop

AWARDS & ACHIEVEMENTS (ACADEMIC):

The Lorne F. Lambier Q.C., Scholarship
McMaster University, Hamilton, ON

- Awarded to a doctoral student in Faculties of Health Science and Science whose research is directed toward the understanding and/or cure of cancer.

The Lee Nielson Roth Award ($1000)
McMaster University, Hamilton, ON

- Awarded to a doctoral student in Medical Sciences, Biochemistry, or Biology of high academic standing who is working in the area of cancer research.
- Awarded in 2016 and 2019

Faculty of Health Sciences Graduate Programs Excellence Award
McMaster University, Hamilton, ON

- Given to a student in the thesis-based program who achieved a rating of excellent for their last two or more supervisory committee meetings
- Awarded in 2014, 2015, 2016, 2017

Faculty of Health Sciences Excellence in Oral Presentation Award
McMaster University, Hamilton, ON

- Given to a student in the thesis-based program for ranking in the top 5 of oral presentation at the annual Faculty of Health Science Research Day

Thomas Neilson Award ($2,000)
McMaster University, Hamilton, ON

- Awarded on recommendation of the Departmental Graduate Admission Committee based on performance in the program with the emphasis on academic standing, contribution to teaching, the seminar presentation, transfer report and research contributions and publications.

The W.E Rawls Memorial Scholarship ($1000)
McMaster University, Hamilton, ON

- Awarded to a student in the Faculty of Health Sciences currently conducting research in molecular virology and oncology, including applications in clinical epidemiology and biostatistics.

Graduate School Entrance Scholarship ($2,500)
McMaster University, Hamilton, ON

- Awarded for academic excellence in undergraduate program upon admission to graduate school